Defining Endocytic Pathways to Characterise the Cellular Uptake of Extracellular Vesicles

A thesis submitted for the degree of Philosophiae Doctor in Cardiff University

by

Hope Daphne Roberts-Dalton

March 2017

Cardiff School of Pharmacy and Pharmaceutical Sciences

Cardiff University

Abstract

There is a need for vectors that, with high efficiency, can deliver small and macromolecular therapeutics into cells and defined intracellular locations. Extracellular vesicles (EVs), including exosomes, are naturally derived nanovesicles generated in and released by numerous cell types. As extracellular entities they have the capacity to interact with neighbouring cells and distant tissues and affect physiological processes as well as being implicated in numerous diseases including tumorigenesis and neurodegeneration. They are also under intense investigation as delivery vectors for biotherapeutics. The ways in which EVs interact with recipient cells to influence cell physiology and deliver a macromolecular payload are at the early stages of exploration, but are believed to involve endocytosis. For endocytic characterisation a significant challenge is having the ability to label exosomes directly or indirectly with fluorescent probes to qualitatively and quantitatively monitor exosome-cell interaction and uptake without compromising functionality.

In this thesis, techniques to inhibit different pathways of endocytosis were investigated and further developed order to establish high content *in vitro* platforms to study the uptake mechanisms of potential drug delivery vectors focusing here exosomes as a model system. These techniques involved siRNA depletion of prospective endocytic proteins and chemical inhibitors of endocytosis. A simple and rapid method for fluorescent labelling purified Du145 exosomes covalently was for the first time utilised to allow comprehensive analysis of the

cellular uptake of differentiation competent prostate cancer derived EVs in live cells using confocal microscopy.

For endocytosis analyses, depletion of key endocytic proteins and the use of chemical inhibitors (Dynasore, EIPA, Rottlerin and IPA-3) indicated that a fluid-phase endocytosis and/or macropinocytosis-like mechanism dependent on dynamin were involved in exosome internalisation. Over a period of six hours exosomes were observed to increasingly co-localise with lysosomes, indicating a possible intracellular terminus with significance with respects to utilisation of exosomes as drug delivery vectors. Overall this labelling method, when used in conjunction with established models of endocytic inhibition, provides new opportunities for analysing the cellular dynamics of exosomes and other extracellular vesicles as biological entities affecting cell and whole body physiology as well as investigating their potential as drug delivery vectors. The work also further enhances our ability to study multiple endocytic pathways as potential routes for entry of other drug delivery vectors to gain important information towards the design of more efficient formulations targeting a number of diseases.

Acknowledgements

Firstly I would like to thank my principle supervisor Prof. Arwyn Jones for all of his support, guidance and understanding throughout my time in the lab and throughout the project. Special thanks for the time and patience always found when in need.

Many thanks also to my co-supervisor Dr. Pete Watson and other members of the Watson group whose expertise and rigor helped to constantly develop the project from start to finish.

The warmest thank you to all of those members of the Jones lab, past and present, whose kindness, support and wit will not soon be forgotten, particularly: Dr. Helen Wiggins, Dr. Lin He, Dr. Noura Eissa and Dr. Paul Moody. Special mentions particularly for Dr. Edd Sayers and Dr. Jennifer Wymant. I honestly could not have completed this project, or my time in Cardiff, without your patience, understanding, friendship and food provision. You really are the most wonderful humans.

I am immeasurably grateful to my other friends in Cardiff who were there for every tear and every giggle. Particular note goes to Sophie Emery. There is always room for more pizza.

I would wholeheartedly like to thank Prof. Aled Clayton for the huge collaborative opportunity that transformed the project and of course for his unwavering support and kindness during our time working together.

Specials thanks also to Dr. Jason Webber and to the other members of the Clayton group for their support, both technically and socially, during my time at the Velindre.

Thank you also goes to all of those involved within the COMPACT Consortium, the opportunities provided by this collaboration have been extremely valuable and always a joy to be part of.

A final and most heartfelt thank you to my awesome family. Alfie Roberts-Dalton, Ed Roberts-Dalton, Robin Roberts-Dalton and Gabrielle Roberts-Dalton: my eternal lefty partners in crime. Cheers.

Table of Contents

List of Figures and Tables

List of Publications and Presentations

Roberts-Dalton, H.D., Brown, E., Webber, J., Watson, P., Clayton, A., Jones, A.T. 2015. **Characterisation of the Endocytic Uptake of Prostate-Derived Exosomes.** *UK Extracellular Vesicle Forum*, Cardiff, 2015. Poster Presentation.

Roberts-Dalton, H.D., Webber, J., Watson, P., Clayton, A., Jones, A.T. 2016. **Thiol-Based Labelling of Prostate-Derived Exosomes for Analysis of Cellular Uptake and Intracellular Traffic.** *International Society of Extracellular Vesicles (ISEV) Meeting*, Rotterdam, 2016. Poster Presentation.

Roberts-Dalton, H.D., Brown, E., Webber, J., Watson, P., Clayton, A., Jones, A.T. 2016. **Thiol-Based Labelling of Prostate-Derived Exosomes for Analysis of Cellular Uptake and Intracellular Traffic.** *UK and Ireland Controlled Release Society (UKICRS) Meeting*, Cardiff, 2016. Verbal Presentation.

Roberts-Dalton, H.D., Cocks, A., Falcon-Perez, J.M., Sayers, E.J., Webber, J., Watson, P., Clayton, A., Jones, A.T. 2017. **Fluorescence Labelling of Extracellular vesicles Using a Novel Thiol-Based Strategy for Quantitative Analysis of Cellular Delivery and Intracellular Traffic.** *Nanoscale*. Accepted for publication 2017.

Abbreviations

Arf6	ADP-ribosylation factor 6
BACE-1	Beta-secretase 1
BBB	Blood brain barrier
BCA	Bicinchoninic
BODIPY-LacCer	BODIPY-Lactosylceramide
BSA	Bovine Serum Albumin
BSA647	Alexa647-BSA
Cav1/2/3	Caveolin-1/-2/-3
CCP	Clathrin coated pit
CCV	Clathrin coated vesicle
Cdc42	Cell division control protein 42 homolog
CFDA	5(6) carboxyfluorescein succinimidyl diacetate
CFSE	Carboxyfluorescein succinimidyl ester
CHC	Clathrin heavy chain
CIE	Clathrin independent endocytosis
CLC	Clathrin light chain
CLIC	Clathrin independent carriers
CMDR	Cell mask deep red
CMO	Cell mask orange

CME	Clathrin-mediated endocytosis
CPP	Cell penetrating peptide
CtBP1/BARS	Brefeldin A ADP-ribosylated substrate
CTxB	Cholera toxin B
DDS	Drug delivery system
dH_2O	Deionised water
DIC	Differential Interference contrast
DMEM	Dulbecco's Modified Eagle Medium
DMSO	Dimethyl sulfoxide
DTT	Dithiothreitol
Dx488/647	10kDa Alexa488/647-Dextran
EEA1	Early endosomal antigen 1
EGF	Epidermal growth factor
eGFP	Enhanced Green Fluorescent Protein
EGFR	Epidermal growth factor receptor
EIPA	5-(N-ethyl-N-isopropyl) amiloride
EPC	Endothelial progenitor cell
ESCRT	Endosomal sorting complexes required for transport
EV	Extracellular vesicle
Exo488/633	Alexa488/633-Exosomes

FBS	Foetal bovine serum
FCHo	F-BAR domain containing proteins
FEME	Fast endophilin-mediated endocytosis
FITC	Fluoresceine
Flot1/2	Flotillin-1/-2
FRα	Folate Receptor alpha
GEEC	GPI-linked proteins enriched in early endosomal compartments
GFP	Green Fluorescent protein
GM	Geometric mean
GPI	Glycosylphosphatidylinositol
GRAF1	GTPase regulator associated with focal adhesion kinase 1
HGF	Hepatocyte growth factor
HIV	Human immunodeficiency virus
hnRNPA2B1	Heterogeneous nuclear ribonucleoprotein A2B1
HRP	Horseradish Peroxidase
Hsc70	70kDa heat-shock cognate protein
Hsp90	Heat shock protein 90
HSPG	Heparin sulphate proteoglycan
IL-2R	Interleukin-2 Receptor
LacCer	Lactosylceramide

LDL	Low density lipoprotein
LDLR	Low density lipoprotein receptor
Lyso647	Alexa647 labelled lysosome
MβCD	Methyl-β cyclodextrin
MEM	Minimum Essential Media
MFI	Mean fluorescence intensity
MHCII	Major histocompatibility complex II
M.Tb	Mycobacterium tuberculosis
MVB	Multivesicular body
NEAA	Non-Essential Amino Acids
NK	Natural killer
NTA	Nanoparticle tracking analysis
PAK1	P21-activated kinase 1
PBS	Phosphate buffered Saline
PBST	PBS supplemented with 0.025% Tween
PDGF	Platelet-derived growth factor
PI3K	Phosphoinositide 3-kinase
PIP_2	Phosphatidylinositol-4,5-bisphosphate
PIP_3	Phosphatidylinositol (3,4,5)-trisphosphate
PLC	Phospholipase C

PKC	Protein Kinase C
PVDF	Polyvinylidene difluoride
Rac1	Ras-related C3 botulinum toxin substrate 1
RhoA/G	Ras homolog A/G
RPMI 1640	Roswell Park Memorial Institute Media 1640
ROI	Region of interest
R/T	Room temperature
RVG	Rabies Virus Glycoprotein
SFIM	Serum-free imaging media
siRNA	Small interfering RNA
SV40	Simian Virus 40
Tf	Transferrin
Tf488/647	Alexa488/647-Transferrin
TfR	Transferrin Receptor
TGFβ	Transforming growth factor β
TGFβR	TGFβ receptor
TGN	Trans-golgi network
TSG101	Tumor susceptibility gene 101
Utx	Untransfected control
WT	Wildtype

1 Introduction

The intracellular environment is regarded by many to be a vault full of therapeutic targets for disease intervention. Hundreds of proteins residing within the cell could be potential targets for entities defined as macromolecular therapeutics; these include proteins, peptides (Cleal et al., 2013; Ye et al., 2016) and nucleotides (Khvorova and Watts, 2017). Unfortunately, there are a number of major obstacles that need to be overcome if these therapeutics are to reach their intracellular targets and be of clinical value (Agrahari et al., 2016). One of these is effective crossing of biological barriers that stand between a therapeutic and its target including the plasma membrane and the endolysosomal network (Cerrato et al., 2017; Cleal et al., 2013; Dowdy, 2017; Saffari et al., 2016; Yang et al., 2017).

1.1 Macromolecular Therapeutics

The functional outcome of therapeutic macromolecules that act within the cell relies upon their protection from extracellular degradation once administered inside the body. Following this, they must cross the plasma membrane and then reach their intracellular destination without degradation at the lysosome that contained hydrolases that will degrade biotherapeutics described above. The fate of internalised cargo depends upon cell type and physiological context within the endocytosis remit: endosomal escape to the cytosol, lysosomal delivery, recycling back to the plasma membrane and cellular escape via exosomes are common journeys taken by endocytosed materials. Therapeutic efficiency of endocytosed macromolecules require escape from the endosomal sorting machinery, or remain in the lysosome yet avoid

degradation (Cleal et al., 2013). Functional outcome of therapeutic molecules does indeed depend on several other processes. For instance, the use of monoclonal antibodies often results in the instigation of a natural immunoregulatory response; the ability to circumvent the activation of an immune response is therefore essential (Tyagi and Santos, 2018). Metabolic stability is also necessary for a functional outcome, whereby clearance of the therapeutic from the bloodstream is reduced and an extended half-life are necessary in order to improve its bioavailability (Masimirembwa et al., 2003).

Drug delivery systems need to surpass a number of obstacles in order to transfer a macromolecule efficiently to its therapeutic target, where it can then perform processes such as inhibition or silencing of aberrant proteins or genes at the functional and expression level. Before identifying potential vectors, the biochemical nature of one of these obstacles, the plasma membrane, must be considered. Many therapeutic macromolecules, such as nucleic acids, are hydrophilic, and this polarity together with their large size negates the possibility that they can diffuse through the membrane directly into the cytosol. A number of studies have now shown that by conjugating or encapsulating a biotherapeutic with a variety of different vector types, they are able to cross this barrier via endocytosis or direct translocation (Kristensen et al., 2016; Veldhoen et al., 2008; Zylberberg and Matosevic, 2016). Vectors can be developed from a variety of sources. Those of viral origin, for instance, have previously provided efficient cell specific gene delivery; they are acknowledged however as highly immunogenic, meaning efforts to avoid activation of the immune response are required (Manjila et al., 2013). Viral vectors with low toxicity *in vitro* exist, such as the

adeno-associated virus compounds, which demonstrate promise as carriers for DNA-delivery systems (Skubis-Zegadlo et al., 2013). However, *in vivo* studies and clinical trials have demonstrated the high immunogenicity of these compounds, exemplifying a major obstacle in the application of viral based delivery systems (Mingozzi and High, 2011; Mingozzi and High, 2013; Zaiss and Muruve, 2005). Unwanted integration of viral DNA into the host genome has also been described (Thomas et al., 2003).

1.2 The Plasma Membrane: A Biological Barrier to Macromolecular Therapeutics

The plasma membrane is a dynamic barrier that lies between the internal and external milieu of a eukaryotic cell and is composed of phospholipids, sphingolipids, cholesterol, carbohydrates and membrane proteins and glycoproteins such as heparin sulphate proteoglycans (HSPGs) (Doherty and McMahon, 2009). The equilibrium of small molecules, such as ions and hormones, and larger particles, such as cell debris and pathogens, across the interior and exterior of the cell is tightly regulated by this structure. For these reasons, the membrane is paramount for homeostatic control of not just the individual cell, but of the whole cellular population and the tissue to which it belongs.

A phospholipid bilayer provides the foundation of the plasma membrane, creating a barrier between the aqueous regions either side. The hydrophobic head of each phospholipid lies in the inner layer, meaning that water-soluble particles, a group that includes many biological molecules, are incapable of passing the membrane. The flexibility of these hydrophobic fatty acid tails also provides a structural fluidity to the

membrane, exemplified by the plasma membrane fluid mosaic model (Cooper, 2000). Cholesterol is also a key part in the dynamics of fluidity via its interaction with the fatty acid tails, but also through its association with sphingolipids in distinct regions of the membrane commonly referred to as 'lipid-rafts' (Frank et al., 2006). The fluid mosaic model also describes the dynamic lateral movement of membrane proteins. Functionally, the membrane relies upon these proteins, which include transmembrane receptors, cytoskeletal components, ion channels and adhesion proteins, amongst numerous others. With regards to endocytosis however several proteins are key. The essential interaction between the different classes of membrane constituents is exemplified by glycosylphosphatidylinositol (GPI)-linked proteins. The C-terminus of these transmembrane proteins associates with a glycolipid anchor termed a GPI at the endoplasmic reticulum, and following transport to the plasma membrane are exposed either within or outside of the cell (Alberts et al., 2008). GPI-linked proteins are generally organised within the membrane as rafts, but also have extensive physiological roles outside of endocytosis such as acting as adhesion molecules, within immune regulation and as receptors (Kinoshita et al., 2008). The GPI-linked proteins CD59 and CD55, for instance are involved in the regulation of the complement cascade (Ruiz-Argüelles and Llorente, 2007) and T-cadherin is a significant regulator of vascularisation (Parker-Duffen et al., 2013).

An endocytic event, whereby an external entity is internalised by encapsulation in a plasma-membrane derived vesicle, relies upon the interaction of several membrane components. Different components and cargo molecules result in diverse interactions

at this interface that ultimately necessitate distinct pathways of endocytosis to operate with a variety of physiological functions (Doherty and McMahon, 2009).

1.3 Mechanisms of Endocytosis

One natural mechanism allowing extracellular molecules can gain access to the intracellular region of the cell is termed endocytosis. This phenomenon involves the envelopment of materials from the exterior region of the cell by the plasma membrane, eventually forming an internal structure consisting of membrane-bound cargo and a portion of the detached membrane, otherwise termed a vesicle (Doherty and McMahon, 2009; Robinson, 2015). The constituents of these vesicles vary depending on the endocytic pathway utilised and one termed macropinocytosis involves an initial outward projection of the membrane before engulfment is initiated. Endocytosis is extremely important for both the individual cell and for communication with adjacent cells and the surrounding extracellular environment. A number of endocytic mechanisms/pathways, resulting from the interactions between different membrane and cytosolic components, are performed by eukaryotic cells. These are generally divided into phagocytosis and pinocytosis, the former being implicated in the uptake of larger molecules, pathogens and cell debris as performed by specialised cell types, such as dendritic cells and macrophages (Aderem and Underhill, 1999). This mechanism is responsible for pathogen, microbial, and apoptotic cell clearance (Maderna and Godson, 2003; Underhill and Ozinsky, 2002), although some phagocytic components are also involved in autophagy (Mehta et al., 2014; Romao and Munz, 2014). Pinocytic mechanisms, of which there may be several are, aside from clathrin

mediated endocytosis (CME), more difficult to characterise due to the lack of information regarding their requirements for specific proteins and unique endocytic probes to study their function. Different physiological and environmental contexts also make it difficult to characterise the different pathways, in addition to differing endocytic profiles between cell-types. A high level of the molecular mechanisms governing CME has allowed greater exploration of its role in physiology. The less well defined mechanisms that are deemed to exist independent of clathrin, have been show to require regulation by the proteins: caveolin-1, flotillin-1, Arf-6, GRAF-1 (Bastiani and Parton, 2010; Hansen and Nichols, 2009), and more recently endophilin-A2 (Boucrot et al., 2015; Renard et al., 2015). All of these pathways and examples of the methods used to study them in this thesis are presented in Figure 1.1, and will be discussed later in this Chapter.

The capacity of these pathways to act as portals for various drug delivery vectors requires further investigation, as many of the context dependent mechanisms involved still require characterisation. Additionally the fate of the drug delivery vector and its therapeutic cargo within the cell may also be dependent on the uptake mechanism. For these reasons, the established mechanisms and physiological functions of each pathway, including their potential as portals for drug delivery systems, will be discussed in this introduction. Methods for exploring the molecular mechanisms involved in each pathway will also be discussed, particularly through the use of high content technologies. The hunt for specific inhibitory methods and cargoes remains a principle challenge in the characterisation of the different endocytic pathways.

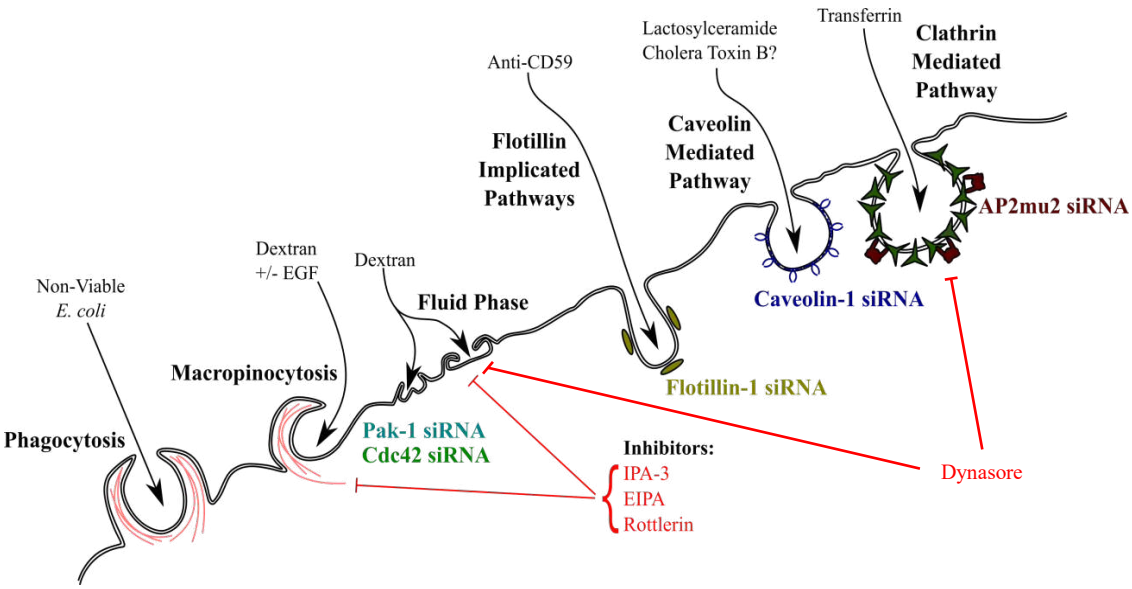

Fig 1.1 ***Key Endocytic Mechanisms and methods of endocytic inhibition utilised in this thesis*** Key examples of entities that have been shown to gain intracellular access via these routes are presented. Courtesy of Dr Edd Sayers.

1.3.1 Clathrin Mediated Endocytosis (CME)

Clathrin mediated endocytosis is by far the most well defined and widely studied endocytic system, and can be performed by all known eukaryotic cells to date, with the possible exception of red blood cells (McMahon and Boucrot, 2011). A variety of extracellular materials can be internalised at membrane localised clathrin coated pits (CCPs), where pinching into clathrin coated vesicles (CCVs) occurs. The molecular events involved are part of a complex regulatory network and was in part initially determined through the use of *Saccharomyces cerevisiae* as a model organism (Boettner et al., 2012; Myers and Payne, 2013). The physiological flexibility of CME is demonstrated by its ability to internalise a vast number of molecules including the iron

transporter, transferrin. The uptake of this protein via binding to the transferrin receptor has been extensively studied and involves a variety of different proteins (Collinet et al., 2010) that will be further discussed in this chapter. The actions of clathrin and the other proteins involved in CME are vital for physiological regulation. The integrity of the plasma membrane also relies upon this process, and CME is operational in signal transduction, nutrient selection and uptake, in addition to the maintenance of cellular and tissue homeostasis (Godlee and Kaksonen, 2013; McMahon and Boucrot, 2011).

The structure of the clathrin molecule, composed of the clathrin heavy chain (CHC) isoforms and clathrin light chain (CLC) has been studied extensively, and is responsible for CCP formation and receptor endocytosis. Endosomal sorting and recycling are also dependant on clathrin, demonstrating a cell-wide role for clathrin in processes regulating cellular homeostasis (Brodsky, 2012). Clathrin also operates at the trans-Golgi network (TGN), and together with adaptor complexes (AP1/3) regulate secretion into the endocytic pathway and to lysosomes (cathepsins) (Shiba et al., 2013) or to the plasma membrane for secreted proteins (Ponnambalam and Baldwin, 2003). Effective endocytosis however begins with the recruitment of specific proteins such those forming the AP2 adaptor complex to the plasma membrane, this initiates formation of the clathrin triskelia and formation of the CCP (Takei and Haucke, 2001). Early CCP budding has been shown to rely on the activities of F-BAR domain containing proteins (FCHo proteins), resulting in recruitment of the scaffold proteins, intersectin and eps15, to the site (Henne et al., 2010). Investigations in zebrafish have suggested a more cargo-specific relationship between FCHo proteins and CCP formation,

exemplifying the complexity of the relationship between specific adaptor proteins and different cargoes in CME (Umasankar et al., 2012). Otherwise characterised as clathrin pit nucleation, this phenomenon allows CCP formation to occur, the processes of which illustrated in Figure 1.2.

The core AP2 adaptor provides the essential linkage between clathrin and plasma membrane regions rich in phosphatidylinositol-4,5-bisphosphates (PIP_2). AP2 is characterised as a 200kDa core, composed of four subunits of varying size and function: the α and β2 trunks, the μ2 subunit, and the σ2 unit (Collins et al., 2002).

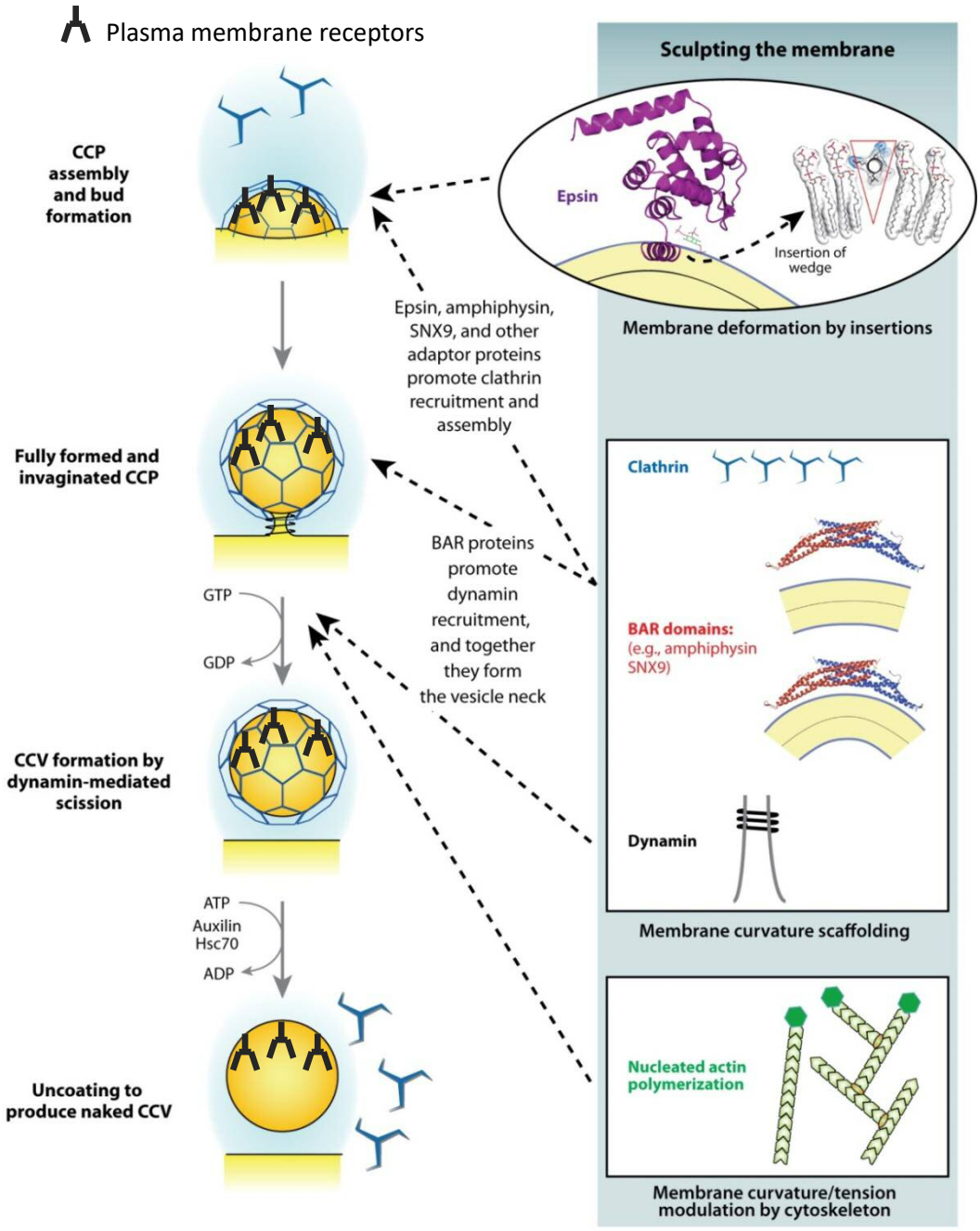

Fig 1.2 ***Mechanism of Clathrin-Mediated Endocytosis*** CPP formation begins with recruitment of accessory proteins, before invagination and dynamin recruitment. Following membrane curvature, dynamin mediated scission removes the budding structure from the plasma membrane, resulting in an intracellular clathrin coated vesicle. This coat is removed and the resulting vesicle merges with the early endosome. Adapted from (Doherty and McMahon, 2009).

Via cargo, clathrin, PIP_2 and further accessory protein binding, AP2 regulates cargo anchoring to the CCP and, following scission, clathrin coated vesicle (CCV) formation (Jackson et al., 2010). Scission is carried out by the 100kDa GTPase dynamin. Helical dynamin arrays result in the formation of a dynamin collar around the neck of the CCP, facilitating GTP hydrolysis and removal of the pit complex and its cargo from the plasma membrane.

Characterisation of these events was performed using dynamin mutants deficient in vital biochemical abilities such as GTPase binding (S45N mutant) (Chappie and Dyda, 2013; Liu et al., 2013). The implication of dynamin II in CCP scission is well established, though its involvement at early stages of clathrin lattice recruitment and importance in CCP stabilisation has also been demonstrated, suggesting both mechanical and regulatory roles (Mettlen et al., 2009). Subsequent detachment of the scission machinery, adaptor proteins and clathrin from the internalised vesicle primarily involves the chaperone Hsc70 (70kDa heat-shock cognate protein) and auxilin, where an ATP-dependent interaction lifts the clathrin lattice to allow recruitment of further chaperones for further vesicle trafficking (Xing et al., 2010; Young et al., 2013). These proteins demonstrate a role additional to that of their involvement in clathrin disassembly, further exemplifying the duplicate roles of the numerous proteins involved in CME regulation. Clathrin pit invagination is also reliant on the hsc70-auxilin relationship, in addition to clathrin recycling back to the plasma membrane (Eisenberg and Greene, 2007).

Bitsikas et al. explored, in HeLa cells, the importance of different pathways in endocytic flux, concluding that CME is solely responsible for endocytic entry in this cell line (Bitsikas et al., 2014). This contentious observation needs further proof but raised interesting questions regarding thousands of papers focusing on clathrin independent endocytosis, in HeLa cells and others, within the context of cell biology and drug delivery.

1.3.2 Caveolin Mediated Endocytosis

Internalisation of structures called caveolae at membrane regions of high sphingolipid and cholesterol density, termed lipid rafts, occurs during Caveolin-1 (Cav1) mediated endocytosis (Cheng and Nichols, 2016; Lajoie and Nabi, 2007; Nichols, 2003). Definition of the mechanistic processes involved in this pathway are less clear than those defined in CME, yet knowledge of the pathway has escalated in recent years mainly due to a greater range of molecular research technologies. The involvement of caveolae is not restricted to endocytosis, and comparable to CME, is implicated in exocytosis, transcytosis and signal transduction.

Caveolae formation relies on the small 20kDa caveolin proteins, caveolin-1, -2 and -3, which have variable expression patterns based on cell and tissue type (Parton and Simons, 2007; Williams and Lisanti, 2004). Caveolin-1 and -2 are expressed in most non-skeletal muscle cell types, whereas caveolin-3 resides solely in striated and cardiac muscle tissue (Bastiani and Parton, 2010). Cav1 is most commonly investigated for its involvement in caveolae formation and internalisation at lipid rafts, where the protein

interacts with up to two cholesterol molecules (Murata et al., 1995) and anchors itself to the membrane via a hydrophobic loop (Kiss and Botos, 2009). Cav1 derived vesicles are primarily composed of caveolin, cavins and cholesterol. The interaction between these proteins at lipid rafts is performed by up to 200 Cav1 molecules per caveolae, creating structures of approximately 60-80 nm in diameter (Parton and del Pozo, 2013). Caveolae are lacking in cells that do not express Cav1 protein, such as leukocytes (Doherty and McMahon, 2009). Scission of the caveolae derived vesicle is also reliant upon the GTPase activity of dynamin (Henley et al., 1998; Oh et al., 2012) again demonstrating one of the numerous commonalities between mechanisms in the endocytic regulatory network.

Much of the information available regarding the internalisation and trafficking capacity of caveolae has been provided through exploration of possible caveolin-dependant endocytic probes, such as cholera toxin B (CTxB), GPI-linked proteins, Simian-Virus 40 (SV40) and albumin (Nichols, 2002). More recently, evidence of caveolae dependent internalisation of oxidised low density lipoprotein in endothelial cells has been described (Sun et al., 2010). The internalisation mechanism of the glycosphingolipid lactosylceramide (LacCer) is also demonstrated to be caveolin related, but this uptake displays a certain level of context dependence, whereby uptake mechanism used is dependent upon Cav1 expression levels (Singh et al., 2003). Here, caveolin dependent uptake of CTxB was also shown to be heavily context dependent. This work went on to further describe how caveolin dependent LacCer uptake results in its merging with the CME early endosome (Sharma et al., 2003).

SV40 internalisation has suggested one possible trafficking route of caveolae derived vesicles. This virus most commonly localises at multivesicular bodies of neutral pH, which are locations distinct from the endosomal transport of CME markers such as transferrin. Termed caveosomes, these distinct vesicles do not travel via the lysosomal system, providing the virus with an escape from intracellular degradation (Pelkmans et al., 2001). However, subsequent studies have indicated that internalisation of this virus is cholesterol and lipid-raft dependant, yet independent of clathrin, caveolin and the scission events controlled by dynamin II. The pH neutral vesicles positive for the virus were found to be devoid of caveolin (Damm et al., 2005), which could either suggest an entirely different uptake route or removal of the protein from these vesicles during downstream trafficking. Cav1 positive caveosomes have been demonstrated to traffic to the late endosomal compartments, suggesting that cargo are trafficked to the lysosome (Hayer et al., 2010; Parton and Howes, 2010). The lack of pathway specificity of distinct cargo is exemplified here.

Notably, the endocytic functions of Cav1 are not isolated to caveolae formation and internalisation. For instance, observation of greater apoptotic cell accumulation in Cav1 knockout mice when compared with wildtype indicates a lack of clearance by phagocytic macrophages, suggesting the involvement of this protein in phagocytosis (Li et al., 2005). Cav1 is also has a regulatory role in other cellular processes such as cholesterol homeostasis. Via interaction with the ATP binding cassette transporter, G1, Cav1 has been demonstrated to be a prime regulatory element in cholesterol efflux, particularly in macrophages (Frank et al., 2006; Gu et al., 2014). Findings such as these have identified Cav1 as a possible target for preventative treatment against diseases

aberrant in cholesterol homeostasis, atherosclerosis and cardiovascular disease (Frank et al., 2007) and also demonstrate the existence of diverse regulatory and mechanical roles of this protein.

1.3.3 Clathrin-Independent Carriers with GPI-linked proteins enriched in early endosomal compartments (CLIC-GEEC) Endocytosis

Other clathrin-independent pathways with distinct regulatory mechanisms have been proposed. Interest in these pathways initially arose due to the ability of cells depleted of clathrin and Cav1 dependant events to internalise cargoes originally thought to gain cellular access only by these mechanisms. CLIC-GEEC endocytosis is one such mechanism, determined by the involvement of clathrin independent carriers (CLIC) with GPI-linked proteins enriched in early endosomal compartments (GEEC). In regions of potential endocytosis, GPI-linked proteins within the plasma membrane are more enriched than in the comparable regions of CCPs and caveolae, and result in tubular, rather than pit-shaped invagination. Suggested cargoes include a number of GPI-linked proteins, such as the alpha subunit of the folate receptor (FRα). Previous studies indicate that internalisation of GPI-linked proteins requires cross-linked Cav1 (Fujimoto, 1996); however, during caveolae endocytosis cross-linking is not always evident, suggesting that a large amount of FRα gains intracellular access by a different route. Investigations utilising the detergent-insoluble nature of caveolae indicate that a vast number of FRα subunits can circumvent caveolae in order to internalise (Rijnboutt et al., 1996).

During and following internalisation, the fate of cargo via CLIC-GEEC may be dependent on the actin cytoskeleton (Doherty and McMahon, 2009). The actin-associated small RhoGTPase Cdc42 was shown to be directed to GEECs on the plasma membrane via N-terminal BAR domains, where it co-localised with the protein GRAF1 (GTPase regulator associated with focal adhesion kinase-1) (Lundmark et al., 2008). GRAF1 has therefore been suggested as a chief regulatory factor of the CLIC/GEEC pathway, meaning that this pathway is also referred to as the GRAF1-dependent pathway. Following GRAF1 depletion, CLIC domain formation is prevented and cell migration was also affected, demonstrating the association between cytoskeletal dynamics, the CLIC/GEECs and GRAF1 (Doherty et al., 2011; Doherty and Lundmark, 2009).

1.3.4 Flotillin-Dependant Endocytosis

Uptake mechanisms which demonstrate dependence upon Flotillin-1 and flotillin-2 have also been described. Endocytosis of anti-CD59, an antibody involved in complement activation, has been linked to this pathway (Doherty and McMahon, 2009; Sugita and Masuho, 1995). In hepatocytes the process of GPI-linked protein uptake demonstrates dependency on Flot2, a finding identified by depleting this protein via transfection with an anti Flot2 siRNA (Ait-Slimane et al., 2009). Flot1 dependency during prion protein endocytosis has also been demonstrated in neuroblastoma cells (Ren et al., 2013).

1.3.5 Endophilin-A2 and Arf6 dependent endocytosis

The discovery of an uncharacterised endocytic pathway has recently been described. The BAR-domain containing protein, EndophilinA2, was found in endocytic structures positive for the supposed activators of this pathway, Shiga-toxin and Cholera-toxin. Furthermore, these membrane tubulations were not associated with CME associated markers, yet required dynamin for scission (Renard et al., 2015). The observations made here are further supported by a lack of established endocytic cargoes, such as transferrin, within these structures yet clathrin-independent cargoes, such as the IL-2R, were internalised via this route. This pathway has subsequently been given the name: fast-endophilin-mediated endocytosis (FEME) (Boucrot et al., 2015).

ADP-ribosylation factor 6 (Arf6) is a GTPase binding protein that has demonstrated involvement in its own regulatory pathway (Radhakrishna and Donaldson, 1997), shown to be responsible for the uptake of growth factor receptors (Pellon-Cardenas et al., 2013) and in the uptake of fibrinogen (Rondina and Weyrich, 2016). It has also been linked with the regulation of other pathways including macropinocytosis (Tang et al., 2015) and via its activation by dynamin II in CME (Okada et al., 2015).

1.3.6 Fluid-Phase Endocytosis vs Macropinocytosis

Fluid and associated small molecules will conceivably enter the cytoplasm of cells via all described endocytic pathways and it still largely remains to be determined whether there exists a constitutive pinocytosis pathway that only function to internalise fluid. Larger molecules of up to 1 µm in size and much higher volumes of fluid can enter via a

phenomenon that is absolutely reliant on the dynamics of actin. This is macropinocytosis and although described as separate processes, definitive distinction of the molecular mechanisms dividing fluid-phase endocytosis and macropinocytosis remain elusive. A reliance on actin for the latter may be one deciding factor together with the fact that macropinocytosis is initiated by outward projection of the plasma membrane in the form of lamellapodia, circular ruffles or blebs. For macropinocytosis to manifest itself prominently cells often need to be serum starved and activated by growth factors such as EGF or PDGF (Kerr and Teasdale, 2009). The extent to which constitutive macropinocytosis occurs in any cell type remains to be determined.

As noted, extensive folding and protrusion of the plasma membrane characterise macropinocytosis, resulting in cargo and fluid engulfment following fusion of distinct membrane protrusions (Figure 1.3). These widespread membrane modifications are dependent upon cytoskeletal activity, and particularly that of actin. Formation of the intracellular macropinosome has two stages that are dependent upon meticulous organisation of the actin cytoskeleton. The process begins with the formation of membrane ruffles, which then fuse at their distal margins to create circular ruffles. A second closure of the ruffles forms the macropinocytic cup, which is pinched from the membrane to form a macropinosome (Buckley and King, 2017; Swanson, 2008). Any extracellular fluids or proteins caught within these ruffles are internalised, creating an endocytic pathway with relatively little cargo specificity. Nevertheless, any membrane receptor bound ligands present at the region of membrane ruffling, and the receptors themselves will be internalised. This process shares many characteristics with the mechanism of phagosome formation (Lim and Gleeson, 2011).

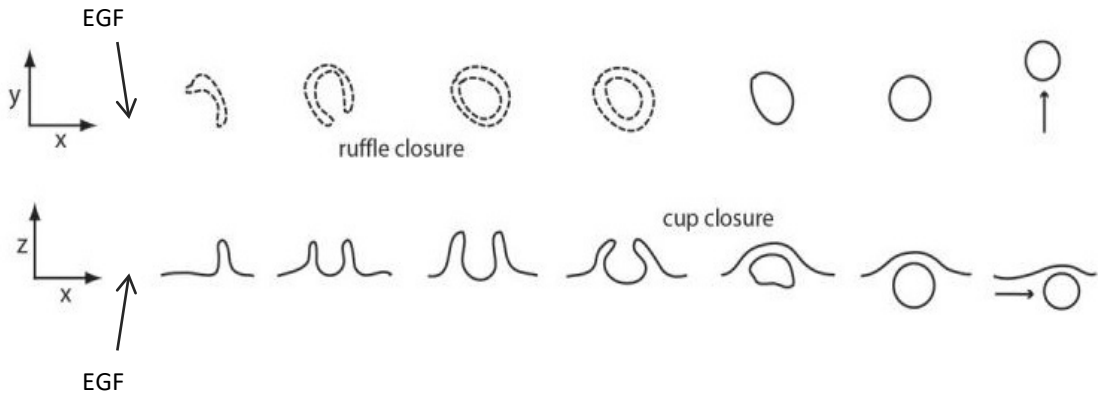

Fig 1.3 ***Macropinocytic Cup Formation and Closure*** Growth factor stimulation induces circular ruffle formation and closure followed by cup closure viewed from above and laterally. Adapted from (Swanson, 2008).

Macropinocytosis results in much larger uncoated vesicles than other pinocytic pathways which result from growth factor stimulation. Activation of growth factor receptors results in a cell-wide increase in cytoskeletal activity, rather than the endocytic organisation at specific membrane regions seen in other pinocytic mechanisms (Kerr and Teasdale, 2009).

Following scission of the macropinocytic cup from the membrane, suggested to occur via a brefeldin A ADP-ribosylated substrate (CtBP1/BARS) dependant mechanism (Liberali et al., 2008; Valente et al., 2013), the recruitment of pinocytic regulators was shown to occur (Feliciano et al., 2011). These include the early endocytic marker Rab5 and CtBP1/BARS, which is responsible for several cytoplasmic fission events including trans-Golgi network (TGN) vesicle scission and macropinosome excision from the plasma membrane (Valente et al., 2013). Although comparable with phagocytosis,

macropinocytosis can be carried out by cells that are not professional phagocytes. Cell lines such as A431s that express high levels of epidermal growth factor receptor (EGFR) demonstrate an increased level of cell-wide plasma membrane ruffling and macropinosome formation when subjected to epidermal growth factor (EGF) stimulation (Araki et al., 2007; Araki et al., 2006). As previously stated, actin-dependant membrane ruffling is recognised as a characteristic feature of macropinocytosis. Macropinocytosis in response to growth factor stimulation is often measured as an increase in the uptake of the fluid phase endocytic probe dextran (Al Soraj et al., 2012; Haigler et al., 1979).

A number of major actin regulatory proteins have demonstrated involvement in macropinocytosis. Primary investigation indicated the importance of phosphoinositide 3-kinase (PI3K) and phospholipase C (PLC) interaction, which are proteins involved in actin remodelling, actin polymerisation, and focal contact turnover during chemokine directed migration (Kolsch et al., 2008; Kortholt et al., 2007). These studies were performed in *Dictyostelium*, a model organism in the study of phagocytosis and macropinocytosis, thereby indicating a role for PI3K, PLC and related factors in actin dynamics during these processes. Actin reorganisation involved in motility of classically phagocytic leukocytes is also reliant on these proteins, particularly with regards to RhoGTPases such as Rac1 (Alon and Shulman, 2011). It must be noted however that chemotactic events are distinct from macropinocytic events. The non-phagocytic cell line, A431, with high EGFR expression, is recognised for high levels of macropinosome formation and membrane ruffling following EGF stimulation, indicating the importance of PI3K and its binding partners in this phenomenon. Ruffling in regions of

macropinocytic cup formation is accompanied by phosphatidylinositol 4,5-bisphosphate (PIP_2) accumulation and a simultaneous surge in phosphatidylinositol (3,4,5)-trisphosphate (PIP_3) before closure and scission (Araki et al., 2007). Compositional organisation of these processes suggests PI3K-dependance, establishing a possible role in the macropinocytic events of A431 cells. Fusion of macropinosomes with early endocytic compartments, as indicated by co-localisation with early endosomal antigen 1 (EEA1) in A431 cells, is reliant on PI3K (Araki et al., 2006), indicating the further involvement of this kinase in downstream trafficking events. These observations provide both evidence for the importance of PI3K in the events following internalisation, and indicate association with the early endocytic pathway where trafficking of the macropinosome joins vesicles from other pinocytic pathways.

P21-activated kinase 1 (PAK1), a downstream serine-threonine kinase targeted by the small RhoGTPase actin regulators, has been defined as a chief regulator of macropinocytic events (Dharmawardhane et al., 2000; Liberali et al., 2008; Redelman-Sidi et al., 2013). Regions of ruffling are often accompanied by membrane localised PAK1, providing a binding platform for other actin regulators such as Cdc42, Rac1 and RhoA. The role of this kinase was initially delineated through the use of PAK1 mutants in a study that demonstrated its role in both macropinocytosis, and during cellular motility through its involvement in actin dynamics (Dharmawardhane et al., 2000). PAK1 has been shown to coordinate a variety of cellular processes through its upstream effectors Cdc42 and Rac1, particularly at the cell periphery (Delorme-Walker et al., 2011). These aspects of cytoskeletal regulation further support the importance of PAK1 in the regulation of the actin dynamics associated with macropinocytosis.

Increased levels of the PAK1 effector, Rac1, synchronise with regions of PIP_3 accumulation at late ruffling events, activating closure of the macropinocytic cup following deactivation in macrophages (Fujii et al., 2013; Yoshida et al., 2009). The events following ruffling and downstream macropinosome formation are further indicated as Rac-dependent in dendritic cells (West et al., 2000). It must be noted here that constitutive events are most likely distinct from growth factor stimulated events.

Although linked to membrane ruffling through its association with Rac1 in leukocytes (Cox et al., 1997), and constitutive endocytosis for antigen presentation in dendritic cells (Garrett et al., 2000) the role of Cdc42 in growth factor stimulated macropinocytosis requires further delineation. In the absence of Rac1, Cdc42 and RhoG (another small GTPase) fibroblasts were unable to initiate actin lamellipodia (extensions that incorporate ruffling) at the plasma membrane. The action of these small GTPases however can activate filopodia independent of Rac1, perhaps through interaction with other signalling molecules (Steffen et al., 2013). It must be considered that much of this work is cell-type dependant, suggesting that effects may be cell-line specific and cannot be applied universally. A number of endocytic probes and their suggested mechanisms of entry are presented in Table 1.1, which nicely demonstrates this cell-type dependency.

Table 1.1 – Endocytic Pathways involved in the cellular uptake of different probes *Macropinocytosis is most extensively characterised as an increase in uptake of this probe following growth factor activation

Entity	Endocytic Pathway(s)	Cell type	Reference
Transferrin Receptor (TfR)	CME	Rat reticulocytes	(Harding et al., 1983; Pearse and Robinson, 1990)
Dextran	Fluid-phase Macropinocytosis*	 HeLa, coelomocytes Dendritic cells	 (Li et al., 2015) (Falcone et al., 2006)
Albumin	Caveolae	HRGEC	(Moriyama et al., 2017)
Low density Lipoprotein (LDL)	CME Fluid-phase	K562 erythroleukemia cells Macrophages	(Bos et al., 1995) (Barthwal et al., 2013)
Cholera Toxin B (CTxB)	Caveolae/CME CME/Caveolae	HeLa HeLa, Baby hamster kidney (BHK), Caco-2	(Singh et al., 2003) (Torgersen et al., 2001)
GPI-linked proteins	CLIC-GEEC Flotillin-1	HeLa, NIH 3T3 HeLa	(Lundmark et al., 2008) (Glebov et al., 2006)
CD59	Flotillin-1 Arf-6	HeLa, A431 HeLa	(Al Soraj et al., 2012) (Naslavsky et al., 2004)
Simian Virus 40 (SV40)	Caveolin-1 CIE	African Green Monkey Kidney Fibroblasts (CV-1), HeLa Fibroblasts	(Anderson et al., 1996) (Damm et al., 2005)
Lactosylceramide (LacCer)	Caveolae CIE	HeLa, A431 HeLa	(Al Soraj et al., 2012) (Singh et al., 2003)

1.4 Establishment of Endocytic Specific Models of Inhibition

A collection of methods are available for studying endocytosis in *in vitro* models. These can largely be classified into two groups: chemical inhibitors and molecular biology. Chemical inhibitors of various types have been used for decades to study endocytic events. Experiments with these are relatively easy to perform involving simple incubations with cell culture models to assess uptake of a measurable probe and/or a plasma membrane protein. The main problem with these agents is their lack of selectivity for distinct endocytic pathways and other off target effects that could also influence viability and thus endocytosis (Dutta and Donaldson, 2012; Ivanov, 2008). In drug delivery research they have been extensively used to study uptake of drug delivery vectors with the aim of them providing information on uptake route of targeted and non-targeted formulations (Vercauteren et al., 2012).

The birth of RNA interference technologies has allowed a much greater level of protein target specificity via silencing expression of key endocytic regulators of endocytosis. These techniques have been established for just over a decade and a half (Fire et al., 1998), yet are utilised universally across the field of molecular biology. Small interfering RNA (siRNA) allows a more specific approach to understanding the involvement of distinct proteins during the various mechanisms of endocytosis. These technologies perform post-transcriptional gene silencing via the two short (~21-23) nucleotide sequences of the siRNA molecule, which are specific to a distinct mRNA sequence (Hamilton and Baulcombe, 1999). Silencing of transcription is facilitated following binding of the siRNA molecule to its target mRNA sequence, where the

sequence is cleaved and then degraded (Zamore et al., 2000). Due to the half-life of the proteins targeted using these technologies, longer incubation times of 24-72 hours are generally required, potentially affecting cellular homeostasis. From the cell biology literature, in some commonly used cell types (HeLa, A431, RPE) the Jones laboratory working in collaboration with the University of Ghent invested in developing siRNA models of endocytosis for drug delivery research (Vercauteren et al., 2011; Vercauteren et al., 2010). Although beneficial for target specificity, the secondary effects on endocytic activity of the cell must be considered when using these technologies but in association with chemical inhibitors much information can be obtained regarding uptake mechanisms for a particular delivery formulation under consideration.

1.4.1 Endocytic Probes

Fluorescently labelled markers or probes such as transferrin can be utilised in flow cytometry or microscopy studies in order to observe and evaluate the onset, trafficking dynamics and terminus of a specific pathway. Labels commonly used to tag endocytic markers include the broad range of AlexaFluors (488, 647), BODIPY labels, Fluoresceine (FITC), Rhodamine, and Biotinylation, amongst others. When used in conjunction with inhibitory techniques such as those briefly discussed, the mechanics of a specific pathway and the regulatory proteins involved can be analysed by observing how the internalisation of a probe is different from its internalisation in cells where endocytosis has not been compromised. Co-localisation studies with different pathway specific probes can also be performed in order to characterise the trafficking events of

different endocytic mechanisms. Identification of pathway specific probes and selective methods of inhibition however is difficult due to the regulatory network that spans across the different endocytic mechanisms. One probe can be internalised by different pathways and the same endocytic protein can be involved in the regulation of more than one pathway. It is also likely that a protein required for endocytosis is also involved in other cellular processes. Pathway specific probes are much needed as are the identification of proteins that regulate only one pathway. The current systems available for studying different endocytic pathways will now be discussed, highlighting the ways that the lack of specificity for these methods has been approached.

1.4.2 Analyses of Clathrin-mediated Endocytosis (CME)

The original inhibitors used to target CME include sucrose and chlorpromazine, to respectively remove or sequester clathrin and its adaptor proteins from the plasma membrane (Day et al., 2003; Heuser and Anderson, 1989; Ivanov, 2008). Other inhibitors include those which target dynamin, such as Dynasore (Macia et al., 2006) and dyngo-4a (McCluskey et al., 2013), although studies that use these generally refer to the uptake pathway that has been inhibited as dynamin dependent rather than CME (Fletcher et al., 2012; Harper et al., 2011; Wang et al., 2012). Dynasore is a GTPase inhibitor that reversibly prevents the GTPase scission activity of dynamin, thereby stopping scission of CCPs from the plasma membrane (Preta et al., 2015). These inhibitors obstruct clathrin stabilisation at, and scission of, CCPs at the plasma membrane, reducing the net occurrence of CME. The efficient nature of dynamin's scission activity is not just utilised by the cell for CME however. Dynamin has been

implicated in mitochondrial fission (van der Bliek et al., 2013) and in the regulation of various cytoskeletal processes including cell-wide actomyosin organisation (Mooren et al., 2009) and remodelling of F-actin in lamellipodia (Menon et al., 2014; Menon and Schafer, 2013). Together with its involvement in other pinocytic mechanisms such as those dependant on the caveolin family (Henley et al., 1998), dynamin appears to be a relatively unspecific target for CME inhibition. In spite of their lack of specificity however, these inhibitors have proved useful for the elucidation of the distinct role of dynamin in CME, for example at the early steps of CCP formation (Nankoe and Sever, 2006).

The wider roles of clathrin (light and heavy chain) and dynamin that are independent of endocytosis suggest that non-specific effects are likely to be produced when these proteins are targeted by chemical inhibition or siRNA transfection. However, currently they remain the only viable methods to study CME endocytosis in detail and the dependence of this pathway for the uptake of any probe or drug delivery formulation.

Using these approaches has identified an exclusive or joint role for CME in the uptake of plasma membrane localised receptors and their associated ligands. These include the transferrin receptor (TfR)(Dautry-Varsat, 1986; Gammella et al., 2017), EGFR (Vieira et al., 1996) and the low-density lipoprotein receptor (LDLR)(Brown and Goldstein, 1979). Recent studies however have demonstrated that LDLR can also internalise via a clathrin-independent mechanisms (Ivaturi et al., 2014; Scotti et al., 2013), indicating that this receptor is not a reliable marker for studying CME specifically. EGFR has also been shown to be internalised via a clathrin independent

mechanism that is dependent on the concentration of added EGF (Sigismund et al., 2005). Constitutive internalisation of the transferrin receptor (TfR) is specifically dependent on CME and once internalised this and its ligand is sorted to recycling endosomes where the receptor and ligand are returned to the membrane (Mayle et al., 2012). During this endocytic cycle the iron bound to the transferrin is released into the cytosol for use in several different processes. There are similarities and differences in endocytic traffic between TfR, LDLR and EGFR highlighting that uptake via one route may lead to delivery of the receptor and ligand to different locations including delivery to lysosomes (EGFR, EGF and LDL) and recycling to the plasma membrane (TfR, Tf and LDLR).

1.4.3 Analyses of Caveolin-Dependant Endocytosis

Targeting cholesterol dynamics is classically used to prevent caveolae formation and internalisation, due to the essential nature of this sterol in these processes. Sequestration of cholesterol from the plasma membrane is directed by the cyclodextrin molecules, a group to which the widely utilised methyl-β cyclodextrin (MβCD) belongs. Typically pre-incubation of cells in culture with this agent is performed before assessing its effects on endocytic uptake. This method is useful in that depletion is reversible, meaning that cholesterol can be restored to the plasma membrane (Watkins et al., 2009). Evident effects on the structure of cells in the presence of this inhibitor are however apparent (Dutta and Donaldson, 2012), suggesting a range of secondary effects caused by MβCD. CME is also affected through the use of this inhibitor (Rodal et al., 1999), further reducing its specificity for targeting

caveolae. Additional inhibitors include those that prevent the synthesis of cholesterol, such as statins, and molecules that directly associate with the cholesterol molecule, such as nystatin (Cleal et al., 2013). Although effective for prevention of caveolin-dependant endocytosis, all of these mechanisms cause secondary effects within the cell due to the universal depletion of cholesterol at the plasma membrane. Much of the information available regarding the internalisation and trafficking capacity of caveolae has been provided through exploration of caveolin-dependent endocytic probes, such as cholera toxin B (CtxB), GPI-linked proteins, Simian-Virus 40 (SV40) (Nichols, 2002) and albumin (Botos et al., 2008).

siRNA depletion methods targeting Cav-1 have also been used as a means to prevent caveolin-1 mediated endocytosis by our group (Al Soraj et al., 2012) and others (Sun et al., 2010). In collaboration with the University of Ghent, previous members of the lab found that depletion of the protein resulted in a decrease in LacCer uptake, providing further evidence of caveolin-1 dependent endocytosis of this glycolipid (Vercauteren et al., 2011). Depletion of flot-1 however also resulted in reduced uptake of LacCer, demonstrating an ability to internalise via multiple CIE pathways. This has also been described through the investigation of its uptake in cells treated with chemical inhibitors of this process, which also indicated that the pathway used was cell type dependent (Vercauteren et al., 2010).

1.4.4 Analyses of Fluid-phase Endocytosis and Macropinocytosis

Inhibitory methods that target the extensive actin remodelling that is indicative of macropinocytosis are most commonly used to study this pathway. Several inhibitors are currently in use for exploring these pathways. Amiloride and its more potent derivative 5-(N-ethyl-N-isopropyl) amiloride (EIPA), are Na^+/H^+ exchange inhibitors that obstruct macropinocytosis (Dowrick et al., 1993; Nakase et al., 2004), by acidifying sites of macropinocytic cup formation at the membrane. This process inhibits actin regulatory GTPases in this region, such as Cdc42 and Rac1, thereby preventing cup formation (Koivusalo et al., 2010).

ML-7, a myosin light chain kinase inhibitor, has previously been used at concentrations identified as specific for targeting myosin II, a protein that localises to the region of macropinocytic cups in leukocytes (Araki et al., 2003). Myosin II uses its contractile capacity (Shutova et al., 2012) in association with actin to modulate actomyosin turnover (Even-Ram et al., 2007), which in this instance leads to cup closure. Here, ML-7 was able to lower internalisation of a macropinocytic probe, dextran, in macrophages, whereby treated cells were unable to successfully close a shallower macropinocytic cup structure (Araki et al., 2003).

Rottlerin is a commonly used inhibitor of fluid-phase endocytosis and macropinocytosis, though its mechanism of inhibition is currently unknown. Although little is known about this inhibitor, it was deemed appropriate for use in these studies due to its extensive use in previous endocytic studies. When Rottlerin was incubated

with dendritic cells, actin reorganisation following cytokine stimulation was found to be reduced (Sarkar et al., 2005). Rottlerin has also been shown to inhibit the uptake of Vaccinia virus in conjunction with EIPA in monocyte-derived dendritic cells, suggesting macropinocytosis as the mechanism of uptake used by this virus (Sandgren et al., 2010).

Vaccinia virus (Mercer et al., 2010), adenovirus (Kalin et al., 2010), herpes simplex and human immunodeficiency virus (HIV) have also been suggested to enter cells via macropinocytosis (Mercer and Helenius, 2009). Notably, entry is via clathrin-, caveolin- and dynamin-independent mechanisms, yet demonstrates reliance on PAK1 through uncoated vacuolar vesicles similar to macropinosomes. Widely utilised probes for the study of fluid-phase and macropinocytosis are the dextran molecules (Al Soraj et al., 2012; Aleksandrowicz et al., 2011). These comprise of a group of glucan polymers of varying lengths linked by α-D-1,6-glucose bonds, do not have an identified receptor in mammalian cells and are therefore internalised into endosomes in the core fluid. The dextran molecules can be purchased in a range of chain lengths (1- 2,000,000 Da) though the differences between their hydrodynamic radii does not vary to the extent of their molecular weights (Armstrong et al., 2004). The difference in radii between 10kDa and 70kDa dextran is approximately 3.5 nm, a relatively small difference considering the variance in chain length. Unfortunately none of these probes has been able to segregate fluid phase endocytosis from macropinocytosis but the work in our laboratory showed that another myosin II inhibitor blebbistatin (Kovacs et al., 2004) was able to inhibit the increase in dextran uptake in serum starved A431 cells activated with EGF but had no effect on baseline uptake of dextran (Al Soraj et al., 2012).

In conclusion to this section it is fair to say that a wide range of chemical inhibitors are available to study endocytosis but that they all have drawbacks. Until the protein machinery of more endocytic pathways is identified we are currently in the situation that it is very difficult to specifically study endocytic pathways beyond CME using siRNA approaches. For both types of analysis new probes are also required that show a higher level of endocytic selectivity.

1.5 Extracellular Vesicles (EVs)

Extracellular vesicles are defined as 'membrane-contained vesicles released in an evolutionally conserved manner by cells ranging from organisms such as prokaryotes to higher eukaryotes and plants' (Yanez-Mo et al., 2015). They can be found in all bodily fluids including blood plasma, cerebrospinal fluid, urine, semen, breast milk and sweat (Keller et al., 2011; Zaborowski et al., 2015). Various types of EV have been described including three main groups: exosomes (30-150 nm), microvesicles (50-1000 nm) and apoptotic bodies (50-5000 nm), all of which consist of a lumen encased by a lipid bilayer membrane. Other classifications include microparticles and ectosomes, however these subsets are less well defined (Raposo and Stoorvogel, 2013). The lumen contains proteins, lipids and nucleotides (mRNA, DNA) that are derived from their cell of origin (Penfornis et al., 2016). The ability of EVs to carry and transfer these functional materials between adjacent and distant cells as a form of intercellular communication suggests that they have a variety of roles in both normal physiology and disease pathology (Gopal et al., 2017; Tkach and Thery, 2016). Many studies initially focussed on delineating the pathological involvement of these vesicles in

diseases such as cancer and autoimmunity, rather than the possibility that they may actually have a physiological role. There has also been more recent studies on their putative use as disease biomarkers and biotherapeutics or vectors for drug delivery (Ha et al., 2016; Maas et al., 2017; van der Meel et al., 2014).

The first evidence of EVs was suggested as early as 1946 (Chargaff and West, 1946), followed by visualisation of platelet derived lipid-based structures (Wolf, 1967) and matrix derived membrane bound vesicles via electron microscopy (Anderson, 1969). A small number of further observations of this type of entity were made in the decades following these studies, before vesicles involved in reticulocyte maturation were found to be released from multivesicular bodies (MVBs)(Johnstone et al., 1987). Literature states that the term 'Exosome' for a type of these EVs was coined in 1981 (Trams et al., 1981). The next significant observation of vesicular type structures came in 1996, when B lymphocyte derived exosomes were found to induce a functional effect via antigen presentation and membrane fusion in T cells (Raposo et al., 1996). The capacity for functional intercellular communication between different cell types suggested by these observations accelerated research in the EV field, resulting in collection and isolation from different kinds of body fluids and cell culture media. The great heterogeneity between the structure, composition and lumen contents of the EVs collected indicated the existence of different types of vesicle, having been derived via different mechanisms and cell types. This variation has necessitated greater standardisation of what defines each class of EV, and the factors required in order for a population of isolated vesicles to fulfil their identity as a particular subset of vesicle:

exosomes or microvesicles, for instance (Gould and Raposo, 2013; Lotvall et al., 2014; Yanez-Mo et al., 2015).

1.5.1 EV Collection, Purification and Characterisation

Recommended isolation techniques to study vesicles across research groups have been established (Witwer et al., 2013) to ensure consistency between different reports, particularly due to the growing knowledge of their importance in disease pathogenesis. Consistency between techniques, particularly with regards to collection, isolation, and storage, ensure that the secreted vesicles being studied both fulfil the criteria as extracellular vesicles (Lotvall et al., 2014) and are from a pure vesicle preparation (Webber and Clayton, 2013). The range of membrane derived products (from shedding to debris) and types of vesicle contained in cell culture supernatant and bodily fluids can complicate the characterisation of isolated preparations of 'vesicles' (Kreimer et al., 2015). This problem is exemplified in the 'vesicle' preparations obtained via commercial isolation kits, which can contain non-vesicular nucleotide carriers, such as lipo-proteins (Van Deun et al., 2014). Several distinct methods are used for EV collection, and enrichment including differential ultracentrifugation, density-gradient/sucrose-cushion ultracentrifugation and size exclusion chromatography, immunoaffinity-based purification methods and commercial precipitation methods such as ExoQuick™ (Szatanek et al., 2015; Thery et al., 2006; Van Deun et al., 2014). Differential ultracentrifugation is currently the most common technique used to isolate and purify vesicle preparations from cell culture supernatants and biofluids. This process is involves centrifugation and pelleting of the

sample at increasingly greater speeds (Figure 1.4). Microvesicles, other larger vesicles and cell debris are believed to pellet before exosomes at approximately 10,000-20,000 x gravitational force (g), isolating the final EV pellet containing exosomes after two longer sequential centrifugation steps of 100,000 x g. Sucrose-cushion ultracentrifugation can be incorporated into this method, which separates exosomes from other vesicles/debris using a 30% sucrose/D_2O cushion (approx. density 1.2 g/cm^3) (Zhang et al., 2014). Size exclusion chromatography methods also involve ultracentrifugation steps in conjunction with the use of a gel filtration column. This separates structures in the sample based on the theory that larger particles will elute through the column at a quicker rate than smaller particles, meaning that elutions collected at specified times will contain similar sized vesicles that can then be further characterised.

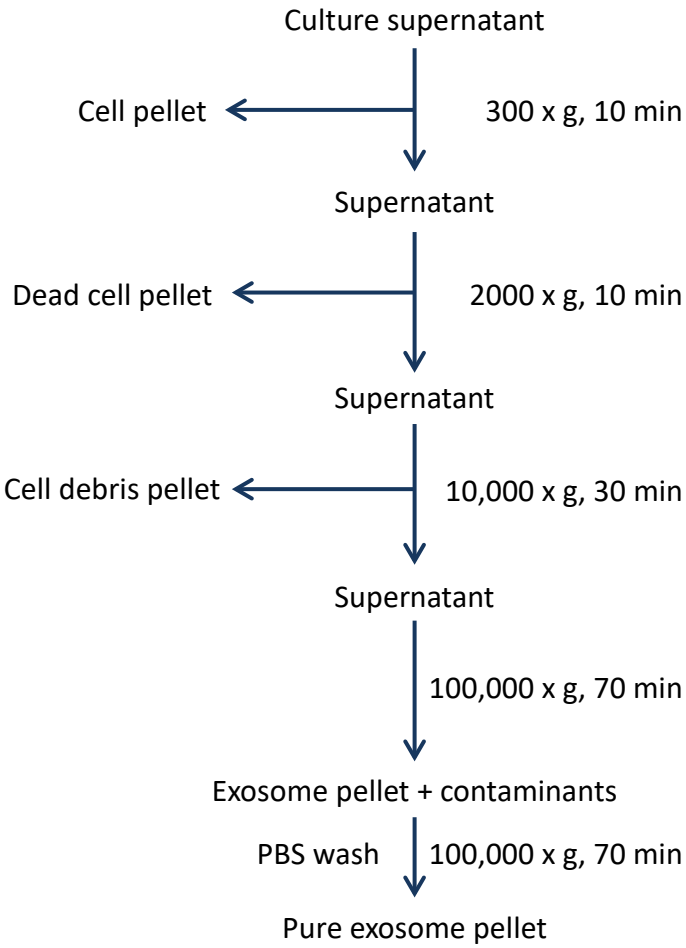

Fig 1.4 ***Isolation of different EV subgroups via the different stages of differential ultracentrifugation*** Based on (Thery et al., 2006)

Affinity-based methods of vesicle isolation and purification are an additional method of isolating vesicles from cell culture supernatant or biofluids. These techniques generally involve the use of a commercial kit incorporating exosome specific antibodies that have been immobilised onto either specialised columns, ELISA plates, magnetic beads or microfluidic devices, for instance (Abramowicz et al., 2016). Antibody targeted proteins include CD63, CD9 and Annexin. This method is useful for the collection of vesicles from a specific cell type in a sample that contains vesicles from multiple cell types, resulting in vesicles with similar characteristics and

composition. For example, the colon epithelial specific protein A33 has been used to isolate exosomes specifically from this cell line in order to identify exosomal proteins that could be used as diagnostic markers for colon cancer (Mathivanan et al., 2010). The vesicle yield using affinity-based methods however is relatively low in comparison to other isolation techniques (Zaborowski et al., 2015). To remove large aggregates and cell debris, an extra filtration step can be performed prior to these isolation techniques. Filtration is often simply carried out by gently pushing the sample through a 0.22 µm filter, removing large aggregates and larger vesicles. These different methods of isolation produce vesicles with variable functionality with regards to both cargo and composition (Mol et al., 2017; Tauro et al., 2012; Taylor and Shah, 2015).

Following collection and isolation, an established set of criteria needs to be fulfilled to ensure the collection of as pure an EV preparation as currently possible. Proteomic analysis has indicated that cytosolic-, cytoskeletal- and membrane-proteins are of particular abundance in exosomes, whereas intracellular proteins associated with organelles are not (Yanez-Mo et al., 2015). It is clear, however, that the proportion of these proteins varies between different vesicle populations, meaning that an abundance of one particular protein in a sample is not sufficient to confirm a pure vesicle/exosome population. An enrichment of several proteins is therefore required to define a preparation as containing mostly exosomes. For example, current protein markers that are abundant in exosomes include Alix, tetraspanins (e.g. CD63), Tumor susceptibility gene 101 (TSG101), Hsp70 and Major histocompatibility complex II (MHCII) (Kalra et al., 2012; Kreimer et al., 2015). Electron microscopy analysis of isolated samples can also be performed to ensure structures between 30-150nm

containing a bilayer enclosing a lumen are clearly defined. This analysis also indicates the presence of debris and non-vesicular structures that result in a 'dirty' preparation. Evaluation of the protein content of vesicle samples allows an approximate exosome concentration to be established, and is most commonly performed using a protein detection assay such as a BCA- or a Bradford assay (Thery et al., 2006). In conjunction with Nanoparticle tracking analysis (NTA), the purity of the sample can be further evaluated via calculation of a particle:protein (P/μg) ratio (Webber and Clayton, 2013). A high ratio value (>$3x10^{10}$ P/μg) indicates that the majority of the sample protein is associated with the particles in the sample, here referring to vesicles. Hence, this is an indicator of the presence of proteins within the sample that are not associated with the EVs.

Due to the variety of factors required to establish their identity as a particular type of vesicle, terminology can be loose. Here, 'EVs' will be used to refer to vesicles not solely defined as either exosomes or microvesicles, but defined as a collection of both. From here on in the EV isolates will be referred to as exosomes due to the rigorous characterisation (discussed in Appendix B) performed by the team of collaborators at the Velindre Hospital lead by Professor Aled Clayton and Dr Jason Webber, who defined the samples as exosomes.

1.6 Exosomes

Exosomes are an EV subgroup derived from the multivesicular bodies (MVBs) of the endolysosomal system, and are expelled from numerous cell types (Edgar, 2016). To

date, exosomes have been established as essential components of numerous physiological processes, including intercellular communication and immune regulation via the transfer of functional proteins, lipids and nucleotides (DNAs, mRNAs, siRNAs) through the extracellular environment between cells and tissues (Mulcahy et al., 2014; Qin and Xu, 2014). Exosomes are 30-150 nm vesicles, composed of a single phospholipid bilayer encapsulating cargo from their cell of origin. This structure allows exosomes to effectively transport a variety of entities through the extracellular milieu, affording protection from degradation. This in a sense describes a form of drug delivery vector leading to interest in their potential use as carriers or therapeutics for the treatment of a variety of diseases (Keller et al., 2011; Simpson et al., 2009).

1.6.1 Exosome Structure and Cargo

1.6.1.1 Exosome RNA

The exosome lumen also encompasses complex entities derived from the cell of origin, including cytosolic proteins and a subset of cellular RNAs (Yanez-Mo et al., 2015; Zaborowski et al., 2015). One may envisage that exosomes may also contain fluid internalised by the endocytic process that generated the MVBs. Coding and non-coding RNA species have been detected in EV isolates, including microRNAs, transfer RNAs, silencing RNAs, small nuclear RNAs and small cytoplasmic RNAs, amongst others. RNA sorting into exosomes is increasingly observed to be a regulated process (Villarroya-Beltri et al., 2014), indicating that transfer of RNA between cells by exosomes is pertinent to normal homeostasis, particularly with regards to immunity (Mittelbrunn et al., 2011; Nolte-'t Hoen et al., 2012), and possibly within disease onset

and pathogenesis (Kosaka et al., 2013; Takahashi et al., 2017). The sorting mechanism responsible for miRNA packaging had been shown to involve the heterogeneous nuclear ribonucleoprotein A2B1 (hnRNPA2B1), which binds to specific miRNA motifs, targeting them for exosome packaging (Villarroya-Beltri et al., 2013). These specific motifs have been termed EXOmotifs, which are GGAG tetranucleotides, found on the miRNA to be sorted (Yanez-Mo et al., 2015) However, the involvement of other mechanisms for different RNA species is still under investigation; other mRNA and miRNA motifs are also being studied for involvement in their sorting into exosomes.

1.6.2.2 DNA

Double stranded DNA fragments of a variety of sizes (100 base pairs to 2.5 kilobase pairs) have been identified in EV isolates, and have been given the title EV-DNAs (Thakur et al., 2014). Whether EV-DNA is homologous to genomic DNA remains to be fully established, and in comparison to EV-RNA, the functional impact of EV-DNA currently remains unknown.

1.6.2.3 Proteins on EV membranes

The protein signature of isolated EVs is shaped by the physiological context and cell-type from which the vesicles are derived. As previously discussed, exosomes have several proteins that look to be universally enriched in exosomes, regardless of the identity of their cell of origin. These include a number of tetraspanins (CD37, CD53, CD63, CD81, and CD82) and MHCII proteins. Sorting of proteins into MVBs is dependent on the endosomal sorting complexes required for transport

(ESCRT)(Schmidt and Teis, 2012), which results in variants of these complexes being enriched on exosomes. These include Alix and TSG101, in addition to the protein chaperones, Hcs70 and Heat shock protein 90 (Hsp90). The use of this intraendosomal sorting machinery for packaging proteins into vesicles strongly suggests that exosomes generally have greater enrichment of these proteins than a standard cell lysate or other EV sample. However, enrichment of these proteins, including the heat shock proteins and MHCII, has recently been suggested to occur in all EV subtypes (Kowal et al., 2016), thereby questioning their exclusivity to exosomes alone.

1.6.2 Function of Exosomes and Extracellular Vesicles

Exosomes naturally shuttle cargo between adjacent and distant cells as a mode of communication, modulating important physiological and pathological processes such as cancer, cardiovascular diseases, and neurodegeneration, as well as transferring pathogenic virulence factors (Yanez-Mo et al., 2015). This natural ability to functionally transfer a spectrum of macromolecular cargo between cells also raises opportunities for exploiting exosomes as vectors for drug delivery (Batrakova and Kim, 2015; Vader et al., 2016; van Dommelen et al., 2012).

1.6.2.1 Exosomes as Shuttles for Communication Between Cells

The communicative abilities of extracellular vesicles have been widely studied with regards to both normal physiology and disease pathogenesis. Having been isolated from all human bodily fluids and from the biofluids of other organisms, including plants (Lange and Gagliardi, 2012), fungi (Rodrigues et al., 2011) and bacteria (Kim et al.,

2014; Lefebvre and Lecuyer, 2017), it can be hypothesised that their roles are extensive. Transfer of a range of functional cargoes between adjacent and distant cells is apparent. However, little is known about the ways in which exosomes initially interact with the cell, gain intracellular access and are trafficked through the cell to their final destination. Even less is known about how intravesicular cargo is released and directed towards the intended target within the cytosol or other intracellular compartments. There is an abundance of information regarding the importance of EV mediated cargo transfer in the processes involved in an extensive range of physiological systems (Yanez-Mo et al., 2015; Zaborowski et al., 2015). For example, involvement within cardiovascular regulation, influence over sexual reproduction and importance for immune surveillance and activation has been suggested (S et al., 2013; Vlassov et al., 2012). There are many systems in which EVs have been found to have involvement and some of these are briefly described below.

1.6.2.2 Cardiovascular Regulation

With the earliest EV work having been performed with blood plasma isolates (Chargaff and West, 1946; Wolf, 1967), it is of no wonder that much work has been performed to characterise their roles within vascular homeostasis.

The involvement of EVs in vascularisation has been extensively characterised with regards to their roles in angiogenesis but also with reference to vascular regeneration. Angiogenesis will be discussed below in the context of cancer. Vascular regeneration has been studied with exosomes derived from stem cells of endothelial nature in both

an *in vitro* and an *in vivo* setting. In both instances, endothelial progenitor cells (EPCs) were harvested from human umbilical cord samples, and exosomes isolated. After injury to the rat carotid artery, EPC exosomes were observed to accelerate the early regeneration of endothelial tissue of the injured artery. Further to this, these exosomes were found to increase proliferation of cultured endothelial cells in *in vitro* wound models (Li et al., 2016a; Li et al., 2016b). This remarkable ability has undoubtedly identified stem cell vesicle isolates as possible therapeutics for cardiovascular repair, targeting damaged tissues through localised engraftment or transplants (Huang et al., 2015; Lai et al., 2011). Inter-cell communication and regulation of the events following a myocardial infarction have also been associated with EV released from cardiomyocytes, indicating use of a variety of cell-derived vesicles for similar therapeutics (Yuan et al., 2016) or help to influence or aid these mechanisms to improve recovery (Sahoo and Losordo, 2014).

1.6.2.3 Immunity

EVs are released from a number of leukocytes of both the innate and activated immune system. These include macrophages, dendritic cells, natural killer (NK) cells, B cells, and T cells (Robbins and Morelli, 2014). The cellular system from which they are derived influences their immune associated activities, and cargoes shown to be associated with EV and exosome isolates from these cell types are diverse. For example, a great number of cytokines and chemokines have been designated as vesicle cargoes, with many of these believed to be involved in processes such as inflammation and antigen presentation (Benito-Martin et al., 2015; Thery et al., 2002). It must be

noted however that many of these studies investigate the involvement of the immune system in the context of cancer onset and progression.

Cargoes associated with EVs also extend to those originating from pathogens such as viruses, and these could even play a role in prevention of pathogenesis (Kouwaki et al., 2017). Hepatitis C viral RNA carried on the exosome surface from infected hepatocytes can be recognised by pattern recognition receptors on dendritic cells and macrophages, causing activation of an antiviral cascade (Dreux et al., 2012; Kouwaki et al., 2016). Similar actions have been demonstrated by exosomes released from Epstein-Barr virus infected cells, which carry small-RNAs from the virus. These exosomes transfer immunity to non-infected dendritic cells (Baglio et al., 2016). Pathogenic bacterial RNA has also been found in exosomes. For example, exosomes produced by *Mycobacterium tuberculosis* (M.Tb) infected macrophages contain M.Tb derived RNA that demonstrates functionality (Singh et al., 2015). These exosomes have the ability to recruit macrophages and other immune cells during tuberculosis granuloma formation, though the exact mechanism responsible for this is unknown (Singh et al., 2012). M.Tb derived protein cargo may well be responsible. Alternately, tumour-derived exosomes have been found to carry cargoes that can act to suppress the immune system (Whiteside, 2017). Increased rates of apoptosis and a reduction in proliferation of T cells (Wieckowski et al., 2009), in addition to a reduced cytotoxicity of natural killer cells (Szczepanski et al., 2011), are some other examples of how exosomes influence immune activity. These abilities are most likely due to their capacity to successfully transfer functional cargo and/or activate plasma membrane receptors.

1.6.2.4 Cancer

Exosomes and other EVs have been extensively studied with regards to their involvement in cancer onset and progression (Whiteside, 2017; Zha et al., 2017). The tumour microenvironment is responsible for these activities, and has key influence over the behaviour of cancer cells (Fouad and Aanei, 2017; Pickup et al., 2014). EVs, including exosomes, have been found to be produced by cells within the cancer structure, indicating their involvement in the processes regulated by this environment (Meehan and Vella, 2016; Webber et al., 2015). Their roles in these processes are broad ranging, having relevance in angiogenesis, immune inactivation and evasion, alteration of cellular metabolism and transfer of metastatic factors to adjacent and distant tissues.

Progressive diseases have the ability to generate their own vascular system (Hanahan and Weinberg, 2011). Angiogenic factors are often secreted by tumour cells, inducing angiogenesis from surrounding tissues, and it has been demonstrated that tumour derived exosomes have to the ability to induce this effect. Tetraspanins are one such angiogenic factor, harnessing the ability to activate branching of adjacent vessels. As previously discussed, these proteins are highly enriched in the membranes of exosomes and other EVs, suggesting a possibility for their interaction via tetraspanins with tumor vasculature to induce angiogenesis (Webber et al., 2015).

The ability of tumour cells to evade clearance by the immune system is important for early disease progression and tumour growth. Tumour-derived exosomes have been

found to carry cargoes that can act to suppress the immune system at various different levels in a variety of ways (Whiteside, 2017). Effects include increased rates of apoptosis and a reduction in proliferation of T cells (Wieckowski et al., 2009), in addition to a reduced cytotoxicity of natural killer cells (Szczepanski et al., 2011).

1.6.3 Exosomes as Diagnostics

Via profiling methods commonly utilising PCR, a number of miRNAs have been identified in exosomes derived from a range of different biofluids, suggesting their use in the diagnosis of a variety of diseases, from gastrointestinal (Matsumura et al., 2015; Nedaeinia et al., 2017; Ogata-Kawata et al., 2014), pancreatic (Que et al., 2013) and cancers (Schwarzenbach, 2015), Alzheimer's disease (Van Giau and An, 2016) and Multiple Sclerosis. Notably, it has been suggested that exosomal transfer between cancer cells is involved in the propagation of drug resistance in prostate (Corcoran et al., 2012), and other cancers (Chen et al., 2014).

1.6.4 Exosomes as Drug Delivery Vectors

The involvement of exosomes and other EVs within normal physiological processes and within a variety of diseases suggests they have ability to transfer bioactive cargo of different types between different cells as a form of cell-cell communication. Their proficiency here makes them promising vectors for small molecule and macromolecular drug delivery (Batrakova and Kim, 2015; Vader et al., 2016; van Dommelen et al., 2012). As more information about their involvement in different pathogeneses also increases, ways in which exosomes could be harnessed for

treatment and prevention is also promising. The treatment of a variety of diseases could benefit from their use due to their ability to reach distant tissues that are oftentimes protected by highly specialised barriers that other drug delivery systems are unable to transgress, such as the BBB (Ha et al., 2016). These diseases include Alzheimer's and other cerebrospinal diseases such as Parkinson's disease (Rufino-Ramos et al., 2017; Wu et al., 2017). Exosomes also possess a number of other factors that make them suitable for drug delivery, including the ability to genetically modify the cell of origin so that the exosomes produced express tissue specific targeting proteins (Batrakova and Kim, 2015). Additionally, some cell types such as dendritic cells produce a proportion of exosomes without T cell activators, such as MHCII, resulting in low levels of immunogenicity (Quah and O'Neill, 2005).

Several studies have endeavoured to explore this function in a variety of contexts. For instance, functional delivery of siRNA to the brain has been demonstrated *in vivo* (Alvarez-Erviti et al., 2011). Here, siRNA targeting GAPDH and Beta-secretase 1 (BACE1), a protein target for Alzheimer's disease, was loaded into dendritic cell derived EVs loaded with siRNA by electroporation, before intravenous injection of the preparation into mice. Targeting to brain tissues was attempted via modification of exosomes with Rabies Virus Glycoprotein (RVG), a neuron-specific peptide for BBB targeting. A reduction in both GAPDH and BACE1 expression in excised brain tissue was presented using Western blot analysis, indicating successful delivery of functional cargo. Protein delivery by exosomes has also been demonstrated in neuronal cells, where loading of exosomes with catalase via sonication or permeabilisation was performed. Increased uptake of exosomes was observed in neuronal cells and via the

measurement of microglial activation in the mouse brain it was found that catalase loaded exosomes had a neuroprotective effect (Haney et al., 2015). Exosome delivery potential also extends to small molecule chemotherapeutics. Loading dendritic cell derived exosomes with doxorubicin resulted in the inhibition of tumour growth in mice *in vivo* (Tian et al., 2014b) and paclitaxel and doxorubicin encapsulated in exosomes derived from a number of brain tumour cell lines resulted in decreased viability of the same cell lines *in vitro* and a loss of cancer cells in the brains of a zebrafish model of brain cancer (Yang et al., 2015).

Methods to improve the uptake of exosomes as a means of improving their delivery capacity for potential therapeutics will be discussed in the following section.

1.6.5 Methods to study Endocytosis of Exosomes

The ways in which exosomes and other EVs interact with and enter cells still remain largely undetermined. Increased knowledge on this is required to elucidate their roles in normal physiology, disease and also to determine how best to exploit them as drug delivery vectors. An array of endocytic inhibitors to target various endocytic pathways has previously been employed in exosomal uptake assays to identify potential routes of internalisation. Studies utilising inhibitors such as EIPA and Cytochalasin D suggest that macropinocytosis, an actin-dependent process, is involved in exosome internalisation (Escrevente et al., 2011), whereas the use of dynamin inhibitors such as dynasore suggests a role for clathrin- and caveolin-mediated endocytosis. Phagocytosis has also been suggested as a preferential uptake route in a study utilising both

phagocytic and non-phagocytic cell types, whereby exosomes were shown to be localised to phagosomal-like structures (Feng et al., 2010). Interestingly, it has also been suggested that exosomes are able to travel along cell filopodia to activate their own uptake (Heusermann et al., 2016). Here downstream of the plasma membrane they were trafficked to lysosomes.

Exosome modification to improve cell uptake capacity has been explored. Exosome conjugation with GALA, a pH-sensitive peptide, and other cationic lipids results in increased uptake and cytosolic release of dextran molecules loaded into HeLa derived exosomes. This method also resulted in the increased cytosolic release of the ribosome inactivating protein, saporin (Nakase and Futaki, 2015). Loading with EGF induced uptake via activation of macropinocytosis It is suggested that encapsulated EGF released to the cytosol following internalisation of a small proportion of exosomes travels back to the cellular plasma membrane to induce macropinocytosis and thereby increases internalisation of the extracellular exosomes not yet internalised (Nakase et al., 2015). Induction of macropinocytosis as an internalisation mechanism was further explored by modifying the exosome membrane with the cell penetrating peptide steryl-octaarginine, resulting in enhanced uptake. Improved cytosolic delivery of encapsulated saporin was again demonstrated (Nakase et al., 2017; Nakase et al., 2016).

Exploring how exosomes interact with *in vitro* cell models for high content analyses can be facilitated by fluorescently labelling them using several different methods. The quickest way of labelling a preparation of isolated exosomes is by using a lipophilic

dye. These dyes come in many different forms including the Di (DiI, DiO) and the PKH (PKH26, 27, etc) molecules (Jensen, 2012). These fluorescent molecules embed within the membrane bilayer of the exosome (Figure 1.5) following a simple incubation with a purified vesicle preparation, resulting in a fluorescently labelled sample. Another method includes the use of exosome permeable compounds including carboxyfluorescein succinimidyl ester (CFSE) and 5(6) carboxyfluorescein succinimidyl diacetate (CFDA) (Temchura et al., 2008). Both molecules are membrane permeable, yet their labelling mechanisms are different. CFSE associates with molecules within the lumen of the exosome via their succinimidyl group and is constitutively fluorescent, whereas the fluorescence of CFDA requires activation by exosomal esterases. Other more labour intensive methods of acquiring fluorescent exosomes include transfection of a cell line with a Green Fluorescent Protein (GFP)-tagged exosomally enriched protein, such as CD63-GFP. Exosomes isolated from these transfected cells are therefore already fluorescently tagged at the point of origin. Both stable and transient transfection have been utilised for this approach. Advantages and disadvantages exist for all of these methods, and discussed in the next section.

1.6.5.1 Labelling Exosomes with Lipophilic Dyes

A variety of lipophilic dyes have been utilised to generate fluorescently labelled extracellular vesicle populations, including exosomes, for many applications. These dyes have also been used in the exploration of possible isolation and characterisation applications including microfluidic devices (Kanwar et al., 2014) and size exclusion chromatography (Xu et al., 2016). By embedding within the membrane bilayer, these

dyes enable qualitative and quantitative measurements of cell-exosome interactions, via microscopy and flow cytometry respectively. The lipophilic carbocyanine Di molecules, which include DiD, DiL and DiO, amongst others, have been used extensively for this purpose, the structure of which is presented in Figure 1.5.

The PKH dyes utilise a similar mechanism to embed within the membrane bilayer to generate a fluorescently labelled whole cell or vesicle population, and this is also presented again in Figure 1.5. These molecules also provide a certain extent of flexibility with regards to colour of fluorescence, PKH26 having red fluorescence for instance and PKH67 green. This method has been used to label bladder cancer cell exosomes indicating that their uptake in the same cell line is time and dose dependent (Franzen et al., 2014).

Labelling of exosomes using these methods is easy to perform but the literature does not disclose experiments that have been performed to characterise the functional integrity of these entities

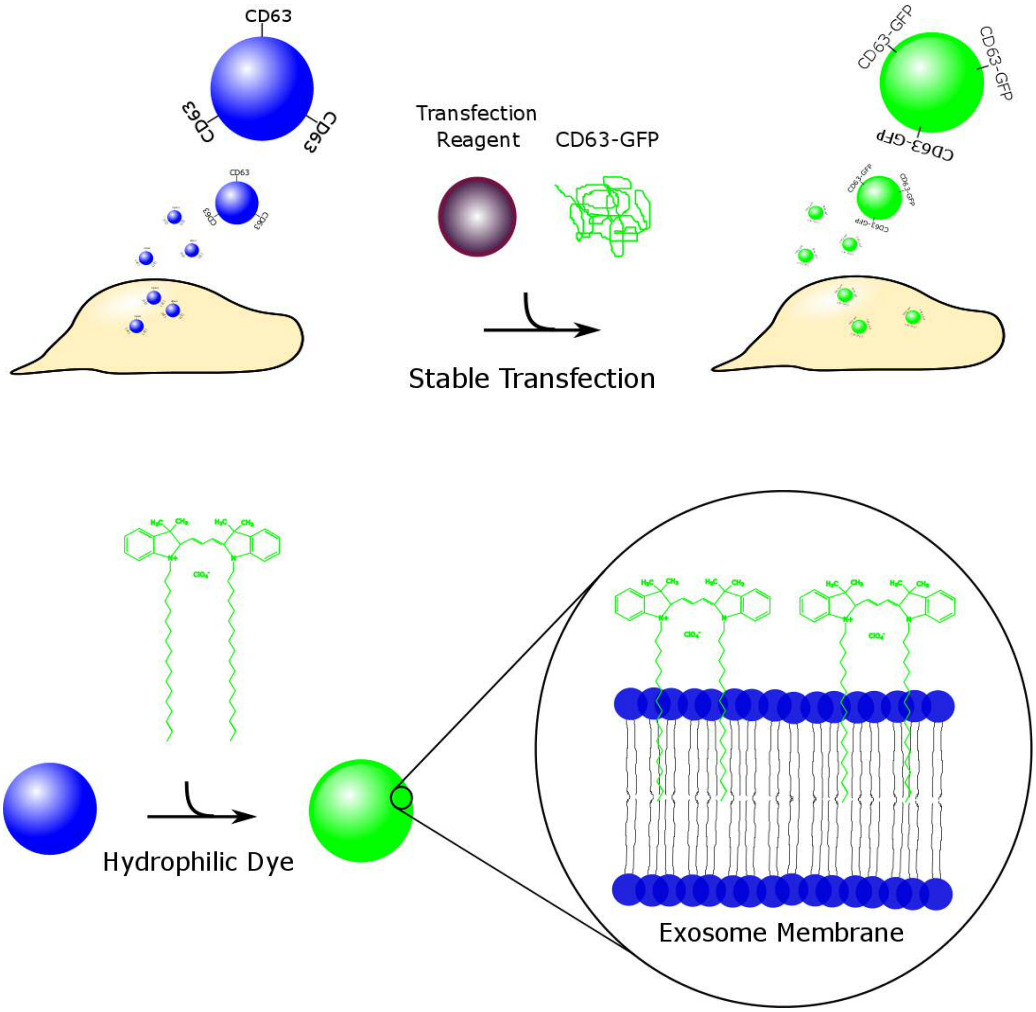

Fig 1.5 Current methods used to produce fluorescently labelled exosome preparations Stable transfection of a GFP-tagged exosomally enriched protein (such as CD63) into a cell line from which exosomes will be collected, results in the subsequent production of GFP-labelled exosomes. Below, fluorescent hydrophilic dyes (Di/PKH molecules) non-covalently embed in the exosome membrane.

1.6.5.2 Labelled Exosomes from Stable Cell Lines

Transient transfection is a quick and efficient method of altering gene expression, and is most commonly used to perform this type of experiment. If expression with greater stability is required however, the generation of a stably transfected cell line is a better option, and are commonly utilised for a variety of applications (Bussow, 2015). These

range from cells that do not express specific proteins to cells that express recombinant proteins, such as mutant proteins or tagged proteins. A sustained gene expression is provided using this method, rather than loss of expression following cell division (Assenberg et al., 2013; Dyson, 2016). Tagged proteins include proteins that have been engineered to express a fluorescent protein, such as GFP or mCherry, and has proved particularly useful in the generation of fluorescently labelled exosomes (Figure 1.5).

Exosome profiling has identified proteins that are highly enriched in these vesicles (Duijvesz et al., 2013; Webber et al., 2014), generating a list of potential proteins that could be targeted for labelling. The most commonly used protein for this process is the tetraspanin CD63, which is commonly transfected as a GFP/mCherry recombinant. CD63 is also called LAMP3, a protein often labelled in cells for immunofluorescence microscopy identification of late endosomes and lysosomes. Exosomes that are collected from stably transfected CD63-GFP cells are therefore fluorescent due to their GFP enrichment and can be further used for analysis using methods such as microscopy or flow cytometry. For instance, exosomes collected from HeLa generated to stably express CD63-GFP have been utilised for exosome microscopy studies (Nakase et al., 2015; Suetsugu et al., 2013). Unfortunately these techniques can result in differential expression of tetraspanins in the structure of the vesicle, with overexpression potentially altering the composition of vesicles collected from such cell lines (Lin et al., 2008; Perez-Hernandez et al., 2013).

These methods exemplify the ways in which exosomes have been labelled for subsequent analysis of cell uptake and intracellular traffic in different *in vitro* models.

The capacity of exosomes to enter via endocytosis has been suggested primarily through the proposition that entry requires an energy-dependent process (Escrevente et al., 2011; Mulcahy et al., 2014). In dendritic cells it has been shown that localisation of internalised exosomes is confined to endosomal sorting networks, further supporting a role for endocytosis as a portal for exosomal entry (Morelli et al., 2004). Studies by Tian et al (Tian et al., 2010; Tian et al., 2014a) used a combination of siRNA depletion of endocytic proteins and pharmacological inhibitors to study possible entry mechanisms of PC12 derived exosomes in PC12 cells.

Once labelled, the cell-type specific endocytic profile of exosomes, and other discussed drug delivery systems, can be elucidated by using the techniques of pathway specific modelling previously discussed. As presented in Table 1.3 a combination of both flow cytometry and microscopy analysis can be used to determine exosome uptake and quantify fluorescence in *in vitro* models. Flow cytometry can provide quantification of intracellular fluorescence, if removal of cell surface fluorescence can be guaranteed. This process involves several trypsinisation steps, potentially altering the plasma membrane so to avoid this, intracellular fluorescence can be quantified from microscopy images and this process is described in Section 2.13.1.

Table 1.3 – Proposed uptake mechanisms of exosomes labelled using different probes

Exosome derivation	Label	Recipient cell type	Method – FACS/Microscopy	Endocyt Pathwa
SW780 human bladder cancer	PKH26	Human bladder cancer - SW780 and UMUC3	Both	Recepto
U87 MG human glioblastoma cells	PKH67/26, cellvue midklaret	HeLa, mouse embryonic fibroblasts (MEF)	Both	Lipid-raf
U87 MG human glioblastoma cells	PKH26	U87 MG, U118 MG and LN18 human glioblastoma, CHO hamster ovary	Both	HSPG-de
K562 human lymphoblasts, MT-4 human T-cell	PKH67/26	Human – Macrophages (RAW 264.7, J774A.1, THP-1), Lymphocytes (Jurkat T cells), Kidney (293T cells, COS-7), HEL299 lung fibroblast, Mouse - NIH-3T3 fibroblast	Both	Phagocy
PC12 rat embryonic brain	DiD, CFSE	PC12, Rat bone marrow stem cells	Both	CME, macropi
SKOV3 human ovarian carcinoma	CFSE	SKOV3	Both	Lipid-raf macropi

1.7 Hypothesis

High-content studies utilising the techniques of endocytic inhibition described will permit a greater level of characterisation of many drug delivery systems. Aiming to identify more specific endocytic probes and inhibitory mechanisms will be facilitated through a greater delineation of the molecular mechanisms involved in processes, particularly that of macropinocytosis.

The hypothesis of this study is:

Further identification of methods to attenuate different endocytic pathways will lead to higher level of evaluation of the cellular internalisation mechanisms utilised by established and novel drug delivery vectors such as exosomes.

1.8 Objectives

The overall aim of this project is to provide high content *in vitro* endocytic platforms using siRNA transfection of endocytic proteins and chemical inhibitors of endocytosis to analyse the uptake of potential drug delivery systems. Provide an *in vitro* platform for specific inhibition of Clathrin-mediated endocytosis

- Further investigate the proteins involved in macropinocytosis to identify a more specific method of targeting this pathway
- Use established and newly developed techniques of endocytic inhibition to better characterised the uptake of model prostate cancer derived exosomes

1.9 References

Abramowicz, A., P. Widlak, and M. Pietrowska. 2016. Proteomic analysis of exosomal cargo: the challenge of high purity vesicle isolation. *Molecular bioSystems*. 12:1407-1419.

Aderem, A., and D.M. Underhill. 1999. Mechanisms of phagocytosis in macrophages. *Annual review of immunology*. 17:593-623.

Agrahari, V., V. Agrahari, and A.K. Mitra. 2016. Nanocarrier fabrication and macromolecule drug delivery: challenges and opportunities. *Therapeutic delivery*. 7:257-278.

Ait-Slimane, T., R. Galmes, G. Trugnan, and M. Maurice. 2009. Basolateral internalization of GPI-anchored proteins occurs via a clathrin-independent flotillin-dependent pathway in polarized hepatic cells. *Molecular biology of the cell*. 20:3792-3800.

Al Soraj, M., L. He, K. Peynshaert, J. Cousaert, D. Vercauteren, K. Braeckmans, S.C. De Smedt, and A.T. Jones. 2012. siRNA and pharmacological inhibition of endocytic pathways to characterize the differential role of macropinocytosis and the actin cytoskeleton on cellular uptake of dextran and cationic cell penetrating peptides octaarginine (R8) and HIV-Tat. *Journal of controlled release : official journal of the Controlled Release Society*. 161:132-141.

Alberts, B., A. Johnson, J. Lewis, M. Raff, K. Roberts, and P. Walter. 2008. Molecular Biology of the Cell. Garland Science, Taylor & Francis Group, New York, USA.

Aleksandrowicz, P., A. Marzi, N. Biedenkopf, N. Beimforde, S. Becker, T. Hoenen, H. Feldmann, and H.J. Schnittler. 2011. Ebola virus enters host cells by macropinocytosis and clathrin-mediated endocytosis. *The Journal of infectious diseases*. 204 Suppl 3:S957-967.

Alon, R., and Z. Shulman. 2011. Chemokine triggered integrin activation and actin remodeling events guiding lymphocyte migration across vascular barriers. *Experimental cell research*. 317:632-641.

Alvarez-Erviti, L., Y. Seow, H. Yin, C. Betts, S. Lakhal, and M.J. Wood. 2011. Delivery of siRNA to the mouse brain by systemic injection of targeted exosomes. *Nature biotechnology*. 29:341-345.

Anderson, H.A., Y. Chen, and L.C. Norkin. 1996. Bound simian virus 40 translocates to caveolin-enriched membrane domains, and its entry is inhibited by drugs that selectively disrupt caveolae. *Molecular biology of the cell*. 7:1825-1834.

Anderson, H.C. 1969. Vesicles associated with calcification in the matrix of epiphyseal cartilage. *The Journal of cell biology*. 41:59-72.

Araki, N., Y. Egami, Y. Watanabe, and T. Hatae. 2007. Phosphoinositide metabolism during membrane ruffling and macropinosome formation in EGF-stimulated A431 cells. *Experimental cell research*. 313:1496-1507.

Araki, N., M. Hamasaki, Y. Egami, and T. Hatae. 2006. Effect of 3-methyladenine on the fusion process of macropinosomes in EGF-stimulated A431 cells. *Cell structure and function*. 31:145-157.

Araki, N., T. Hatae, A. Furukawa, and J.A. Swanson. 2003. Phosphoinositide-3-kinase-independent contractile activities associated with Fcgamma-receptor-mediated phagocytosis and macropinocytosis in macrophages. *Journal of cell science*. 116:247-257.

Armstrong, J.K., R.B. Wenby, H.J. Meiselman, and T.C. Fisher. 2004. The hydrodynamic radii of macromolecules and their effect on red blood cell aggregation. *Biophysical journal*. 87:4259-4270.

Assenberg, R., P.T. Wan, S. Geisse, and L.M. Mayr. 2013. Advances in recombinant protein expression for use in pharmaceutical research. *Current opinion in structural biology*. 23:393-402.

Baglio, S.R., M.A. van Eijndhoven, D. Koppers-Lalic, J. Berenguer, S.M. Lougheed, S. Gibbs, N. Leveille, R.N. Rinkel, E.S. Hopmans, S. Swaminathan, S.A. Verkuijlen, G.L. Scheffer, F.J. van Kuppeveld, T.D. de Gruijl, I.E. Bultink, E.S. Jordanova, M. Hackenberg, S.R. Piersma, J.C. Knol, A.E. Voskuyl, T. Wurdinger, C.R. Jimenez, J.M. Middeldorp, and D.M. Pegtel. 2016. Sensing of latent EBV infection through exosomal transfer of 5'pppRNA. *Proceedings of the National Academy of Sciences of the United States of America*. 113:E587-596.

Barthwal, M.K., J.J. Anzinger, Q. Xu, T. Bohnacker, M.P. Wymann, and H.S. Kruth. 2013. Fluid-phase pinocytosis of native low density lipoprotein promotes murine M-CSF differentiated macrophage foam cell formation. *PloS one*. 8:e58054.

Bastiani, M., and R.G. Parton. 2010. Caveolae at a glance. *Journal of cell science*. 123:3831-3836.

Batrakova, E.V., and M.S. Kim. 2015. Using exosomes, naturally-equipped nanocarriers, for drug delivery. *Journal of controlled release : official journal of the Controlled Release Society*. 219:396-405.

Benito-Martin, A., A. Di Giannatale, S. Ceder, and H. Peinado. 2015. The new deal: a potential role for secreted vesicles in innate immunity and tumor progression. *Frontiers in immunology*. 6:66.

Bitsikas, V., I.R. Corrêa, and B.J. Nichols. 2014. Clathrin-independent pathways do not contribute significantly to endocytic flux.

Boettner, D.R., R.J. Chi, and S.K. Lemmon. 2012. Lessons from yeast for clathrin-mediated endocytosis. *Nature cell biology*. 14:2-10.

Bos, C.R., S.L. Shank, and M.D. Snider. 1995. Role of clathrin-coated vesicles in glycoprotein transport from the cell surface to the Golgi complex. *The Journal of biological chemistry*. 270:665-671.

Botos, E., J. Klumperman, V. Oorschot, B. Igyarto, A. Magyar, M. Olah, and A.L. Kiss. 2008. Caveolin-1 is transported to multi-vesicular bodies after albumin-induced endocytosis of caveolae in HepG2 cells. *Journal of cellular and molecular medicine*. 12:1632-1639.

Boucrot, E., A.P.A. Ferreira, L. Almeida-Souza, S. Debard, Y. Vallis, G. Howard, L. Bertot, N. Sauvonnet, and H.T. McMahon. 2015. Endophilin marks and controls a clathrin-independent endocytic pathway. *Nature*. 517:460-465.

Brodsky, F.M. 2012. Diversity of clathrin function: new tricks for an old protein. *Annual review of cell and developmental biology*. 28:309-336.

Brown, M.S., and J.L. Goldstein. 1979. Receptor-mediated endocytosis: insights from the lipoprotein receptor system. *Proceedings of the National Academy of Sciences of the United States of America*. 76:3330-3337.

Buckley, C.M., and J.S. King. 2017. Drinking problems: mechanisms of macropinosome formation and maturation. *The FEBS journal*.

Bussow, K. 2015. Stable mammalian producer cell lines for structural biology. *Current opinion in structural biology*. 32:81-90.

Cerrato, C.P., K. Kunnapuu, and U. Langel. 2017. Cell-penetrating peptides with intracellular organelle targeting. *Expert opinion on drug delivery*. 14:245-255.

Chappie, J.S., and F. Dyda. 2013. Building a fission machine--structural insights into dynamin assembly and activation. *Journal of cell science*. 126:2773-2784.

Chargaff, E., and R. West. 1946. The biological significance of the thromboplastic protein of blood. *The Journal of biological chemistry*. 166:189-197.

Chen, W.X., X.M. Liu, M.M. Lv, L. Chen, J.H. Zhao, S.L. Zhong, M.H. Ji, Q. Hu, Z. Luo, J.Z. Wu, and J.H. Tang. 2014. Exosomes from drug-resistant breast cancer cells transmit chemoresistance by a horizontal transfer of microRNAs. *PloS one*. 9:e95240.

Cheng, J.P., and B.J. Nichols. 2016. Caveolae: One Function or Many? *Trends in cell biology*. 26:177-189.

Christianson, H.C., K.J. Svensson, T.H. van Kuppevelt, J.P. Li, and M. Belting. 2013. Cancer cell exosomes depend on cell-surface heparan sulfate proteoglycans for their internalization and functional activity. *Proceedings of the National Academy of Sciences of the United States of America*. 110:17380-17385.

Cleal, K., L. He, P.D. Watson, and A.T. Jones. 2013. Endocytosis, intracellular traffic and fate of cell penetrating peptide based conjugates and nanoparticles. *Current pharmaceutical design*. 19:2878-2894.

Collinet, C., M. Stoter, C.R. Bradshaw, N. Samusik, J.C. Rink, D. Kenski, B. Habermann, F. Buchholz, R. Henschel, M.S. Mueller, W.E. Nagel, E. Fava, Y.

Kalaidzidis, and M. Zerial. 2010. Systems survey of endocytosis by multiparametric image analysis. *Nature*. 464:243-249.

Collins, B.M., A.J. McCoy, H.M. Kent, P.R. Evans, and D.J. Owen. 2002. Molecular architecture and functional model of the endocytic AP2 complex. *Cell*. 109:523-535.

Cooper, G. 2000. Structure of the Plasma Membrane. *In* The Cell: A Molecular Approach. Sinauer Associates

Corcoran, C., S. Rani, K. O'Brien, A. O'Neill, M. Prencipe, R. Sheikh, G. Webb, R. McDermott, W. Watson, J. Crown, and L. O'Driscoll. 2012. Docetaxel-resistance in prostate cancer: evaluating associated phenotypic changes and potential for resistance transfer via exosomes. *PloS one*. 7:e50999.

Cox, D., P. Chang, Q. Zhang, P.G. Reddy, G.M. Bokoch, and S. Greenberg. 1997. Requirements for both Rac1 and Cdc42 in membrane ruffling and phagocytosis in leukocytes. *The Journal of experimental medicine*. 186:1487-1494.

Damm, E.M., L. Pelkmans, J. Kartenbeck, A. Mezzacasa, T. Kurzchalia, and A. Helenius. 2005. Clathrin- and caveolin-1-independent endocytosis: entry of simian virus 40 into cells devoid of caveolae. *The Journal of cell biology*. 168:477-488.

Dautry-Varsat, A. 1986. Receptor-mediated endocytosis: the intracellular journey of transferrin and its receptor. *Biochimie*. 68:375-381.

Day, P.M., D.R. Lowy, and J.T. Schiller. 2003. Papillomaviruses infect cells via a clathrin-dependent pathway. *Virology*. 307:1-11.

Delorme-Walker, V.D., J.R. Peterson, J. Chernoff, C.M. Waterman, G. Danuser, C. DerMardirossian, and G.M. Bokoch. 2011. Pak1 regulates focal adhesion strength, myosin IIA distribution, and actin dynamics to optimize cell migration. *The Journal of cell biology*. 193:1289-1303.

Dharmawardhane, S., A. Schurmann, M.A. Sells, J. Chernoff, S.L. Schmid, and G.M. Bokoch. 2000. Regulation of macropinocytosis by p21-activated kinase-1. *Molecular biology of the cell*. 11:3341-3352.

Doherty, G.J., M.K. Ahlund, M.T. Howes, B. Moren, R.G. Parton, H.T. McMahon, and R. Lundmark. 2011. The endocytic protein GRAF1 is directed to cell-matrix adhesion sites and regulates cell spreading. *Molecular biology of the cell*. 22:4380-4389.

Doherty, G.J., and R. Lundmark. 2009. GRAF1-dependent endocytosis. *Biochemical Society transactions*. 37:1061-1065.

Doherty, G.J., and H.T. McMahon. 2009. Mechanisms of endocytosis. *Annual review of biochemistry*. 78:857-902.

Dowdy, S.F. 2017. Overcoming cellular barriers for RNA therapeutics. *Nature biotechnology*. 35:222-229.

Dowrick, P., P. Kenworthy, B. McCann, and R. Warn. 1993. Circular ruffle formation and closure lead to macropinocytosis in hepatocyte growth factor/scatter factor-treated cells. *European journal of cell biology*. 61:44-53.

Dreux, M., U. Garaigorta, B. Boyd, E. Decembre, J. Chung, C. Whitten-Bauer, S. Wieland, and F.V. Chisari. 2012. Short-range exosomal transfer of viral RNA from infected cells to plasmacytoid dendritic cells triggers innate immunity. *Cell host & microbe*. 12:558-570.

Duijvesz, D., K.E. Burnum-Johnson, M.A. Gritsenko, A.M. Hoogland, M.S. Vredenbregt-van den Berg, R. Willemsen, T. Luider, L. Pasa-Tolic, and G. Jenster. 2013. Proteomic profiling of exosomes leads to the identification of novel biomarkers for prostate cancer. *PloS one*. 8:e82589.

Dutta, D., and J.G. Donaldson. 2012. Search for inhibitors of endocytosis: Intended specificity and unintended consequences. *Cellular logistics*. 2:203-208.

Dyson, M.R. 2016. Fundamentals of Expression in Mammalian Cells. *Advances in experimental medicine and biology*. 896:217-224.

Edgar, J.R. 2016. Q&A: What are exosomes, exactly? *BMC biology*. 14:46.

Eisenberg, E., and L.E. Greene. 2007. Multiple roles of auxilin and hsc70 in clathrin-mediated endocytosis. *Traffic (Copenhagen, Denmark)*. 8:640-646.

Escrevente, C., S. Keller, P. Altevogt, and J. Costa. 2011. Interaction and uptake of exosomes by ovarian cancer cells. *BMC cancer*. 11:108.

Even-Ram, S., A.D. Doyle, M.A. Conti, K. Matsumoto, R.S. Adelstein, and K.M. Yamada. 2007. Myosin IIA regulates cell motility and actomyosin-microtubule crosstalk. *Nature cell biology*. 9:299-309.

Falcone, S., E. Cocucci, P. Podini, T. Kirchhausen, E. Clementi, and J. Meldolesi. 2006. Macropinocytosis: regulated coordination of endocytic and exocytic membrane traffic events. *Journal of cell science*. 119:4758-4769.

Feliciano, W.D., S. Yoshida, S.W. Straight, and J.A. Swanson. 2011. Coordination of the Rab5 cycle on macropinosomes. *Traffic (Copenhagen, Denmark)*. 12:1911-1922.

Feng, D., W.L. Zhao, Y.Y. Ye, X.C. Bai, R.Q. Liu, L.F. Chang, Q. Zhou, and S.F. Sui. 2010. Cellular internalization of exosomes occurs through phagocytosis. *Traffic (Copenhagen, Denmark)*. 11:675-687.

Fire, A., S. Xu, M.K. Montgomery, S.A. Kostas, S.E. Driver, and C.C. Mello. 1998. Potent and specific genetic interference by double-stranded RNA in Caenorhabditis elegans. *Nature*. 391:806-811.

Fletcher, S.J., N.S. Poulter, E.J. Haining, and J.Z. Rappoport. 2012. Clathrin-mediated endocytosis regulates occludin, and not focal adhesion, distribution during epithelial wound healing. *Biology of the cell*. 104:238-256.

Fouad, Y.A., and C. Aanei. 2017. Revisiting the hallmarks of cancer. *American journal of cancer research*. 7:1016-1036.

Frank, P.G., M.W. Cheung, S. Pavlides, G. Llaverias, D.S. Park, and M.P. Lisanti. 2006. Caveolin-1 and regulation of cellular cholesterol homeostasis. *American journal of physiology. Heart and circulatory physiology*. 291:H677-686.

Franzen, C.A., P.E. Simms, A.F. Van Huis, K.E. Foreman, P.C. Kuo, and G.N. Gupta. 2014. Characterization of uptake and internalization of exosomes by bladder cancer cells. *Biomed Res Int*. 2014:619829.

Fujii, M., K. Kawai, Y. Egami, and N. Araki. 2013. Dissecting the roles of Rac1 activation and deactivation in macropinocytosis using microscopic photo-manipulation. *Scientific reports*. 3:2385.

Fujimoto, T. 1996. GPI-anchored proteins, glycosphingolipids, and sphingomyelin are sequestered to caveolae only after crosslinking. *The journal of histochemistry and cytochemistry : official journal of the Histochemistry Society*. 44:929-941.

Gammella, E., P. Buratti, G. Cairo, and S. Recalcati. 2017. The transferrin receptor: the cellular iron gate. *Metallomics : integrated biometal science*.

Garrett, W.S., L.M. Chen, R. Kroschewski, M. Ebersold, S. Turley, S. Trombetta, J.E. Galan, and I. Mellman. 2000. Developmental control of endocytosis in dendritic cells by Cdc42. *Cell*. 102:325-334.

Glebov, O.O., N.A. Bright, and B.J. Nichols. 2006. Flotillin-1 defines a clathrin-independent endocytic pathway in mammalian cells. *Nature cell biology*. 8:46-54.

Godlee, C., and M. Kaksonen. 2013. Review series: From uncertain beginnings: initiation mechanisms of clathrin-mediated endocytosis. *The Journal of cell biology*. 203:717-725.

Gopal, S.K., D.W. Greening, A. Rai, M. Chen, R. Xu, A. Shafiq, R.A. Mathias, H.J. Zhu, and R.J. Simpson. 2017. Extracellular vesicles: their role in cancer biology and epithelial-mesenchymal transition. *Biochem J*. 474:21-45.

Gould, S.J., and G. Raposo. 2013. As we wait: coping with an imperfect nomenclature for extracellular vesicles. *Journal of extracellular vesicles*. 2.

Ha, D., N. Yang, and V. Nadithe. 2016. Exosomes as therapeutic drug carriers and delivery vehicles across biological membranes: current perspectives and future challenges. *Acta pharmaceutica Sinica. B*. 6:287-296.

Haigler, H.T., J.A. McKanna, and S. Cohen. 1979. Rapid stimulation of pinocytosis in human carcinoma cells A-431 by epidermal growth factor. *The Journal of cell biology*. 83:82-90.

Hamilton, A.J., and D.C. Baulcombe. 1999. A species of small antisense RNA in posttranscriptional gene silencing in plants. *Science (New York, N.Y.)*. 286:950-952.

Hanahan, D., and R.A. Weinberg. 2011. Hallmarks of cancer: the next generation. *Cell*. 144:646-674.

Haney, M.J., N.L. Klyachko, Y. Zhao, R. Gupta, E.G. Plotnikova, Z. He, T. Patel, A. Piroyan, M. Sokolsky, A.V. Kabanov, and E.V. Batrakova. 2015. Exosomes as drug delivery vehicles for Parkinson's disease therapy. *Journal of controlled release : official journal of the Controlled Release Society*. 207:18-30.

Hansen, C.G., and B.J. Nichols. 2009. Molecular mechanisms of clathrin-independent endocytosis. *Journal of cell science*. 122:1713-1721.

Harding, C., J. Heuser, and P. Stahl. 1983. Receptor-mediated endocytosis of transferrin and recycling of the transferrin receptor in rat reticulocytes. *The Journal of cell biology*. 97:329-339.

Harper, C.B., S. Martin, T.H. Nguyen, S.J. Daniels, N.A. Lavidis, M.R. Popoff, G. Hadzic, A. Mariana, N. Chau, A. McCluskey, P.J. Robinson, and F.A. Meunier. 2011. Dynamin inhibition blocks botulinum neurotoxin type A endocytosis in neurons and delays botulism. *The Journal of biological chemistry*. 286:35966-35976.

Hayer, A., M. Stoeber, D. Ritz, S. Engel, H.H. Meyer, and A. Helenius. 2010. Caveolin-1 is ubiquitinated and targeted to intralumenal vesicles in endolysosomes for degradation. *The Journal of cell biology*. 191:615-629.

Henley, J.R., E.W. Krueger, B.J. Oswald, and M.A. McNiven. 1998. Dynamin-mediated internalization of caveolae. *The Journal of cell biology*. 141:85-99.

Henne, W.M., E. Boucrot, M. Meinecke, E. Evergren, Y. Vallis, R. Mittal, and H.T. McMahon. 2010. FCHo proteins are nucleators of clathrin-mediated endocytosis. *Science (New York, N.Y.)*. 328:1281-1284.

Heuser, J.E., and R.G. Anderson. 1989. Hypertonic media inhibit receptor-mediated endocytosis by blocking clathrin-coated pit formation. *The Journal of cell biology*. 108:389-400.

Heusermann, W., J. Hean, D. Trojer, E. Steib, S. von Bueren, A. Graff-Meyer, C. Genoud, K. Martin, N. Pizzato, J. Voshol, D.V. Morrissey, S.E.L. Andaloussi, M.J. Wood, and N.C. Meisner-Kober. 2016. Exosomes surf on filopodia to enter cells at endocytic hot spots, traffic within endosomes, and are targeted to the ER. *The Journal of cell biology*. 213:173-184.

Huang, L., W. Ma, Y. Ma, D. Feng, H. Chen, and B. Cai. 2015. Exosomes in mesenchymal stem cells, a new therapeutic strategy for cardiovascular diseases? *International journal of biological sciences*. 11:238-245.

Ivanov, A.I. 2008. Pharmacological inhibition of endocytic pathways: is it specific enough to be useful? *Methods in molecular biology (Clifton, N.J.)*. 440:15-33.

Ivaturi, S., C.J. Wooten, M.D. Nguyen, G.C. Ness, and D. Lopez. 2014. Distribution of the LDL receptor within clathrin-coated pits and caveolae in rat and human liver. *Biochemical and biophysical research communications*. 445:422-427.

Jackson, L.P., B.T. Kelly, A.J. McCoy, T. Gaffry, L.C. James, B.M. Collins, S. Honing, P.R. Evans, and D.J. Owen. 2010. A large-scale conformational change couples membrane recruitment to cargo binding in the AP2 clathrin adaptor complex. *Cell*. 141:1220-1229.

Jensen, E.C. 2012. Use of Fluorescent Probes: Their Effect on Cell Biology and Limitations. *The Anatomical Record: Advances in Integrative Anatomy and Evolutionary Biology*. 295:2031-2036.

Johnstone, R.M., M. Adam, J.R. Hammond, L. Orr, and C. Turbide. 1987. Vesicle formation during reticulocyte maturation. Association of plasma membrane activities with released vesicles (exosomes). *The Journal of biological chemistry*. 262:9412-9420.

Kalin, S., B. Amstutz, M. Gastaldelli, N. Wolfrum, K. Boucke, M. Havenga, F. DiGennaro, N. Liska, S. Hemmi, and U.F. Greber. 2010. Macropinocytotic uptake and infection of human epithelial cells with species B2 adenovirus type 35. *Journal of virology*. 84:5336-5350.

Kalra, H., R.J. Simpson, H. Ji, E. Aikawa, P. Altevogt, P. Askenase, V.C. Bond, F.E. Borras, X. Breakefield, V. Budnik, E. Buzas, G. Camussi, A. Clayton, E. Cocucci, J.M. Falcon-Perez, S. Gabrielsson, Y.S. Gho, D. Gupta, H.C. Harsha, A.

Hendrix, A.F. Hill, J.M. Inal, G. Jenster, E.M. Kramer-Albers, S.K. Lim, A. Llorente, J. Lotvall, A. Marcilla, L. Mincheva-Nilsson, I. Nazarenko, R. Nieuwland, E.N. Nolte-'t Hoen, A. Pandey, T. Patel, M.G. Piper, S. Pluchino, T.S. Prasad, L. Rajendran, G. Raposo, M. Record, G.E. Reid, F. Sanchez-Madrid, R.M. Schiffelers, P. Siljander, A. Stensballe, W. Stoorvogel, D. Taylor, C. Thery, H. Valadi, B.W. van Balkom, J. Vazquez, M. Vidal, M.H. Wauben, M. Yanez-Mo, M. Zoeller, and S. Mathivanan. 2012. Vesiclepedia: a compendium for extracellular vesicles with continuous community annotation. *PLoS biology*. 10:e1001450.

Kanwar, S.S., C.J. Dunlay, D.M. Simeone, and S. Nagrath. 2014. Microfluidic device (ExoChip) for on-chip isolation, quantification and characterization of circulating exosomes. *Lab on a chip*. 14:1891-1900.

Keller, S., J. Ridinger, A.K. Rupp, J.W. Janssen, and P. Altevogt. 2011. Body fluid derived exosomes as a novel template for clinical diagnostics. *Journal of translational medicine*. 9:86.

Kerr, M.C., and R.D. Teasdale. 2009. Defining macropinocytosis. *Traffic (Copenhagen, Denmark)*. 10:364-371.

Khvorova, A., and J.K. Watts. 2017. The chemical evolution of oligonucleotide therapies of clinical utility. *Nature biotechnology*. 35:238-248.

Kim, G.H., C.W. Choi, E.C. Park, S.Y. Lee, and S.I. Kim. 2014. Isolation and proteomic characterization of bacterial extracellular membrane vesicles. *Current protein & peptide science*. 15:719-731.

Kiss, A.L., and E. Botos. 2009. Endocytosis via caveolae: alternative pathway with distinct cellular compartments to avoid lysosomal degradation? *Journal of cellular and molecular medicine*. 13:1228-1237.

Koivusalo, M., C. Welch, H. Hayashi, C.C. Scott, M. Kim, T. Alexander, N. Touret, K.M. Hahn, and S. Grinstein. 2010. Amiloride inhibits macropinocytosis by lowering submembranous pH and preventing Rac1 and Cdc42 signaling. *The Journal of cell biology*. 188:547-563.

Kolsch, V., P.G. Charest, and R.A. Firtel. 2008. The regulation of cell motility and chemotaxis by phospholipid signaling. *Journal of cell science*. 121:551-559.

Kortholt, A., J.S. King, I. Keizer-Gunnink, A.J. Harwood, and P.J. Van Haastert. 2007. Phospholipase C regulation of phosphatidylinositol 3,4,5-trisphosphate-mediated chemotaxis. *Molecular biology of the cell*. 18:4772-4779.

Kosaka, N., Y. Yoshioka, K. Hagiwara, N. Tominaga, and T. Ochiya. 2013. Functional analysis of exosomal microRNA in cell-cell communication research. *Methods in molecular biology (Clifton, N.J.)*. 1024:1-10.

Kouwaki, T., Y. Fukushima, T. Daito, T. Sanada, N. Yamamoto, E.J. Mifsud, C.R. Leong, K. Tsukiyama-Kohara, M. Kohara, M. Matsumoto, T. Seya, and H.

Oshiumi. 2016. Extracellular Vesicles Including Exosomes Regulate Innate Immune Responses to Hepatitis B Virus Infection. *Frontiers in immunology*. 7:335.

Kouwaki, T., M. Okamoto, H. Tsukamoto, Y. Fukushima, and H. Oshiumi. 2017. Extracellular Vesicles Deliver Host and Virus RNA and Regulate Innate Immune Response. *International journal of molecular sciences*. 18.

Kovacs, M., J. Toth, C. Hetenyi, A. Malnasi-Csizmadia, and J.R. Sellers. 2004. Mechanism of blebbistatin inhibition of myosin II. *The Journal of biological chemistry*. 279:35557-35563.

Kowal, J., G. Arras, M. Colombo, M. Jouve, J.P. Morath, B. Primdal-Bengtson, F. Dingli, D. Loew, M. Tkach, and C. Thery. 2016. Proteomic comparison defines novel markers to characterize heterogeneous populations of extracellular vesicle subtypes. *Proceedings of the National Academy of Sciences of the United States of America*.

Kreimer, S., A.M. Belov, I. Ghiran, S.K. Murthy, D.A. Frank, and A.R. Ivanov. 2015. Mass-spectrometry-based molecular characterization of extracellular vesicles: lipidomics and proteomics. *Journal of proteome research*. 14:2367-2384.

Kristensen, M., D. Birch, and H. Morck Nielsen. 2016. Applications and Challenges for Use of Cell-Penetrating Peptides as Delivery Vectors for Peptide and Protein Cargos. *International journal of molecular sciences*. 17.

Lai, R.C., T.S. Chen, and S.K. Lim. 2011. Mesenchymal stem cell exosome: a novel stem cell-based therapy for cardiovascular disease. *Regenerative medicine*. 6:481-492.

Lajoie, P., and I.R. Nabi. 2007. Regulation of raft-dependent endocytosis. *Journal of cellular and molecular medicine*. 11:644-653.

Lange, H., and D. Gagliardi. 2012. Plant Exosomes and Cofactors. *The Enzymes*. 31:31-52.

Lefebvre, F.A., and E. Lecuyer. 2017. Small Luggage for a Long Journey: Transfer of Vesicle-Enclosed Small RNA in Interspecies Communication. *Frontiers in microbiology*. 8:377.

Li, L., T. Wan, M. Wan, B. Liu, R. Cheng, and R. Zhang. 2015. The effect of the size of fluorescent dextran on its endocytic pathway. *Cell Biol Int*. 39:531-539.

Li, X., C. Chen, L. Wei, Q. Li, X. Niu, Y. Xu, Y. Wang, and J. Zhao. 2016a. Exosomes derived from endothelial progenitor cells attenuate vascular repair and accelerate reendothelialization by enhancing endothelial function. *Cytotherapy*. 18:253-262.

Li, X., C. Jiang, and J. Zhao. 2016b. Human endothelial progenitor cells-derived exosomes accelerate cutaneous wound healing in diabetic rats by promoting endothelial function. *Journal of Diabetes and its Complications*. 30:986-992.

Liberali, P., E. Kakkonen, G. Turacchio, C. Valente, A. Spaar, G. Perinetti, R.A. Bockmann, D. Corda, A. Colanzi, V. Marjomaki, and A. Luini. 2008. The closure of Pak1-dependent macropinosomes requires the phosphorylation of CtBP1/BARS. *The EMBO journal*. 27:970-981.

Lim, J.P., and P.A. Gleeson. 2011. Macropinocytosis: an endocytic pathway for internalising large gulps. *Immunology and cell biology*. 89:836-843.

Lin, D., E.J. Kamsteeg, Y. Zhang, Y. Jin, H. Sterling, P. Yue, M. Roos, A. Duffield, J. Spencer, M. Caplan, and W.H. Wang. 2008. Expression of tetraspan protein CD63 activates protein-tyrosine kinase (PTK) and enhances the PTK-induced inhibition of ROMK channels. *The Journal of biological chemistry*. 283:7674-7681.

Liu, Y.W., J.P. Mattila, and S.L. Schmid. 2013. Dynamin-catalyzed membrane fission requires coordinated GTP hydrolysis. *PloS one*. 8:e55691.

Lotvall, J., A.F. Hill, F. Hochberg, E.I. Buzas, D. Di Vizio, C. Gardiner, Y.S. Gho, I.V. Kurochkin, S. Mathivanan, P. Quesenberry, S. Sahoo, H. Tahara, M.H. Wauben, K.W. Witwer, and C. Thery. 2014. Minimal experimental requirements for definition of extracellular vesicles and their functions: a position statement from the International Society for Extracellular Vesicles. *Journal of extracellular vesicles*. 3:26913.

Lundmark, R., G.J. Doherty, M.T. Howes, K. Cortese, Y. Vallis, R.G. Parton, and H.T. McMahon. 2008. The GTPase-activating protein GRAF1 regulates the CLIC/GEEC endocytic pathway. *Current biology : CB*. 18:1802-1808.

Maas, S.L., X.O. Breakefield, and A.M. Weaver. 2017. Extracellular Vesicles: Unique Intercellular Delivery Vehicles. *Trends in cell biology*. 27:172-188.

Macia, E., M. Ehrlich, R. Massol, E. Boucrot, C. Brunner, and T. Kirchhausen. 2006. Dynasore, a cell-permeable inhibitor of dynamin. *Developmental cell*. 10:839-850.

Maderna, P., and C. Godson. 2003. Phagocytosis of apoptotic cells and the resolution of inflammation. *Biochimica et biophysica acta*. 1639:141-151.

Manjila, S.B., J.N. Baby, E.N. Bijin, I. Constantine, K. Pramod, and J. Valsalakumari. 2013. Novel gene delivery systems. *International journal of pharmaceutical investigation*. 3:1-7.

Masimirembwa, C.M., U. Bredberg, and T.B. Andersson. 2003. Metabolic stability for drug discovery and development: pharmacokinetic and biochemical challenges. Clinical pharmacokinetics. 42:515-528.

Mathivanan, S., J.W. Lim, B.J. Tauro, H. Ji, R.L. Moritz, and R.J. Simpson. 2010. Proteomics analysis of A33 immunoaffinity-purified exosomes released from the human colon tumor cell line LIM1215 reveals a tissue-specific protein signature. *Molecular & cellular proteomics : MCP*. 9:197-208.

Matsumura, T., K. Sugimachi, H. Iinuma, Y. Takahashi, J. Kurashige, G. Sawada, M. Ueda, R. Uchi, H. Ueo, Y. Takano, Y. Shinden, H. Eguchi, H. Yamamoto, Y. Doki, M. Mori, T. Ochiya, and K. Mimori. 2015. Exosomal microRNA in serum is a novel biomarker of recurrence in human colorectal cancer. *British journal of cancer*. 113:275-281.

Mayle, K.M., A.M. Le, and D.T. Kamei. 2012. The intracellular trafficking pathway of transferrin. *Biochimica et biophysica acta*. 1820:264-281.

McCluskey, A., J.A. Daniel, G. Hadzic, N. Chau, E.L. Clayton, A. Mariana, A. Whiting, N.N. Gorgani, J. Lloyd, A. Quan, L. Moshkanbaryans, S. Krishnan, S. Perera, M. Chircop, L. von Kleist, A.B. McGeachie, M.T. Howes, R.G. Parton, M. Campbell, J.A. Sakoff, X. Wang, J.Y. Sun, M.J. Robertson, F.M. Deane, T.H. Nguyen, F.A. Meunier, M.A. Cousin, and P.J. Robinson. 2013. Building a better dynasore: the dyngo compounds potently inhibit dynamin and endocytosis. *Traffic (Copenhagen, Denmark)*. 14:1272-1289.

McMahon, H.T., and E. Boucrot. 2011. Molecular mechanism and physiological functions of clathrin-mediated endocytosis. *Nature reviews. Molecular cell biology*. 12:517-533.

Meehan, K., and L.J. Vella. 2016. The contribution of tumour-derived exosomes to the hallmarks of cancer. *Critical reviews in clinical laboratory sciences*. 53:121-131.

Mehta, P., J. Henault, R. Kolbeck, and M.A. Sanjuan. 2014. Noncanonical autophagy: one small step for LC3, one giant leap for immunity. *Current opinion in immunology*. 26c:69-75.

Menon, M., O.L. Askinazi, and D.A. Schafer. 2014. Dynamin2 organizes lamellipodial actin networks to orchestrate lamellar actomyosin. *PloS one*. 9:e94330.

Menon, M., and D.A. Schafer. 2013. Dynamin: expanding its scope to the cytoskeleton. *International review of cell and molecular biology*. 302:187-219.

Mercer, J., and A. Helenius. 2009. Virus entry by macropinocytosis. *Nature cell biology*. 11:510-520.

Mercer, J., S. Knebel, F.I. Schmidt, J. Crouse, C. Burkard, and A. Helenius. 2010. Vaccinia virus strains use distinct forms of macropinocytosis for host-cell entry. *Proceedings of the National Academy of Sciences of the United States of America*. 107:9346-9351.

Mettlen, M., T. Pucadyil, R. Ramachandran, and S.L. Schmid. 2009. Dissecting dynamin's role in clathrin-mediated endocytosis. *Biochemical Society transactions*. 37:1022-1026.

Mingozzi, F., and K.A. High. 2011. Immune responses to AAV in clinical trials. *Current gene therapy*. 11:321-330.

Mingozzi, F., and K.A. High. 2013. Immune responses to AAV vectors: overcoming barriers to successful gene therapy. *Blood*. 122:23-36.

Mittelbrunn, M., C. Gutierrez-Vazquez, C. Villarroya-Beltri, S. Gonzalez, F. Sanchez-Cabo, M.A. Gonzalez, A. Bernad, and F. Sanchez-Madrid. 2011. Unidirectional transfer of microRNA-loaded exosomes from T cells to antigen-presenting cells. *Nature communications*. 2:282.

Mol, E.A., M.J. Goumans, P.A. Doevendans, J.P. Sluijter, and P. Vader. 2017. Higher functionality of extracellular vesicles isolated using size-exclusion chromatography compared to ultracentrifugation. *Nanomedicine : nanotechnology, biology, and medicine*.

Mooren, O.L., T.I. Kotova, A.J. Moore, and D.A. Schafer. 2009. Dynamin2 GTPase and cortactin remodel actin filaments. *The Journal of biological chemistry*. 284:23995-24005.

Morelli, A.E., A.T. Larregina, W.J. Shufesky, M.L. Sullivan, D.B. Stolz, G.D. Papworth, A.F. Zahorchak, A.J. Logar, Z. Wang, S.C. Watkins, L.D. Falo, Jr., and A.W. Thomson. 2004. Endocytosis, intracellular sorting, and processing of exosomes by dendritic cells. *Blood*. 104:3257-3266.

Moriyama, T., K. Sasaki, K. Karasawa, K. Uchida, and K. Nitta. 2017. Intracellular transcytosis of albumin in glomerular endothelial cells after endocytosis through caveolae. *Journal of cellular physiology*. 232:3565-3573.

Mulcahy, L.A., R.C. Pink, and D.R. Carter. 2014. Routes and mechanisms of extracellular vesicle uptake. *Journal of extracellular vesicles*. 3.

Murata, M., J. Peranen, R. Schreiner, F. Wieland, T.V. Kurzchalia, and K. Simons. 1995. VIP21/caveolin is a cholesterol-binding protein. *Proceedings of the National Academy of Sciences of the United States of America*. 92:10339-10343.

Myers, M.D., and G.S. Payne. 2013. Clathrin, adaptors and disease: insights from the yeast Saccharomyces cerevisiae. *Frontiers in bioscience (Landmark edition)*. 18:862-891.

Nakase, I., and S. Futaki. 2015. Combined treatment with a pH-sensitive fusogenic peptide and cationic lipids achieves enhanced cytosolic delivery of exosomes. *Scientific reports*. 5:10112.

Nakase, I., N.B. Kobayashi, T. Takatani-Nakase, and T. Yoshida. 2015. Active macropinocytosis induction by stimulation of epidermal growth factor receptor and oncogenic Ras expression potentiates cellular uptake efficacy of exosomes. *Scientific reports*. 5:10300.

Nakase, I., M. Niwa, T. Takeuchi, K. Sonomura, N. Kawabata, Y. Koike, M. Takehashi, S. Tanaka, K. Ueda, J.C. Simpson, A.T. Jones, Y. Sugiura, and S. Futaki. 2004. Cellular uptake of arginine-rich peptides: roles for macropinocytosis and actin rearrangement. *Molecular therapy : the journal of the American Society of Gene Therapy*. 10:1011-1022.

Nakase, I., K. Noguchi, A. Aoki, T. Takatani-Nakase, I. Fujii, and S. Futaki. 2017. Arginine-rich cell-penetrating peptide-modified extracellular vesicles for active macropinocytosis induction and efficient intracellular delivery. *Scientific reports*. 7:1991.

Nakase, I., K. Noguchi, I. Fujii, and S. Futaki. 2016. Vectorization of biomacromolecules into cells using extracellular vesicles with enhanced internalization induced by macropinocytosis. *Scientific reports*. 6:34937.

Nankoe, S.R., and S. Sever. 2006. Dynasore puts a new spin on dynamin: a surprising dual role during vesicle formation. *Trends in cell biology*. 16:607-609.

Naslavsky, N., R. Weigert, and J.G. Donaldson. 2004. Characterization of a nonclathrin endocytic pathway: membrane cargo and lipid requirements. *Molecular biology of the cell*. 15:3542-3552.

Nedaeinia, R., M. Manian, M.H. Jazayeri, M. Ranjbar, R. Salehi, M. Sharifi, F. Mohaghegh, M. Goli, S.H. Jahednia, A. Avan, and M. Ghayour-Mobarhan. 2017. Circulating exosomes and exosomal microRNAs as biomarkers in gastrointestinal cancer. *Cancer gene therapy*. 24:48-56.

Nichols, B. 2003. Caveosomes and endocytosis of lipid rafts. *Journal of cell science*. 116:4707-4714.

Nichols, B.J. 2002. A distinct class of endosome mediates clathrin-independent endocytosis to the Golgi complex. *Nature cell biology*. 4:374-378.

Nolte-'t Hoen, E.N., H.P. Buermans, M. Waasdorp, W. Stoorvogel, M.H. Wauben, and P.A. t Hoen. 2012. Deep sequencing of RNA from immune cell-derived vesicles uncovers the selective incorporation of small non-coding RNA biotypes with potential regulatory functions. *Nucleic acids research*. 40:9272-9285.

Ogata-Kawata, H., M. Izumiya, D. Kurioka, Y. Honma, Y. Yamada, K. Furuta, T. Gunji, H. Ohta, H. Okamoto, H. Sonoda, M. Watanabe, H. Nakagama, J. Yokota, T. Kohno, and N. Tsuchiya. 2014. Circulating exosomal microRNAs as biomarkers of colon cancer. *PloS one*. 9:e92921.

Oh, P., T. Horner, H. Witkiewicz, and J.E. Schnitzer. 2012. Endothelin induces rapid, dynamin-mediated budding of endothelial caveolae rich in ET-B. *The Journal of biological chemistry*. 287:17353-17362.

Okada, R., Y. Yamauchi, T. Hongu, Y. Funakoshi, N. Ohbayashi, H. Hasegawa, and Y. Kanaho. 2015. Activation of the Small G Protein Arf6 by Dynamin2 through Guanine Nucleotide Exchange Factors in Endocytosis. *Scientific reports*. 5:14919.

Parker-Duffen, J.L., K. Nakamura, M. Silver, R. Kikuchi, U. Tigges, S. Yoshida, M.S. Denzel, B. Ranscht, and K. Walsh. 2013. T-cadherin Is Essential for Adiponectin-mediated Revascularization. *The Journal of biological chemistry*. 288:24886-24897.

Parton, R.G., and M.A. del Pozo. 2013. Caveolae as plasma membrane sensors, protectors and organizers. *Nature reviews. Molecular cell biology*. 14:98-112.

Parton, R.G., and M.T. Howes. 2010. Revisiting caveolin trafficking: the end of the caveosome. *The Journal of cell biology*. 191:439-441.

Parton, R.G., and K. Simons. 2007. The multiple faces of caveolae. *Nature reviews. Molecular cell biology*. 8:185-194.

Pearse, B.M., and M.S. Robinson. 1990. Clathrin, adaptors, and sorting. *Annual review of cell biology*. 6:151-171.

Pellon-Cardenas, O., J. Clancy, H. Uwimpuhwe, and C. D'Souza-Schorey. 2013. ARF6-regulated endocytosis of growth factor receptors links cadherin-based adhesion to canonical Wnt signaling in epithelia. *Molecular and cellular biology*. 33:2963-2975.

Penfornis, P., K.C. Vallabhaneni, J. Whitt, and R. Pochampally. 2016. Extracellular vesicles as carriers of microRNA, proteins and lipids in tumor microenvironment. *International journal of cancer*. 138:14-21.

Perez-Hernandez, D., C. Gutierrez-Vazquez, I. Jorge, S. Lopez-Martin, A. Ursa, F. Sanchez-Madrid, J. Vazquez, and M. Yanez-Mo. 2013. The intracellular interactome of tetraspanin-enriched microdomains reveals their function as

sorting machineries toward exosomes. *The Journal of biological chemistry*. 288:11649-11661.

Pickup, M.W., J.K. Mouw, and V.M. Weaver. 2014. The extracellular matrix modulates the hallmarks of cancer. *EMBO reports*. 15:1243-1253.

Ponnambalam, S., and S.A. Baldwin. 2003. Constitutive protein secretion from the trans-Golgi network to the plasma membrane. *Molecular membrane biology*. 20:129-139.

Preta, G., J.G. Cronin, and I.M. Sheldon. 2015. Dynasore - not just a dynamin inhibitor. *Cell communication and signaling : CCS*. 13:24.

Qin, J., and Q. Xu. 2014. Functions and application of exosomes. *Acta poloniae pharmaceutica*. 71:537-543.

Quah, B.J., and H.C. O'Neill. 2005. The immunogenicity of dendritic cell-derived exosomes. *Blood cells, molecules & diseases*. 35:94-110.

Que, R., G. Ding, J. Chen, and L. Cao. 2013. Analysis of serum exosomal microRNAs and clinicopathologic features of patients with pancreatic adenocarcinoma. *World journal of surgical oncology*. 11:219.

Radhakrishna, H., and J.G. Donaldson. 1997. ADP-ribosylation factor 6 regulates a novel plasma membrane recycling pathway. *The Journal of cell biology*. 139:49-61.

Raposo, G., H.W. Nijman, W. Stoorvogel, R. Liejendekker, C.V. Harding, C.J. Melief, and H.J. Geuze. 1996. B lymphocytes secrete antigen-presenting vesicles. *The Journal of experimental medicine*. 183:1161-1172.

Raposo, G., and W. Stoorvogel. 2013. Extracellular vesicles: exosomes, microvesicles, and friends. *The Journal of cell biology*. 200:373-383.

Redelman-Sidi, G., G. Iyer, D.B. Solit, and M.S. Glickman. 2013. Oncogenic activation of Pak1-dependent pathway of macropinocytosis determines BCG entry into bladder cancer cells. *Cancer research*. 73:1156-1167.

Ren, K., C. Gao, J. Zhang, K. Wang, Y. Xu, S.B. Wang, H. Wang, C. Tian, Q. Shi, and X.P. Dong. 2013. Flotillin-1 mediates PrPc endocytosis in the cultured cells during Cu(2)(+) stimulation through molecular interaction. *Molecular neurobiology*. 48:631-646.

Renard, H.-F., M. Simunovic, J. Lemiere, E. Boucrot, M.D. Garcia-Castillo, S. Arumugam, V. Chambon, C. Lamaze, C. Wunder, A.K. Kenworthy, A.A. Schmidt, H.T. McMahon, C. Sykes, P. Bassereau, and L. Johannes. 2015. Endophilin-A2 functions in membrane scission in clathrin-independent endocytosis. *Nature*. 517:493-496.

Rijnboutt, S., G. Jansen, G. Posthuma, J.B. Hynes, J.H. Schornagel, and G.J. Strous. 1996. Endocytosis of GPI-linked membrane folate receptor-alpha. *The Journal of cell biology*. 132:35-47.

Robbins, P.D., and A.E. Morelli. 2014. Regulation of immune responses by extracellular vesicles. *Nature reviews. Immunology*. 14:195-208.

Robinson, M.S. 2015. Forty Years of Clathrin-coated Vesicles. *Traffic (Copenhagen, Denmark)*. 16:1210-1238.

Rodal, S.K., G. Skretting, O. Garred, F. Vilhardt, B. van Deurs, and K. Sandvig. 1999. Extraction of cholesterol with methyl-beta-cyclodextrin perturbs formation of clathrin-coated endocytic vesicles. *Molecular biology of the cell*. 10:961-974.

Rodrigues, M.L., J.D. Nosanchuk, A. Schrank, M.H. Vainstein, A. Casadevall, and L. Nimrichter. 2011. Vesicular transport systems in fungi. *Future microbiology*. 6:1371-1381.

Romao, S., and C. Munz. 2014. LC3-associated phagocytosis. *Autophagy*. 10.

Rondina, M.T., and A.S. Weyrich. 2016. Arf6 arbitrates fibrinogen endocytosis. *Blood*. 127:1383-1384.

Rufino-Ramos, D., P.R. Albuquerque, V. Carmona, R. Perfeito, R.J. Nobre, and L. Pereira de Almeida. 2017. Extracellular vesicles: Novel promising delivery systems for therapy of brain diseases. *Journal of controlled release : official journal of the Controlled Release Society*. 262:247-258.

Ruiz-Argüelles, A., and L. Llorente. 2007. The role of complement regulatory proteins (CD55 and CD59) in the pathogenesis of autoimmune hemocytopenias. *Autoimmunity Reviews*. 6:155-161.

S, E.L.A., I. Mager, X.O. Breakefield, and M.J. Wood. 2013. Extracellular vesicles: biology and emerging therapeutic opportunities. *Nature reviews. Drug discovery*. 12:347-357.

Saffari, M., H.R. Moghimi, and C.R. Dass. 2016. Barriers to Liposomal Gene Delivery: from Application Site to the Target. *Iranian journal of pharmaceutical research : IJPR*. 15:3-17.

Sahoo, S., and D.W. Losordo. 2014. Exosomes and cardiac repair after myocardial infarction. *Circulation research*. 114:333-344.

Sandgren, K.J., J. Wilkinson, M. Miranda-Saksena, G.M. McInerney, K. Byth-Wilson, P.J. Robinson, and A.L. Cunningham. 2010. A differential role for macropinocytosis in mediating entry of the two forms of vaccinia virus into dendritic cells. *PLoS Pathog*. 6:e1000866.

Sarkar, K., M.J. Kruhlak, S.L. Erlandsen, and S. Shaw. 2005. Selective inhibition by rottlerin of macropinocytosis in monocyte-derived dendritic cells. *Immunology*. 116:513-524.

Schmidt, O., and D. Teis. 2012. The ESCRT machinery. *Current biology : CB*. 22:R116-120.

Schwarzenbach, H. 2015. The clinical relevance of circulating, exosomal miRNAs as biomarkers for cancer. *Expert review of molecular diagnostics*. 15:1159-1169.

Scotti, E., M. Calamai, C.N. Goulbourne, L. Zhang, C. Hong, R.R. Lin, J. Choi, P.F. Pilch, L.G. Fong, P. Zou, A.Y. Ting, F.S. Pavone, S.G. Young, and P. Tontonoz. 2013. IDOL stimulates clathrin-independent endocytosis and multivesicular body-mediated lysosomal degradation of the low-density lipoprotein receptor. *Molecular and cellular biology*. 33:1503-1514.

Sharma, D.K., A. Choudhury, R.D. Singh, C.L. Wheatley, D.L. Marks, and R.E. Pagano. 2003. Glycosphingolipids internalized via caveolar-related endocytosis rapidly merge with the clathrin pathway in early endosomes and form microdomains for recycling. *The Journal of biological chemistry*. 278:7564-7572.

Shiba, Y., S. Kametaka, S. Waguri, J.F. Presley, and P.A. Randazzo. 2013. ArfGAP3 regulates the transport of cation-independent mannose 6-phosphate receptor in the post-Golgi compartment. *Current biology : CB*. 23:1945-1951.

Shutova, M., C. Yang, J.M. Vasiliev, and T. Svitkina. 2012. Functions of nonmuscle myosin II in assembly of the cellular contractile system. *PloS one*. 7:e40814.

Sigismund, S., T. Woelk, C. Puri, E. Maspero, C. Tacchetti, P. Transidico, P.P. Di Fiore, and S. Polo. 2005. Clathrin-independent endocytosis of ubiquitinated cargos.

Proceedings of the National Academy of Sciences of the United States of America. 102:2760-2765.

Simpson, R.J., J.W. Lim, R.L. Moritz, and S. Mathivanan. 2009. Exosomes: proteomic insights and diagnostic potential. *Expert review of proteomics*. 6:267-283.

Singh, P.P., L. Li, and J.S. Schorey. 2015. Exosomal RNA from Mycobacterium tuberculosis-Infected Cells Is Functional in Recipient Macrophages. *Traffic (Copenhagen, Denmark)*. 16:555-571.

Singh, P.P., V.L. Smith, P.C. Karakousis, and J.S. Schorey. 2012. Exosomes isolated from mycobacteria-infected mice or cultured macrophages can recruit and activate immune cells in vitro and in vivo. *Journal of immunology (Baltimore, Md. : 1950)*. 189:777-785.

Singh, R.D., V. Puri, J.T. Valiyaveettil, D.L. Marks, R. Bittman, and R.E. Pagano. 2003. Selective caveolin-1-dependent endocytosis of glycosphingolipids. *Molecular biology of the cell*. 14:3254-3265.

Skubis-Zegadlo, J., A. Stachurska, and M. Malecki. 2013. Vectrology of adeno-associated viruses (AAV). *Medycyna wieku rozwojowego*. 17:202-206.

Steffen, A., M. Ladwein, G.A. Dimchev, A. Hein, L. Schwenkmezger, S. Arens, K.I. Ladwein, J. Margit Holleboom, F. Schur, J. Victor Small, J. Schwarz, R. Gerhard, J. Faix, T.E. Stradal, C. Brakebusch, and K. Rottner. 2013. Rac

function is crucial for cell migration but is not required for spreading and focal adhesion formation. *Journal of cell science*. 126:4572-4588.

Suetsugu, A., K. Honma, S. Saji, H. Moriwaki, T. Ochiya, and R.M. Hoffman. 2013. Imaging exosome transfer from breast cancer cells to stroma at metastatic sites in orthotopic nude-mouse models. *Advanced drug delivery reviews*. 65:383-390.

Sugita, Y., and Y. Masuho. 1995. CD59: its role in complement regulation and potential for therapeutic use. *Immunotechnology : an international journal of immunological engineering*. 1:157-168.

Sun, S.W., X.Y. Zu, Q.H. Tuo, L.X. Chen, X.Y. Lei, K. Li, C.K. Tang, and D.F. Liao. 2010. Caveolae and caveolin-1 mediate endocytosis and transcytosis of oxidized low density lipoprotein in endothelial cells. *Acta pharmacologica Sinica*. 31:1336-1342.

Svensson, K.J., H.C. Christianson, A. Wittrup, E. Bourseau-Guilmain, E. Lindqvist, L.M. Svensson, M. Morgelin, and M. Belting. 2013. Exosome uptake depends on ERK1/2-heat shock protein 27 signaling and lipid Raft-mediated endocytosis negatively regulated by caveolin-1. *The Journal of biological chemistry*. 288:17713-17724.

Swanson, J.A. 2008. Shaping cups into phagosomes and macropinosomes. *Nature reviews. Molecular cell biology*. 9:639-649.

Szatanek, R., J. Baran, M. Siedlar, and M. Baj-Krzyworzeka. 2015. Isolation of extracellular vesicles: Determining the correct approach (Review). *International journal of molecular medicine*. 36:11-17.

Szczepanski, M.J., M. Szajnik, A. Welsh, T.L. Whiteside, and M. Boyiadzis. 2011. Blast-derived microvesicles in sera from patients with acute myeloid leukemia suppress natural killer cell function via membrane-associated transforming growth factor-beta1. *Haematologica*. 96:1302-1309.

Takahashi, R.U., M. Prieto-Vila, A. Hironaka, and T. Ochiya. 2017. The role of extracellular vesicle microRNAs in cancer biology. *Clinical chemistry and laboratory medicine*. 55:648-656.

Takei, K., and V. Haucke. 2001. Clathrin-mediated endocytosis: membrane factors pull the trigger. *Trends in cell biology*. 11:385-391.

Tang, W., J.H. Tam, C. Seah, J. Chiu, A. Tyrer, S.P. Cregan, S.O. Meakin, and S.H. Pasternak. 2015. Arf6 controls beta-amyloid production by regulating macropinocytosis of the Amyloid Precursor Protein to lysosomes. *Mol Brain*. 8:41.

Tauro, B.J., D.W. Greening, R.A. Mathias, H. Ji, S. Mathivanan, A.M. Scott, and R.J. Simpson. 2012. Comparison of ultracentrifugation, density gradient separation, and immunoaffinity capture methods for isolating human colon cancer cell line LIM1863-derived exosomes. *Methods (San Diego, Calif.)*. 56:293-304.

Taylor, D.D., and S. Shah. 2015. Methods of isolating extracellular vesicles impact down-stream analyses of their cargoes. *Methods (San Diego, Calif.)*. 87:3-10.

Temchura, V.V., M. Tenbusch, G. Nchinda, G. Nabi, B. Tippler, M. Zelenyuk, O. Wildner, K. Uberla, and S. Kuate. 2008. Enhancement of immunostimulatory properties of exosomal vaccines by incorporation of fusion-competent G protein of vesicular stomatitis virus. *Vaccine*. 26:3662-3672.

Thakur, B.K., H. Zhang, A. Becker, I. Matei, Y. Huang, B. Costa-Silva, Y. Zheng, A. Hoshino, H. Brazier, J. Xiang, C. Williams, R. Rodriguez-Barrueco, J.M. Silva, W. Zhang, S. Hearn, O. Elemento, N. Paknejad, K. Manova-Todorova, K. Welte, J. Bromberg, H. Peinado, and D. Lyden. 2014. Double-stranded DNA in exosomes: a novel biomarker in cancer detection. *Cell research*. 24:766-769.

Thery, C., S. Amigorena, G. Raposo, and A. Clayton. 2006. Isolation and characterization of exosomes from cell culture supernatants and biological fluids. *Current protocols in cell biology / editorial board, Juan S. Bonifacino ... [et al.]*. Chapter 3:Unit 3.22.

Thery, C., L. Zitvogel, and S. Amigorena. 2002. Exosomes: composition, biogenesis and function. *Nature reviews. Immunology*. 2:569-579.

Thomas, C.E., A. Ehrhardt, and M.A. Kay. 2003. Progress and problems with the use of viral vectors for gene therapy. *Nature reviews. Genetics*. 4:346-358.

Tian, T., Y. Wang, H. Wang, Z. Zhu, and Z. Xiao. 2010. Visualizing of the cellular uptake and intracellular trafficking of exosomes by live-cell microscopy. *Journal of cellular biochemistry*. 111:488-496.

Tian, T., Y.L. Zhu, Y.Y. Zhou, G.F. Liang, Y.Y. Wang, F.H. Hu, and Z.D. Xiao. 2014a. Exosome uptake through clathrin-mediated endocytosis and macropinocytosis and mediating miR-21 delivery. *The Journal of biological chemistry*. 289:22258-22267.

Tian, Y., S. Li, J. Song, T. Ji, M. Zhu, G.J. Anderson, J. Wei, and G. Nie. 2014b. A doxorubicin delivery platform using engineered natural membrane vesicle exosomes for targeted tumor therapy. *Biomaterials*. 35:2383-2390.

Tkach, M., and C. Thery. 2016. Communication by Extracellular Vesicles: Where We Are and Where We Need to Go. *Cell*. 164:1226-1232.

Torgersen, M.L., G. Skretting, B. van Deurs, and K. Sandvig. 2001. Internalization of cholera toxin by different endocytic mechanisms. *Journal of cell science*. 114:3737-3747.

Trams, E.G., C.J. Lauter, N. Salem, Jr., and U. Heine. 1981. Exfoliation of membrane ecto-enzymes in the form of micro-vesicles. *Biochimica et biophysica acta*. 645:63-70.

Tyagi, P., and J.L. Santos. 2018. Macromolecule nanotherapeutics: approaches and challenges. Drug discovery today.

Umasankar, P.K., S. Sanker, J.R. Thieman, S. Chakraborty, B. Wendland, M. Tsang, and L.M. Traub. 2012. Distinct and separable activities of the endocytic clathrin-coat components Fcho1/2 and AP-2 in developmental patterning. *Nature cell biology*. 14:488-501.

Underhill, D.M., and A. Ozinsky. 2002. Phagocytosis of microbes: complexity in action. *Annual review of immunology*. 20:825-852.

Vader, P., E.A. Mol, G. Pasterkamp, and R.M. Schiffelers. 2016. Extracellular vesicles for drug delivery. *Advanced drug delivery reviews*. 106:148-156.

Valente, C., A. Luini, and D. Corda. 2013. Components of the CtBP1/BARS-dependent fission machinery. *Histochemistry and cell biology*. 140:407-421.

van der Bliek, A.M., Q. Shen, and S. Kawajiri. 2013. Mechanisms of mitochondrial fission and fusion. *Cold Spring Harbor perspectives in biology*. 5.

van der Meel, R., M.H. Fens, P. Vader, W.W. van Solinge, O. Eniola-Adefeso, and R.M. Schiffelers. 2014. Extracellular vesicles as drug delivery systems: Lessons from the liposome field. *Journal of controlled release : official journal of the Controlled Release Society*.

Van Deun, J., P. Mestdagh, R. Sormunen, V. Cocquyt, K. Vermaelen, J. Vandesompele, M. Bracke, O. De Wever, and A. Hendrix. 2014. The impact of disparate isolation methods for extracellular vesicles on downstream RNA profiling. *Journal of extracellular vesicles*. 3.

van Dommelen, S.M., P. Vader, S. Lakhal, S.A. Kooijmans, W.W. van Solinge, M.J. Wood, and R.M. Schiffelers. 2012. Microvesicles and exosomes: opportunities for cell-derived membrane vesicles in drug delivery. *Journal of controlled release : official journal of the Controlled Release Society*. 161:635-644.

Van Giau, V., and S.S. An. 2016. Emergence of exosomal miRNAs as a diagnostic biomarker for Alzheimer's disease. *Journal of the neurological sciences*. 360:141-152.

Veldhoen, S., S.D. Laufer, and T. Restle. 2008. Recent developments in peptide-based nucleic acid delivery. *International journal of molecular sciences*. 9:1276-1320.

Vercauteren, D., M. Piest, L.J. van der Aa, M. Al Soraj, A.T. Jones, J.F. Engbersen, S.C. De Smedt, and K. Braeckmans. 2011. Flotillin-dependent endocytosis and a phagocytosis-like mechanism for cellular internalization of disulfide-based poly(amido amine)/DNA polyplexes. *Biomaterials*. 32:3072-3084.

Vercauteren, D., J. Rejman, T.F. Martens, J. Demeester, S.C. De Smedt, and K. Braeckmans. 2012. On the cellular processing of non-viral nanomedicines for nucleic acid delivery: mechanisms and methods. *Journal of controlled release : official journal of the Controlled Release Society*. 161:566-581.

Vercauteren, D., R.E. Vandenbroucke, A.T. Jones, J. Rejman, J. Demeester, S.C. De Smedt, N.N. Sanders, and K. Braeckmans. 2010. The use of inhibitors to

study endocytic pathways of gene carriers: optimization and pitfalls. *Molecular therapy : the journal of the American Society of Gene Therapy*. 18:561-569.

Vieira, A.V., C. Lamaze, and S.L. Schmid. 1996. Control of EGF receptor signaling by clathrin-mediated endocytosis. *Science (New York, N.Y.)*. 274:2086-2089.

Villarroya-Beltri, C., F. Baixauli, C. Gutierrez-Vazquez, F. Sanchez-Madrid, and M. Mittelbrunn. 2014. Sorting it out: regulation of exosome loading. *Seminars in cancer biology*. 28:3-13.

Villarroya-Beltri, C., C. Gutierrez-Vazquez, F. Sanchez-Cabo, D. Perez-Hernandez, J. Vazquez, N. Martin-Cofreces, D.J. Martinez-Herrera, A. Pascual-Montano, M. Mittelbrunn, and F. Sanchez-Madrid. 2013. Sumoylated hnRNPA2B1 controls the sorting of miRNAs into exosomes through binding to specific motifs. *Nature communications*. 4:2980.

Vlassov, A.V., S. Magdaleno, R. Setterquist, and R. Conrad. 2012. Exosomes: current knowledge of their composition, biological functions, and diagnostic and therapeutic potentials. *Biochimica et biophysica acta*. 1820:940-948.

Wang, Y., Y. Yang, X. Liu, N. Wang, H. Cao, Y. Lu, H. Zhou, and J. Zheng. 2012. Inhibition of clathrin/dynamin-dependent internalization interferes with LPS-mediated TRAM-TRIF-dependent signaling pathway. *Cellular immunology*. 274:121-129.

Watkins, C.L., D. Schmaljohann, S. Futaki, and A.T. Jones. 2009. Low concentration thresholds of plasma membranes for rapid energy-independent translocation of a cell-penetrating peptide. *Biochem J*. 420:179-189.

Webber, J., and A. Clayton. 2013. How pure are your vesicles? *Journal of extracellular vesicles*. 2.

Webber, J., T.C. Stone, E. Katilius, B.C. Smith, B. Gordon, M.D. Mason, Z. Tabi, I.A. Brewis, and A. Clayton. 2014. Proteomics analysis of cancer exosomes using a novel modified aptamer-based array (SOMAscan) platform. *Molecular & cellular proteomics : MCP*. 13:1050-1064.

Webber, J., V. Yeung, and A. Clayton. 2015. Extracellular vesicles as modulators of the cancer microenvironment. *Seminars in cell & developmental biology*. 40:27-34.

West, M.A., A.R. Prescott, E.L. Eskelinen, A.J. Ridley, and C. Watts. 2000. Rac is required for constitutive macropinocytosis by dendritic cells but does not control its downregulation. *Current biology : CB*. 10:839-848.

Whiteside, T.L. 2017. Exosomes carrying immunoinhibitory proteins and their role in cancer. *Clinical and experimental immunology*.

Wieckowski, E.U., C. Visus, M. Szajnik, M.J. Szczepanski, W.J. Storkus, and T.L. Whiteside. 2009. Tumor-derived microvesicles promote regulatory T cell expansion and induce apoptosis in tumor-reactive activated CD8+ T

lymphocytes. *Journal of immunology (Baltimore, Md. : 1950)*. 183:3720-3730.

Williams, T.M., and M.P. Lisanti. 2004. The Caveolin genes: from cell biology to medicine. *Annals of medicine*. 36:584-595.

Witwer, K.W., E.I. Buzas, L.T. Bemis, A. Bora, C. Lasser, J. Lotvall, E.N. Nolte-'t Hoen, M.G. Piper, S. Sivaraman, J. Skog, C. Thery, M.H. Wauben, and F. Hochberg. 2013. Standardization of sample collection, isolation and analysis methods in extracellular vesicle research. *Journal of extracellular vesicles*. 2.

Wolf, P. 1967. The nature and significance of platelet products in human plasma. *British journal of haematology*. 13:269-288.

Wu, X., T. Zheng, and B. Zhang. 2017. Exosomes in Parkinson's Disease. *Neuroscience bulletin*. 33:331-338.

Xing, Y., T. Bocking, M. Wolf, N. Grigorieff, T. Kirchhausen, and S.C. Harrison. 2010. Structure of clathrin coat with bound Hsc70 and auxilin: mechanism of Hsc70-facilitated disassembly. *The EMBO journal*. 29:655-665.

Xu, R., A. Fitts, X. Li, J. Fernandes, R. Pochampally, J. Mao, and Y.M. Liu. 2016. Quantification of Small Extracellular Vesicles by Size Exclusion Chromatography with Fluorescence Detection. *Analytical chemistry*. 88:10390-10394.

Yanez-Mo, M., P.R. Siljander, Z. Andreu, A.B. Zavec, F.E. Borras, E.I. Buzas, K. Buzas, E. Casal, F. Cappello, J. Carvalho, E. Colas, A. Cordeiro-da Silva, S. Fais, J.M. Falcon-Perez, I.M. Ghobrial, B. Giebel, M. Gimona, M. Graner, I. Gursel, M. Gursel, N.H. Heegaard, A. Hendrix, P. Kierulf, K. Kokubun, M. Kosanovic, V. Kralj-Iglic, E.M. Kramer-Albers, S. Laitinen, C. Lasser, T. Lener, E. Ligeti, A. Line, G. Lipps, A. Llorente, J. Lotvall, M. Mancek-Keber, A. Marcilla, M. Mittelbrunn, I. Nazarenko, E.N. Nolte-'t Hoen, T.A. Nyman, L. O'Driscoll, M. Olivan, C. Oliveira, E. Pallinger, H.A. Del Portillo, J. Reventos, M. Rigau, E. Rohde, M. Sammar, F. Sanchez-Madrid, N. Santarem, K. Schallmoser, M.S. Ostenfeld, W. Stoorvogel, R. Stukelj, S.G. Van der Grein, M.H. Vasconcelos, M.H. Wauben, and O. De Wever. 2015. Biological properties of extracellular vesicles and their physiological functions. *Journal of extracellular vesicles*. 4:27066.

Yang, R., T. Wei, H. Goldberg, W. Wang, K. Cullion, and D.S. Kohane. 2017. Getting Drugs Across Biological Barriers. *Advanced materials (Deerfield Beach, Fla.)*.

Yang, T., P. Martin, B. Fogarty, A. Brown, K. Schurman, R. Phipps, V.P. Yin, P. Lockman, and S. Bai. 2015. Exosome delivered anticancer drugs across the blood-brain barrier for brain cancer therapy in Danio rerio. *Pharmaceutical research*. 32:2003-2014.

Ye, J., E. Liu, Z. Yu, X. Pei, S. Chen, P. Zhang, M.C. Shin, J. Gong, H. He, and V.C. Yang. 2016. CPP-Assisted Intracellular Drug Delivery, What Is Next? *International journal of molecular sciences*. 17.

Yoshida, S., A.D. Hoppe, N. Araki, and J.A. Swanson. 2009. Sequential signaling in plasma-membrane domains during macropinosome formation in macrophages. *Journal of cell science*. 122:3250-3261.

Young, A., S. Stoilova-McPhie, A. Rothnie, Y. Vallis, P. Harvey-Smith, N. Ranson, H. Kent, F.M. Brodsky, B.M. Pearse, A. Roseman, and C.J. Smith. 2013. Hsc70-induced changes in clathrin-auxilin cage structure suggest a role for clathrin light chains in cage disassembly. *Traffic (Copenhagen, Denmark)*. 14:987-996.

Yuan, M.J., T. Maghsoudi, and T. Wang. 2016. Exosomes Mediate the Intercellular Communication after Myocardial Infarction. *International journal of medical sciences*. 13:113-116.

Zaborowski, M.P., L. Balaj, X.O. Breakefield, and C.P. Lai. 2015. Extracellular Vesicles: Composition, Biological Relevance, and Methods of Study. *Bioscience*. 65:783-797.

Zaiss, A.K., and D.A. Muruve. 2005. Immune responses to adeno-associated virus vectors. *Current gene therapy*. 5:323-331.

Zamore, P.D., T. Tuschl, P.A. Sharp, and D.P. Bartel. 2000. RNAi: double-stranded RNA directs the ATP-dependent cleavage of mRNA at 21 to 23 nucleotide intervals. *Cell*. 101:25-33.

Zha, Q.B., Y.F. Yao, Z.J. Ren, X.J. Li, and J.H. Tang. 2017. Extracellular vesicles: An overview of biogenesis, function, and role in breast cancer. *Tumour biology : the journal of the International Society for Oncodevelopmental Biology and Medicine*. 39:1010428317691182.

Zhang, Z., C. Wang, T. Li, Z. Liu, and L. Li. 2014. Comparison of ultracentrifugation and density gradient separation methods for isolating Tca8113 human tongue cancer cell line-derived exosomes. *Oncology letters*. 8:1701-1706.

Zylberberg, C., and S. Matosevic. 2016. Pharmaceutical liposomal drug delivery: a review of new delivery systems and a look at the regulatory landscape. *Drug delivery*. 23:3319-3329.

2 Materials and Methods

2.1 Materials

General materials and their suppliers are listed in Appendix A. All tissue culture plasticware was manufactured by Corning and purchased from Fisher Scientific (Loughborough, UK), as were laboratory disposables and organic solvents. General usage chemicals and reagents were supplied by Sigma-Aldrich (Poole, UK). Glass bottomed 35 mm MatTek imaging dishes were purchased from MatTek Corporation (MA, USA). Cell lines for *in vitro* barrier models were supplied by GSK through the COMPACT Consortium, the details of which are presented in Table 2.1.

2.2 General cell culture

2.2.1 Cell lines

All cell lines were maintained as sub-confluent monolayers with 10% foetal bovine serum (FBS) supplemented growth media (details provided in Section 2.2.2). All were cultured in a humidified incubator at 5% CO_2, 37°C.

All cell culture materials used and protocols for maintaining COMPACT Consortium cell lines (HeLa, A549, bEND3) were as agreed by the COMPACT Consortium based on guidelines provided from GSK and Cardiff University. This was to establish and maintain consistency across all partners of the COMPACT Consortium (Table 2.1). Each cell line used has also been sequence verified by GSK before provision. Non-COMPACT Consortium cell lines utilised in this project are provided in Table 2.2.

Table 2.1 – COMPACT Consortium verified Cell Lines and Culture Guidelines

	HeLa	**A549**	**bEnd.3**
Tissue	Cervical, epithelial	Lung epithelial	Brain endothelial
Species	Human	Human	Mouse
Growth Medium	sensi-cell MEM	Ham's F-12 Nutrient	DMEM
Maximum Passage	20 (/10 weeks)	20 (/10 weeks)	20 (/10 weeks)
Seeding Density (T75)	18.75×10^4	37.5×10^4	75×10^4
Passage Frequency	90% confluency	90% confluency	90% confluency
Media Change	3 days	3 days	3 days
Centrifugation	300g/4 min	300g/4 min	300g/4 min

Table 2.2 – Non-COMPACT Consortium Cell Lines and Culture Details. H1299eGFP were stably transfected to express eGFP (Cun et al., 2011)

	AG02262	**H1299eGFP**	**H1299WT**
Supplier	Coriell Institute Medical Research	University of Copenhagen	University of Copenhagen
Cell type	Human Primary Lung Fibroblasts	Human Lung Carcinoma	Human Lung Carcinoma
Growth Medium	DMEM F-12 (1:1 mix)	RPMI 1640	RPMI 1640
Max. Passage	Received P7-8, Max. P10	20	20
Split Ratio (T75)	1:2	1:6	1:6
Passage Frequency	90% confluency	90% confluency	90% confluency
Media Change	3 days	3 days	3 days
Centrifugation	300g/4 min	300g/4 min	300g/4 min

2.2.2 Media

HeLa cells were cultured in Minimum Essential Media (MEM) containing phenol red and supplemented without antibiotics but containing 10% FBS, 1% L-glutamine and 1% Non-Essential Amino Acids (NEAA). A549 cells were maintained in Ham's F-12 Nutrient Media containing phenol red and supplemented with 10% FBS. Mouse-derived bEnd.3 endothelial brain cells were grown in Dulbecco's Modified Eagle Medium (DMEM) with phenol red and 10% FBS.

H1299eGFP (enhanced green fluorescent protein)/wildtype (WT) cells were grown in Roswell Park Memorial Institute Media 1640 (RPMI 1640) with phenol red and supplemented with 10% FBS, 1% L-glutamine and 0.4% Geneticin (H1299eGFP cells). AG02262 were cultured in DMEM F-12 (1:1 mix) supplemented with 1% L-glutamine and 10% exosome-depleted FBS. Exosome-depleted FBS was provided by the Clayton lab and was produced by centrifuging the FBS overnight (18 hours) at 100,000 *x g*. The FBS was then filtered through a 0.22 µm vacufilter, followed by further filtration through a 0.1 µm vacufilter.

2.2.3 Routine cell culture maintenance

All cells were maintained in a humidified incubator at 37°C with 5% CO_2. Cells were passaged every 3-5 days via one phosphate buffered saline (PBS) wash and incubation with 2.5 µL 0.05% trypsin ethylenediaminetetraacetic acid (EDTA) for 3-5 min (37°C, 5%CO_2) to detach the cells. bEnd.3 cells were incubated for 10 min (37°C, 5% CO_2). After trypsinisation the cells were collected in 8ml of culture media before centrifugation at 300 *x g* for 4 min. The supernatant was removed and the pellet re-

suspended in a specified volume of media depending on split ratio and addition to a new T75 flask depending on the split ratio of the cell line and seeding density (see Tables 2.1 and 2.2).

2.2.4 Cell counting for splitting and plating

Following pellet resuspension, 10 µL cell suspension was added to 10 µL Trypan Blue Solution to allow visualisation of dead cells. The haemocytometer was assembled and 10 µL cell-Trypan Blue mix was added before cells were counted. Cell concentration of the complete cell suspension was calculated based on this value and appropriate volume for correct cell density added to a new T75 flask for culture, or per well for experiments.

2.3 siRNA Transfection

The siRNAs provided in Table 2.3 were custom designed and provided by Eurofins MWG Operon (Ebesburg, Germany). siRNA targeting eGFP was used as a negative control due to the absence of this gene in the mammalian genome.

2.3.1 Standard Single siRNA Transfection

A day prior to transfection, HeLa and A549 cells were seeded at a density of $1.5x10^5$ per 35 mm well (6 well-plate for lysate collection, 35 mm MatTeK dish for live imaging). bEnd.3 cells were seeded at a density of $1.0x10^5$ cells per 35 mm well three days prior to transfection. Per well: siRNA was diluted with Opti-MEM I to generate a volume of 185 µL, and mixed via inversion (siRNAs and working concentrations used

are listed in Table 2.3). Oligofectamine (2 µL per 13 µL Opti-MEM) was added to the siRNA, inverted, and incubated at room temperature (R/T) for 30 min. Following two Opti-MEM I washes to remove serum, 800 µL Opti-MEM I was added per well followed by the drop-wise addition of the transfection medium (200 µL). Cells were incubated for 4 hours (37°C, 5% CO_2) before addition of 500 µL FBS (30%) in Opti-MEM I, followed by a 48 hour incubation (37°C, 5% CO_2). All transfection protocols were followed as according to the Invitrogen transfection guidelines. Untransfected control cells were seeded and treated with Opti-MEM I in the same manner as transfected cells, omitting the addition of Oligofectamine and siRNA. Cells were then used for microscopy studies or the lysates collected for Western blot analysis (Section 2.12).

2.3.2 Double siRNA Transfection

HeLa and A549 cells were seeded at a density of $1.5x10^5$ per 35 mm well (6 well-plate for lysate collection, 35 mm MatTeK dish for live imaging) a day prior to transfection. Transfection was performed as specified in Section 2.3.1 followed by a second identical siRNA transfection 48 hours following the initial transfection, followed by further 48 hour incubation (37°C, 5% CO_2).

Table 2.3 – siRNA Targets and Sequences

Target	Sequence	Stock	Working	Referenc
AP2µ2	GUGGAUGCCUUUCGGGUCAdTdT	50 µg/mL	100 nM	Custom d
Caveolin-1	AGACGAGCUGAGCGAGAAGdTdT	100 µg/mL	100 nM	(Al Soraj
Cdc42	GACUCCUUUCUUGCUUGUUdTdT	100 µg/mL	100 nM	Custom d
Flotillin-1	UGAGGCCAUGGUGGUCUCCdTdT	100 µg/mL	100 nM	Custom d
PAK1	AUAACGGCCUAGACAUUCAdTdT	100 µg/mL	100 nM	(Al Soraj
Protein Kinase C (PKC)δ	GGCUGAGUUCUGGCUGGACdTdT	100 µg/mL	100 nM	(Llado et
GFP	GGCUACGUCCAGGAGCGCAdTdT	100 µg/mL	100 nM	(Al Soraj
eGFP/Cy5-eGFP	UGCGCUCCUGGACGUAGCCdTdT	100 µg/mL	100 nM	Custom d
Scrambled (Scram) eGFP	GCACGGACCGCGUCUAGGAdTdT	100 µg/mL	100 nM	Custom d

2.3.3 Synchronous siRNA Transfection

The siRNA and Oligofectamine transfection complexes were prepared as for forward siRNA transfection (Section 2.3.1). During complex formation, HeLa cells were trypsinised and seeded at a density of $2.0x10^5$ per 35 mm well in 800 µL Opti-MEM I. siRNA complexes were added (200 µL) directly to the cell suspension, pipetted to mix, placed in 35 mm MatTek dishes and incubated for 4 hours (37°C, 5% CO_2). Addition of 500 µL FBS (30%) in Opti-MEM I and 72 hour incubation (37°C, 5% CO_2) were then performed before the cells were used for confocal microscopy studies.

2.3.4 siRNA targeted depletion of eGFP in H1299eGFP cells

2.3.4.1 Oligofectamine

Oligofectamine/siRNA complexes were prepared and cells transfected (as detailed in Section 2.3.1) but with 100 nM of either scrambled eGFP siRNA (+ Oligofectamine), Cy5-labelled eGFP siRNA (no Oligofectamine), Cy5-labelled eGFP siRNA (+ Oligofectamine) or unlabelled eGFP siRNA (+ Oligofectamine) for a period of 48 hours (37°C, 5% CO_2). Cells were incubated with 1 µM Hoechst33342 for 5 min before imaging live on the confocal microscope (R/T).

2.3.4.2 Exosomes

Unlabelled exosomes (2 or 20 µg/ml) were incubated with 100 nM of Cy5-eGFP siRNA in Opti-MEM I media for 30 min (R/T). Cells (seeded in 35 mm dishes as described in Section 2.3.1) were washed three times with Opti-MEM I before the addition of 800 µL

fresh media. Exosome/siRNA mixtures, 20 µg/ml exosomes only, 100 nM Cy5-eGFP siRNA only, or 100 nM Cy5-eGFP siRNA with Oligofectamine (prepared as described in Section 2.3.4.1) (200 µL of each) were added to the cells and incubated for 4 hours (37°C, 5% CO_2) before the addition of 500 µL FBS in Opti-MEM I (30%). Hoechst33342 (1 µM) was added for 5 min before live confocal imaging (R/T). Untransfected control cells were treated as transfected cells, omitting the addition of siRNA or transfection reagent.

2.4 Live Cell Endocytic Uptake Assays for siRNA transfection studies

2.4.1 Alexa488/647-Transferrin (Tf488/647)

Following transfection of cells in 35 mm MatTeK dishes (as described in Section 2.3.1-3), cells were washed twice with pre-warmed serum-free imaging media (SFIM - phenol red-free DMEM, 0.1% Bovine Serum Albumin (BSA), 20 mM HEPES pH 7.4), before serum starvation for 30 min (37°C, 5% CO_2). Cells were subjected to two further washes with SFIM before addition of Tf488/647 (at the concentrations specified in Table 2.4) and incubated for 10 min (37°C, 5% CO_2). Cells were subjected to two further SFIM washes, followed by incubation with fresh SFIM supplemented with 1 µM Hoeschst33342 for 5 min (37°C, 5% CO_2). Cells were then washed three times with SFIM and confocal imaging was carried out live at R/T in SFIM.

2.4.2 Fluorescent Dextrans

Following transfection of cells in 35 mm MatTeK dishes (as described in Section 2.3.1-2), cells were washed twice with pre-warmed serum-free imaging media. Dextran was added for a period of 60 min (37°C, 5% CO_2), and the specific fluorescent dextran concentrations are specified in Table 2.4. Cells were washed once 55 min after the addition of dextran, followed by incubation with 1 µM Hoescht33342 for 5 min before confocal imaging live at R/T in SFIM.

2.4.3 Alexa647-BSA (BSA647)

Following transfection of cells in 35 mm MatTeK dishes (as described in Section 2.3.1), cells were washed twice with pre-warmed SFIM. BSA647 (50 µg/mL) was added for a period of either 30 or 60 min (37°C, 5% CO_2). Cells were washed with SFIM 5 min before the incubation period was complete and 1 µM Hoescht33342 added for 5 min (37°C, 5% CO_2) before cells were imaged live on the confocal at R/T in SFIM.

2.4.4 BODIPY-Lactosylceramide (BODIPY-LacCer)

Cells were washed twice following transfection of cells in 35 mm MatTek dishes (as described in Section 2.3.1) with pre-warmed SFIM. BODIPY-LacCer (1 µg/mL) was added for 15 min (37°C, 5% CO_2) before three 5% non-fatty acid BSA in phosphate buffered saline (PBS) washes were performed. Hoechst33342 (1 µM) was added for 5 min before live confocal imaging at R/T in SFIM.

Table 2.4 – Endocytic Probes Used

Endocytic Probe	**Incubation**	**Stock Conc**	**Working Conc**		
			HeLa	**A549**	**bEND3**
Transferrin488/647	10 min pulse 5 min chase	5 mg/mL	5 µg/mL	5 µg/mL	1 µg/mL
10kDa Dextran488	30, 60 min	10 mg/mL	100 µg/mL	100 µg/mL	100 µg/mL
10kDa Dextran647	60 min	10 mg/mL	-	100 µg/ml	-
2MDa FITC-Dextran	60 min	10 mg/mL	1 mg/mL	-	-
BSA647	30, 60 min	10 mg/ml	50 µg/mL	-	-
BODIPY-LacCer	15 min	0.1 mM	1 µg/mL	1 µg/mL	-

2.5 Treatment of Cells with Chemical Inhibitors of Endocytosis

2.5.1 Cell Culture

HeLa cells were seeded at a density of 2.75×10^5 and A549 cells at a density of 3.0×10^5 per 35 mm MatTek dish in complete media and cultured in a humidified incubator until 80-90% confluent.

2.5.2 Inhibitor Treatment and Live cell Endocytic Probe Assays

Cells were washed three times with SFIM before inhibitor pre-treatment for 30 min (37°C, 5% CO_2) in fresh SFIM. Cells were then co-incubated with the specific inhibitor at

the specified concentration and endocytic probe (details in Table 2.5) for the period stated (37°C, 5% CO_2) in SFIM. Cells were imaged live on the confocal microscope in SFIM following three washes. Hoescht33342 (1 µM) was added 5 min before live cell confocal imaging at R/T. All inhibitors were prepared in dimethyl sulfoxide (DMSO) and stored at the temperatures and concentrations detailed in Table 2.5. DMSO was used as a diluent control for all experiments.

Table 2.5 – Chemical Inhibitors of Endocytosis

Inhibitor	**Target**	**Incubation Period**		**Storage Temperature**	**Stock Concentra**
		Dextran/Exosomes	**Transferrin**		
EIPA	Macropinocytosis Na^+/H^+ Exchange	90 min	45 min	4°C	100 mM
Rottlerin	Fluid-phase PKCδ?	90 min	45 min	4°C	20 mM
IPA-3	PAK1	90 min	45 min	-20°C	50mM
ML-7	Myosin II	90 min	45 min	-20°C	20 mM
Dynasore	Dynamin II	90 min	45 min	-20°C	100 µM

2.6 Fixed Cell Confocal Fluorescence Microscopy

2.6.1 Cell Culture

HeLa and A549 cells were seeded onto glass coverslips in 6-well plates at a density of $2.5x10^5$ per 35 mm well and grown in complete media in a humidified incubator (37°C, 5% CO_2) until 80-90% confluent. For siRNA transfection, cells were seeded in the same manner but at a density of $1.5x10^5$ before transfection according to (Section 2.3.1).

2.6.2 Epidermal Growth Factor (EGF) stimulation of HeLa and A549 cells

HeLa cells were plated at a density of $2.5x10^5$ per 35 mm well a day before the experiment was carried out. Cells were washed three times with DMEM (0.1% BSA) and serum-starved for one hour (37°C, 5% CO_2) with DMEM (0.1% BSA) before the addition of 20 nM EGF and a further 10 min incubation (37°C, 5% CO_2). Cells not subjected to EGF stimulation were treated identically to stimulated cells but with an equal aliquot of deionised water (dH_2O, solvent used for EGF). Cells were then fixed using the protocol in Section 2.6.3. For HeLa and A549 cells transfected with siRNA, this protocol was carried out 48 hours following transfection.

2.6.3 Fixation and permeabilisation with Paraformaldehyde and Triton X-100

Cells were washed three times in PBS before fixation in 3% paraformaldehyde for 15 min. Cells were again washed three times with PBS and 50 mM ammonium chloride added for 10 min to block free aldehyde groups. After three PBS washes, 0.2% Triton

X-100 was added for 5 min to permeabilise the cells before a further three PBS washes were performed.

2.6.4 Rhodamine-Phalloidin and Hoescht33342 Labelling

Following fixation actin filaments were labelled by incubation with 2 µg/mL Rhodamine-Phalloidin and the nucleus labelled by incubation with 1 µg/mL Hoechst33342 for 10 min at R/T. Both labels were diluted in PBS. Cells were washed twice with PBS before dipping coverslips once into fresh PBS and then once into dH_2O. Coverslips were mounted onto glass slides using 10 µL DAKO mounting media, left at R/T for one hour before sealing with clear nail polish. Slides were stored at 4°C until fixed cell confocal imaging was performed.

2.7 Extracellular vesicle isolation, purification and characterisation

Using the methodology outlined in Appendix B, the isolation and subsequent analyses performed by the Clayton lab satisfy the criterion set by the International Society for Extracellular Vesicles (ISEV), for defining this specimen as exosomes (Lotvall et al., 2014).

2.8 Labelling of Du145 exosomes with Alexa488/633

C_5-maleimide-Alexa488 or C_5-maleimide-Alexa633 (200 µg/mL - 2.5 µL) was added to a 30 µL exosome aliquot containing 60 to 100 µg protein, and made up to 50 µL with PBS before incubation, with no agitation, for 60 min in the dark (R/T). During incubation

exosome spin columns (Invitrogen) were prepared according to manufacturer's instructions and powdered resin was hydrated with 650 µL for 15-30 min at R/T. Spin columns placed in the collection tubes were centrifuged for 2 min (750 *x g*), in a swing-out rotor. The collection tubes were discarded before the addition of the labelled EV aliquot to the resin. Columns were placed in 1.5 mL eppendorf tubes and centrifuged for 3 min (750 *x g*) to collect labelled exosomes. Non-incorporated, excess dye was retained by the resin, and controls involving dye but no exosomes were performed in parallel to confirm dye retention by the column. For microscopy analysis, labelled exosomes were gently mixed to 1000 µL in phenol red free DMEM, before filtration through a 0.22 µm filter (Millex), aliquoted and stored at -80°C until required.

2.9 Live Alexa488/633-Exosome (Exo488/633) Endocytic Uptake Assay

2.9.1 Standard endocytic uptake assay

As for live cell endocytic probe uptake assay experiments, HeLa cells were seeded at $2.5x10^5$, primary human lung fibroblasts at $2.5x10^5$ and H1299eGFP cells at $3.0x10^5$ in 35 mm MatTek imaging dishes in complete media before being cultured to reach 80-90% confluency. Cells were washed three times with SFIM before the addition of 60 µg/mL of either Exo488 (HeLa) or Exo633 (Fibroblasts/HeLa) in SFIM for 30-360 min (37°C, 5% CO_2) before confocal imaging (R/T). For siRNA transfection and inhibitor experiments in HeLa, Exo488 were incubated for 60 min (37°C, 5% CO_2). For uptake in H1299eGFP cells, Exo633 were incubated for 60 min at either 2 µg/ml or 20 µg/ml. Cells were incubated with 1 µM Hoechst33342 for 5 min (37°C, 5% CO_2) before washing thrice with SFIM and imaging live (R/T). For time-lapse confocal imaging, HeLa

cells were incubated with 1 µM Hoechst33342 and Cell Mask Deep Red Plasma Membrane Stain (1:5000) and fibroblasts incubated with 1 µM Hoechst33342 for 5 min before washing with SFIM and time lapse confocal imaging (37°C).

2.9.2 Endocytic Uptake in siRNA transfected cells

Following transfection of HeLa cells (described in Section 2.3.1), cells were subjected to three SFIM washes before the addition of 60 µg/mL of Exo488 or Exo633 (Fibroblasts) in SFIM for 60 min (37°C, 5% CO_2). Media was removed and Hoescht33342 (1 µM) added for the final 5 min of incubation before cells were washed thrice with SFIM and imaged live on the confocal microscope (R/T).

2.9.3 Endocytic Uptake in cells treated with Chemical Inhibitors of Endocytosis

Following inhibitor pre-treatment (detailed in Section 2.5.2), Exo488 (60 µg/mL) in SFIM were added to cells in the continued presence of the specified inhibitor for 60 min (37°C, 5% CO_2). Hoescht33342 (1 µM) was added for the final 5 min before live cell confocal imaging (R/T).

2.10 Labelling of lysosomes with Dx647

Cells were seeded in complete media at $2.0x10^5$ in 35 mm MatTek dishes and cultured in a humidified chamber (37°C, 5% CO_2) to be 50-60% confluent on the day of Dx647 incubation. Dx647 (100 µg/mL) was incubated with cells for 2 hours (5% CO_2, 37°C), before washing with PBS and re-addition of complete media. Cells were then

incubated for approximately 18 hours (37°C, 5% CO_2) before incubating with 60 µg/mL Exo488 (as described in Section 2.9.1) for colocalisation analysis.

2.11 Microscopy

2.11.1 Live Cell Confocal Microscopy

Fluorescent images were taken using a Leica SP5 Confocal Microscope system and LASAF software. Cells were imaged at R/T with either a 40x 1.25 NA or a 63x 1.4 NA Oil Objective. Hoechst33342 emission was collected after excitation at 405 nm; Alexa488 and FITC fluorophores were excited by a 488 Argon laser rhodamine fluorescence was excited by a 543 Helium-Neon laser and Alexa633/647 and Cy5 fluorophores were excitation by a 633 Helium-Neon laser. Bi-directional, sequential scanning was applied to ensure spectral separation of fluorophores. Gain and offset settings were optimised for each fluorescent channel within an experiment. Images were collected using a line average of three and scanned at 200-400 Hz to reduce noise. Where Xyz projections are shown, images were taken beginning at the basal surface of the cell and at every 0.5 µm within the z plane until the apical surface of the cell, to produce a z-stack of each field of view.

2.11.2 Live Cell Time-Lapse Imaging

This was performed to visualise the intracellular dynamics of Exo488/647 in HeLa/Fibroblasts, respectively. Microscope settings used were as described in Section

2.11.1 but with cells maintained at 37°C. Images were scanned every 1-2 sec over a period of 5 min.

2.11.3 Fixed Cell Confocal Microscopy

This was performed to visualise rhodamine-phalloidin labelled actin filaments. Objectives and lasers used were as used for live cell microscopy, unless otherwise stated. Images were collected at 100Hz using uni-directional and sequential scanning. Images were taken every 0.2-0.5 µm within the z-plane.

2.12 SDS PAGE and Western Blotting

2.12.1 Lysate collection

Following siRNA transfection (Section 2.3.1-2) cells, , were washed twice with ice-cold PBS before the addition of 100 µL of lysis buffer (150 mM NaCl, 50 mM Tris-base pH 8.0, 10% Triton X-100, dH_2O) with protease inhibitor per 35 mm well. One cOmplete Mini Protease Inhibitor Cocktail Tablet was dissolved per 10 mL of lysis buffer. Cells were incubated with the lysis buffer on a lateral, circular shaker (high speed setting) for 5 min (4°C). Cells were scraped using a sterilised cell scraper, suspension removed and centrifuged for 10 min at 4°C (13,000 *x g*). Supernatant was collected for further analysis and the pellet discarded.

2.12.2 Bicinchoninic (BCA) Assay for protein quantification

A 200 µL aliquot of BCA working solution (49:1, Bicinchoninic Acid: Copper Sulphate Pentahydrate) was added per well of a 96-well plate. Cell lysates to be quantified were added to triplicate wells at 10 µL per well. BSA protein standards (0, 0.2, 0.4, 0.6, 0.8, 1 mg/mL in Triton X-100 lysis buffer) were added to duplicate wells at 10 µL, in order to generate a protein standard curve. Samples were incubated for 30 min at 37°C before absorbance reading at 562 nm. Quantification of each lysate supernatant was calculated through analyses of the protein concentration standard curve generated based on the absorbance readings of the BSA standards.

2.12.3 SDS-PAGE Electrophoresis

Stock samples of each lysate were prepared at concentrations of 1 mg/mL in lysis buffer and stored at -20°C until required. One part sample buffer (2% SDS, 10% glycerol, 0.02% Bromophenol Blue (0.8% w/v), 62.5 mM Tris-HCL, 400 mM Dithiothreitol (DTT), dH_2O, pH 6.8) was added to three parts lysate before incubation at 95°C for 5 min to denature the sample protein. Samples were then centrifuged for 1 min at 4°C (13,000 *x g*). Prepared samples were loaded onto pre-cast 10% or 12% resolving and stacking gels (Life Science BIO-RAD, Hertfordshire, UK) at between 18-24 µg of protein per well. Dual Color molecular weight marker was loaded at 10 µL. Electrophoresis was carried out at 100 V for approximately 85 min (R/T) using a BIO-RAD 300W PowerPac HC.

2.12.4 Wet Protein Transfer

Protein was transferred from the resolving gel to Polyvinylidene difluoride (PVDF) membrane at 100 V for 1 hour (approximately 4°C). PVDF membrane was removed and washed once in dH_2O, followed by incubation with PonceauS solution for approximately 5 min to allow protein visualisation. Relevant parts of the membrane were retained regarding relevant molecular weights before three 5 min PBS washes were performed to remove remaining PonceauS from the membrane.

2.12.5 Semi-dry Protein Transfer

Resolving gels were transferred to a 0.2 µm PVDF mini-gel transfer system (BIO-RAD) and protein transfer carried out at 1.3 A, 25 V for 7 min (2 gels) or 4 min (single gel) using a BIO-RAD Transblot TURBO. This setting is defined by BIO-RAD for the universal transfer of proteins with mixed molecular weights on the same gel. PVDF membrane was removed and treated with PonceauS solution as described in Section 2.12.4.

2.12.6 Immunoblotting for protein detection

PVDF membrane was blocked with 5% milk (Marvel in PBS-0.0025% Tween (PBST)) for 1 hour on an oscillator (low speed setting) to prevent non-specific antibody binding. Primary antibody incubation was carried out on the oscillator (low speed setting) for either 1 hour at R/T, or overnight at 4°C. Membranes were subjected to three 5 min washes with PBS supplemented with 0.025% Tween (PBST) on a lateral, circular shaker (medium speed setting). Secondary species specific Horseradish Peroxidase (HRP)

conjugated antibody incubation for 1 hour (R/T) on the oscillator (low speed setting) was performed followed by three 5 min PBST washes. Primary and secondary antibodies and the dilution used are presented in Table 2.6. Incubations of membranes with mouse anti-β-tubulin-HRP conjugate were carried out in 5% milk for 1 hour (R/T) and required no secondary antibody incubation.

Table 2.6 - Antibodies used for Immunoblotting

Antibody	**Dilution**	**Supplier**
Primary Antibodies		
Mouse Anti-AP50	1:200	BD Transduction Laboratories (Oxford, U.K.)
Rabbit Anti-Caveolin 1	1:200	Cell Signalling Technologies (Hertfordshire, U.K.)
Rabbit Anti-Cdc42	1:200	Sigma-Aldrich (Dorset, U.K.)
Rabbit Anti-Flotillin1	1:500	BD Transduction Laboratories (Oxford, U.K.)
Rabbit Anti-PAK1	1:500	Cell Signalling Technologies (Hertfordshire, U.K.)
Rabbit Anti-PKCδ	1:200	Sigma-Aldrich (Dorset, U.K.)
Rabbit Anti-GAPDH	1:1000	Cell Signalling Technologies (Hertfordshire, U.K.)
Anti-δ-Tubulin-HRP	1:50000	Sigma-Aldrich (Dorset, U.K.)
Secondary Antibodies		
Goat anti-mouse HRP	1:2000	(Thermo-Scientific Pierce, Loughborough, U.K.)
Goat anti-rabbit HRP	1:2000	(Thermo-Scientific Pierce, Loughborough, U.K.)

2.12.7 HRP Detection

Membranes were incubated with Clarity Western ECL Solution (BIO-RAD) for 5 min at R/T before imaging. AP50 and Cdc42 bands were imaged following 2.5 min incubation with SuperSignal West Femto ECL solution (Thermo Scientific-Pierce). The membrane was wrapped in cling film, placed in a developer cassette and imaged in an x-ray developer with ECL hyperfilm or excess ECL solution was shaken from the membrane before being imaged using a BioRad ChemiDoc system.

2.13 Data Analysis

2.13.1 Mean Fluorescence Intensity Quantification of Individual Cells

Individual cells from Leica Application Suite Advanced Fluorescence (LAS AF) Software files were manually selected as regions of interest (ROIs) using ImageJ software (Schindelin, J. et al., 2012). Mean fluorescence intensity (MFI) of each was calculated, resulting in the quantification of approximately 150-160 cells per experimental sample from 8-10 fields of view. The geometric mean (GM) of each sample group was calculated to provide an average MFI for repeat experiments; the mean of the GM from three independent experiments was calculated and used for statistical calculations. Figure 2.1 demonstrates this protocol.

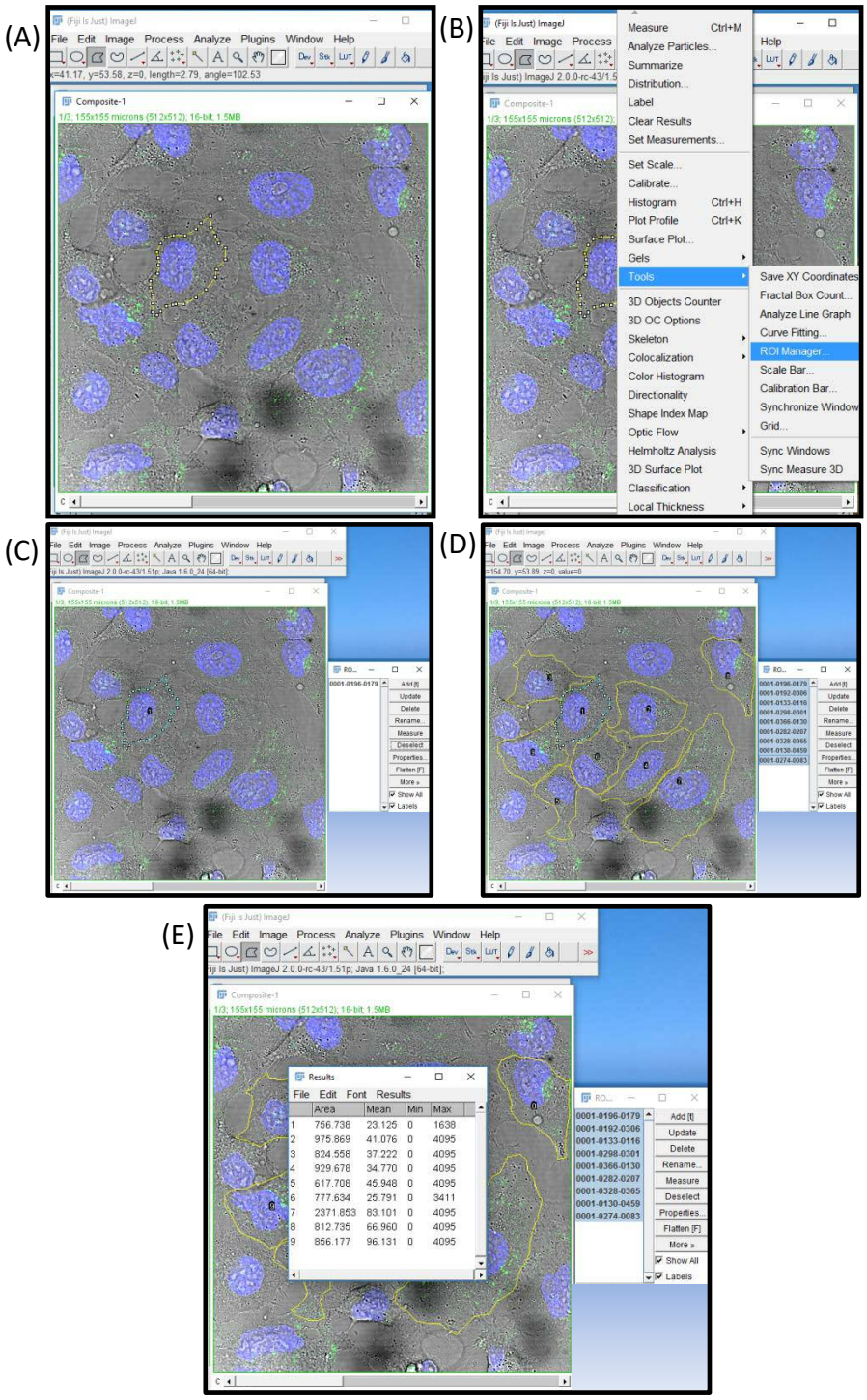

Fig. 2.1. ***Method to calculate MFI (ImageJ software).*** (A) Brightfield (BF) channel, Hoechst33342 channel and channel containing fluorescence intensity to be measured (shown as green) of one field of view were merged. Drawing tool was selected and the peripheries of individual cells identified and marked as shown for one cell. (B) ROI Manager was opened and (C) the selected cell added as a new ROI. (D) The periphery of all cells in the field of view were selected and added as ROIs to the ROI Manager. Only cells completely within the field of view were selected. (E) All ROIs were selected and measured using the ROI manager. This process was repeated for another field of view, the mean intensity of each cell collected and the GM of approximately 160 cells per sample calculated.

The data generated from this method can be presented in a variety of ways. Using the GM, as described above, the data could be presented in a bar graph. The GM has an advantage in that intensity values obtained from cells containing saturated pixels would not skew the resulting average value.

2.13.2 Calculation of Colocalisation Coefficients from Confocal Microscopy

To determine the proportion of exosomes (green fluorescence) associated with lysosomes (red fluorescence) in the cells treated as described in Section 2.10 the M1 Mander's coefficient (a metric used to calculate the 'fraction of probe 1 in compartments containing probe 2' (Dunn et al., 2011)) was calculated using the JaCop ImageJ plug-in and thresholded using the automated default algorithm. Six fields of view (approximately 60 cells) per time point were analysed and the mean M1 coefficient of the six fields of view calculated to provide an average colocalisation value for each repeat. The mean of the average colocalisation value for three separate experiments was plotted.

2.13.3 Statistical Analysis

To compare control treated samples against experimental samples, a Student's unpaired t-test was utilised using the geometric mean of each separate experiment. Significance was calculated for geometric means normalised to either the untransfected control (Utx) value for siRNA transfection uptake experiments or the DMSO Control value for inhibitor uptake experiments. Significance was specified as *$p<0.05$, **$p<0.01$, or ***$p<0.001$.

2.14 References

Al Soraj, M., L. He, K. Peynshaert, J. Cousaert, D. Vercauteren, K. Braeckmans, S.C. De Smedt, and A.T. Jones. 2012. siRNA and pharmacological inhibition of endocytic pathways to characterize the differential role of macropinocytosis and the actin cytoskeleton on cellular uptake of dextran and cationic cell penetrating peptides octaarginine (R8) and HIV-Tat. *Journal of controlled release : official journal of the Controlled Release Society*. 161:132-141.

Cun, D., D.K. Jensen, M.J. Maltesen, M. Bunker, P. Whiteside, D. Scurr, C. Foged, and H.M. Nielsen. 2011. High loading efficiency and sustained release of siRNA encapsulated in PLGA nanoparticles: quality by design optimization and characterization. *European journal of pharmaceutics and biopharmaceutics : official journal of Arbeitsgemeinschaft fur Pharmazeutische Verfahrenstechnik e.V*. 77:26-35.

Dunn, K.W., M.M. Kamocka, and J.H. McDonald. 2011. A practical guide to evaluating colocalization in biological microscopy. *American Journal of Physiology - Cell Physiology*. 300:C723-C742.

Llado, A., F. Tebar, M. Calvo, J. Moreto, A. Sorkin, and C. Enrich. 2004. Protein kinaseCdelta-calmodulin crosstalk regulates epidermal growth factor receptor exit from early endosomes. *Molecular biology of the cell*. 15:4877-4891.

Lotvall, J., A.F. Hill, F. Hochberg, E.I. Buzas, D. Di Vizio, C. Gardiner, Y.S. Gho, I.V. Kurochkin, S. Mathivanan, P. Quesenberry, S. Sahoo, H. Tahara, M.H. Wauben,

K.W. Witwer, and C. Thery. 2014. Minimal experimental requirements for definition of extracellular vesicles and their functions: a position statement from the International Society for Extracellular Vesicles. *Journal of extracellular vesicles*. 3:26913.

Schindelin, J., Arganda-Carreras, I. and Frise, E. et al. 2012. "Fiji: an open-source platform for biological-image analysis". Nature methods 9(7): 676-682.

3 Developing and optimizing methodologies: siRNA targeting methods for analysing endocytic pathways

3.1 Introduction

A variety of methodologies have previously been utilised by a number of groups to specifically inhibit different endocytic mechanisms. These most notably involve siRNA targeted depletion of a number of endocytic proteins, transfecting cells to overexpress mutant endocytic proteins and pharmacological inhibition (Dutta and Donaldson, 2012). Targeting known endocytic regulatory proteins using siRNA transfection in distinct model cell lines defined by the COMPACT Consortium was initially performed.

This work began by using the *in vitro* barrier models provided by GSK as part of the COMPACT consortium, the details of which are presented in Table 3.1.

Table 3.1 – Biological Barrier models of COMPACT Consortium Cell Lines

Cell line	**Species**	**Biological Barrier**
HeLa cervical epithelial	Human	Cervical mucous membrane
A549 alveolar epithelial	Human	Deep Lung epithelia
bEnd.3 brain endothelial	Mouse	Blood Brain barrier (BBB)
Caco.2 colorectal epithelial	Human	Gut epithelia
Calu.3 lung epithelial	Human	Upper Lung epithelia
HaCaT keratinocyte	Human	Skin

HeLa, A549 and bEnd.3 cells were initially used for these studies due to their ease of culture and transfection. Other members of the lab have found that Caco.2 and Calu.3 cells form a thick mucal layer that is useful for their use as a barrier model to test drug delivery systems, but makes their culture difficult. This physical barrier also prevents efficient transfection, which rendered them unsuitable for the aims of this project, which included the use of siRNA transfection as a method of targeting endocytosis.

3.2 Aims and Objectives

- To explore protein targets and techniques for siRNA depletion in order to inhibit Clathrin-Mediated Endocytosis (CME) in the barrier model cell lines supplied by the COMPACT Consortium.
- To use the same siRNA techniques in order to identify proteins which are involved in the regulation of fluid-phase endocytosis and macropinocytosis in these same cell lines.
- To assess the effects on both cell structure and on the uptake of different endocytic probes following the depletion of the proteins targeted in Aim 1. and 2.
- As an overall aim, to become comfortable and efficient in the basic laboratory techniques, cell culture, and confocal microscopy that will be essential for the completion of this project.

3.3 Results

3.3.1 Exploration siRNA depletion methods to inhibit Clathrin-Mediated Endocytosis (CME)

In this section the HeLa cell line was utilised as the laboratory has been developing *in vitro* endocytosis assays in this cell line (Al Soraj et al., 2012; Moody et al., 2015). By depleting the levels of AP2µ2, a subunit of the AP2 complex to which CME is dependent, it was postulated that internalisation of the CME marker, transferrin, would be prevented; an observation that has been previously demonstrated (Moody et al., 2015; Motley et al., 2003). Cells were transfected with siRNA targeting this protein and then analysed for AP2µ2 expression and transferrin uptake. A single 48 hour AP2µ2 siRNA transfection demonstrated a significant decrease in AP2µ2 expression via Western blotting (Figure 3.1a). Indeed, a double band was evident at 50 kDa (AP2µ2), yet the higher weight band was reduced in cells transfected with siAP2µ2 indicating that expression of the protein was reduced. Furthermore, many cells of the transfected population demonstrated membrane bound transferrin after 10 min (Figure 3.1b), suggesting an inability of these cells to carry out CME. To ensure that the depletion of AP2µ2 did not affect the internalisation capacity of other endocytic pathways, a dextran488 (Dx488) and albumin647 (BSA647) endocytosis assay was performed using the method described in Section 2.4.2-3, as these two probes do not enter the cell via CME. Dextran is a widely recognised fluid-phase endocytosis/macropinocytosis probe and BSA is believed to enter the cell via clathrin independent endocytosis (CIE).

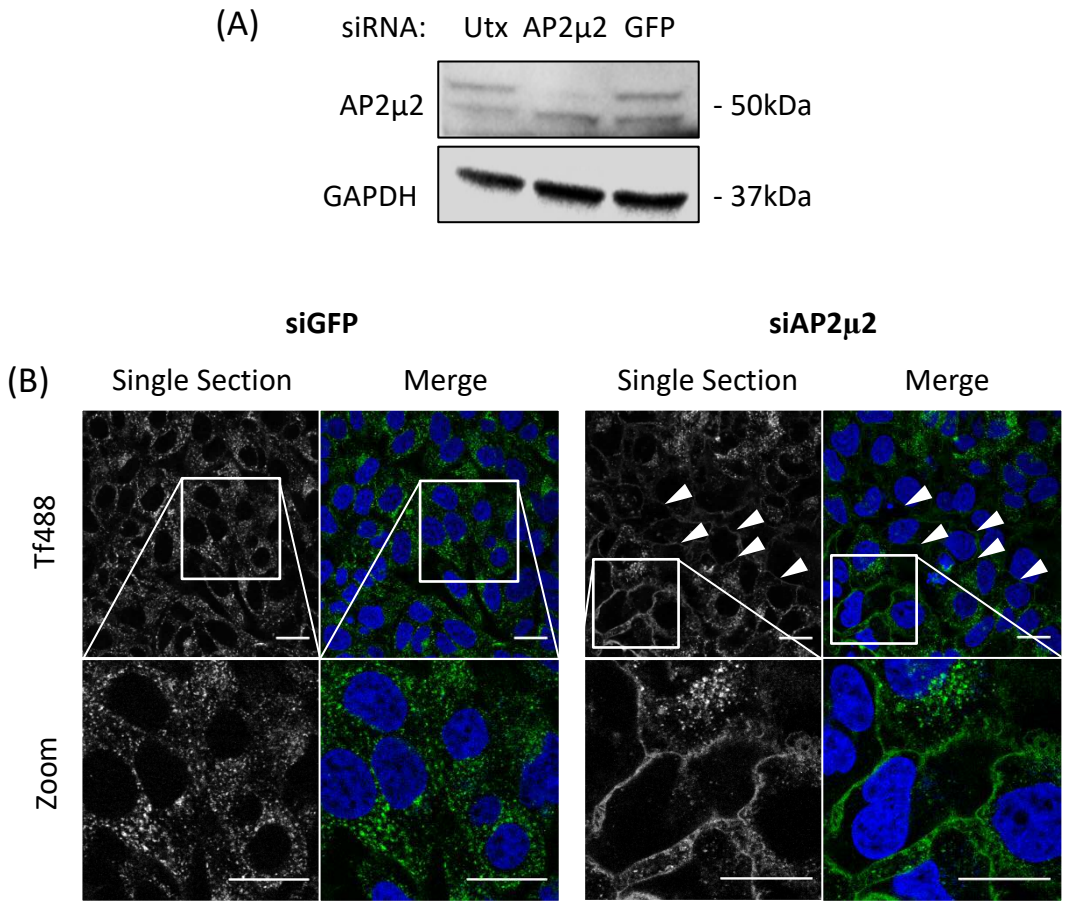

Fig. 3.1. ***AP2µ2 depletion via single 100nM siRNA transfection successfully inhibits Tf488 endocytosis in HeLa cells.*** (A) Representative Western blot analysis demonstrates successful depletion of AP2µ2 following 100 nM siRNA transfection. Blots representative of two separate experiments. (B) Following a 48 h period of siRNA transfection, cells were serum starved for 30 min (37°C, 5% CO_2). Tf488 (5 µg/ml) was pulsed for 10 min, washed and incubated with Hoeschst33342 for 5 min before imaging live (R/T). Arrows indicate membrane bound Tf488. Scale bar: 20 µm. Images summarise of three separate experiments.

Fluid-phase endocytosis and caveolin-mediated endocytosis are both proposed. Following a 30 min pulse of both probes, both Dx488 and BSA647 positive vesicles could be observed in cytoplasmic vesicular structures in control and AP2µ2 depleted cells to a similar extent. This thesis demonstrates an ability to quantify the fluorescence in cell populations as described in Section 2.13.3 and mean fluorescence

intensity (MFI) quantification of each population supports these findings, providing further evidence that AP2µ2 depletion via this method does not affect the endocytic ability of dextran and albumin (Figure 3.2) and the pathway(s) that are utilised by them. In both populations the appearance of large BSA647 aggregates was apparent, though the number was greater in cells depleted of AP2µ2. This could be for a number of reasons, but as this was a single experiment it may be an issue with the probe used or problem with the treatment.

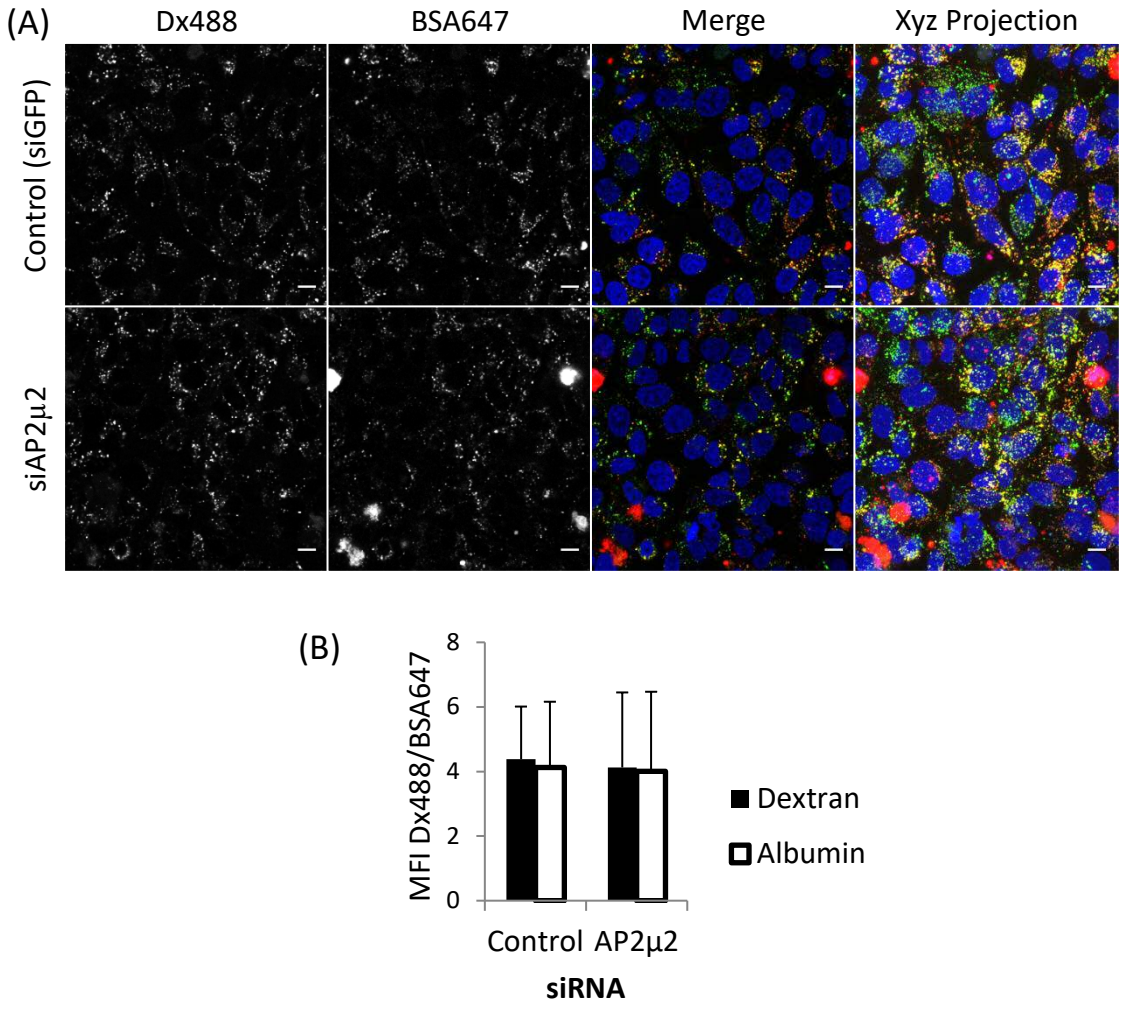

Fig. 3.2. ***HeLa cells retain the ability to internalise Dextran488 and Albumin647 following depletion of AP2µ2 via siRNA transfection.*** (A) Following 48 h transfection, cells were subjected to a 30 min Dx488 (100 µg/ml) and Albumin647 (50 µg/ml) pulse (37°C, 5% CO_2) before imaging live (R/T). Scale bar: 10 µm. (B) MFI quantified for both Dx488 and BSA647 in each cell population. Bars: Standard deviation of cell variability within population.

Though the described 48 hour single transfection method successfully depleted the AP2 subunit, double transfection experiments were also investigated (as described in Section 2.3.2) having been utilised previously (Motley et al., 2003). Similar results were obtained following double transfection (Figure 3.3), with transferrin labelling punctate structures in control cells and largely contained on the plasma membrane of siAP2µ2 cells. Cells subjected to this double transfection, however, were less confluent and had

formed a greater number of stress fibres, suggesting that this technique may have detrimental effects on overall cell physiology. Secondary effects of depleting a target protein for extended periods must be considered regarding these assays, as results comparable to a 'physiological norm' will be the most reliable. For these reasons, all further transfections, where possible, were restricted to a single application for a 48 hour period. Notably, such low expression levels of AP2µ2 from double transfections could indicate the occurrence of undesirable secondary effects due to the inability of successfully transfected cells to perform CME.

Reverse transfection is primarily used in high-throughput analyses and involves simultaneous siRNA complex application and cell seeding (synchronous siRNA transfection), or the addition of cells to dry siRNA (Erfle et al., 2007; Fujita et al., 2010). By removing a day of culture and returning to a single application of siRNA it was hoped that cells would be subject to less physiological stress and therefore yield more reliable results. Tf488 uptake in cells subjected to synchronous siRNA transfection of AP2µ2 was non-uniform across the cell population (Figure 3.3). Although some cells had clearly internalised transferrin, others presented only membrane bound transferrin, indicating that AP2µ2 had been successfully depleted in these cells. In cells transfected (synchronous) with GFP siRNA, transferrin could be clearly observed at early endocytic compartments in the perinuclear region 15 min following addition of the probe (Figure 3.3). This indicated that the synchronous transfection protocol did not cause a consistent observable effect regarding the ability of the cell to internalise transferrin.

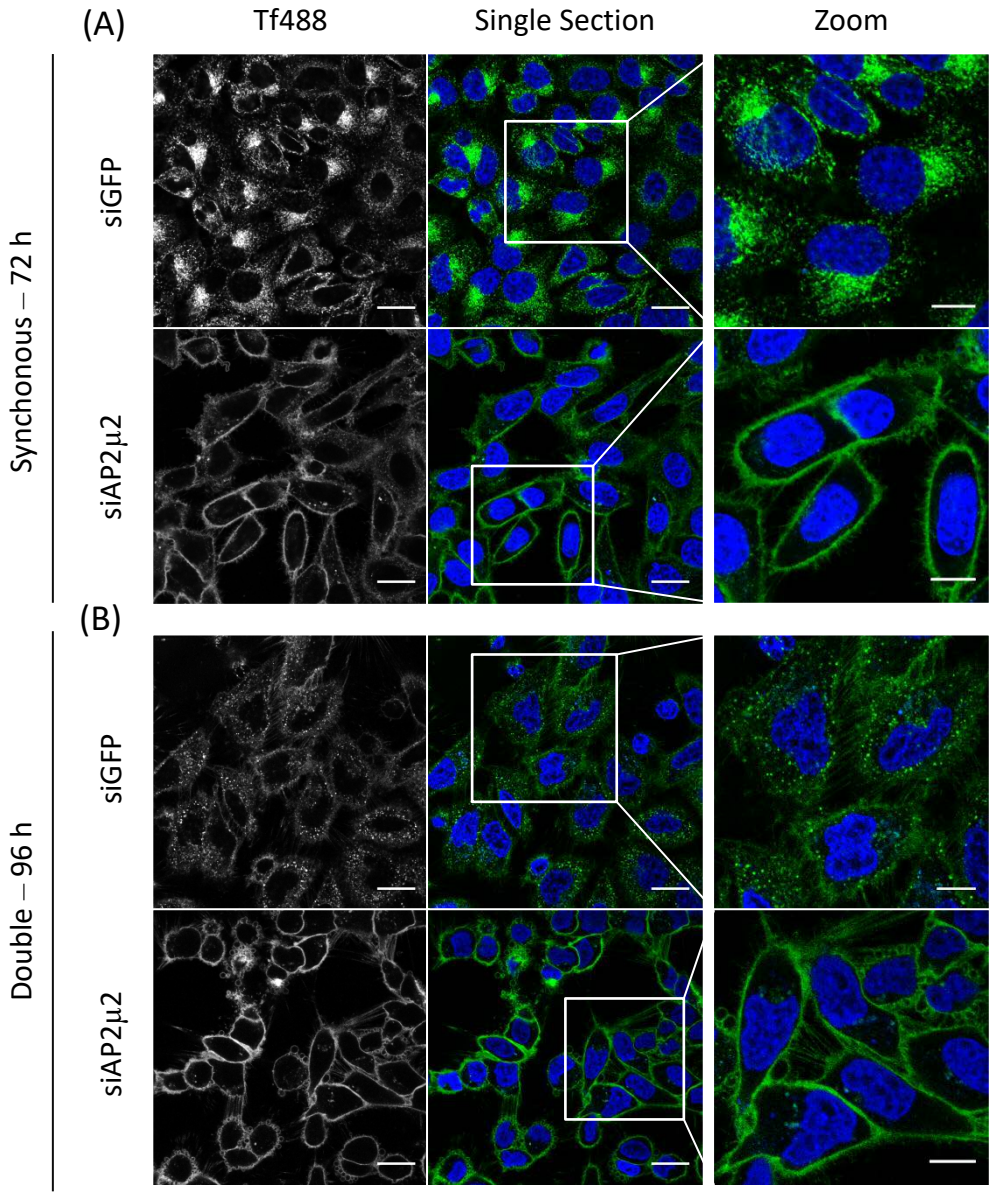

Fig. 3.3. ***AP2µ2 depletion via synchronous and double siRNA transfection successfully inhibits Tf488 endocytosis in HeLa cells.*** Following either a 72 h synchronous transfection (A) or two 48 h periods of siRNA transfection (B), cells were serum starved for 30 min (37°C, 5% CO_2). Tf488 (5 µg/ml) was pulsed for 10 min, washed and Hoechst33342 added for 5 min (37°C, 5% CO_2) before imaging live (R/T). Scale bar: 20 µm. n=1

These observations indicated that a single 48 hour siRNA transfection provided greater efficiency for the obstruction of transferrin endocytosis without causing effects such as elongation and greater production of intercellular stress fibres observed with double transfections.

The establishment of a specific endocytic model for CME inhibition in HeLa is demonstrated from these studies. The use of a single siRNA transfection targeting AP2µ2 as a specific inhibitory method, with the use of a transferrin pulse as a specific probe can now be applied at the high content level to assess CME as an entry route for specified drug delivery systems (DDSs) via microscopy. To compliment this data, forward siRNA transfection targeting AP2µ2 was carried out in A549 cells, a COMPACT Consortium barrier model for the deep lung epithelia. Initial analysis with A549 cells demonstrated the presence of punctate auto-fluorescence, which in some cells is particularly extensive (Figure 3.4). These structures can be observed from 405 and 488nm excitation lasers set at low power settings, but not by the 633 laser. For these reasons, it was decided that markers conjugated to Alexa647 or those which fluoresce in the far-red would be used for further uptake studies in A549 cells.

Western blot analysis indicates that AP2µ2 could be successfully depleted in these cells (Figure 3.5a). As expected control siRNA cells internalised transferrin647 (Tf647), which was visualised within the cell 15 min following addition (Figure 3.5b). In contrast, an extensive number of the cell population transfected with siRNA targeting AP2µ2 are unable to internalise transferrin, where it is confined to the plasma membrane.

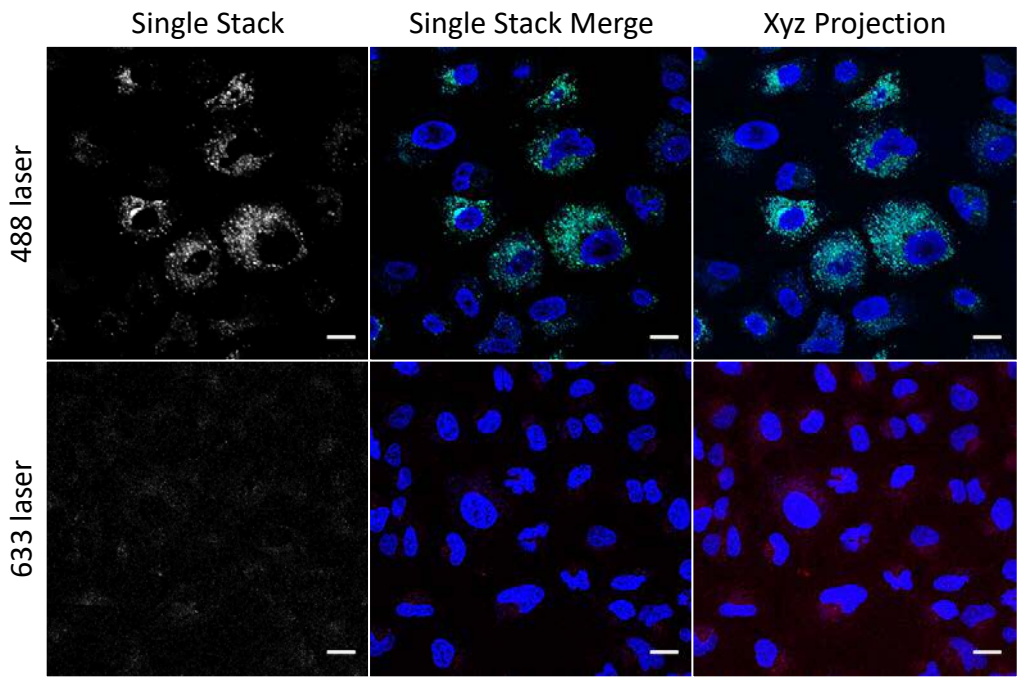

Fig. 3.4. ***Autofluorescent structures in A549 cells visualised by the 488 laser but not the 633 laser.*** Cells were incubated with Hoechst33342 for 5 min (37°C, 5% CO_2) before imaging live (R/T). Scale bar: 20 µm.

The efficiency of synchronous transfection in this cell line was investigated, but unlike single transfection, transferrin uptake was largely unaffected and, as observed in control cells it was located in punctate cytoplasmic structures in a high percentage of the population (Figure 3.5b). These results provide evidence that the use of a single siRNA transfection as a depletion method in conjunction with a CME specific endocytic model can also be applied in A549 cells at a high content level. CME as an endocytic route for drug delivery systems, such as those provided by COMPACT Consortium partners, could then be evaluated in HeLa and A549 cells.

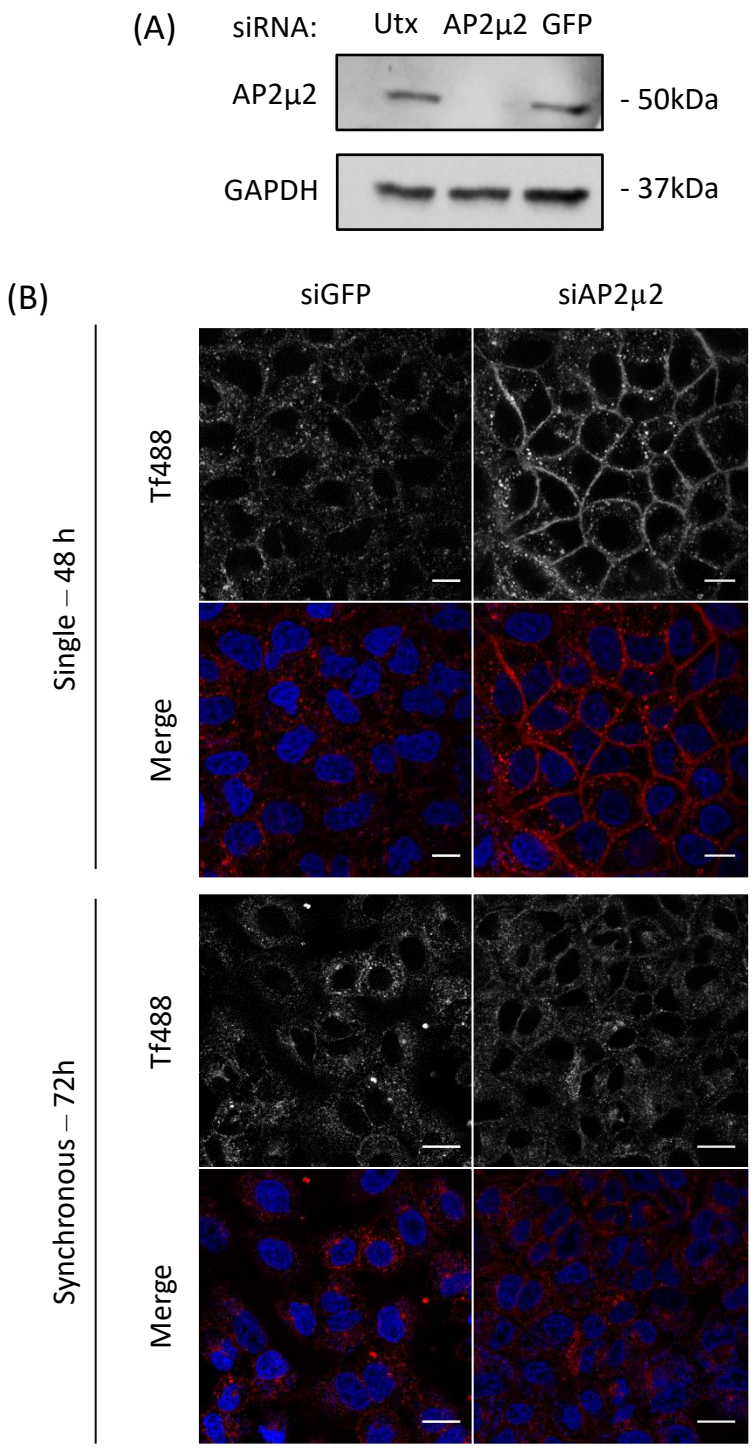

Fig. 3.5. ***Tf647 endocytosis is prevented following 48 h depletion of AP2µ2 via siRNA transfection in A549 cells.*** (A) Western blot analysis indicates that AP2µ2 is depleted 48 h following single transfection. (B) Following a 48 h single transfection or 72 h synchronous transfection, cells were serum starved for 30 min (37°C, 5% CO_2) before being subjected to a 10 min Tf647 (5 µg/ml) pulse, washed and addition of Hoechst33342 (37°C, 5% CO_2) for 5 min before imaging live (R/T). For single transfection images are representative of two separate experiments. Scale bar: 20 µm.

Lactosylceramide (LacCer) is a glycosphingolipid believed to preferentially reside in lipid-rafts, and is therefore used as a marker for Caveolin- and Flotillin-mediated endocytosis, or more generally CIE (Marks et al., 2005; Singh et al., 2007). Here, BODIPY-labelled LacCer was used to assess whether siRNA mediated depletion of AP2µ2 also affected the uptake of the probe. Uptake has been assessed through the use of chemical inhibitors of endocytosis (Vercauteren et al., 2010) but to our knowledge this was the first time that this experiment had been performed using siRNA depletion of endocytic proteins. In HeLa cells treated with control siRNA (GFP) and LacCer (as described in Section 2.4.4), the probe was strongly localised to the plasma membrane and was also observed within the intracellular region of the cell as punctate structures (Figure 3.6). LacCer positive punctate structures indicate internalisation via endosomes, possibly derived from caveolae. Association of BODIPY-LacCer with endosomal membranes has indeed been previously observed in human fibroblasts (Marks et al., 2008). Dispersion throughout the cytosol may be lipid resultant from endosomal escape or direct translocation through the membrane. This pattern of uptake is replicated in control transfected A549 cells (Figure 3.6), indicating that LaCer has similar cellular interaction and mode of uptake between these two cell lines. Following depletion of AP2µ2, uptake of LacCer is unaffected, strongly labelling the plasma membrane and intracellular vesicles (Figure 3.6). These observations indicate that depletion of AP2µ2 via siRNA transfection does not affect the uptake of probes believed to internalise independent of CME, suggesting that other endocytic mechanisms are not affected by this method. It also confirmed that robust *in vitro* assays for CME and CIE in these two cell lines were now available in the laboratory.

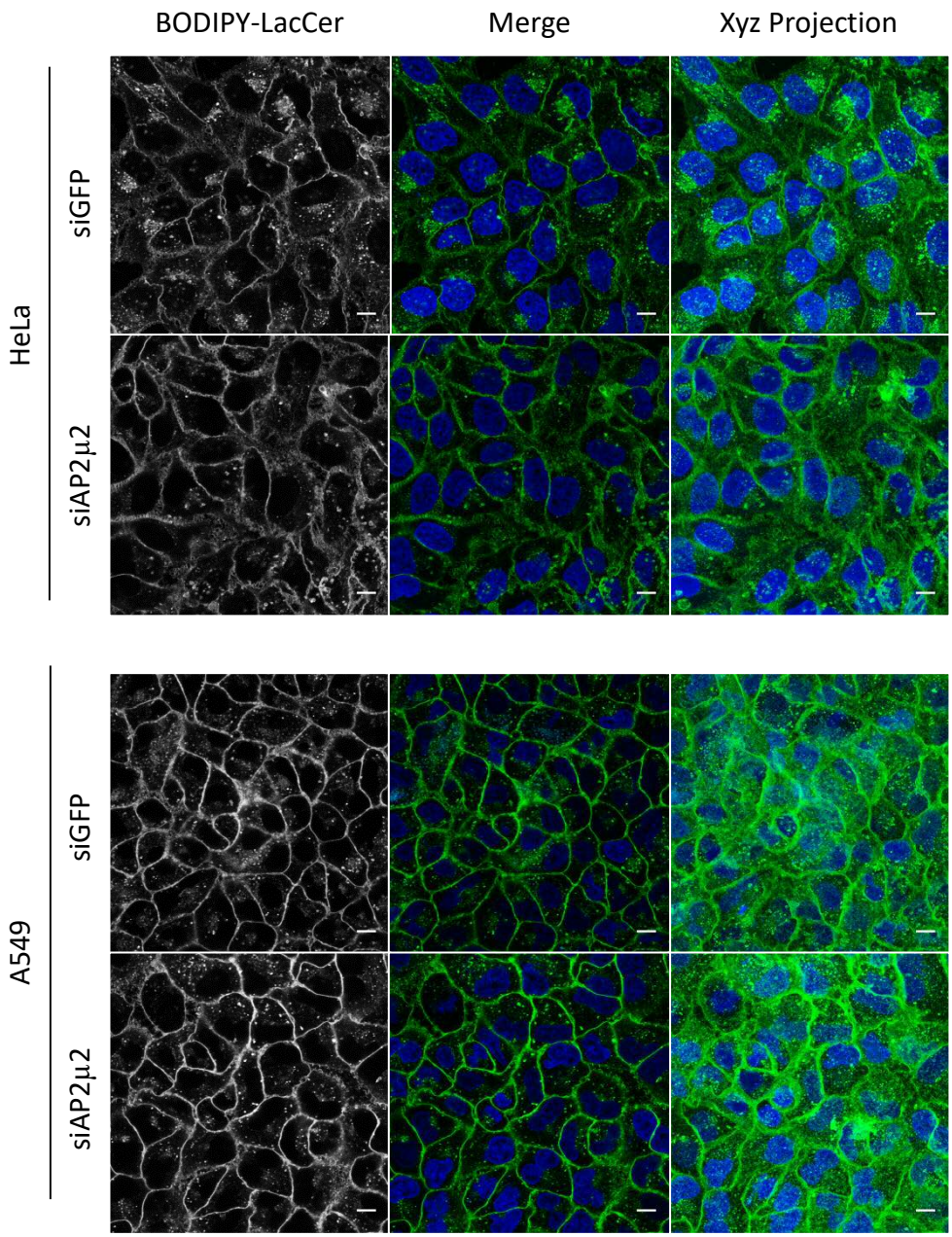

Fig. 3.6. ***BODIPY-LacCer endocytosis is not affected in either HeLa or A549 cells following depletion of AP2µ2.*** *F*ollowing 48 h transfection, cells were washed and subjected to a 15 min pulse of BODIPY-LacCer (1 µg/ml) followed by 3x 5% non-fatty acid BSA in PBS (37°C, 5% CO_2) washes. Hoechst33342 was added 5 min before imaging live (R/T). Scale bar: 10 µm.

bEnd.3 cells are a mouse derived brain endothelial line, and a commonly used *in vitro* model for the BBB. Using a single siRNA transfection targeting mouse AP2µ2, the protein was successfully depleted after 48 hours (Figure 3.7a). Transferrin uptake was

then assessed in these cells including an acid wash step to remove surface bound label. This was in an attempt to better differentiate surface from intracellular staining that was difficult to separate in these very thin cells (5-7 µm) that also, compared with HeLa and A549 had relatively low transferrin uptake.

Uptake of both Tf488 and Tf647 in control transfected cells was observed in vesicular structures in control cells (Figure 3.7b). Following AP2µ2 transfection, cells appear to internalise Tf488 to the same extent as control cells (Figure 3.7b) but uptake of Tf647 appeared to be compromised. MFI quantification to obtain quantifiable results was very difficult for this cell line due to low fluorescence and they also tended to stack on top of each other. For these reasons, it was difficult to assess whether the decrease in Tf647 uptake observed in siAP2µ2 transfected cells was significant using this method.

The effect of siAP2µ2 targeting on fluid-phase uptake of dextran was then analysed in bEnd.3 cells. Dextran presented as punctate structures in control transfected cells after 60 min of uptake (Figure 3.8) and there was no evidence that inhibition of CME affected uptake or distribution of this probe.

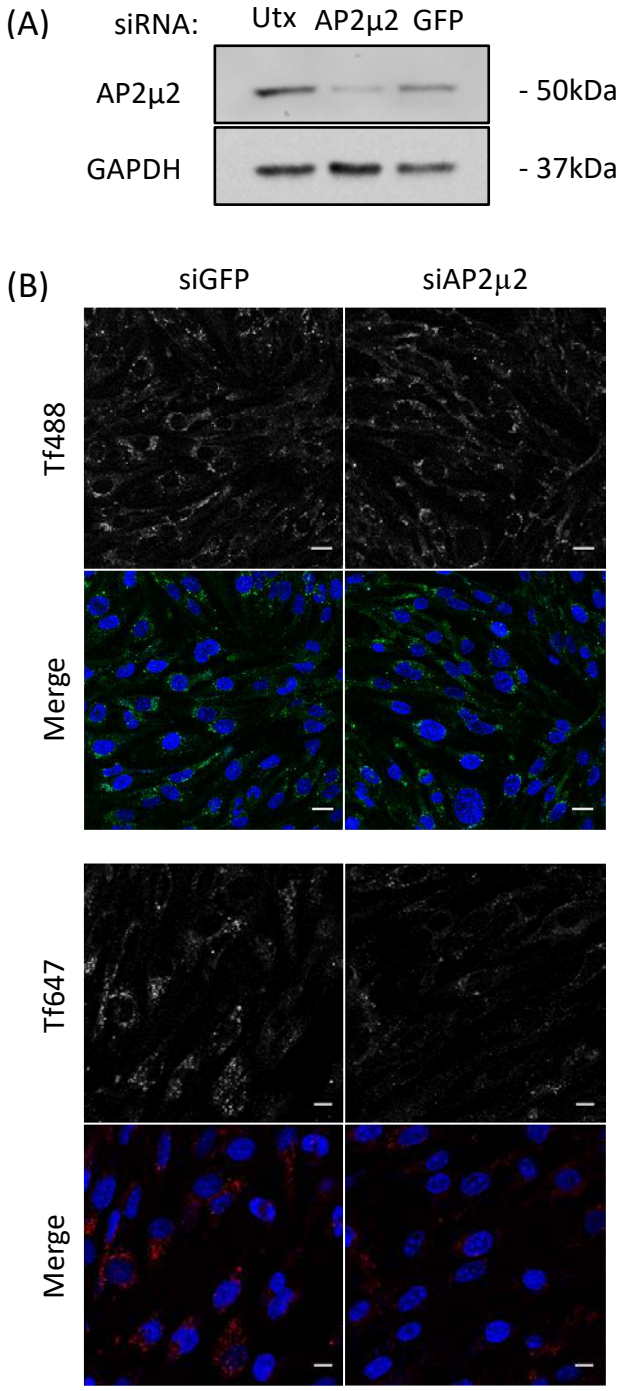

Fig. 3.7. ***Tf488 and Tf647 endocytosis is not prevented following depletion of AP2µ2 in bEnd.3 cells.*** (A) Western blot analysis indicates that AP2µ2 is depleted 48 h following single transfection. (B) Following 48 h transfection, cells were serum starved before being subjected to a 10 min Tf647 (5 µg/ml) pulse, wash and 5 min Hoechst33342 incubation. An ice cold 3 min acid wash (pH 4.5) was performed before imaging live (R/T). Scale bar: 10 µm.

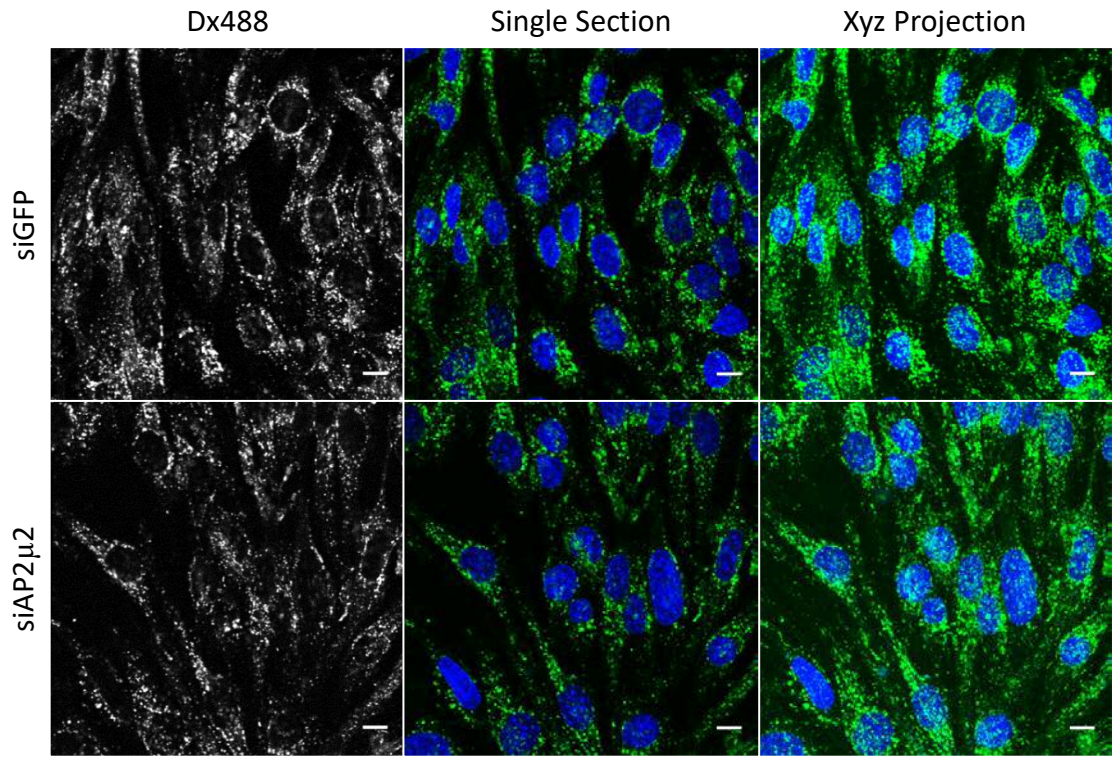

Fig. 3.8. ***Dx488 endocytosis is not prevented following depletion of AP2µ2 via siRNA transfection in bEnd.3 cells.*** Following a 48 h transfection, cells were subjected to a 60 min Dx488 (100 µg/ml) pulse. Hoechst33342 was added 5 min before imaging live (R/T). Images representative of three separate experiments. Scale bar: 10 µm.

These studies began to indicate which cell lines would be suitable to study the uptake of exosomes. Transfection and endocytic probe uptake efficiency of HeLa and A549 cells, over bEnd.3 suggested that these would be the most appropriate choice at this stage of the project.

3.3.2 Exploring the role of P21-associated kinase 1 (PAK1) in actin cytoskeletal dynamics and fluid-phase endocytosis/macropinocytosis in HeLa and A549 cells

The involvement of PAK1 in actin regulation, through its interaction with small GTPases such as Cdc42 and Rac1, has been demonstrated in growth factor mediated macropinocytosis (Dharmawardhane et al., 2000; Edwards et al., 1999) and indeed other cellular processes that rely on actin (Ong et al., 2011; Tunduguru et al., 2014). However, it must be noted that the distinction between fluid-phase endocytosis, constitutive and growth factor induced macropinocytosis is still relatively undefined. PAK1 was further investigated in this thesis including the effects of its depletion on actin, which was visualised in cells using Rhodamine-Phalloidin. Unlike previous experiments performed in this chapter that were performed with live cells, labelling with this fluorophore required cell fixing using established methods.

Western blot analysis indicated successful depletion of PAK1 protein in both HeLa and A549 cells subjected to a single 48 hour transfection with siRNA targeting PAK1 (Figure 3.9). Epidermal growth factor (EGF) acting through the Epidermal growth factor receptor (EGFR) is a powerful stimulator of macropinocytosis that can be visualised by looking at actin causing membrane ruffling and also stimulating the internalisation of fluid as large gulps into macropinosomes (Buckley and King, 2017; Jones, 2007) is routine. HeLa have very low EGFR levels (Al Soraj et al., 2012) but A549 cells with higher EGFR levels have been used to demonstrate EGF effects on actin (Peter et al., 2009); the extent of actin response following EGF treatment was then mostly explored in this cell line.

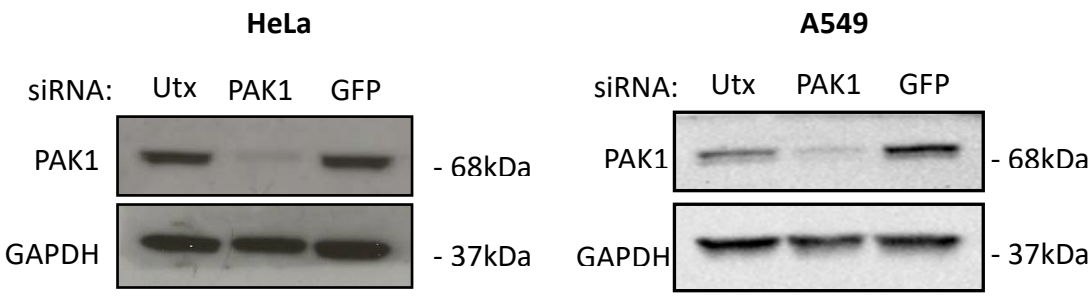

Fig. 3.9. ***PAK1 is successfully depleted 48 h after siRNA transfection in HeLa and A549 cells.*** Following 48 h siRNA transfection, Western blot analysis confirms PAK1 depletion in HeLa and A549 cells in comparison with the loading control GAPDH.

Introducing EGF to serum starved A549 cells, as described in Section 2.6.2 induced clear effects on the actin cytoskeleton, which manifest by classic signs of actin ruffling and filopodia formation (Figure 3.10). Growth factor induced macropinocytosis involves extensive ruffling of the plasma membrane and the formation of filopodia within 10 min of EGF stimulation. These protrusions are also observed in control cells but are much more prominent in stimulated cells (Figure 3.10). Here images were captured through the Z axis and then separated as Basal, Centre and Apical using methodology developed in the laboratory (He et al., 2015). This allowed closer scrutiny of distinct locations of the cell in response to EGF and in PAK1 depleted cells.

Following a 48 h depletion of PAK1 via siRNA transfection, the effect of EGF on the actin cytoskeleton was investigated in order to evaluate the necessity for PAK1 in filopodia formation and macropinocytosis. The cellular response to EGF stimulation in cells transfected with control siRNA was analogous to the response observed in untransfected cells (Figure 3.11), indicating that the ability of the cells to perform and respond to EGFR signalling is unaffected by the transfection process. With regards to

PAK1 depleted cells, no major differences in actin response to EGF stimulation was observed. There was little observable difference between these two populations with regards to actin dynamics. A difference between the control siRNA and PAK1 siRNA treated cells under non-EGF stimulated conditions would suggest a necessity for PAK1 in constitutive actin dynamics, yet no distinguishable difference between these populations can be observed either (Figure 3.11). There are several reasons for these observations. PAK1 may not be directly and solely responsible for the events leading up to macropinocytosis; it may have a greater role in later events, such as cup formation and closure. As PAK1 activity has previously been linked with growth factor induced stimulation of dextran endocytosis the involvement of this kinase in fluid-phase mechanisms cannot be ignored (Dharmawardhane et al., 2000). Further studies were performed in in PAK1 depleted cells.

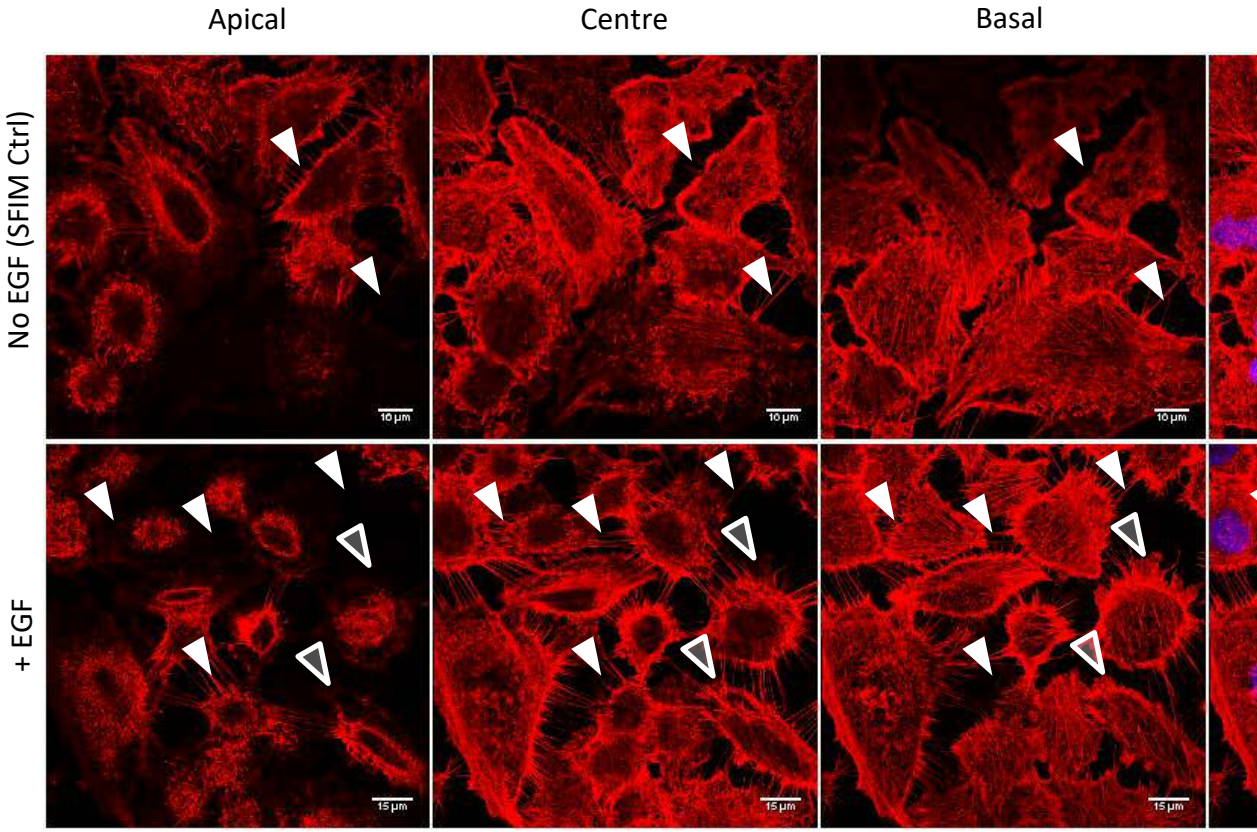

Fig. 3.10. ***Actin demonstrates greater activity following EGF stimulation in untransfected A549 cells*** before 10 min incubation with either SFIM only or 20 ng/ml EGF (37°C, 5% CO_2). PFA fixation was carried Rhodamine-Phalloidin (1:500) and Hoechst33342 (1 µM) at R/T before imaging. Empty arrows indicate r indicate extensive filopodia-like cell-cell connections.

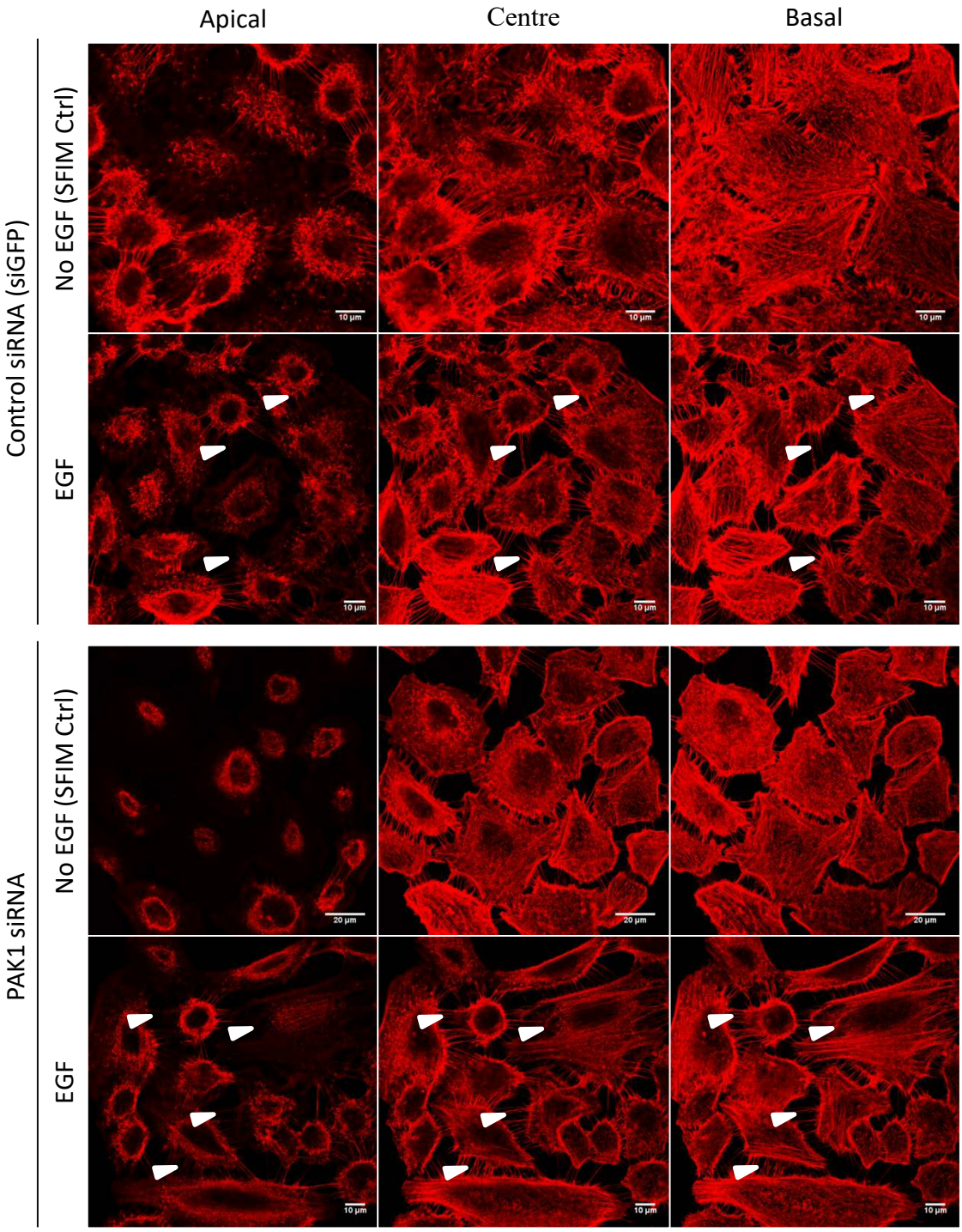

Fig. 3.11. ***Actin demonstrates no difference in activity following EGF stimulation in A549 cells with depleted PAK1 levels.*** Cells were transfected with either GFP or PAK1 siRNA for 48 h followed by serum starvation for 1 h. Incubation with either SFIM only or 20 ng/mL EGF for 10 min was performed (37°C, 5% CO_2) before PFA fixation and 10 min incubation with Rhodamine-Phalloidin (1:500) and Hoechst33342 (1 µM) at R/T.

After a 48 h depletion of PAK1 in A549 cells, dextran was found to internalise to the same degree as in untransfected and control cells. MFI quantification confirmed the microscopy images, in that there was no significant difference in uptake (Figure 3.12). These observations indicate that depletion of PAK1 does not affect the fluid-phase in A549 cells. This was further explored in HeLa cells confirming the data in A549 (Figure 3.13). Uptake of a larger dextran molecule (2 MDa) was also investigated to explore whether the fluid-phase uptake of larger molecules was affected by depletion of this protein. Control transfected cells were found to internalise 2 MDa dextran as intracellular punctate structures, not dissimilar to those resultant from 10 kDa dextran uptake (Figure 3.13). The effect of PAK1 depletion on the uptake of the CME probe transferrin was also explored in order to assess any effects on CME. Both control and siPAK1 cells internalised to a similar extent and this was confirmed using MFI measurements (Figure 3.14).

Though there is strong data for the involvement of PAK1 in growth factor induced macropinocytosis (Dharmawardhane et al., 2000) and in organising cell shape (Figure 3.11) the protein does not appear to be involved in constitutive fluid phase uptake. This led to studies investigating the role of another actin interacting protein named Cdc42.

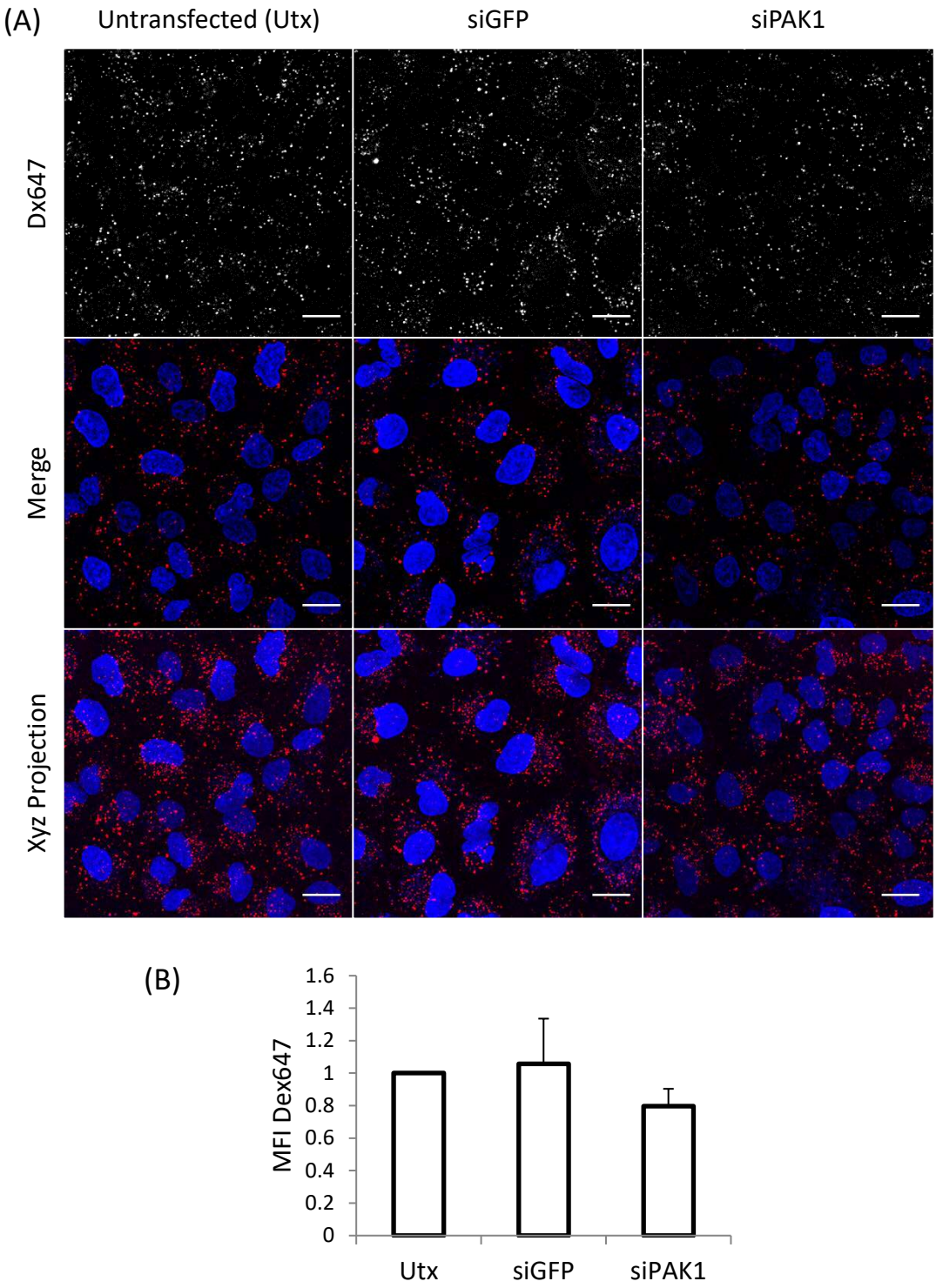

Fig. 3.12. ***Dx647 endocytosis is reduced following depletion of PAK1 48 h following siRNA transfection in A549 cells.*** (A) Following 48 h transfection, cells were washed before being subjected to a 60 min Dx647 (100 µg/ml) pulse before imaging live (R/T). Hoechst33342 was added 5 min before imaging. Scale bar: 20 µm. (B) MFI quantification of Dx647 for each cell population. Bars: Standard deviation. Graph summarises two separate experiments.

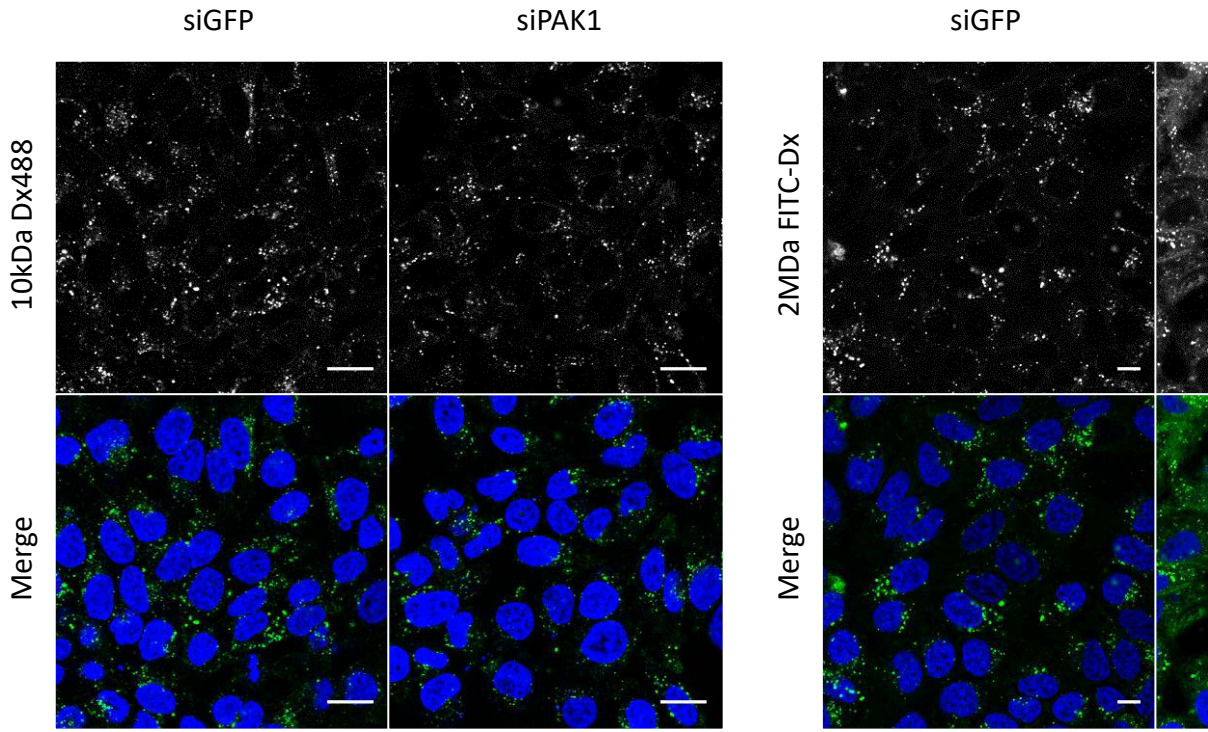

Fig. 3.13. ***Neither 10 kDa Dx488 nor 2 MDa Dex endocytosis is prevented following depletion of PAK1 via siRNA tra***

48 h transfection, cells subjected to a 60 min 10 kDa Dex (100 µg/ml) or 2 MDa Dex (1 mg/ml) pulse before washing a

20 µm and 10 µm respectively.

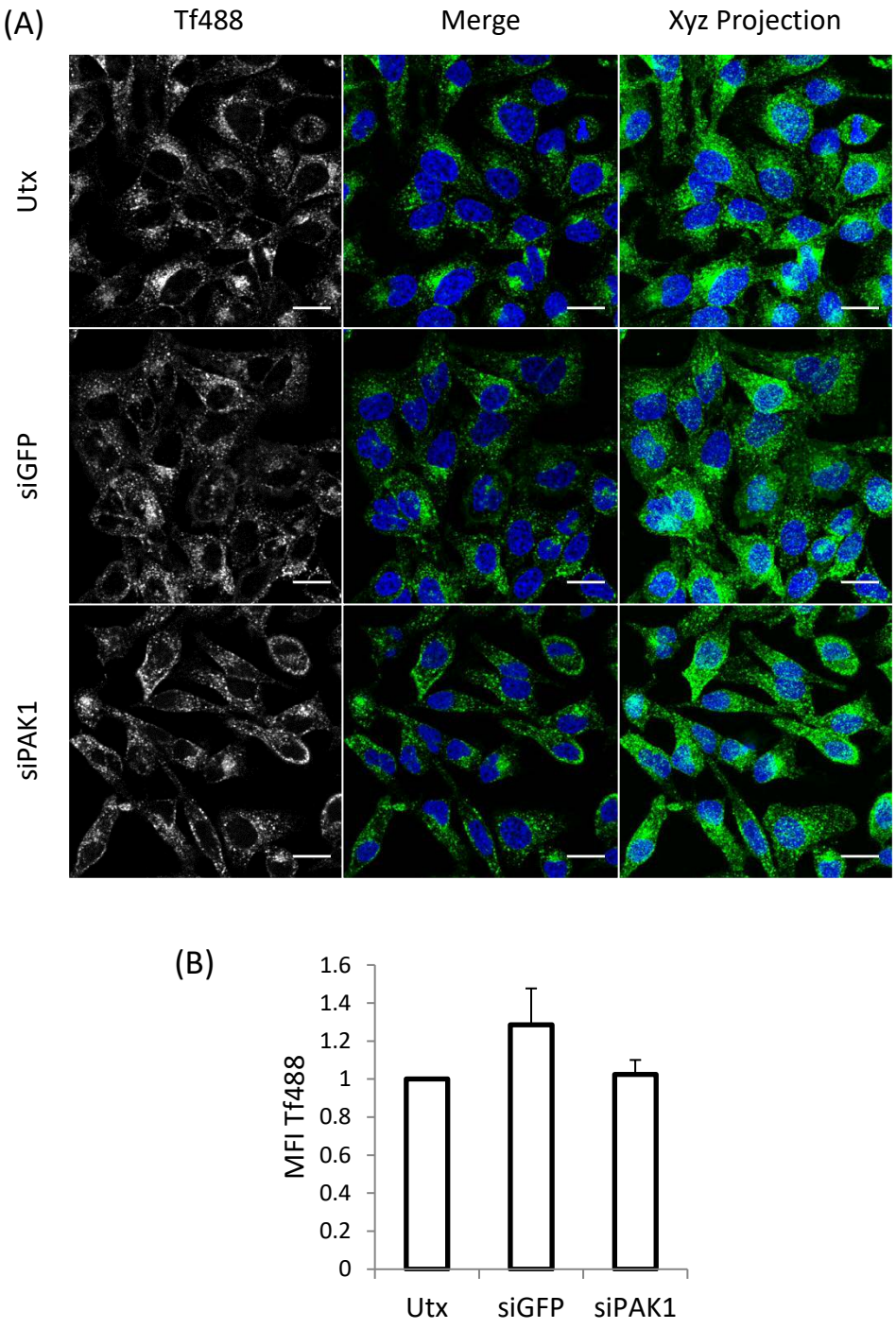

Fig. 3.14. ***Tf488 endocytosis is unaffected following depletion of PAK1 via siRNA transfection in HeLa cells.*** (A) Following 48 h transfection, cells were serum starved before being subjected to a 10 min Tf488 (5 µg/ml) pulse and 5 min chase with Hoechst33342 before imaging live (R/T). Scale Bar: 20 µm. (B) MFI quantification of Tf488 for each cell population in (A). Bars: Standard error. Graph summarises three separate experiments.

3.3.3 Exploring the role of Cdc42 in actin cytoskeletal dynamics and fluid-phase endocytosis /macropinocytosis in HeLa and A549 cells.

Cdc42 is one of several RhoGTPases involved in the regulation of actin function and has been associated with fluid-phase uptake, growth factor induced macropinocytosis and phacocytosis (Beemiller et al., 2010; Cox et al., 1997). Notably, it acts upstream of PAK1. Effects on endocytosis were investigated in cells depleted of this protein, initially focusing on constitutive fluid phase uptake of dextran in HeLa and A549 cells. Western blot analysis indicated that a 48 h siRNA transfection was sufficient for Cdc42 depletion (Figure 3.15), thus permitting further endocytosis studies.

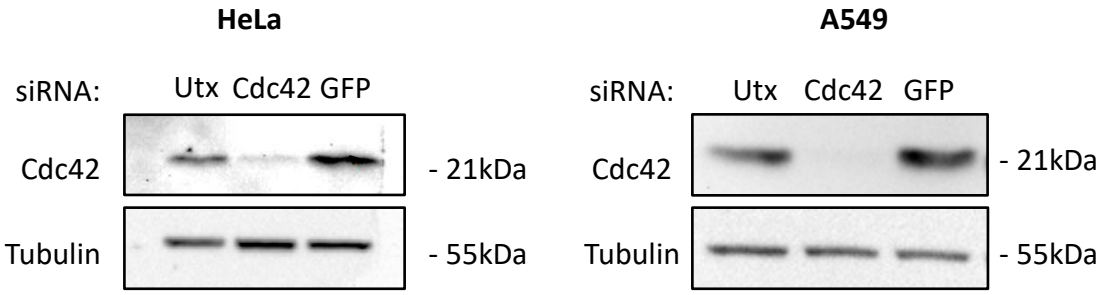

Fig. 3.15. ***Cdc42 is successfully depleted following siRNA transfection in both HeLa and A549 cells.*** Western blot analysis indicates levels of Cdc42 are depleted 48 h following siRNA transfection in HeLa and A549 cells when compared with tubulin as a loading control.

Quantification of microscopy images represented by Figures 4.16 and 4.17 demonstrated that there was no significant effect on dextran uptake in either cell type when they were depleted of Cdc42. Again, uptake of 2 MDa dextran was investigated in HeLa cells depleted of this protein, showing no major requirement for Cdc42 (Figure 3.18). To assess whether Cdc42 regulates CME, HeLa cells were depleted of this

protein and incubated with Tf488 as previously described (Section 2.4.1). The microscopy images clearly suggested that depleting this protein inhibited transferrin uptake and this was confirmed by MFI quantification ((p=0.01), Figure 3.19). This result was somewhat unexpected but suggested that this protein may be an unsuitable target for analysis of fluid phase endocytosis.

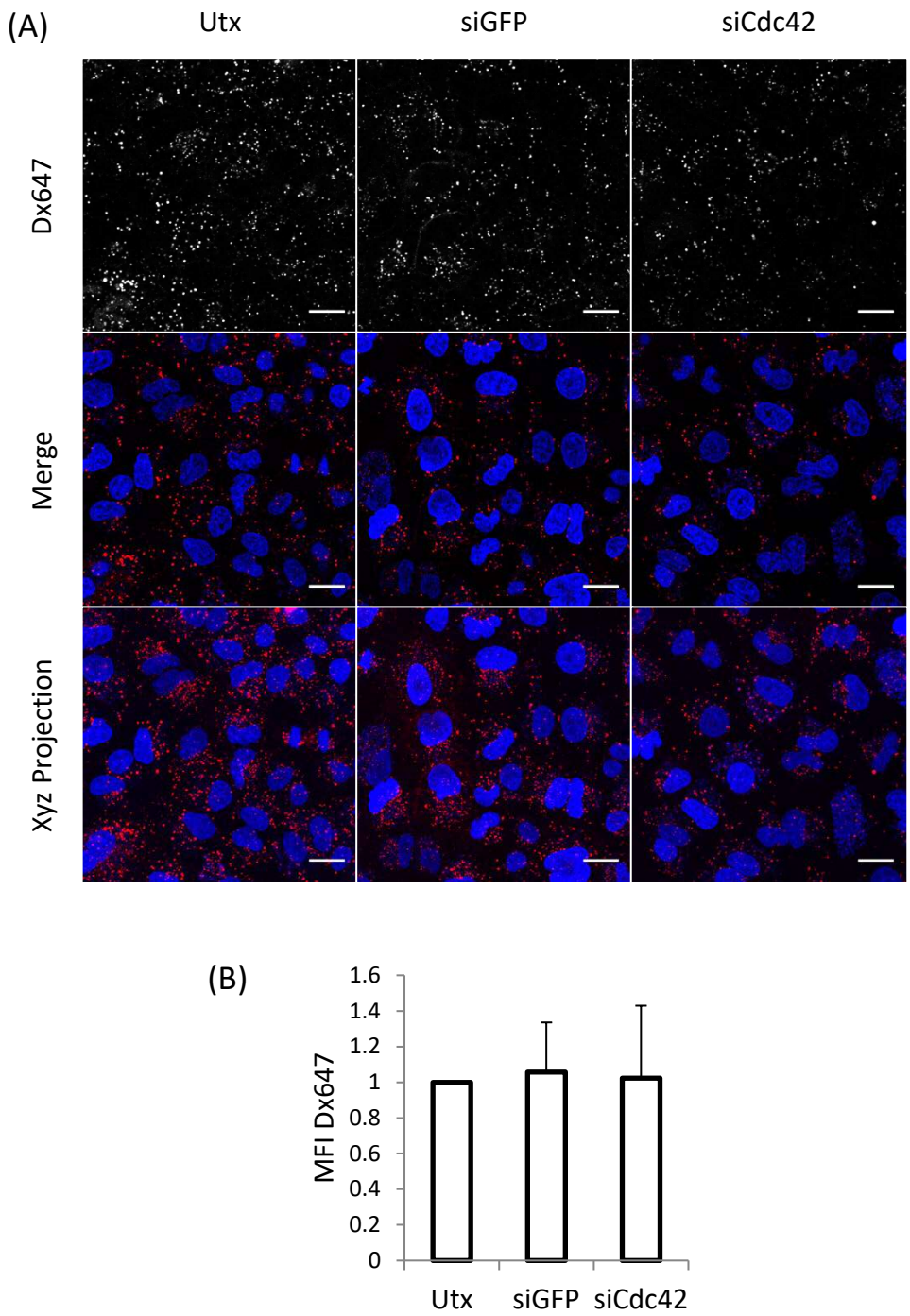

Fig. 3.16. ***Dx647 endocytosis is unaffected following depletion of Cdc42 via siRNA transfection in A549 cells.*** (A) Following 48 h transfection, cells were subjected to a 60 min Dx647 (100 µg/ml) pulse before washing. Hoechst33342 was added 5 min before imaging live (R/T). Scale Bar: 20 µm. (B) MFI quantification of Dx647 in each cell population. Bars: Standard error. Images and graph summarise three separate experiments.

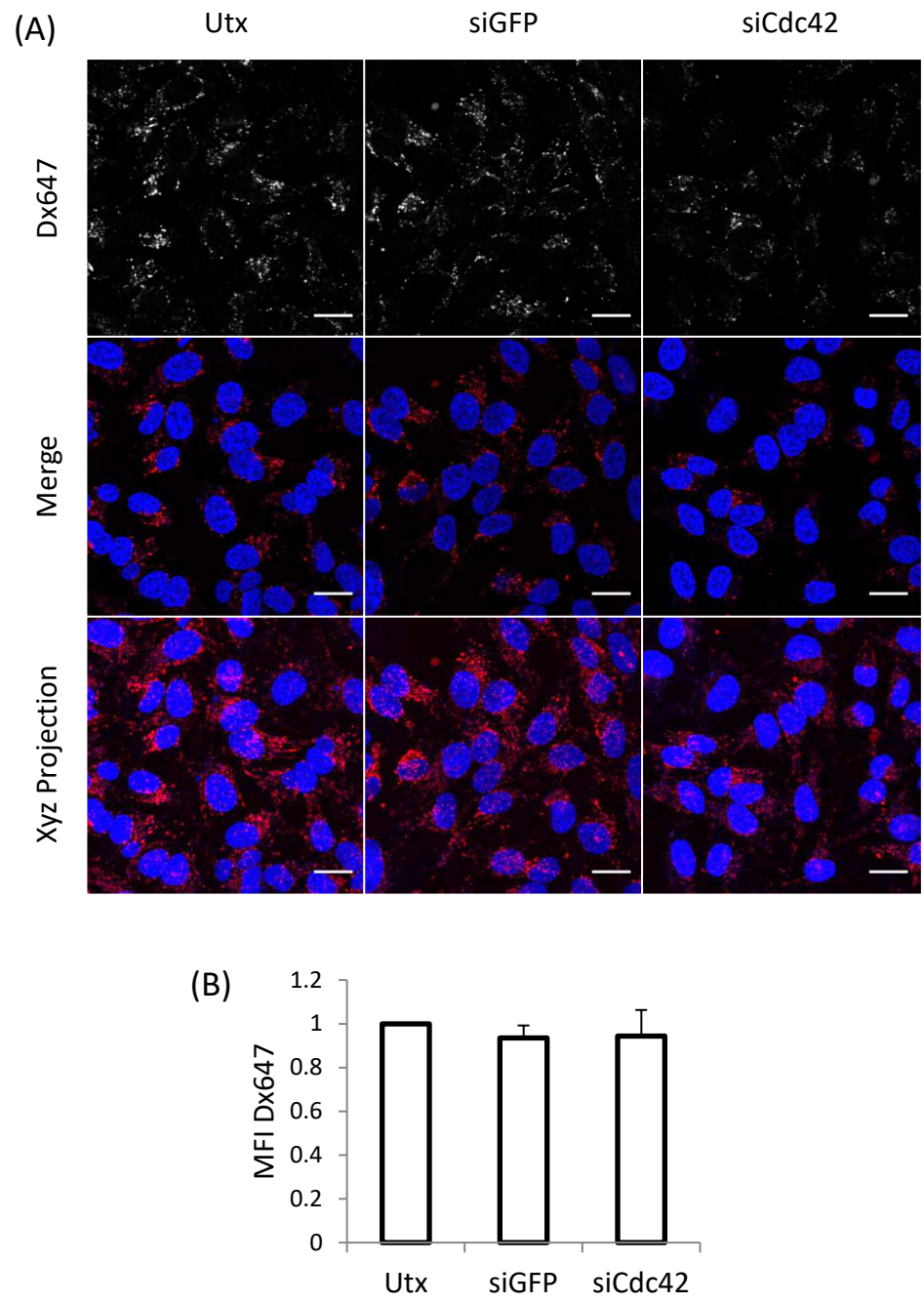

Fig. 3.17. ***Dx647 endocytosis is not affected following depletion of Cdc42 via siRNA transfection in HeLa cells.*** (A) Following 48 h transfection, cells were subjected to a 60 min Dx647 (100 µg/ml) pulse before washing. Hoechst33342 was added 5 min before imaging live (R/T). Scale Bar: 20 µm (B) MFI quantification of Dx647 in each cell population. Bars: Standard error. Images and graph summarise three separate experiments.

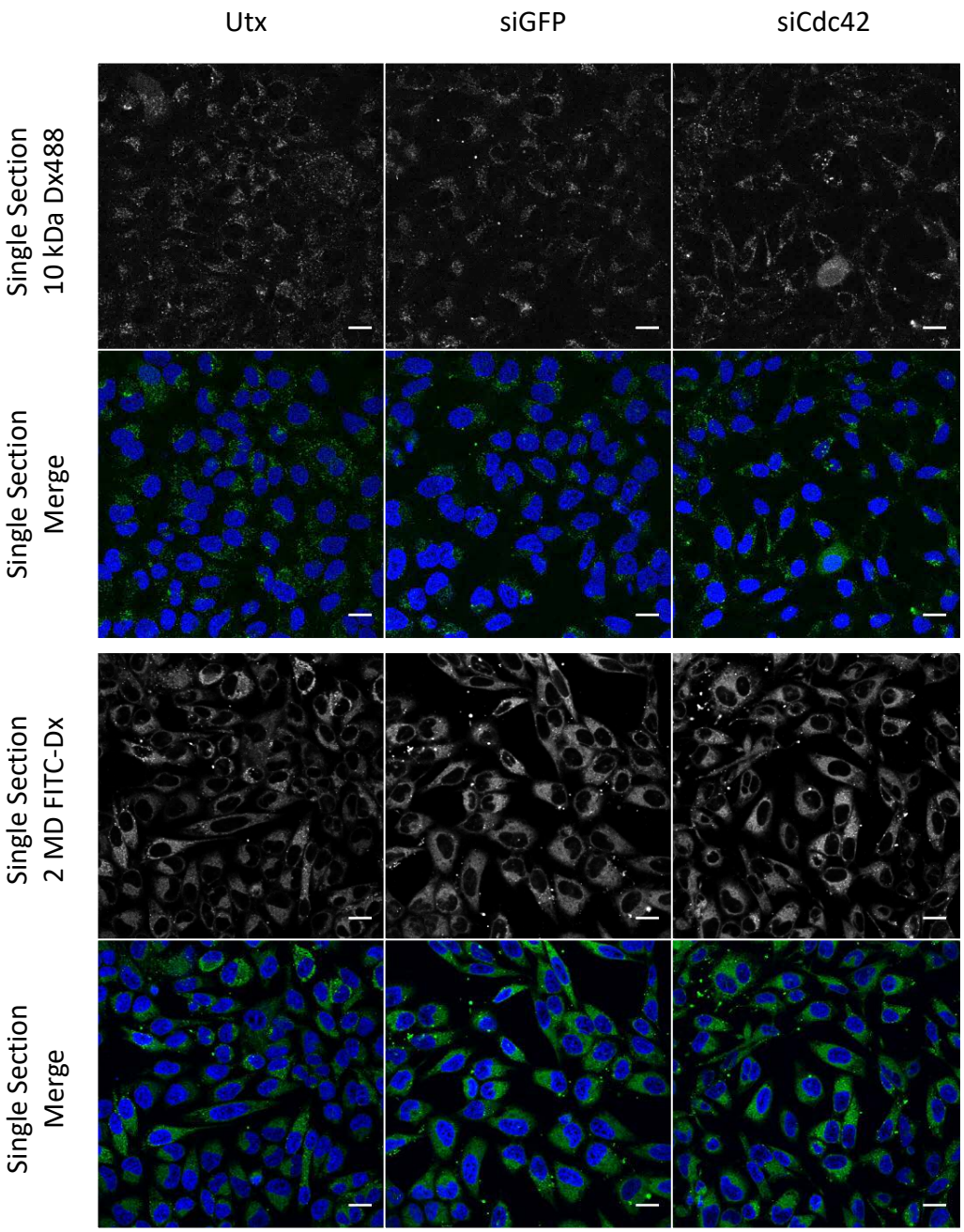

Fig. 3.18. Neither 10 kDa Dex nor 2 MDa Dex *endocytosis is affected following depletion of Cdc42 via siRNA transfection in HeLa cells.* Following 48 h transfection, cells were subjected to a 60 min 10 kDa Dx488 (100 µg/ml) or a 2 MD FITC Dx (1 mg/ml) pulse before washing. Hoechst33342 was added 5 min before imaging live (R/T). Scale Bar: 20 µm.

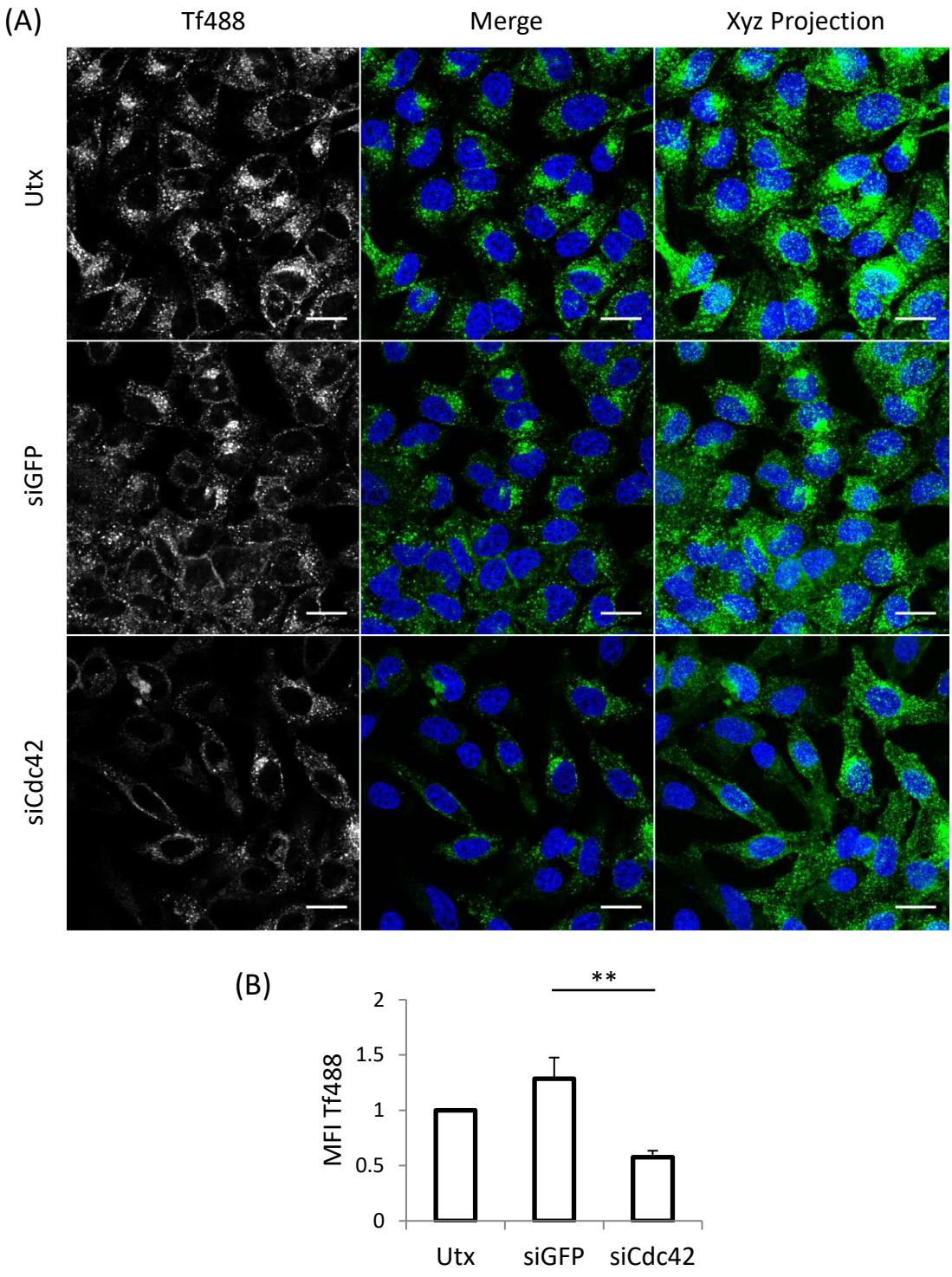

Fig. 3.19. ***Tf488 endocytosis is significantly reduced following depletion of Cdc42 via siRNA transfection in HeLa cells.*** (A) Following 48 h transfection, cells were serum starved for 30 min before being subjected to a 10 min Tf488 (5 µg/ml) pulse and 5 min chase with Hoechst33342 before imaging live (R/T). Scale Bar: 20 µm. (B) MFI quantification of Tf488 in each cell population. Bars: Standard error. Images and graph summarise three separate experiments. **p<0.01

There was a suggestion in Figure 3.11 that PAK1 depletion was affecting cell morphology without having noticeable effects on endocytosis. As PAK1 and Cdc42 are linked with respects to affecting actin function control and Cdc42 depleted A549 cells were labelled with the plasma membrane probe cell mark deep red. Figure 3.20 shows that Cdc42 depleted cells appear narrower and longer than control cells.

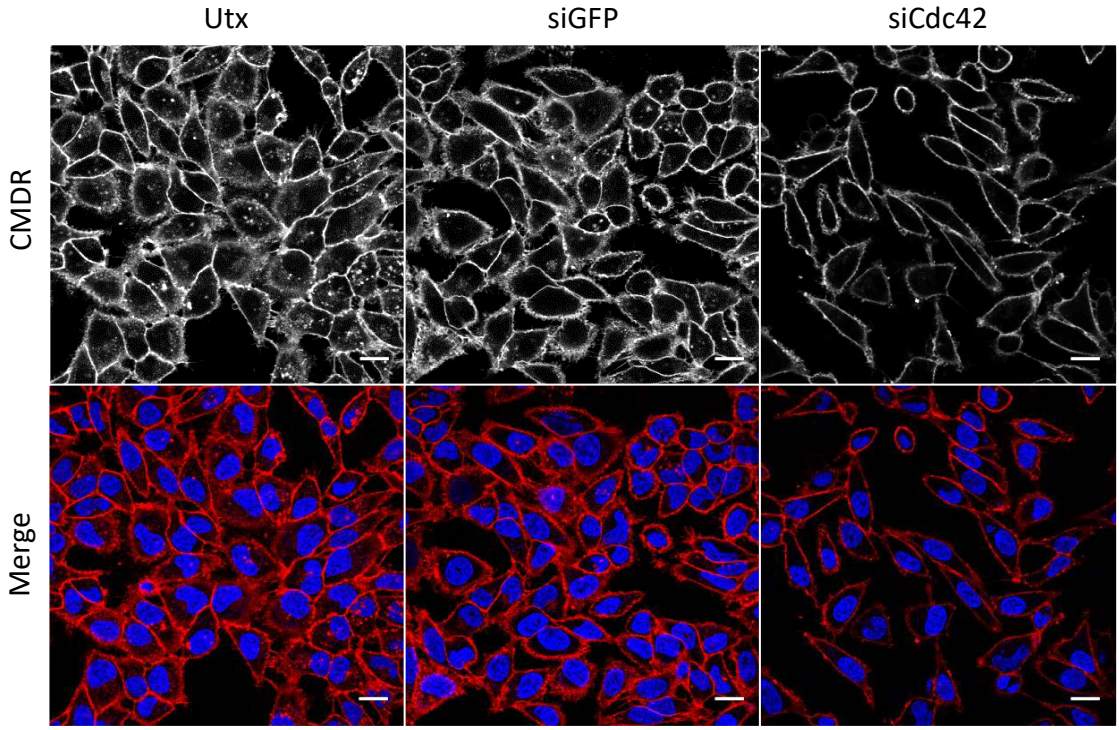

Fig. 3.20. ***Cdc42 depleted HeLa cells present with aberrant morphology.*** Following 48 h siRNA treatment (100 nM siRNA), cells were incubated with cell mask deep red (CMDR) (37°C, 5% CO_2) before confocal imaging live (R/T). Scale bar: 20 µm.

3.4 Discussion

Methods to inhibit specific endocytic pathways *in vitro* should provide reliable platforms for evaluating cellular entry of DDSs. Successful inhibition of CME in HeLa and A549 cells through siRNA targeted depletion of AP2µ2 expression was demonstrated in this chapter, providing two robust models for CME for future studies. Live cell confocal microscopy was chosen as a tool to provide both visual qualitative analysis of cell uptake, in this case transferrin, but methods were also adapted to quantify the fluorescent output from a fraction of the analysed cell population. Imaging cells live also allowed analysis of the live endocytic system, ruling out the possibility of artefacts produced during the fixing process. Quantification of the intracellular fluorescence using these described methods avoided the need to perform further flow cytometry analysis on fixed cells and also provided further relatively high content information on possible more global effects that siRNA targeting of endocytic proteins or chemical inhibition may cause.

PAK1 was targeted as a regulator of induced macropinocytosis due to its close association with actin dynamics (Dharmawardhane et al., 2000; Kalwat et al., 2013; Zhang et al., 2016). Inhibition of this kinase by siRNA transfection does not seem to have a great effect on the dynamics of actin following growth factor stimulation in A549 cells, yet results in some phenotypic effects. Previous studies in the laboratory indicated that targeting PAK1 did inhibit the uptake of cationic cell penetrating peptides (Al Soraj et al., 2012) but only affected stimulated dextran uptake in response to growth factor stimulation – i.e. the fraction of dextran internalised via induced

macropinocytosis rather than the constitutive fraction. Overall PAK1 was not a suitable target for fluid phase uptake or constitutive macropinocytosis in HeLa or A549 cells based on these results so other actin regulatory proteins were explored.

The involvement of the small GTPase, Cdc42, was further investigated as a possible target for macropinocytic inhibition due also to its involvement in actin dynamics (Beemiller et al., 2010; Cox et al., 1997), most notably through its interaction with PAK1 (Kalwat et al., 2013), and suggested involvement in fluid-phase endocytosis (Cheng et al., 2010; Singh et al., 2013). Cdc42 depletion through siRNA transfection however had no effect on the ability of HeLa or A549 to carry out fluid-phase endocytosis. Additionally, similar phenotypic effects of Cdc42 depletion as those observed in PAK1 depleted cells were apparent, consistent with previous reported observations (Monypenny et al., 2009). The significant decrease in transferrin uptake in HeLa cells depleted of Cdc42 supports this idea. This inhibition of CME is not surprising considering that the progression of CPP invagination involves active Cdc42 (Shen et al., 2011) and that Cdc42 regulated actin dynamics are essential for endocytic trafficking from the membrane (Chi et al., 2013; Watson et al., 2014). There is further evidence that a Cdc42 binding kinase (Myotonic dystrophy kinase-related Cdc42-binding kinase alpha-MRCKalpha) is important for internalisation of the transferrin receptor (Cmejla et al., 2010).

Furthermore, cells undergoing migration or undertaking migratory preparation display F-actin ruffles solely at their leading edge (Yi and Coppolino, 2006). Via the introduction of EGF a migratory stimulus is provided, a common and well established

consequence of EGF signalling particularly in epithelial cells (Jiang et al., 2006; Zeineldin and Hudson, 2006). This knowledge was used to assess the effect of EGF stimulus on the actin cytoskeleton in this project. The involvement of Cdc42 and Rac1 activity in dendritic dextran uptake has previously been shown, indicating that these proteins are involved in these processes (Tourkova et al., 2007); this cell line however is classically phagocytic unlike HeLa cells. Fluid-phase endocytosis may well have different dependencies on Cdc42 across the different cell-types, as the actin cytoskeleton in dendritic cells is more likely to be carrying out these processes at a much higher constitutive rate. Furthermore, it has been suggested that antigen presentation in dendritic cells requires macropinocytosis as regulated by Cdc42 and Rac1 (Garrett et al., 2000; Nobes and Marsh, 2000). Notably, the wide-ranging roles of Cdc42 and other factors give cause to question whether this is a suitable target for siRNA depletion. Cell cycle regulation is particularly dependent upon this RhoGTPase, a role that explains the slow growth exhibited by HeLa cells in which the protein has been depleted.

This data presented in this chapter describes an efficient high content platform to assess the involvement of CME in the uptake of novel drug delivery systems. With regards to the inhibition of fluid-phase endocytosis and macropinocytosis the depletion of Rac1 may be a possible avenue to explore further, but the observations made following the PAK1 and Cdc42 studies suggest that siRNA depletion of proteins regulating actin dynamics may affect too many other cellular processes. For these reasons the use of pharmacological inhibitors to study fluid-phase endocytosis and macropinocytic uptake was decided upon.

3.5 References

Al Soraj, M., L. He, K. Peynshaert, J. Cousaert, D. Vercauteren, K. Braeckmans, S.C. De Smedt, and A.T. Jones. 2012. siRNA and pharmacological inhibition of endocytic pathways to characterize the differential role of macropinocytosis and the actin cytoskeleton on cellular uptake of dextran and cationic cell penetrating peptides octaarginine (R8) and HIV-Tat. *Journal of controlled release : official journal of the Controlled Release Society*. 161:132-141.

Beemiller, P., Y. Zhang, S. Mohan, E. Levinsohn, I. Gaeta, A.D. Hoppe, and J.A. Swanson. 2010. A Cdc42 activation cycle coordinated by PI 3-kinase during Fc receptor-mediated phagocytosis. *Molecular biology of the cell*. 21:470-480.

Buckley, C.M., and J.S. King. 2017. Drinking problems: mechanisms of macropinosome formation and maturation. *The FEBS journal*.

Cheng, Z.J., R.D. Singh, E.L. Holicky, C.L. Wheatley, D.L. Marks, and R.E. Pagano. 2010. Co-regulation of caveolar and Cdc42-dependent fluid phase endocytosis by phosphocaveolin-1. *The Journal of biological chemistry*. 285:15119-15125.

Chi, X., S. Wang, Y. Huang, M. Stamnes, and J.L. Chen. 2013. Roles of rho GTPases in intracellular transport and cellular transformation. *International journal of molecular sciences*. 14:7089-7108.

Cmejla, R., P. Ptackova, J. Petrak, F. Savvulidi, J. Cerny, O. Sebesta, and D. Vyoral. 2010. Human MRCKalpha is regulated by cellular iron levels and interferes with

transferrin iron uptake. *Biochemical and biophysical research communications*. 395:163-167.

Cox, D., P. Chang, Q. Zhang, P.G. Reddy, G.M. Bokoch, and S. Greenberg. 1997. Requirements for both Rac1 and Cdc42 in membrane ruffling and phagocytosis in leukocytes. *The Journal of experimental medicine*. 186:1487-1494.

Dharmawardhane, S., A. Schurmann, M.A. Sells, J. Chernoff, S.L. Schmid, and G.M. Bokoch. 2000. Regulation of macropinocytosis by p21-activated kinase-1. *Molecular biology of the cell*. 11:3341-3352.

Dutta, D., and J.G. Donaldson. 2012. Search for inhibitors of endocytosis: Intended specificity and unintended consequences. *Cellular logistics*. 2:203-208.

Edwards, D.C., L.C. Sanders, G.M. Bokoch, and G.N. Gill. 1999. Activation of LIM-kinase by Pak1 couples Rac/Cdc42 GTPase signalling to actin cytoskeletal dynamics. *Nature cell biology*. 1:253-259.

Erfle, H., B. Neumann, U. Liebel, P. Rogers, M. Held, T. Walter, J. Ellenberg, and R. Pepperkok. 2007. Reverse transfection on cell arrays for high content screening microscopy. *Nature protocols*. 2:392-399.

Fujita, S., K. Takano, E. Ota, T. Sano, T. Yoshikawa, M. Miyake, and J. Miyake. 2010. New methods for reverse transfection with siRNA from a solid surface. *Methods in molecular biology (Clifton, N.J.)*. 623:197-209.

Garrett, W.S., L.M. Chen, R. Kroschewski, M. Ebersold, S. Turley, S. Trombetta, J.E. Galan, and I. Mellman. 2000. Developmental control of endocytosis in dendritic cells by Cdc42. *Cell*. 102:325-334.

He, L., P.D. Watson, and A.T. Jones. 2015. Visualizing Actin Architectures in Cells Incubated with Cell-Penetrating Peptides. *Methods in molecular biology (Clifton, N.J.)*. 1324:247-259.

Jiang, Q., C. Zhou, Z. Bi, and Y. Wan. 2006. EGF-induced cell migration is mediated by ERK and PI3K/AKT pathways in cultured human lens epithelial cells. *Journal of ocular pharmacology and therapeutics : the official journal of the Association for Ocular Pharmacology and Therapeutics*. 22:93-102.

Jones, A.T. 2007. Macropinocytosis: searching for an endocytic identity and role in the uptake of cell penetrating peptides. *Journal of cellular and molecular medicine*. 11:670-684.

Kalwat, M.A., S.M. Yoder, Z. Wang, and D.C. Thurmond. 2013. A p21-activated kinase (PAK1) signaling cascade coordinately regulates F-actin remodeling and insulin granule exocytosis in pancreatic beta cells. *Biochemical pharmacology*. 85:808-816.

Marks, D.L., R. Bittman, and R.E. Pagano. 2008. Use of Bodipy-labeled sphingolipid and cholesterol analogs to examine membrane microdomains in cells. *Histochemistry and cell biology*. 130:819-832.

Marks, D.L., R.D. Singh, A. Choudhury, C.L. Wheatley, and R.E. Pagano. 2005. Use of fluorescent sphingolipid analogs to study lipid transport along the endocytic pathway. *Methods (San Diego, Calif.)*. 36:186-195.

Monypenny, J., D. Zicha, C. Higashida, F. Oceguera-Yanez, S. Narumiya, and N. Watanabe. 2009. Cdc42 and Rac family GTPases regulate mode and speed but not direction of primary fibroblast migration during platelet-derived growth factor-dependent chemotaxis. *Molecular and cellular biology*. 29:2730-2747.

Moody, P.R., E.J. Sayers, J.P. Magnusson, C. Alexander, P. Borri, P. Watson, and A.T. Jones. 2015. Receptor Crosslinking: A General Method to Trigger Internalization and Lysosomal Targeting of Therapeutic Receptor:Ligand Complexes. *Molecular therapy : the journal of the American Society of Gene Therapy*. 23:1888-1898.

Motley, A., N.A. Bright, M.N. Seaman, and M.S. Robinson. 2003. Clathrin-mediated endocytosis in AP-2-depleted cells. *The Journal of cell biology*. 162:909-918.

Nobes, C., and M. Marsh. 2000. Dendritic cells: new roles for Cdc42 and Rac in antigen uptake? *Current biology : CB*. 10:R739-741.

Ong, C.C., A.M. Jubb, W. Zhou, P.M. Haverty, A.L. Harris, M. Belvin, L.S. Friedman, H. Koeppen, and K.P. Hoeflich. 2011. p21-activated kinase 1: PAK'ed with potential. *Oncotarget*. 2:491-496.

Peter, Y., A. Comellas, E. Levantini, E.P. Ingenito, and S.D. Shapiro. 2009. Epidermal growth factor receptor and claudin-2 participate in A549 permeability and

remodeling: implications for non-small cell lung cancer tumor colonization. *Molecular carcinogenesis*. 48:488-497.

Shen, H., S.M. Ferguson, N. Dephoure, R. Park, Y. Yang, L. Volpicelli-Daley, S. Gygi, J. Schlessinger, and P. De Camilli. 2011. Constitutive activated Cdc42-associated kinase (Ack) phosphorylation at arrested endocytic clathrin-coated pits of cells that lack dynamin. *Molecular biology of the cell*. 22:493-502.

Singh, R.D., D.L. Marks, and R.E. Pagano. 2007. Using fluorescent sphingolipid analogs to study intracellular lipid trafficking. *Current protocols in cell biology / editorial board, Juan S. Bonifacino ... [et al.]*. Chapter 24:Unit 24.21.

Singh, R.D., A.S. Schroeder, L. Scheffer, E.L. Holicky, C.L. Wheatley, D.L. Marks, and R.E. Pagano. 2013. Prominin-2 expression increases protrusions, decreases caveolae and inhibits Cdc42 dependent fluid phase endocytosis. *Biochemical and biophysical research communications*. 434:466-472.

Tourkova, I.L., G.V. Shurin, S. Wei, and M.R. Shurin. 2007. Small rho GTPases mediate tumor-induced inhibition of endocytic activity of dendritic cells. *Journal of immunology (Baltimore, Md. : 1950)*. 178:7787-7793.

Tunduguru, R., T.T. Chiu, L. Ramalingam, J.S. Elmendorf, A. Klip, and D.C. Thurmond. 2014. Signaling of the p21-activated kinase (PAK1) coordinates insulin-stimulated actin remodeling and glucose uptake in skeletal muscle cells. *Biochemical pharmacology*. 92:380-388.

Vercauteren, D., R.E. Vandenbroucke, A.T. Jones, J. Rejman, J. Demeester, S.C. De Smedt, N.N. Sanders, and K. Braeckmans. 2010. The use of inhibitors to study endocytic pathways of gene carriers: optimization and pitfalls. *Molecular therapy : the journal of the American Society of Gene Therapy*. 18:561-569.

Watson, L.J., G. Rossi, and P. Brennwald. 2014. Quantitative analysis of membrane trafficking in regulation of Cdc42 polarity. *Traffic (Copenhagen, Denmark)*. 15:1330-1343.

Yi, Q., and M.G. Coppolino. 2006. Automated classification and quantification of F-actin-containing ruffles in confocal micrographs. *BioTechniques*. 40:745-746, 748, 750 passim.

Zeineldin, R., and L.G. Hudson. 2006. Epithelial cell migration in response to epidermal growth factor. *In* Epidermal Growth Factor. Springer. 147-158.

Zhang, W., Y. Huang, and S.J. Gunst. 2016. p21-Activated kinase (Pak) regulates airway smooth muscle contraction by regulating paxillin complexes that mediate actin polymerization. *The Journal of physiology*. 594:4879-4900.

4 Investigations on chemical inhibitors of fluid-phase endocytosis and macropinocytosis in HeLa and A549 cells

4.1 Introduction

Useful *in vitro* siRNA targeting models for CME and CIE were now available but there was still a requirement for models to study unstimulated and induced macropinocytosis**.** Inhibitors directly targeting the actin cytoskeleton, such as cytochalasin D, were avoided due to the extensive morphological effects of these agents that is likely to have global cellular effects (He et al., 2015).

This work was performed using HeLa and A549 cells, rather than bEnd.3 cells, as the use of two cell lines in siRNA transfection and endocytic probe uptake had generated an efficient platform for the analysis of CME. Indeed, identification of a protein target for the siRNA inhibition of fluid-phase endocytosis/macropinocytosis had not been as successful, but these cell lines were again used to maintain consistency within the project.

4.2 Aims and Objectives

- To further explore inhibitory methods involving chemical inhibitors to target fluid-phase endocytosis and macropinocytosis, due to the lack of an efficient protein for siRNA targeted depletion.

- To assess the fluid-phase uptake of dextran in HeLa and A549 cells treated with the common inhibitors of fluid-phase endocytosis and macropinocytosis: EIPA, Rottlerin, IPA-3 and ML-7.
- To identify the potential cell-wide effects caused by the treatment of these inhibitors at different concentrations on these cell lines.
- To establish chemical inhibitor based *in vitro* models for the inhibition of fluid-phase endocytosis and macropinocytosis that can be used to evaluate the uptake of novel drug delivery systems via these mechanisms.

4.3 Results

4.3.1 Investigation of the chemical inhibitor of fluid-phase endocytosis and macropinocytosis 5-(N-ethyl-N-isopropyl)amiloride (EIPA)

As previously discussed in Chapter 1, the Na^+/H^+ exchange inhibitor EIPA and the parent molecule amiloride have been widely employed in macropinocytic studies at low micromolar concentration (Al Soraj et al., 2012; Devadas et al., 2014).

At 100 µM, the cells are more rounded and highly autofluorescent in the green channel when compared to control cells (Figure 4.1), indicating that this concentration of EIPA may affect the wider physiology of the cell. Hoechst33342 staining is also uniform across the cell structure and not solely localised to the nucleus. Dextran uptake was noticeably reduced following treatment with 50 µM EIPA yet the Hoechst33342 staining was not confined to the nucleus but was uniform across the cell cytoplasm. The lower concentrations of 25 µM and 10 µM

were subsequently used in an attempt to prevent dextran uptake in HeLa and A549 without visibly affecting Hoechst33342 staining or cell morphology. These concentrations have been utilised in previous studies to assess the macropinocytic uptake of various other entities (Weinberg et al., 2014).

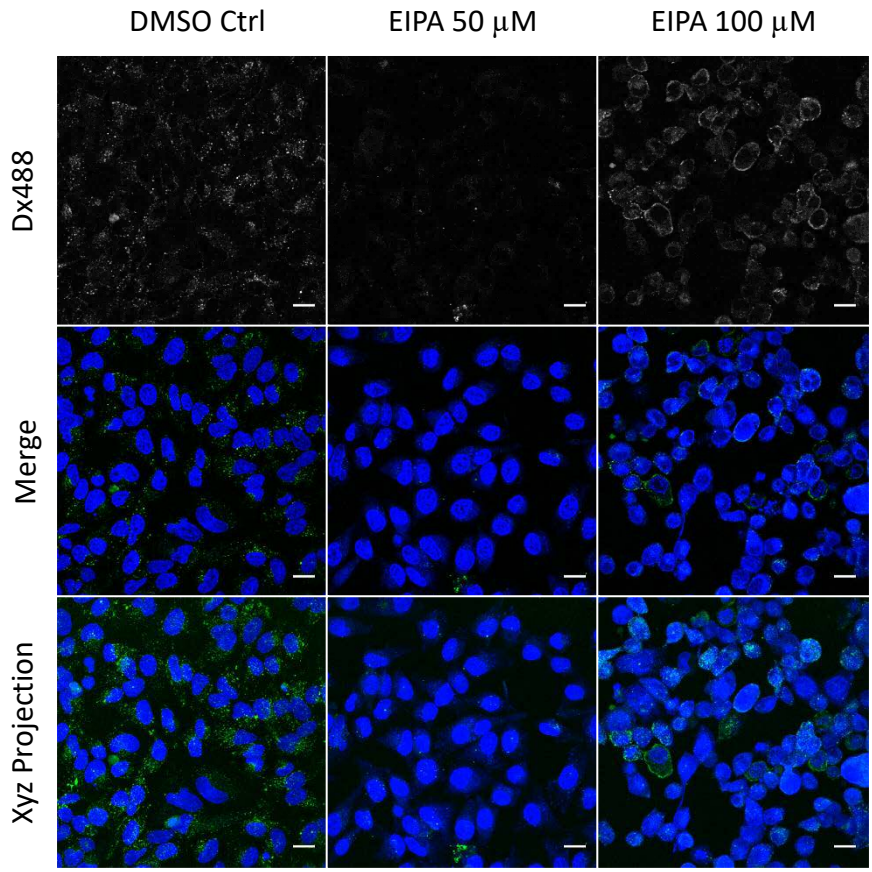

Fig. 4.1. ***Dx488 uptake in HeLa cells treated with 100 µM and 50 µM EIPA.*** Cells were pre-treated with either DMSO (0.05%), 50 µM EIPA or 100 µM EIPA for 30 min before being subjected to a 60 min Dx488 (100 µg/ml) pulse in the continued presence of the inhibitor. Hoechst33342 was added 5 min before imaging live (R/T). Scale bar: 20 µm.

Firstly, the noted effects on cell morphology and Hoechst33342 staining at 25 µM and 10 µM are not apparent in both cell types, indicating that these are adequate concentrations. Following a 60 min dextran pulse in HeLa, dextran positive vesicles can

be observed within the cell (Figure 4.2). A small decrease in intracellular dextran fluorescence was apparent following 25 µM EIPA treatment as viewed via microscopy and MFI quantification (Figure 4.2), suggesting that a proportion of fluid-phase endocytosis has been obstructed. Statistically this was insignificant. Little difference in dextran uptake can be observed between untreated cells and 10 µM EIPA, indicating that an optimum concentration for the inhibition of dextran uptake without having effects on cell morphology is approximately 25 µM.

Treatment with these concentrations also indicated little difference in cell morphology when compared with control treated cells, as demonstrated by Cell Mask deep red (CMDR) staining following treatment (Figure 4.3). Transferrin internalisation in EIPA cells was significantly reduced, indicating an effect on CME (Figure 4.4). Notably, differences in the localisation of transferrin loaded vesicles was apparent, agreeing with our previous studies that show effects on the subcellular localisation of early and late endosomes/lysosomes in cells treated with this drug (Fretz et al., 2006).

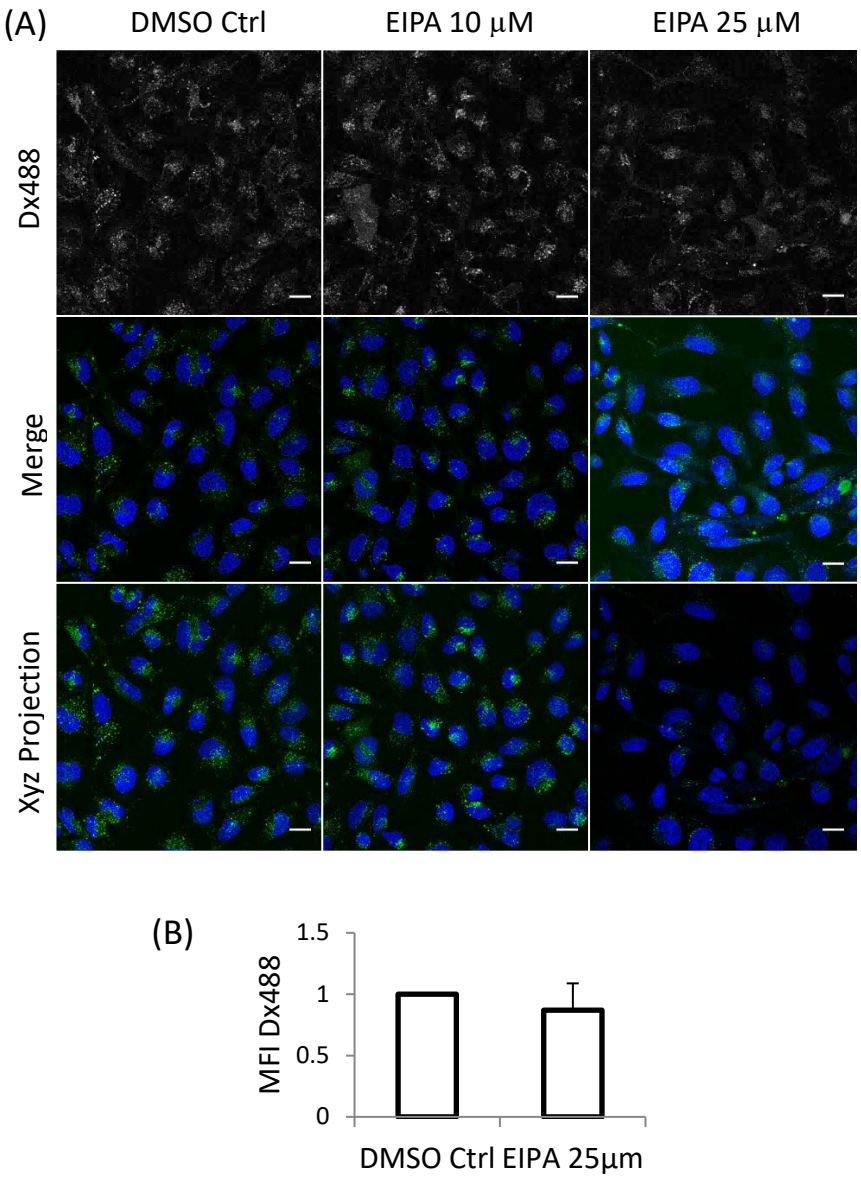

Fig. 4.2. ***Dx488 endocytosis in HeLa cells is not affected by 25 µM EIPA*** (A) Cells were pre-treated with either DMSO (0.05%), 25 µM EIPA or 10 µM EIPA for 30 min before being subjected to a 60 min Dx488 (100 µg/ml) pulse in the continued presence of the inhibitor. Hoechst33342 was added 5 min before imaging live (R/T). Scale bar: 20 µm. (B) MFI quantification of Dx488 in each cell population. Error bars: Standard error. Images (25 µM) and graph summarise three separate experiments.

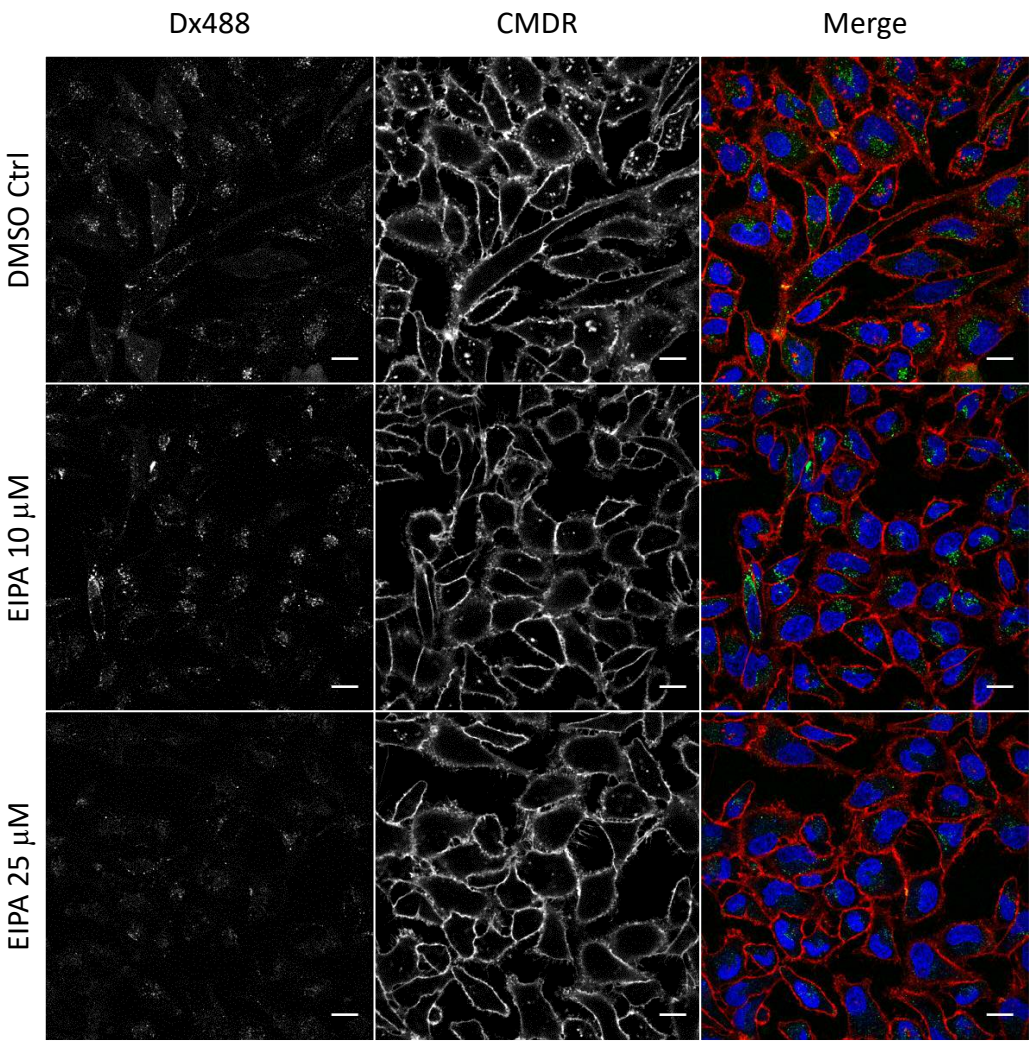

Fig. 4.3. ***Cell Mask Deep Red (CMDR) staining indicates little difference in cell morphology following EIPA treatment in HeLa cells.*** Cells were pre-treated with either DMSO (0.05%), 25 µM EIPA or 10 µM EIPA for 30 min before being subjected to a 60 min Dx488 (100 µg/ml) pulse whilst in the continued presence of the inhibitor. Hoechst33342 and CMDR were added 5 min before imaging live (R/T). Scale bar: 20 µm. Images representative of three separate experiments.

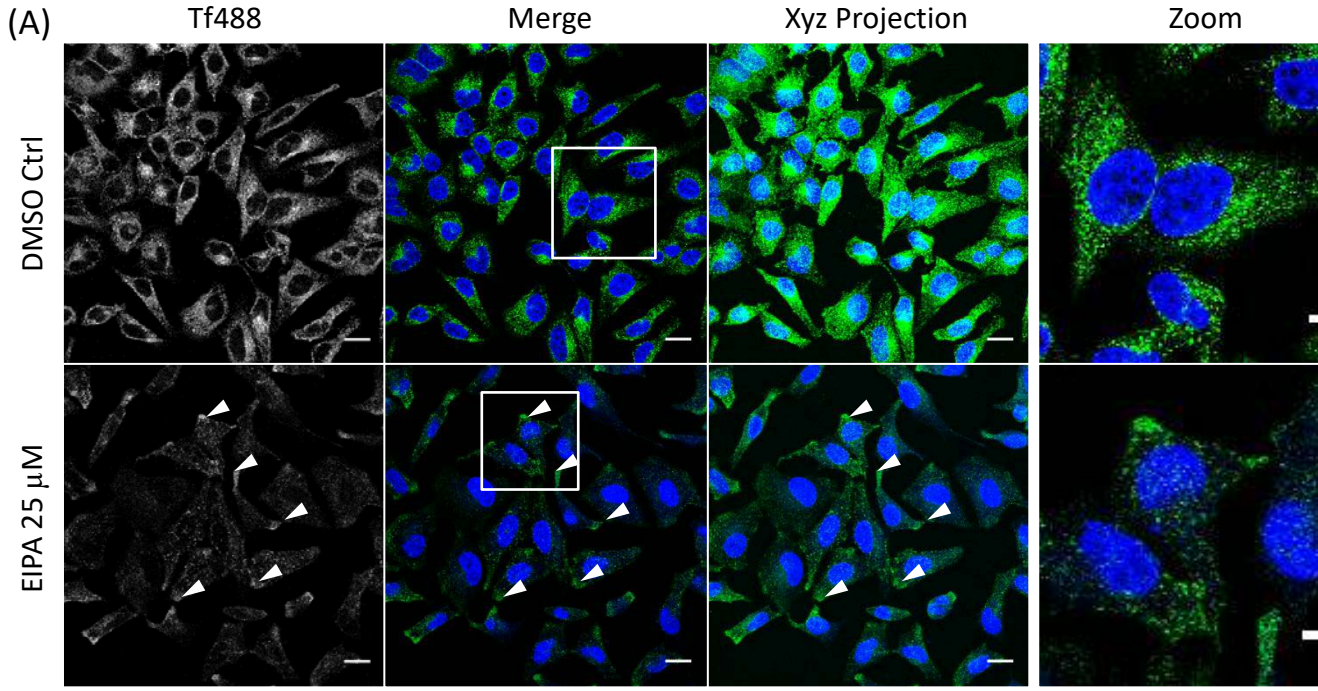

Fig. 4.4. ***Tf488 internalisation following EIPA treatment in HeLa cells.*** (A) Cells were pre-treated with either DMSO (0.0
being subjected to a 10 min Tf488 (5 µg/ml) pulse whilst in the continued presence of the inhibitor. Hoechst33342 was a
Solid arrows indicate concentrated transferrin localisation/fluorescence at the cell periphery. White squares presented
10 µm in zoomed images. (B) Graph presents MFI quantification of Tf488 in each cell population. Error bars: Standard
three separate experiments. **p<0.01

Identical experiments were carried out in A549 cells. Possible effects on cell morphology and therefore the wider physiology of the cell were more observable at 25 µM and 10 µM in this cell line, whereby the production of the autofluorescent structures previously described are extensive (Figure 4.5). This suggests that both concentrations may have global effects in A549 cells.

MFI quantification also indicated that there was little difference in the ability of cells to internalise dextran at both 10 µM and 25 µM EIPA in A549 cells (Figure 4.5b), signifying that fluid-phase endocytosis was not prevented at these concentrations. Transferrin uptake (Section 2.5.2) was assessed following EIPA treatment in A549 cells to observe the effects of this inhibitor treatment on different endocytic pathways, and because of the observations discussed previously.

There was no difference in uptake or localisation of transferrin vesicles between EIPA treated cells and control treated cells (Figure 4.6), indicating that CME and trafficking are not visibly affected by this drug. MFI quantification supports these observations in that there was little difference in uptake intensity (Figure 4.6). Furthermore, a greater number of autofluorescent structures previously described in A549 cells can again be viewed in A549 cells, suggesting that the inhibitor may affect other physiological processes. For these reasons, EIPA may not be an efficient inhibitor for these studies in A549 cells, but its use in HeLa should not be disregarded.

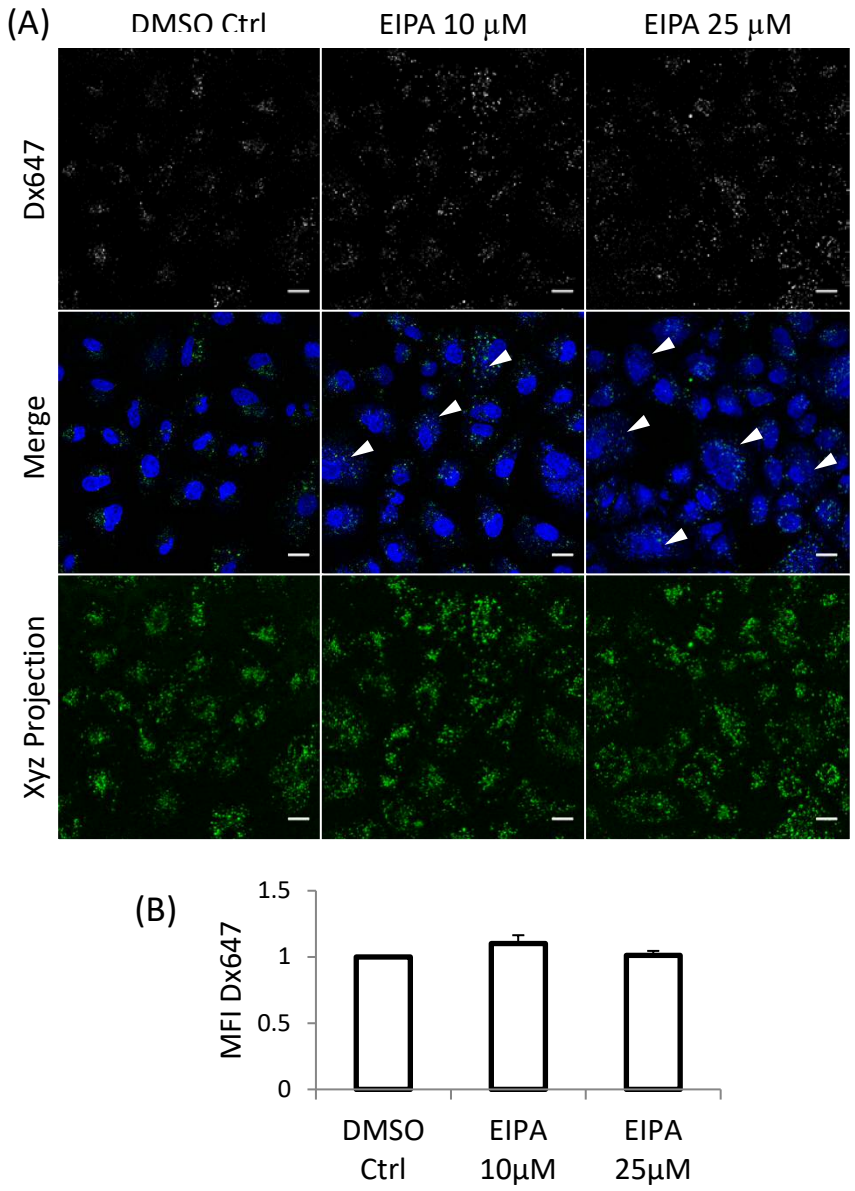

Fig. 4.5. ***Dx647 endocytosis is not affected following EIPA treatment in A549 cells.*** (A) Cells were pre-treated with either DMSO (0.05%), 25 µM or 10 µM EIPA for 30 min before being subjected to a 60 min Dx488 (100 µg/ml) pulse in the continued presence of the inhibitor. Hoechst33342 was added 5 min before imaging live (R/T). White arrows indicate autofluorescent punctate structures. Scale bar: 20 µm. (B) MFI quantification of Dx488 in each cell population. Error bars: Standard error. Images and graph summarise three separate experiments.

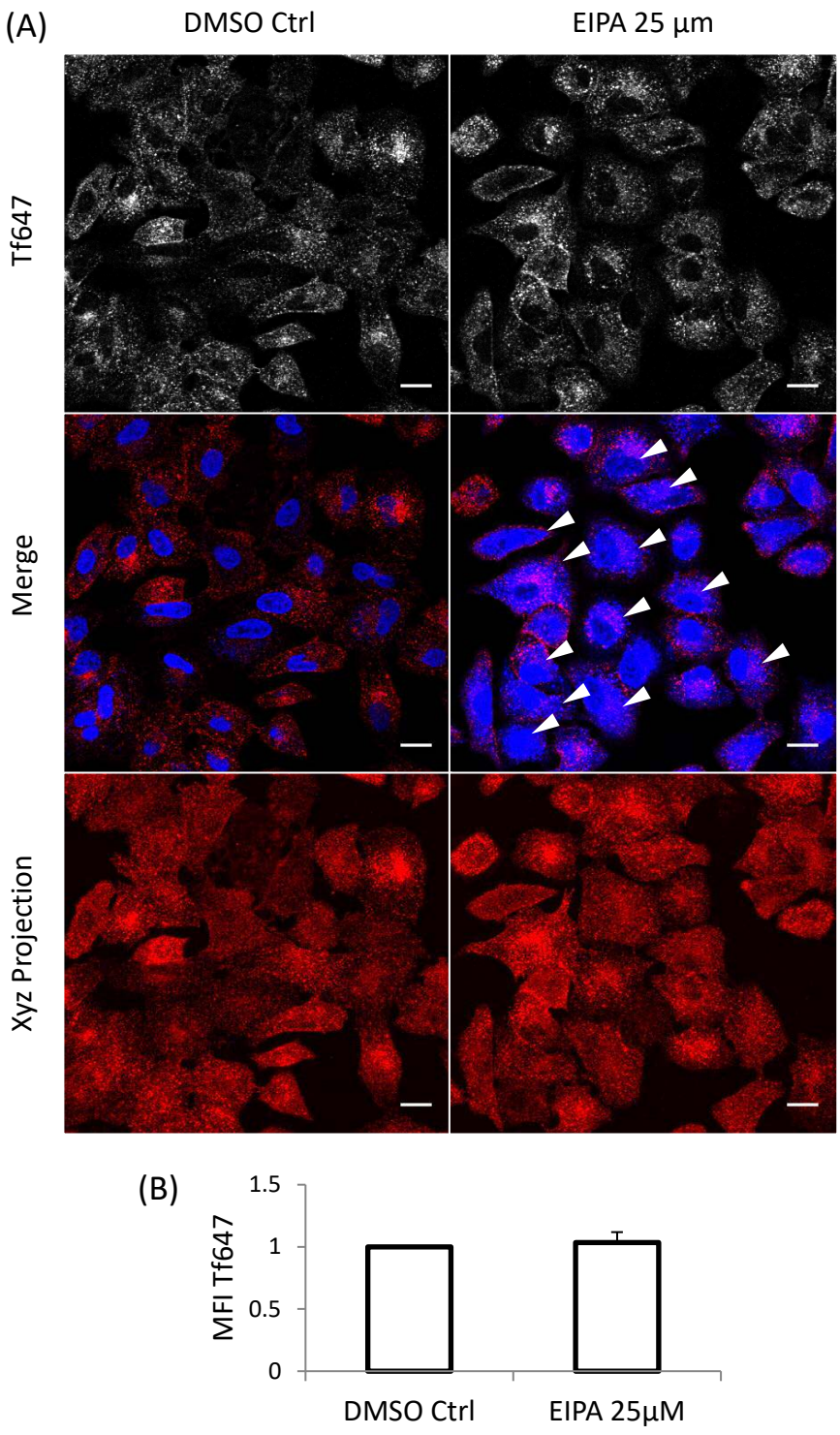

Fig. 4.6. ***Tf647 endocytosis is not affected following EIPA treatment in A549 cells.*** (A) Cells were pre-treated with either DMSO (0.05%) or 25 µM EIPA for 30 min before being subjected to a 10 min Tf647 (5 µg/ml) pulse and 5 min chase whilst in the continued presence of the inhibitor. Hoechst33342 was added 5 min before imaging live (R/T). Arrows indicate autofluorescent punctate structures. Scale bar: 20 µm. (B) MFI quantification of Tf647 in each cell population. Error bars: Standard error. Images and graphs summarise three separate experiments.

4.3.2 Investigation of the fluid-phase inhibitor Rottlerin and its potential target PKCδ

This drug has been utilised to study fluid-phase endocytosis and macropinocytic events in different cell lines through its suggested capacity to inhibit PKCδ in the 5-10 μM range (Fenyvesi et al., 2014; Sarkar et al., 2005; Vercauteren et al., 2011). For instance, 10 μM Rottlerin was previously shown to reduce the uptake of dextran in ARPE-19 cells (Vercauteren et al., 2011) and the uptake of Lucifer yellow and cyclodextrin in Caco-2 cells (Fenyvesi et al., 2014). Here, dextran was again utilised as a fluid phase probe for Rottlerin studies and after 60 min incubation in Hela there was evidence that uptake was inhibited at both 5 μm and 10 μM (Figure 4.7), but MFI scrutiny for a repeated 10 μM concentration revealed that this was not significant. Localisation of dextran fluorescence did however appear to be more disperse through the cytoplasm/cytosol in cells treated with this inhibitor (Figure 4.7). This could suggest that Rottlerin may be affecting endosomes and possibly inducing endocytic escape. Despite this observation, there were no notable effects on cell morphology following Rottlerin treatment in comparison with control cells (Figure 4.7).

Rottlerin treatment in A549 cells produced a significant decrease in dextran fluorescence (Figure 4.8), providing evidence that the target of Rottlerin may be a target for fluid-phase specific inhibition in this cell line.

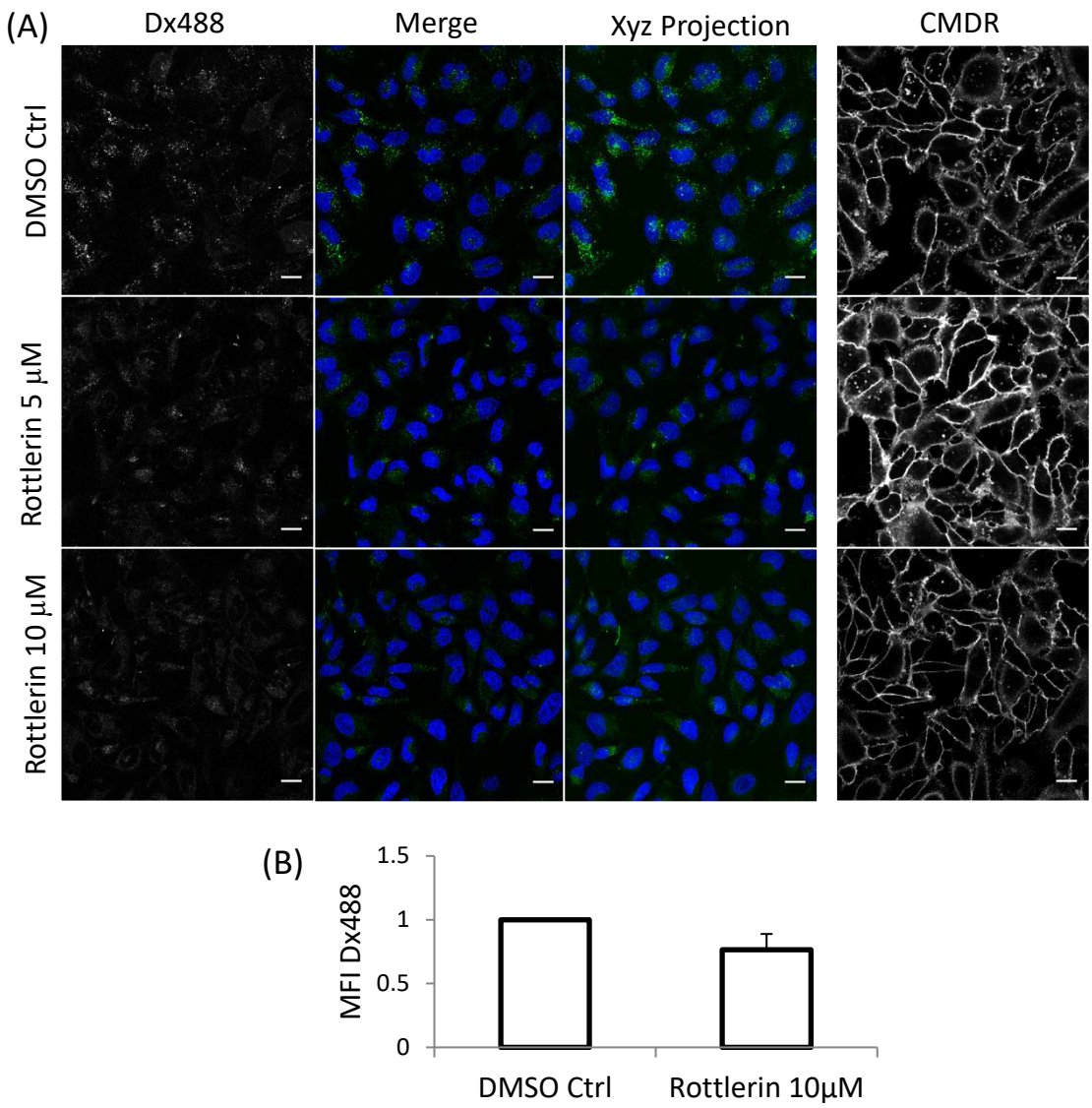

Fig. 4.7. ***Dx488 endocytosis and cell morphology are not affected following Rottlerin treatment in HeLa cells.*** (A) Cells were pre-treated with either DMSO (0.05%), 5 µM Rottlerin or 10 µM Rottlerin for 30 min before being subjected to a 60 min Dx488 (100 µg/ml) pulse whilst in the continued presence of the inhibitor. Hoechst33342 and CMDR were added 5 min before imaging live (R/T). Scale bar: 20 µm. (B) MFI quantification of Dx488 in each cell population. Error bars: Standard error. Images and graph summarise three separate experiments.

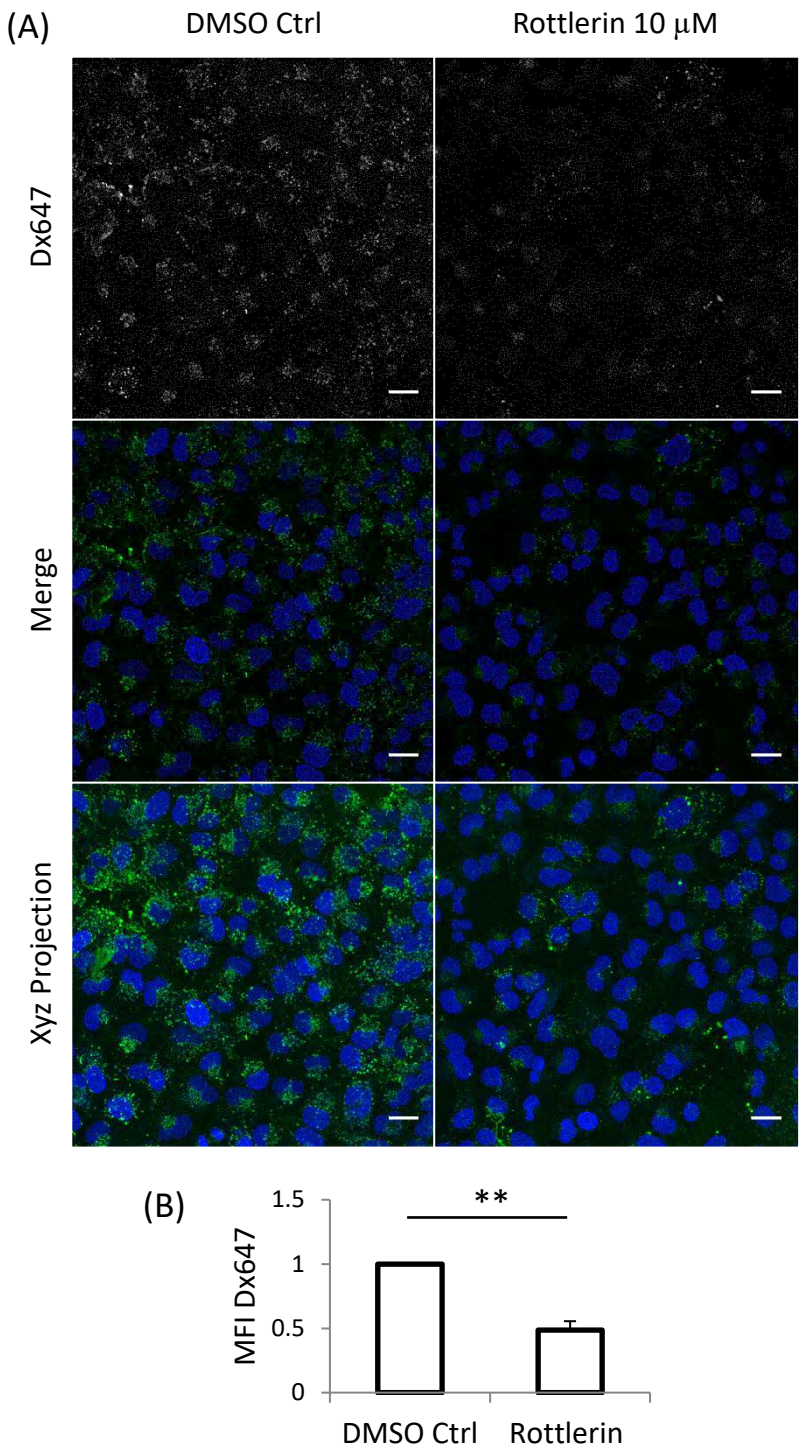

Fig. 4.8. ***Dx488 endocytosis is significantly reduced following Rottlerin treatment in A549 cells.*** (A) Cells were pre-treated with either DMSO (0.05%) or 10 µM Rottlerin for 30 min before being subjected to a 60 min Dx647 (100 µg/ml) pulse whilst in the continued presence of the inhibitor. Hoechst33342 was added 5 min before imaging live (R/T). Scale bar: 20 µm. (B) MFI quantification of Dx647 in each cell population. Error bars: Standard error. Images and graph summarise three separate experiments. **p<0.01

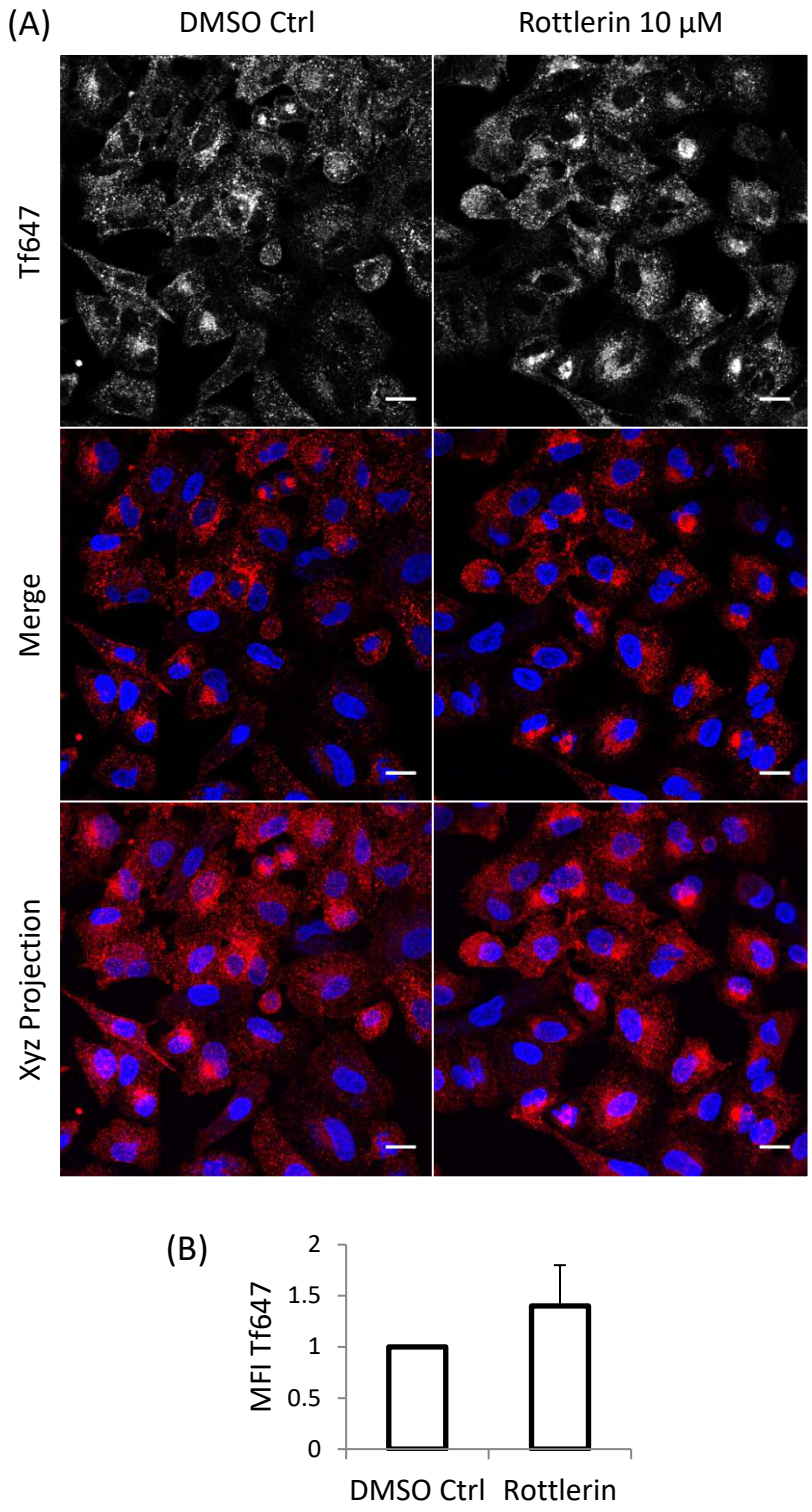

Fig. 4.9. ***Tf647 endocytosis following Rottlerin treatment in A549 cells.*** (A) Cells were pre-treated with either DMSO (0.05%) or 10 µM Rottlerin for 30 min before being subjected to a 10 min Tf647 (5 µg/ml) pulse whilst in the continued presence of the inhibitor. Hoechst33342 was added 5 min before imaging live (R/T). Scale bar: 20 µm. (B) MFI quantification of Tf647 in each cell population. Error bars: Standard error. Images and graphs summarise three separate experiments.

To investigate whether Rottlerin is exclusively affecting fluid-phase uptake in A549 cells, we also performed transferrin uptake assays to evaluate its potential effects on CME. Characteristic transferrin positive vesicles visualised within control cells were also observed in cells treated with Rottlerin, suggesting that the inhibitor has no effect on CME (Figure 4.9a). Quantification of transferrin MFI supports this observation (Figure 4.9b). The ability of Rottlerin to affect the fluid-phase in A549 cells indicates that one of its identified targets Protein Kinase Cδ (PKCδ) (Gschwendt et al., 1994) is involved in this process. siRNA sequences were then identified and purchased to test this hypothesis for macropinocytic studies (Sarkar et al., 2005). For this reason, PKCδ was identified as a possible target for inhibiting fluid-phase endocytosis and macropinocytosis.

Following a 48 hour transfection with PKCδ siRNA, Western blot analysis demonstrated that the protein was successfully depleted in HeLa and A549 cells (Figure 4.10). A dextran uptake assay was then performed to ascertain the effects of PKCδ depletion on fluid-phase endocytosis. Uptake was initially performed in A549 cells, as Rottlerin induced a diminished ability of this cell line to internalise dextran. Data shown in Figure 4.11a however shows no clear difference in dextran uptake in siPKCδ cells compared with controls. MFI quantification supported this observation (Figure 4.11b).

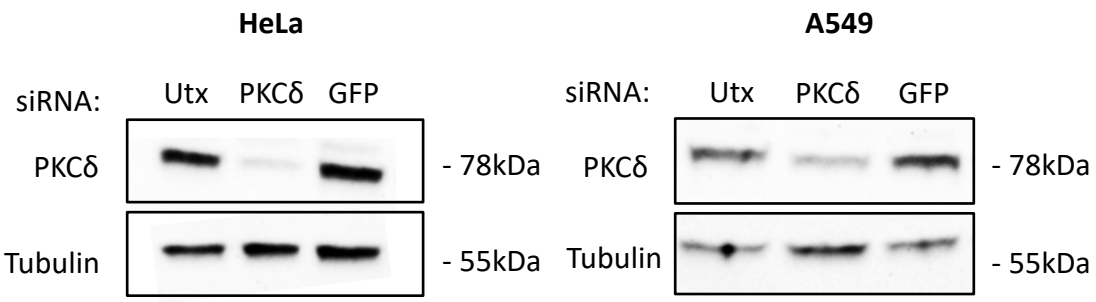

Fig. 4.10. ***PKCδ is successfully depleted following siRNA transfection in both HeLa and A549 cells.*** Western blot analysis indicates levels of PKCδ are depleted 48 h following siRNA transfection in HeLa and A549 cells when compared with tubulin as a loading control.

Many of the PKC isoforms, including PKCδ, have been implicated in regulating actin function (Keenan and Kelleher, 1998; Larsson, 2006) so actin localisation was compared in both control cells and siPKCδ cells using rhodamine-phalloidin staining of fixed cells. PKCδ depletion did induce a minor but consistent change in the structure and organisation of the actin cytoskeleton. Cells depleted of the protein presented with more pronounced stress fibres compared with control cells and this was most pronounced in the basal and central portions of the cells' Z-axis (Figure 4.12).

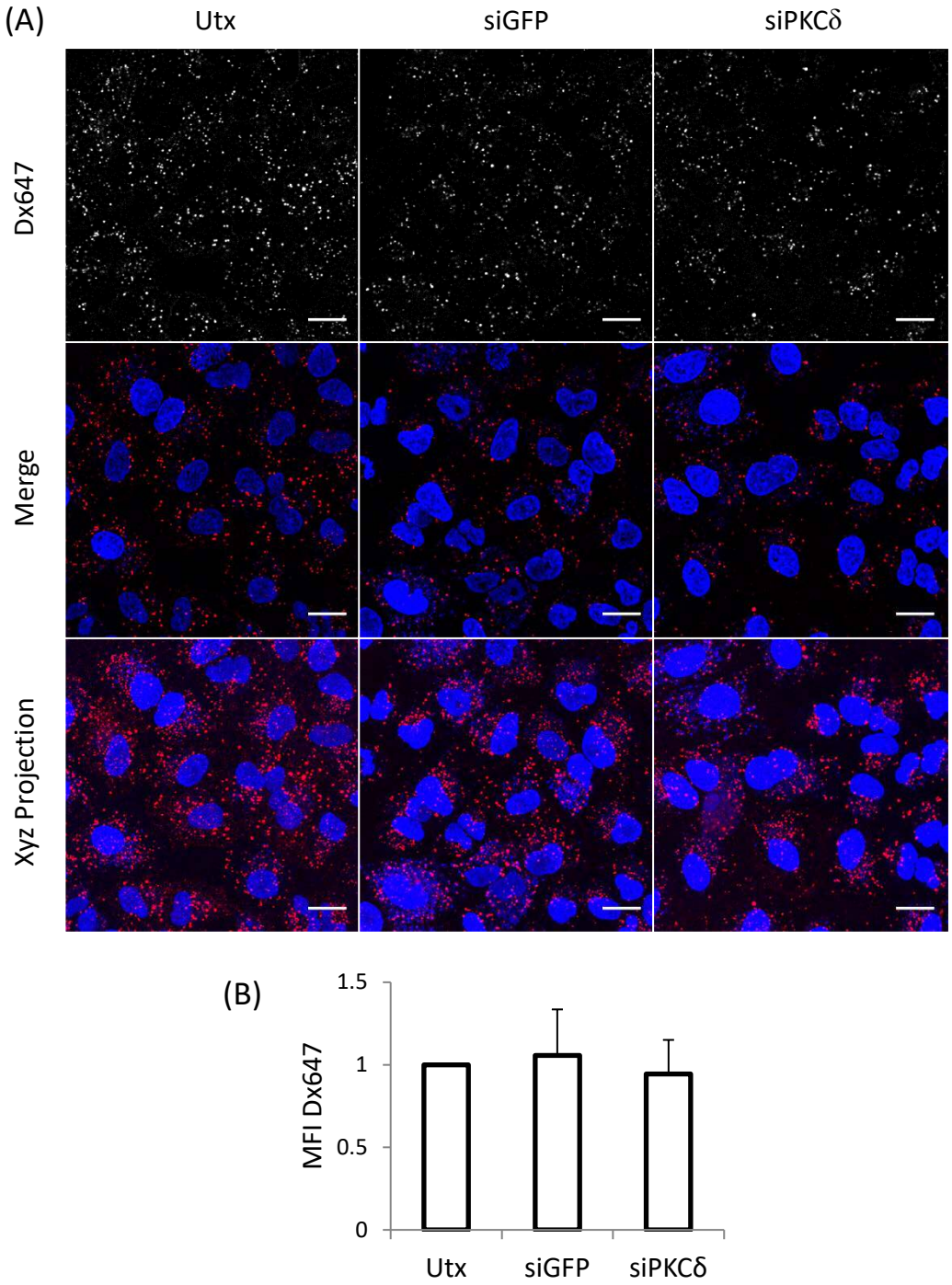

Fig. 4.11. ***Dex647 endocytosis is not affected following depletion of PKCδ via siRNA transfection in A549 cells.*** (A) Following 48 h transfection, cells were subjected to a 60 min Dx647 (100 µg/ml) pulse. Hoechst33342 was added 5 min before imaging live (R/T). Scale Bar: 20 µm. (B) MFI quantification of Dx647 in each cell population. Bars: Standard error. Images and graphs summarise three separate experiments.

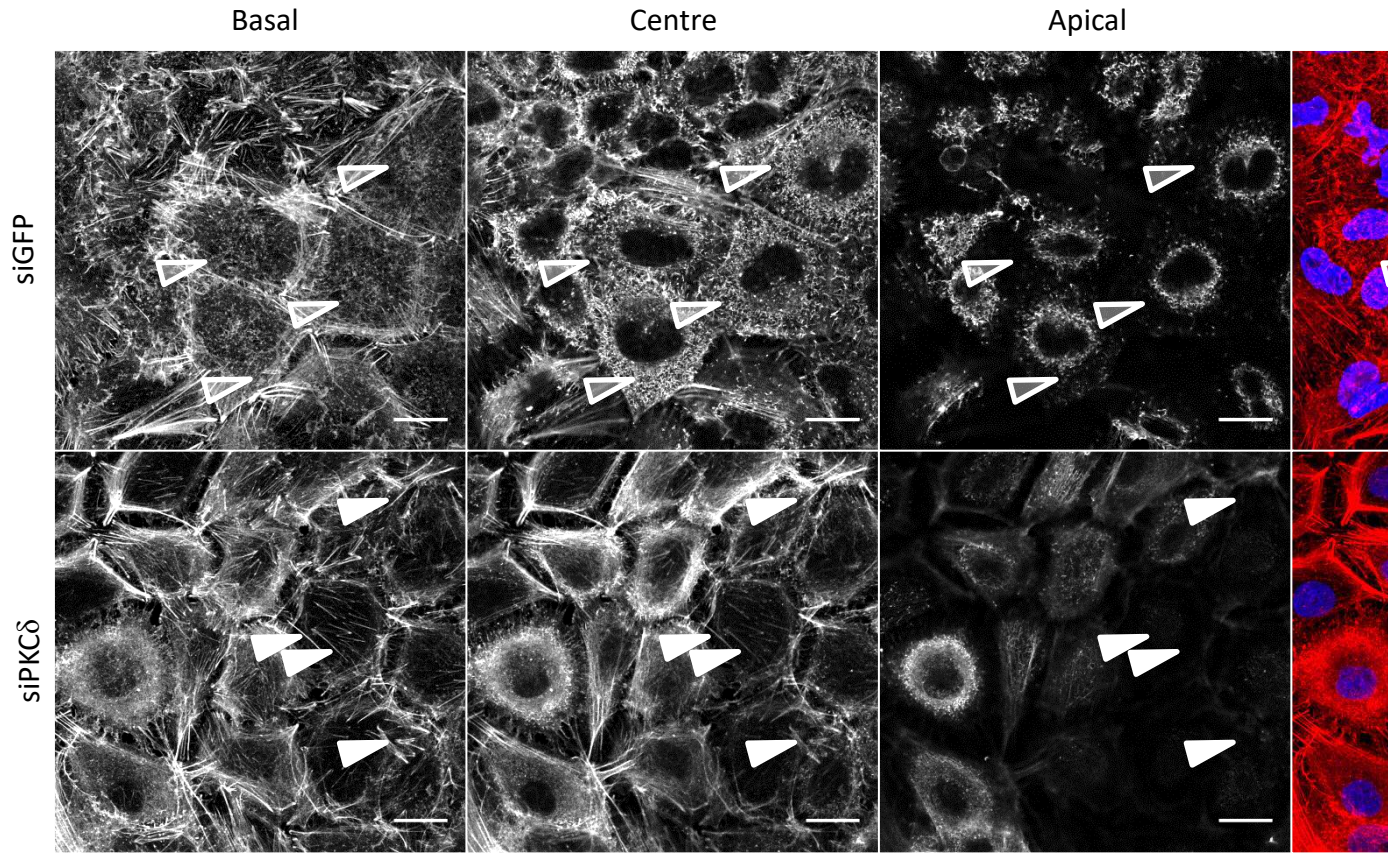

Fig. 4.12. ***The actin cytoskeleton of A549 cells presents with a greater number of stress fibres following PKCδ depletion.*** Cells
(100 nM) for 48 h. PFA fixation was carried out before 10 min incubation with Rhodamine-Phalloidin (1:500) and Hoechst33
Translucent arrows indicate greater actin activity, solid arrows indicate stress fibres. Scale bar: 10 µm.

4.3.3 Exploration of the PAK1 inhibitor IPA-3 to target fluid-phase endocytosis and macropinocytosis

The PAK1 inhibitor IPA-3 has previously been used to propose macropinocytosis as a mechanism for viral cell entry (Krzyzaniak et al., 2013; Wen et al., 2013). The effects of this inhibitor on fluid-phase uptake of dextran were initially explored in HeLa cells. A prominent decrease in dextran uptake was observed (Figure 4.13a), supported by MFI quantification ($p=0.033$)(Figure 4.13b). These experiments were also performed in A549 cells and at 50 µM there was again evidence that dextran uptake was decreased but also some evidence of cell toxicity that manifested as cell loss (floating cells) and cell shrinkage (Figure 4.14). At 25 µM IPA-3 there was no evidence of a reduction in dextran uptake or loss of viability. Further studies on IPA-3 will be presented in the following results chapter.

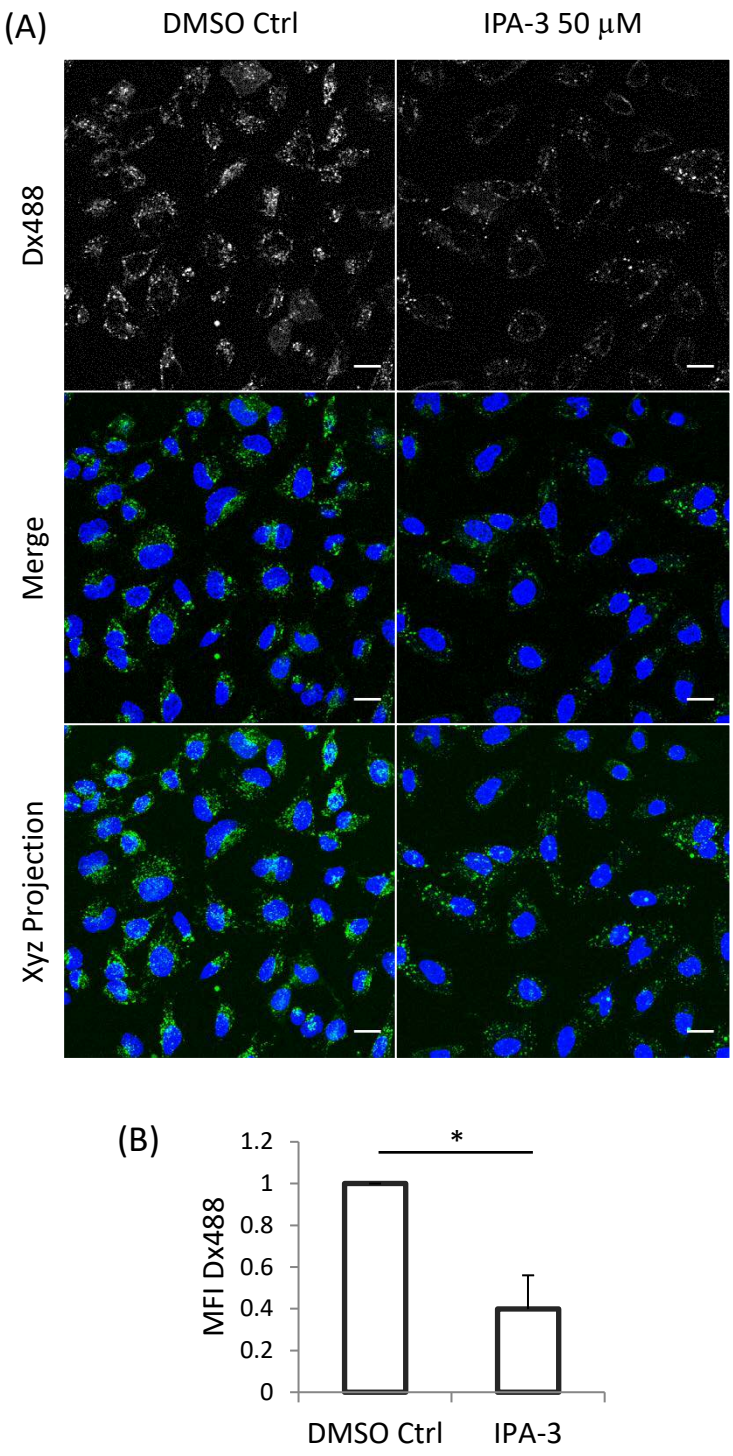

Fig. 4.13. ***Dx488 endocytosis is significantly reduced following IPA-3 treatment in HeLa cells.*** (A) Cells were pre-treated with either DMSO (0.05%) or 50 µM IPA-3 for 30 min before being subjected to a 60 min Dx488 (100 µg/mL) pulse whilst in the continued presence of the inhibitor. Hoechst33342 was added 5 min before imaging live (R/T). Scale bar: 20 µm. (B) MFI quantification of Dx488 in each cell population. Error bars: Standard error. Images and graphs summarise three separate experiments. *p<0.05.

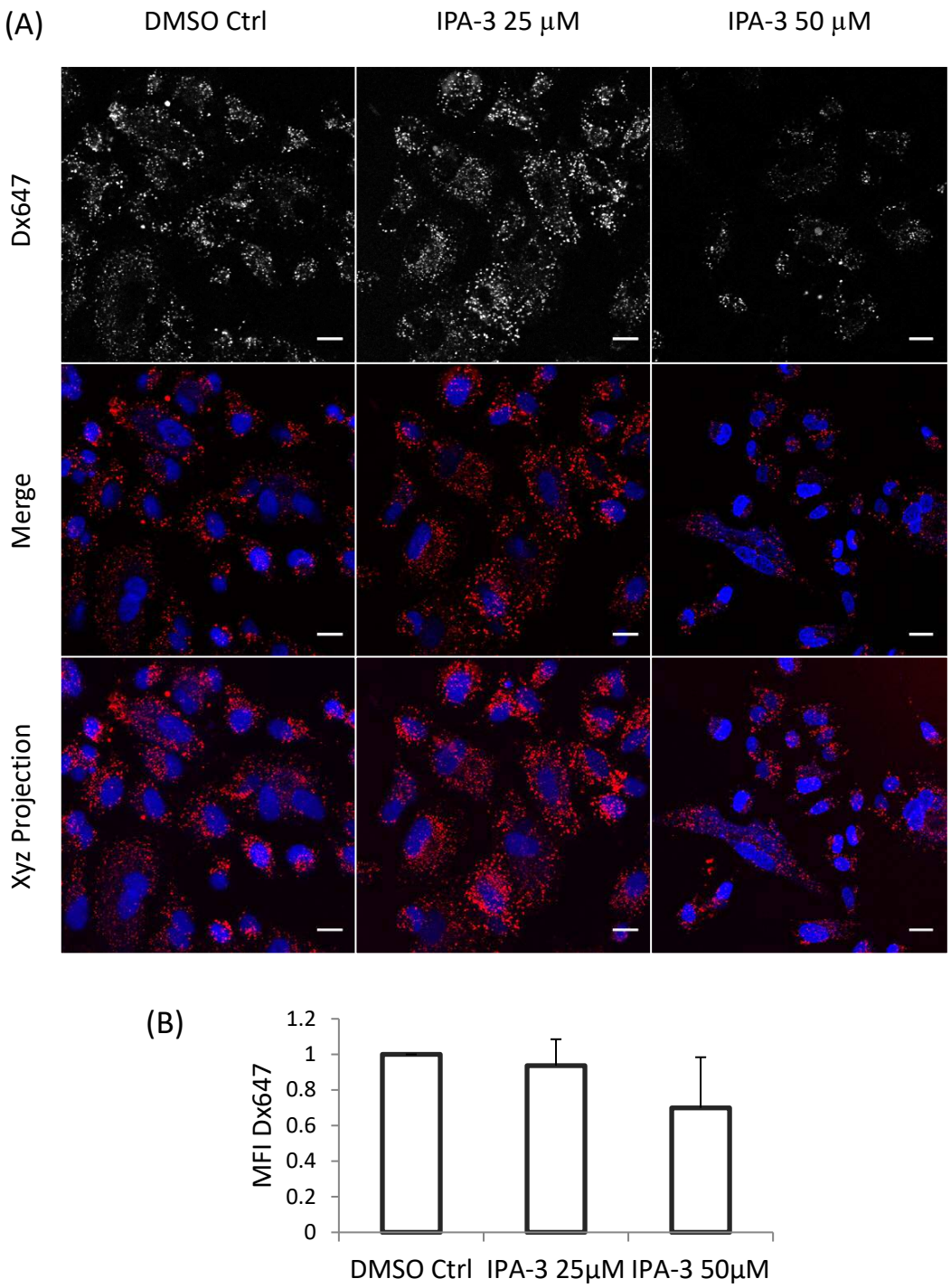

Fig. 4.14. ***Dx647 endocytosis decreases following IPA-3 treatment in A549 cells.*** (A) Cells were pre-treated with either DMSO (0.05%), 25 µM or 50 µM IPA-3 for 30 min before being subjected to a 60 min Dx647 (100 µg/ml) pulse whilst in the continued presence of the inhibitor. Hoechst33342 was added 5 min before imaging live (R/T). Scale bar: 20 µm. (B) MFI quantification of Dx488 in each cell population. Error bars: Standard error. Images and graph summarise three separate experiments.

4.3.4 Investigation of the cellular effects of ML-7, a myosin light chain kinase inhibitor

As a myosin light chain kinase inhibitor, ML-7 has been utilised in a small number of endocytic studies targeting fluid-phase, macropinocytosis and phagocytosis. Dextran uptake experiments were then performed in cells treated with this drug using the methodology outlined in Section 2.5.2. Control treated cells were observed to internalise dextran in a characteristic manner after 60 min of uptake (Figure 4.15). Dextran uptake in 10 µM ML-7 treated Hela cells appeared to be normal (Figure 4.15) but in cells treated with the higher drug concentration obvious morphological changes were apparent. These mostly manifested as cells rounding. These morphological effects were not observed when the same experiments were performed in A549 that showed visibly higher levels of dextran fluorescence when incubated with the drug (Figure 4.16).

Indication that myosin II (which is indirectly targeted by ML-7) is required for the progression of CME (Chandrasekar et al., 2014) let to investigation as to whether the drug also inhibits CME. Data in Figure 4.17 strongly suggests this is the case but this was not followed by MFI quantification as the drug by this time, due to its multiple effects was discontinued as a possible selective marker for fluid-phase endocytosis. Some individuals within the HeLa population were also noted to contain very large dextran loaded vesicles or vacuoles (Figure 4.18). Punctate dextran structures were enlarged and correlated with 2-5 µm vesicles that could be visualised via differential interference contrast (DIC) microscropy (Figure 4.18).

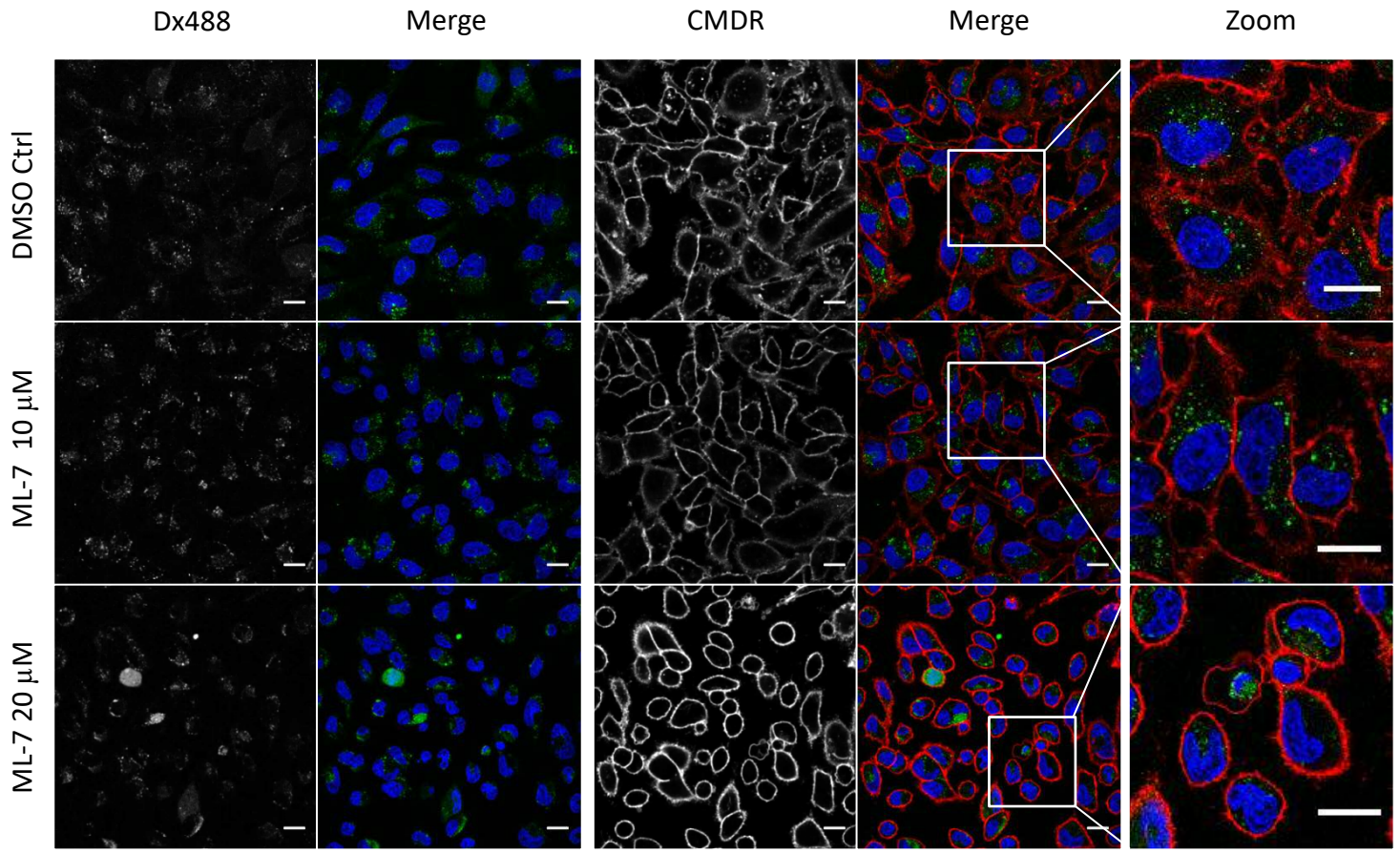

Fig. 4.15. ***Dx488 endocytosis is reduced and cell morphology is affected following ML-7 treatment of increasing concentrations in HeLa cells.*** Cells were pre-treated with either DMSO (0.05%), 10 µM or 20 µM ML-7 for 30 min before being subjected to a 60 min Dx488 (100 µg/ml) pulse whilst in the continued presence of the inhibitor. Hoechst33342 and CMDR were added 5 min before imaging live (R/T). Scale bar: 20 µm.

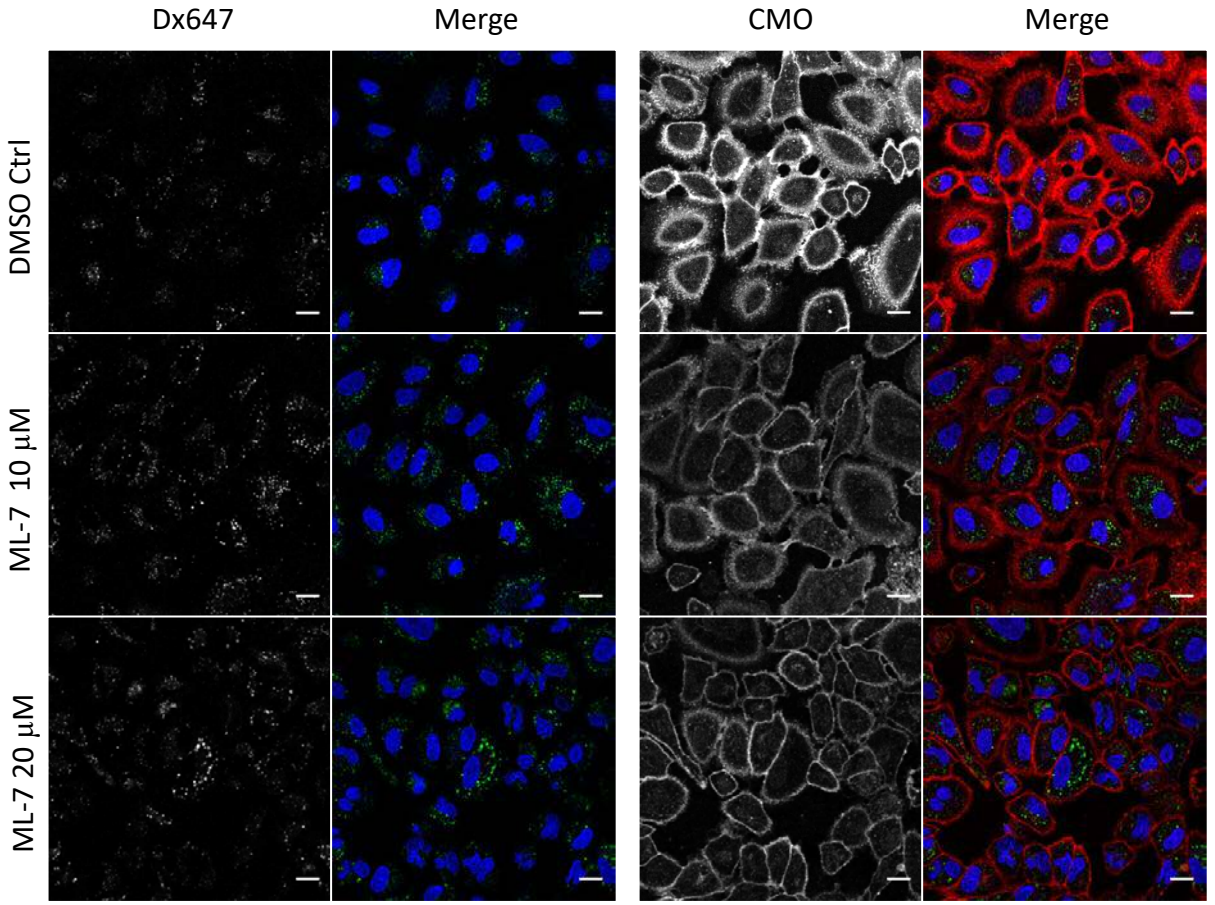

Fig. 4.16. ***Dx647 uptake and cell morphology of ML-7 treated A549 cells.*** Cells were pre-treated with either DMSO (0.05%), 10 µM or 20 µM ML-7 for 30 min before being subjected to a 60 min Dx647 (100 µg/ml) pulse whilst in the continued presence of the inhibitor. Hoechst33342 and Cell Mask Orange (CMO) were added 5 min before imaging live (R/T). Scale bar: 20 µm.

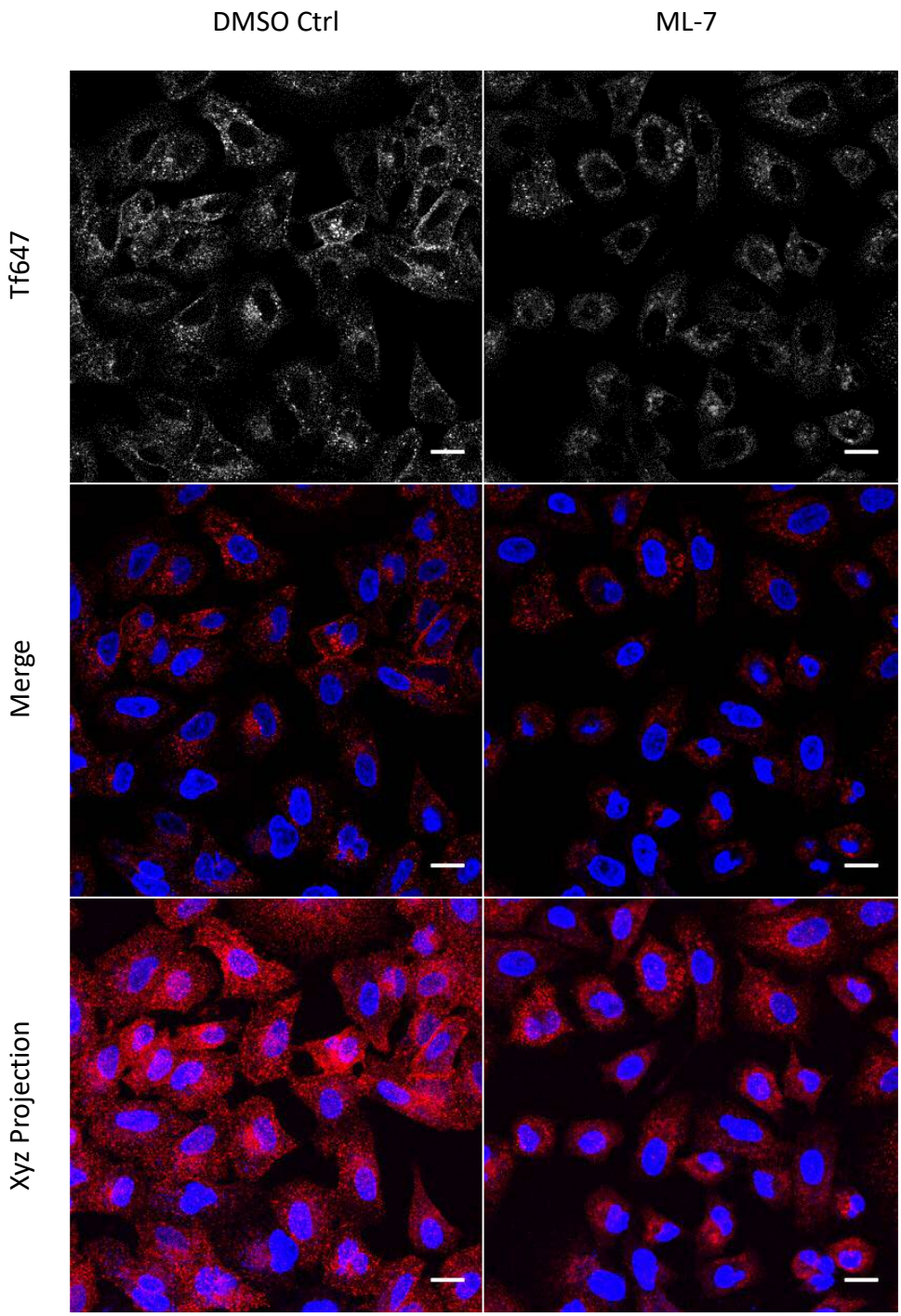

Fig. 4.17. ***Tf647 endocytosis is reduced following ML-7 treatment in A549 cells.*** Cells were pre-treated with either DMSO (0.05%) or 20 µM ML-7 for 30 min before being subjected to a 10 min Tf647 (5 µg/ml) pulse and 5 min chase in the continued presence of the inhibitor. Hoechst33342 was added 5 min before imaging live (R/T). Scale bar: 20 µm.

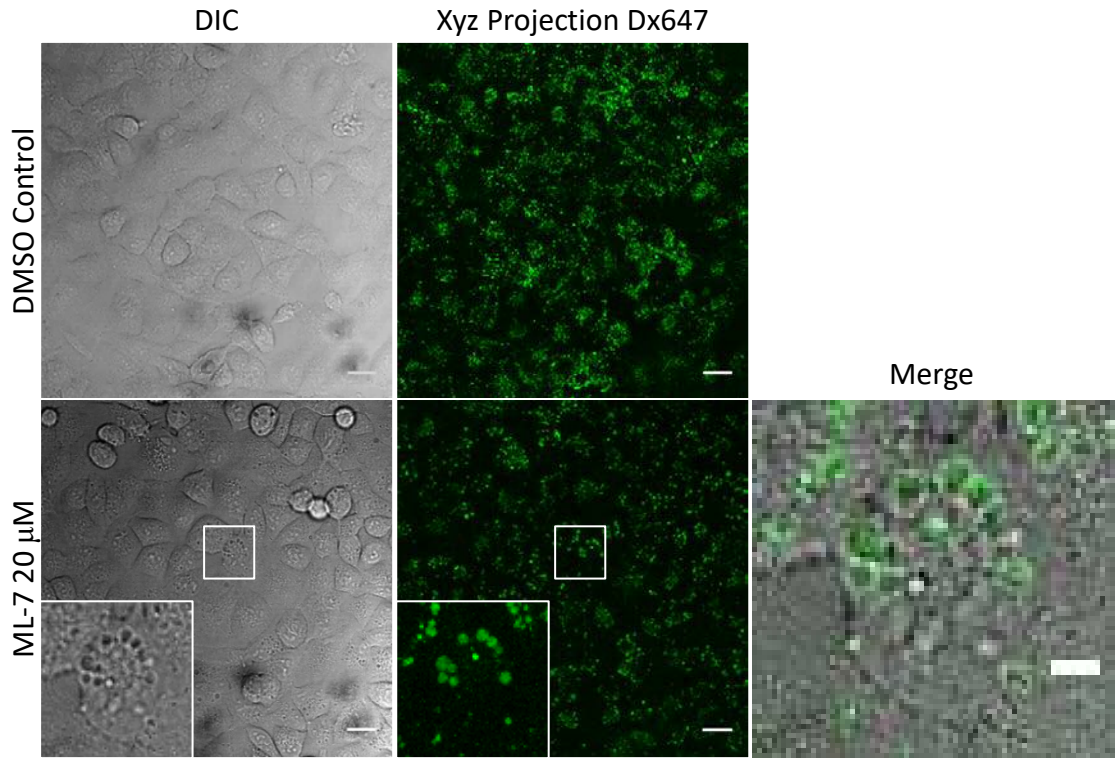

Fig. 4.18. ***Vesicular Dx647 structures are larger following ML-7 treatment in A549 cells.*** Cells were pre-treated with either DMSO (0.05%) or 20 µM ML-7 for 30 min before being subjected to a 60 min Dx647 (100 µg/ml) pulse whilst in the continued presence of the inhibitor. Scale bar: 20 µm, zoomed image: 10 µm.

4.4 Discussion

In this chapter, the search for an efficient technique to inhibit macropinocytosis using pharmacological inhibition was investigated. EIPA resulted in changes in cell morphology as described in Section 3.3.1. These observations were apparent at 100 µM, which is generally the concentration used for endocytic studies. Many of these studies however do not present microscopy images of the cells used for these studies and conclusions are based on analysis of flow cytometry data (Al Soraj et al., 2012). Cell viability had been previously measured by other members of the lab indicating that the concentrations utilised do not affect viability (data not

published). The incubation periods used for this project are generally too short for many commercial viability/cytotoxicity kits which require incubation for over 4 hours. The shorter periods of incubation used for uptake studies are therefore less likely to cause quantifiable effects on viability. Viability does not necessarily correlate to changes in the endocytic network, and the morphology effects observed suggest that cellular homeostasis is altered at these higher concentrations of inhibitor treatment. Regardless of these observations, EIPA treatment had a small effect on the fluid-phase uptake of dextran, suggesting that a proportion of dextran uptake was affected. The obvious effects on trafficking of the CME probe transferrin suggests that EIPA may affect CME, which may account for this proportion of dextran. It is plausible that a number of dextran molecules are caught within internalising clathrin pits, and therefore enter the cell via the CME pathway.

The ability of Rottlerin to prevent fluid-phase uptake of dextran, particularly in A549s suggests that its target is part of the fluid-phase machinery, and may be a possible target for siRNA depletion. PKCδ was investigated due to its original identity as a target of Rottlerin. Depletion of this protein however, did not affect dextran uptake in A549 cells, the line in which Rottlerin had an effect on dextran uptake suggesting that the protein is not the causal factor of Rottlerin's effects in A549 cells.

PKCδ was chosen as siRNA target in A549 cells due to the ability of Rottlerin to reduce dextran uptake. Depletion of this protein however has no effect on the uptake of dextran in either A549 or HeLa cells. This could be for several reasons.

The targets of Rottlerin may range wider than this particular kinase. Rottlerin has most notably been identified to uncouple mitochondria from oxidative phosphorylation (Soltoff, 2001; Soltoff, 2007), which could theoretically result in an indirect effect on PKCδ phosphorylation. It is possible that the other targets of Rottlerin may affect dextran uptake in a manner completely independent of PKCδ. For these reasons, PKCδ is not a suitable target for the inhibition of fluid-phase or macropinocytosis.

In Chapter 3, depletion of the protein PAK1 by siRNA transfection did not significantly affect fluid-phase endocytosis of dextran. Treatment with IPA-3, which allosterically inhibits the activation site of the kinase (Deacon et al., 2008; Viaud and Peterson, 2009), caused a reduction in dextran uptake however. The use of IPA-3 has been utilised to investigate the impact of PAK1 regulation on cell growth, in cancer studies for instance (Wang et al., 2016; Wong et al., 2013). Indeed these studies use concentrations were less than or within the same range as used here (10-50 μM), which could account for the apparent cell loss/shrinkage observed in the uptake studies performed here. Effects on the mechanisms of cell growth would explain this. IPA-3 also causes inhibition of actin polymerisation (Zhang et al., 2016), which as discussed previously, is an essential component of fluid-phase endocytosis, macropinocytosis and endocytic trafficking from the membrane, and this correlates with the observations presented here. Whether this is via the specific inhibition of PAK1 is a question that remains to be answered, as specific depletion of the protein did not have this effect on fluid-phase endocytosis.

These studies continue to work toward finding an efficient target for macropinocytic and fluid-phase inhibition, resulting in the establishment of a specific model for macropinocytic inhibition that can be applied on a high-content scale. From these studies however it is clear that specific models of inhibition will involve the utilisation of both siRNA transfection models and pharmacological inhibition. Preliminary use of such pathway specific models can be utilised to evaluate the entry mechanism of a model drug delivery system.

To begin to test these techniques for intended purpose, the characteristics of prostate derived exosomes was explored in collaboration with the Velindre Hospital. The details of these studies are presented and further discussed within the following Chapter.

4.5 References

Al Soraj, M., L. He, K. Peynshaert, J. Cousaert, D. Vercauteren, K. Braeckmans, S.C. De Smedt, and A.T. Jones. 2012. siRNA and pharmacological inhibition of endocytic pathways to characterize the differential role of macropinocytosis and the actin cytoskeleton on cellular uptake of dextran and cationic cell penetrating peptides octaarginine (R8) and HIV-Tat. *Journal of controlled release : official journal of the Controlled Release Society*. 161:132-141.

Chandrasekar, I., Z.M. Goeckeler, S.G. Turney, P. Wang, R.B. Wysolmerski, R.S. Adelstein, and P.C. Bridgman. 2014. Nonmuscle myosin II is a critical

regulator of clathrin-mediated endocytosis. *Traffic (Copenhagen, Denmark)*. 15:418-432.

Deacon, S.W., A. Beeser, J.A. Fukui, U.E.E. Rennefahrt, C. Myers, J. Chernoff, and J.R. Peterson. 2008. An Isoform-Selective, Small-Molecule Inhibitor Targets the Autoregulatory Mechanism of p21-Activated Kinase. *Chemistry & biology*. 15:322-331.

Devadas, D., T. Koithan, R. Diestel, U. Prank, B. Sodeik, and K. Dohner. 2014. Herpes simplex virus internalization into epithelial cells requires Na+/H+ exchangers and p21-activated kinases but neither clathrin- nor caveolin-mediated endocytosis. *Journal of virology*. 88:13378-13395.

Fenyvesi, F., K. Reti-Nagy, Z. Bacso, Z. Gutay-Toth, M. Malanga, E. Fenyvesi, L. Szente, J. Varadi, Z. Ujhelyi, P. Feher, G. Szabo, M. Vecsernyes, and I. Bacskay. 2014. Fluorescently labeled methyl-beta-cyclodextrin enters intestinal epithelial Caco-2 cells by fluid-phase endocytosis. *PloS one*. 9:e84856.

Fretz, M., J. Jin, R. Conibere, N.A. Penning, S. Al-Taei, G. Storm, S. Futaki, T. Takeuchi, I. Nakase, and A.T. Jones. 2006. Effects of Na+/H+ exchanger inhibitors on subcellular localisation of endocytic organelles and intracellular dynamics of protein transduction domains HIV-TAT peptide and octaarginine. *Journal of controlled release : official journal of the Controlled Release Society*. 116:247-254.

Gschwendt, M., H.J. Muller, K. Kielbassa, R. Zang, W. Kittstein, G. Rincke, and F. Marks. 1994. Rottlerin, a novel protein kinase inhibitor. *Biochemical and biophysical research communications*. 199:93-98.

He, L., P.D. Watson, and A.T. Jones. 2015. Visualizing Actin Architectures in Cells Incubated with Cell-Penetrating Peptides. *Methods in molecular biology (Clifton, N.J.)*. 1324:247-259.

Keenan, C., and D. Kelleher. 1998. Protein Kinase C and the Cytoskeleton. *Cellular signalling*. 10:225-232.

Krzyzaniak, M.A., M.T. Zumstein, J.A. Gerez, P. Picotti, and A. Helenius. 2013. Host cell entry of respiratory syncytial virus involves macropinocytosis followed by proteolytic activation of the F protein. *PLoS Pathog*. 9:e1003309.

Larsson, C. 2006. Protein kinase C and the regulation of the actin cytoskeleton. *Cellular signalling*. 18:276-284.

Sarkar, K., M.J. Kruhlak, S.L. Erlandsen, and S. Shaw. 2005. Selective inhibition by rottlerin of macropinocytosis in monocyte-derived dendritic cells. *Immunology*. 116:513-524.

Soltoff, S.P. 2001. Rottlerin is a mitochondrial uncoupler that decreases cellular ATP levels and indirectly blocks protein kinase Cdelta tyrosine phosphorylation. *The Journal of biological chemistry*. 276:37986-37992.

Soltoff, S.P. 2007. Rottlerin: an inappropriate and ineffective inhibitor of PKCdelta. *Trends in pharmacological sciences*. 28:453-458.

Vercauteren, D., M. Piest, L.J. van der Aa, M. Al Soraj, A.T. Jones, J.F. Engbersen, S.C. De Smedt, and K. Braeckmans. 2011. Flotillin-dependent endocytosis and a phagocytosis-like mechanism for cellular internalization of disulfide-based poly(amido amine)/DNA polyplexes. *Biomaterials*. 32:3072-3084.

Viaud, J., and J.R. Peterson. 2009. An allosteric kinase inhibitor binds the p21-activated kinase autoregulatory domain covalently. *Molecular cancer therapeutics*. 8:2559-2565.

Wang, Y., C. Gratzke, A. Tamalunas, N. Wiemer, A. Ciotkowska, B. Rutz, R. Waidelich, F. Strittmatter, C. Liu, C.G. Stief, and M. Hennenberg. 2016. P21-Activated Kinase Inhibitors FRAX486 and IPA3: Inhibition of Prostate Stromal Cell Growth and Effects on Smooth Muscle Contraction in the Human Prostate. *PloS one*. 11:e0153312.

Weinberg, M.S., S. Nicolson, A.P. Bhatt, M. McLendon, C. Li, and R.J. Samulski. 2014. Recombinant adeno-associated virus utilizes cell-specific infectious entry mechanisms. *Journal of virology*. 88:12472-12484.

Wen, Z., B. Zhao, K. Song, X. Hu, W. Chen, D. Kong, J. Ge, and Z. Bu. 2013. Recombinant lentogenic Newcastle disease virus expressing Ebola virus GP infects cells independently of exogenous trypsin and uses macropinocytosis as the major pathway for cell entry. *Virol J*. 10:331.

Wong, L.L.-Y., I.P.-Y. Lam, T.Y.-N. Wong, W.-L. Lai, H.-F. Liu, L.-L. Yeung, and Y.-P. Ching. 2013. IPA-3 Inhibits the Growth of Liver Cancer Cells By Suppressing PAK1 and NF-κB Activation. *PloS one*. 8:e68843.

Zhang, W., Y. Huang, and S.J. Gunst. 2016. p21-Activated kinase (Pak) regulates airway smooth muscle contraction by regulating paxillin complexes that mediate actin polymerization. *The Journal of physiology*. 594:4879-4900.

5 Exploration of the Cellular Uptake and Trafficking Characteristics of Fluorescently Labelled Prostate Cancer Exosomes

5.1 Introduction

The natural ability to functionally transfer a spectrum of macro-molecular cargo between cells raises opportunities for exploiting exosomes as vectors for drug delivery (Batrakova and Kim, 2015; Vader et al., 2016; van Dommelen et al., 2012). However little is known about the ways in which exosomes initially interact with the cell, gain intracellular access and are trafficked through the cell to their final destination. Even less is known about how intravesicular cargo is released and directed towards the intended target within the cytosol or other intracellular compartments. The capacity of exosomes to mediate these effects, possibly through endocytosis, requires further characterisation in order to fully understand their natural roles in disease pathogenesis and also unlock their potential for drug delivery.

Exosome entry and cargo release has been proposed to occur via endocytosis (Escrevente et al., 2011) and/or through direct exosome-plasma membrane fusion (Montecalvo et al., 2012; Mulcahy et al., 2014). These studies labelled purified exosome preparations with fluorescent probes and then used either microscopy or flow cytometry to monitor cell interaction and uptake. As previously discussed in Chapter 1, labelling strategies include the use of lipophilic dyes such as PKH26 (Feng et al., 2010; Sagar et al., 2016) and the carbocyanine dyes (DiI, DiO) (Tian et al., 2014; Wiklander et al., 2015), which embed within the membrane bilayer of the

exosome. Such dyes can however form dye aggregates or micelles, of similar proportions to exosomes, giving misleading information in uptake experiments. This was highlighted in Figure 1 in Roberts-Dalton *et al* 2017 via work performed by our collaborators at the Velindre Cancer Hospital (Appendix B). Exosome permeable compounds including CFSE and CFDA have also been used for this purpose (Escrevente et al., 2011; Temchura et al., 2008). Any structural modifications on exosomes following labelling with these dyes could alter their physical characteristics but may also affect their functional properties. For cell uptake analysis this functional impact is rarely considered.

In this chapter, a simple and rapid method for fluorescently labelling purified Du145 exosomes is used to provide high content microscopy analysis of the ways in which these exosomes interact with cells *in vitro*. This together with subsequent endocytosis experiments has now been accepted for publication (Roberts-Dalton et al. *Nanoscale*. 2017. Manuscript in Press.). The method takes advantage of thiol (sulph-hydryl) groups on the exosome surface and experiments were also performed by collaborators led by Professor Aled Clayton and Dr Jason Webber at the Velindre Cancer Hospital to assess whether they retain the documented capacity to induce fibroblast differentiation *in vitro* (Webber et al., 2010; Webber et al., 2015).

The Du145 exosome preparations used were subjected to rigorous characterisation by members of the Clayton lab before labelling was performed and this is also presented in Figure 1 of Appendix B. Cryo-electron microscopy (Cryo-EM) indicated

the isolation of vesicular structures with a lipid bi-layer membrane that were mostly around 100 nm in diameter (Appendix B, Figure 1A), and this observation was supported by Nanoparticle Tracking Analysis (NTA) (Appendix B, Figure 1B). Furthermore, these vesicles were found to be enriched in tetraspanins such as CD9, CD81 and CD63, and exosome-related proteins including TGS101, Alix and MHC Class-I (Appendix B, Figure 1C). Using a combination of BCA-protein assay and NanoSight-concentration measurements, the particle to protein ratio for purified exosomes was also calculated. All preparations used had a particle:protein ratio of $>2x10^{10}$ particles/µg protein, indicating specimen purity as previously described (Webber and Clayton, 2013). The isolation and subsequent analyses satisfy the criterion set by the International Society for Extracellular Vesicles for defining this specimen as exosomes (Lotvall et al., 2014).

The exosome is an environment that is cysteine rich through, for example, the presence of tetraspanin webs (Martínez and Yáñez-Mó, 2014). It was postulated that the thiols (-S-H groups) present on these structures would react with a maleimide functional group to form a stable, non-reversible, thio-ether linkage. Fluorophore conjugated maleimides are often used to fluorescently label bio-molecules so C_5-maleimide conjugated to Alexafluor488/633 was used. Other groups have exploited this labelling protocol in order to study micro-particle populations whereby whole blood samples were labelled with BODIPY-maleimide for analysis via flow cytometry (Enjeti et al., 2008; Headland et al., 2014). However, BODIPY itself is used to label membranes, and is therefore likely to integrate onto the exosome bilayer. The capacity for C_5-maleimide-Alexa488/633 to react with

exosome thiols was explored by previous members of the Clayton and Jones labs. This procedure involves the removal of non-bound dye from the exosome-preparations and spin-columns (Invitrogen) that retain molecules of <3000 Da was used to do this. Initial experiments explored incubating a constant quantity of purified exosomes with varying fluorophore concentrations, showing saturating levels of labelling at ≥100 μg/ml after an incubation of 1 hour (R/T) (Appendix B, Figure 1D). At the saturating fluorophore concentration of 200 μg/ml a range of incubation times were investigated revealing that most of the fluorophore-exosome labelling occurred very rapidly within the first 5 min, and saturation was reached at 1 to 2 hours (Appendix B, Figure 1E). Conditions of 200 μg/ml of fluorophore for 1 hour were chosen for labelling the Du145 exosomes for further microscopy studies. To ascertain whether or not the fluorophore was actually forming a covalent bond through the thiol groups, or merely binding passively to the vesicle surface, a competitor that works by capping the available reactive thiol groups was used. Pre-incubating exosomes with doses of N-acetyl-L-cysteine showed a potent (~80%) inhibition of labelling under these same conditions (Appendix B, Figure 1F).

NTA revealed a similar size distribution profile following incubations with C_5-maleimide-Alexa488, suggesting a paucity of gross complexation due to maleimide-vesicle cross-linking. Importantly, NTA in the presence of a low-pass 500 nm filter showed the majority (>90%) of vesicles were fluorescent. The stock C_5-maleimide-Alexa488 reagent was also analysed by NTA (Appendix B, Figure 1G). Unlike for some other fluorescent labels, particularly PKH26, there were negligible particles detected in scatter mode, and there were no particles seen with a fluorescent filter

in place. An example of nano-particulate PKH26 fluorescent aggregates in the absence of exosomes is shown in Appendix C, Figure 1. Particulate material spanning the size range of exosomes was present in the stock solution, and a high proportion (52%) of these were fluorescent. The Jones and Clayton labs therefore concluded that this method was a simple, rapid and highly effective modality for fluorescently labelling exosome preparations that were free of artefacts relating to insoluble dye nano-particulates.

The functional impact of coating exosomes with this fluorescent label was also investigated by the labs; an aspect that is rarely considered in other studies. To do this, a well-established functional assay whereby prostate cancer exosomes trigger the differentiation of fibroblasts to myofibroblasts was used (Webber et al., 2010). This process required delivery of exosome-associated Transforming growth factor β (TGFβ) to fibroblasts, but was also likely to involve additional exosome-cargo as the myofibroblasts generated are distinct from those formed by soluble TGFβ-stimulation in that secretion of Hepatocyte growth factor (HGF) is triggered (Webber et al., 2015). Stimulation of fibroblasts either with native or with C_5-maleimide-Alexa488 labelled exosomes successfully triggered the onset of stress fibres visualized via αSMA labelling; soluble TGFβ also did this as expected. When evaluating the secretion of HGF however, there was clear difference in levels of HGF whether stimulations were by exosomes or soluble TGFβ (Appendix B, Figure 1H). The labelled or unlabelled exosomes were equally proficient at stimulating HGF secretion. In this assay, which represents a major and complex cell differentiation process, the C_5-maleimide-Alexa488 labelling approach showed no signs of

attenuated exosome function. This method was used to fluorescently label Du145 exosomes provided by the Clayton lab and explore their interaction and uptake with cells, using the endocytic models explored and described in Chapters 4 and 5 of this thesis.

5.2 Aims and Objectives

- To provide a simpler and more efficient method of visualising the ways in which Du145 exosomes interact with the cell and possibly gain intracellular access in order to induce their phenotypic effect. As previously stated, this method made use of the free thiol-groups abundant on the surface of the exosome membrane.
- To analyse cell binding and uptake of fluorescent Du145 exosomes in primary lung fibroblasts (AG02262-Coriell Institute of Medical Research), the cell line for which a phenotypic effect has been documented.
- To perform high content analysis of the cellular interaction, uptake and traffic of fluorescently labelled Du145 exosomes using the *in vitro* techniques of endocytic inhibition explored in Chapter 4 and 5 of this thesis. HeLa cells were used for this analysis based on their well-characterised endocytic profile (Al Soraj et al., 2012; Moody et al., 2015; Nakase et al., 2004) and ease of cell culture.
- Based on their ability to induce a phenotypic effect, the possible drug delivery potential of Du145 exosomes was preliminary investigated in a human lung carcinoma line engineered to stably express eGFP (H1299eGFP).

5.3 Results

5.3.1 Uptake of labelled Du145 exosomes in primary lung fibroblasts

Du145 exosomes have been shown to induce primary lung fibroblasts to differentiate into myofibroblasts and secrete an increased level of HGF (Webber et al., 2010; Webber et al., 2015). This represents a major phenotypic change indicating that these exosomes had the capacity to interact with recipient cells and transfer functional cargo, a characteristic of a theoretical drug delivery vector. There is however the possibility that differentiation is induced at the level of the plasma membrane by a ligand on the exosome binding to a receptor on the host cell for example. There is evidence from the Clayton laboratory that TGFβ on the exosome surface is critical for induction of differentiation (Webber et al., 2015), most probably via interaction with the TGFβ receptor (TGFβR). Interaction of this ligand and receptor is well documented to induce differentiation in a number of different cell lines (Grafe et al., 2017). Exosome-fibroblast differentiation could be further explored via high content microscopy analysis following fluorescent labelling. As described in Section 2.8, C_5-maleimide-Alexa488/633 (200 μg/ml) was mixed with exosomes to form a covalent linkage between the fluorophore and the exosome, thereby providing a fluorescent preparation. Preliminary experiments in the Clayton lab identified that exosomes at concentrations of 50-60 μg/ml could be easily visualised on cells using wide field microscopy and a concentration of 60 μg/ml was used for the following studies.

Due to their documented effects in fibroblasts, we investigated the possibility of visualising the labelled exosomes following incubation in this cell line. These cells had high background cellular autofluorescence after excitation at 488 nm (Figure 5.1a), thus distinguishing between this autofluorescence and internalised C_5-maleimide-Alexa488-exosomes (Exo488) was not possible (Figure 5.1b). The purified exosomes were therefore labelled with C_5-maleimide-Alexa633 using the same procedure for uptake in fibroblasts. Figure 5.2 demonstrates that these exosomes (Exo633) were internalised to label punctate structures indicative of endosomes. The movement of these endosomes over a period of 5 minutes (Video 5.1) was also indicative of endocytic trafficking movements in the fibroblasts, further suggesting endocytosis as the mechanisms by which these exosomes gain intracellular access. It also showed that another fluorescent dye could be utilised to label exosomes to monitor their cellular uptake. These cells are however poorly characterised with respects to characterisation of endocytosis and it was decided that focus would be given to the HeLa cell line that from previous work in the Jones laboratory and work presented in this study is much better characterised with respects to endocytosis.

Previous studies on exosome uptake have also been published using HeLa cells allowing for some comparative investigations (Nakase and Futaki, 2015; Nakase et al., 2015; Svensson et al., 2013).

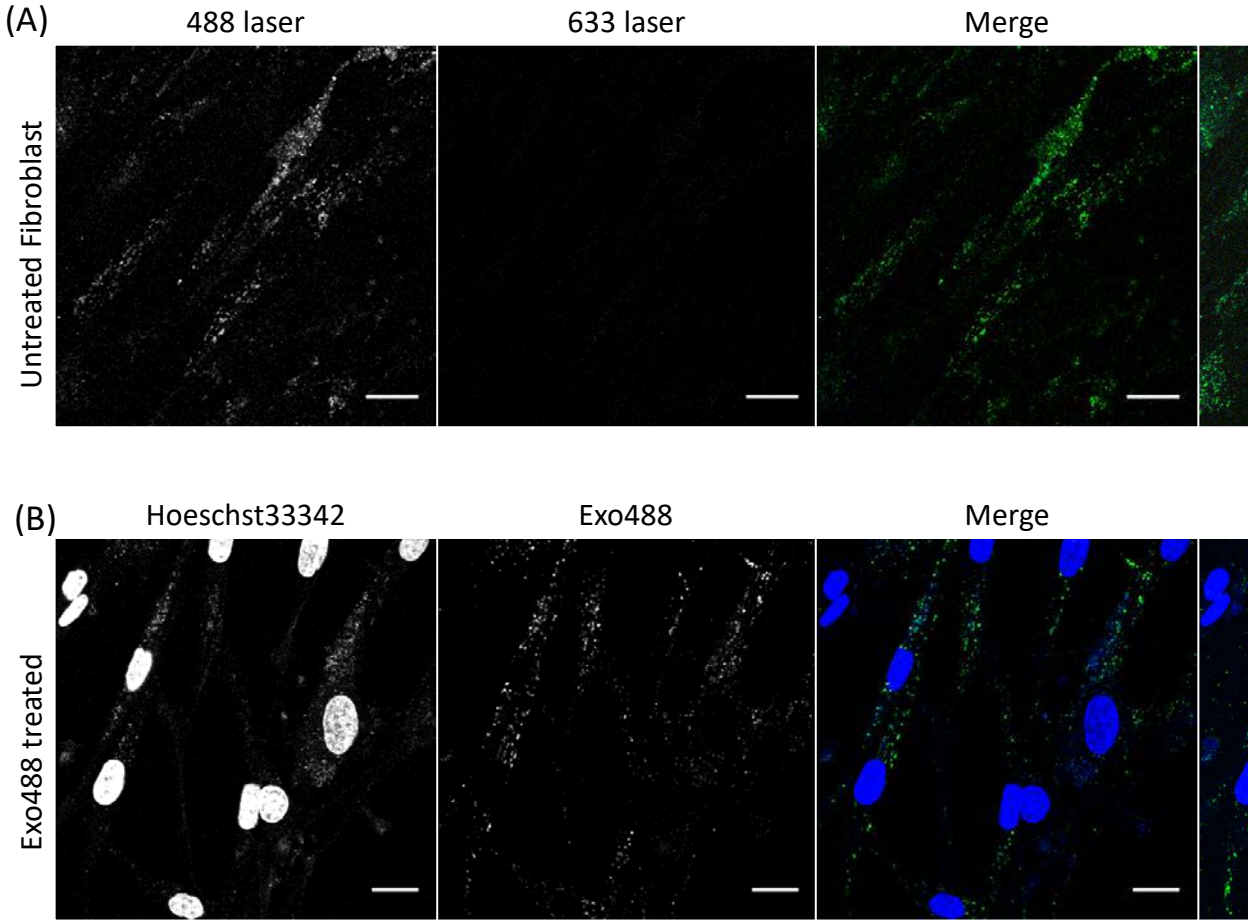

Fig. 5.1. ***Primary lung fibroblasts contain punctate autofluorescent structures detected following excitation with the UV a***

Cells were either untreated (washed with SFIM) before imaging (R/T) or (B) pulsed with Exo488 (60 µg/ml) for 2 h (3
Hoechst33342 for 5 min and imaging live (R/T). Scale bar: 20 µm.

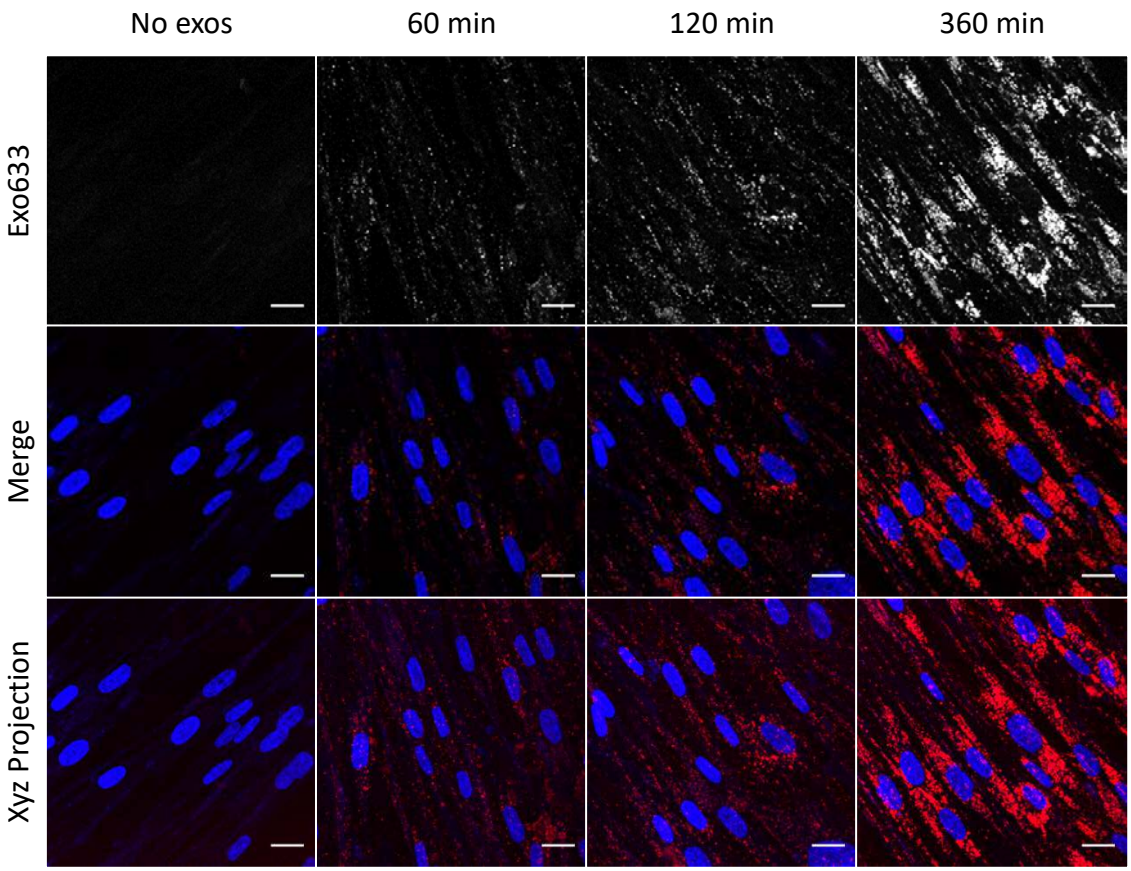

Fig. 5.2. ***Alexa633 labelled exosomes seen as intracellular punctate structures after incubation with primary lung fibroblasts.*** Cells were pulsed with 60 µg/mL Exo633 for 60, 120 or 360 min (37°C, 5% CO_2) before imaging prior to incubation with Hoechst33342 for 5 min before imaging live (R/T). Scale bar: 20 µm. Images representative of three separate experiments.

5.3.2 Endocytic Uptake of C_5-maleimide-Alexa labelled Du145 exosomes in HeLa cells

HeLa cells incubated with Alexa633 labelled exosomes (Exo633) for 30 and 60 min demonstrated a scattered punctate distribution throughout the cell cytoplasm (Figure 5.3). There was a noticeable time dependant increase in fluorescence intensity from 30 min to 360 min (Figure 5.3) and at this later time point fluorescence was more polarised to the perinuclear regions. This uptake pattern was replicated using Alexa488 labelled exosomes in HeLa cells, whereby distribution of punctate structures was initially scattered throughout the cytoplasm followed by a noticeable time dependant

increase in increase in intensity from 30 to 240 min (Figure 5.4a). This increase was further supported by MFI quantification of Exo488 intensity (Figure 5.4b).

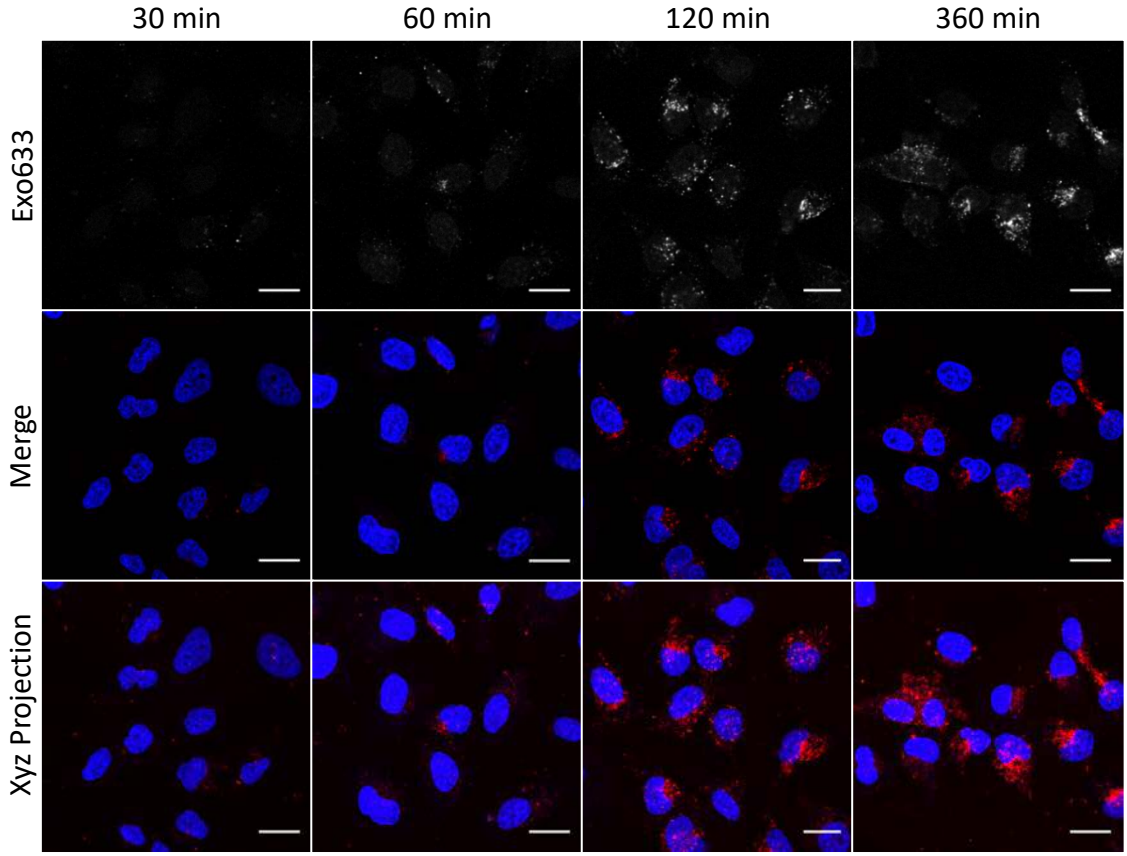

Fig. 5.3. ***Alexa633 labelled exosomes are internalised by HeLa cells and can be visualised as punctate structures.*** Cells were pulsed with 60 µg/mL Exo633 for 30, 60, 120 or 360 min (37°C, 5% CO_2) before imaging. Cells were incubated with Hoechst33342 for 5 min before imaging live (R/T). Scale bar: 20 µm.

Zoomed images of the cells in Figure 5.4a allow greater visualisation of the Exo488 positive punctate structures indicative of endosomes (Figure 5.5). Time lapse imaging of Exo488 incubated with HeLa cells over a period of 3 min (after a 120 min pre-incubation) shows these structures to be highly motile with little evidence of significant accumulation at the plasma membrane (Video 5.2). These experiments, clearly showing the localisation of endosomes in endolysosomal structures prompted

further analysis to investigate how they gain access to cells and whether this can be inhibited chemically or by depleting proteins regulating endocytosis.

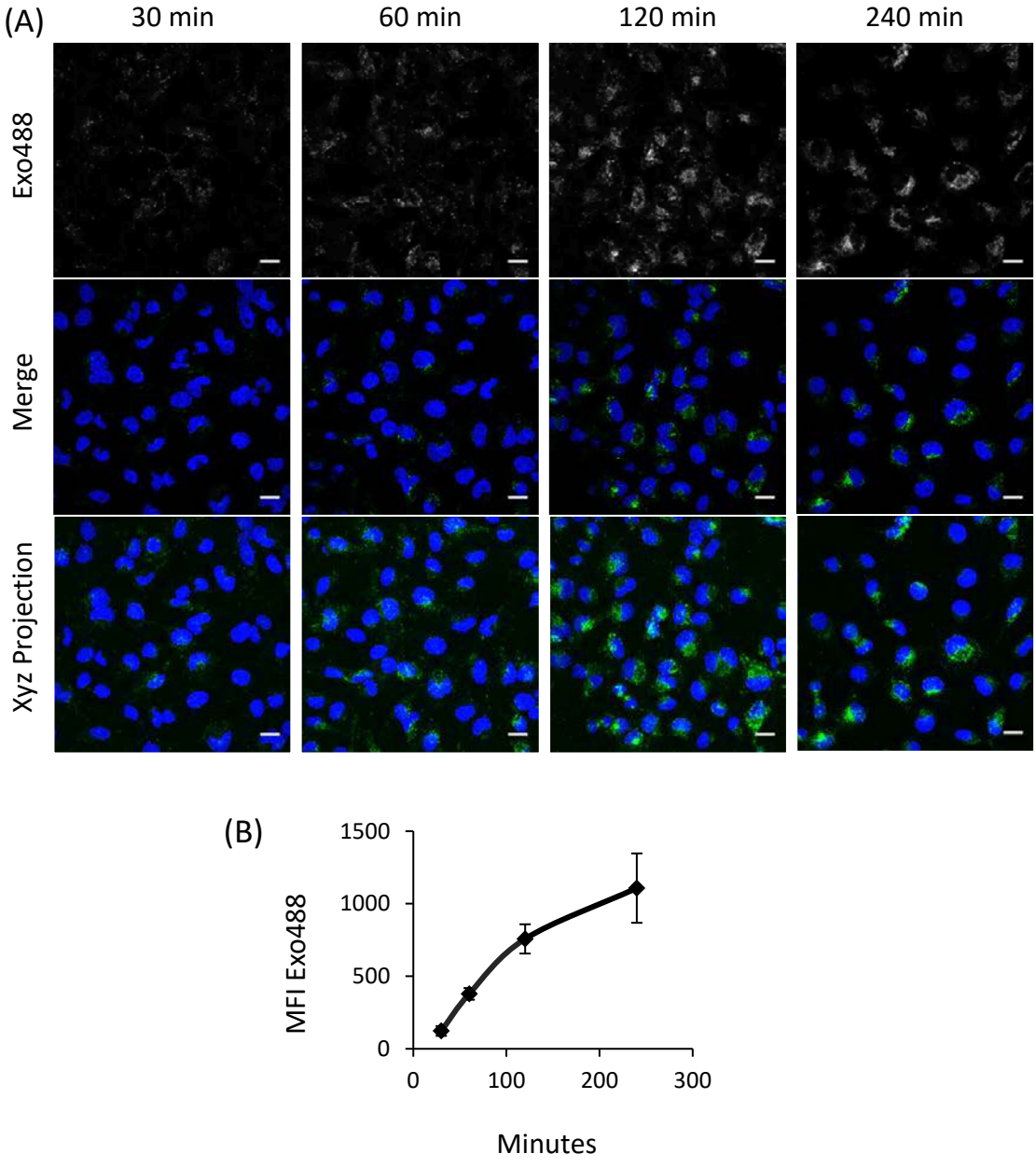

Fig. 5.4. ***Time dependent cellular uptake of Exo488 in HeLa cells*** (A) Cells were pulsed with 60 µg/ml Exo488 for 30, 60, 120 or 360 min (37°C, 5% CO_2) before imaging. Cells were incubated with Hoechst33342 for 5 min before imaging. Scale bar: 20 µm. (B) MFI quantification of each cell population in (A). Error bars represent Standard error. Images and graph summarise three separate experiments.

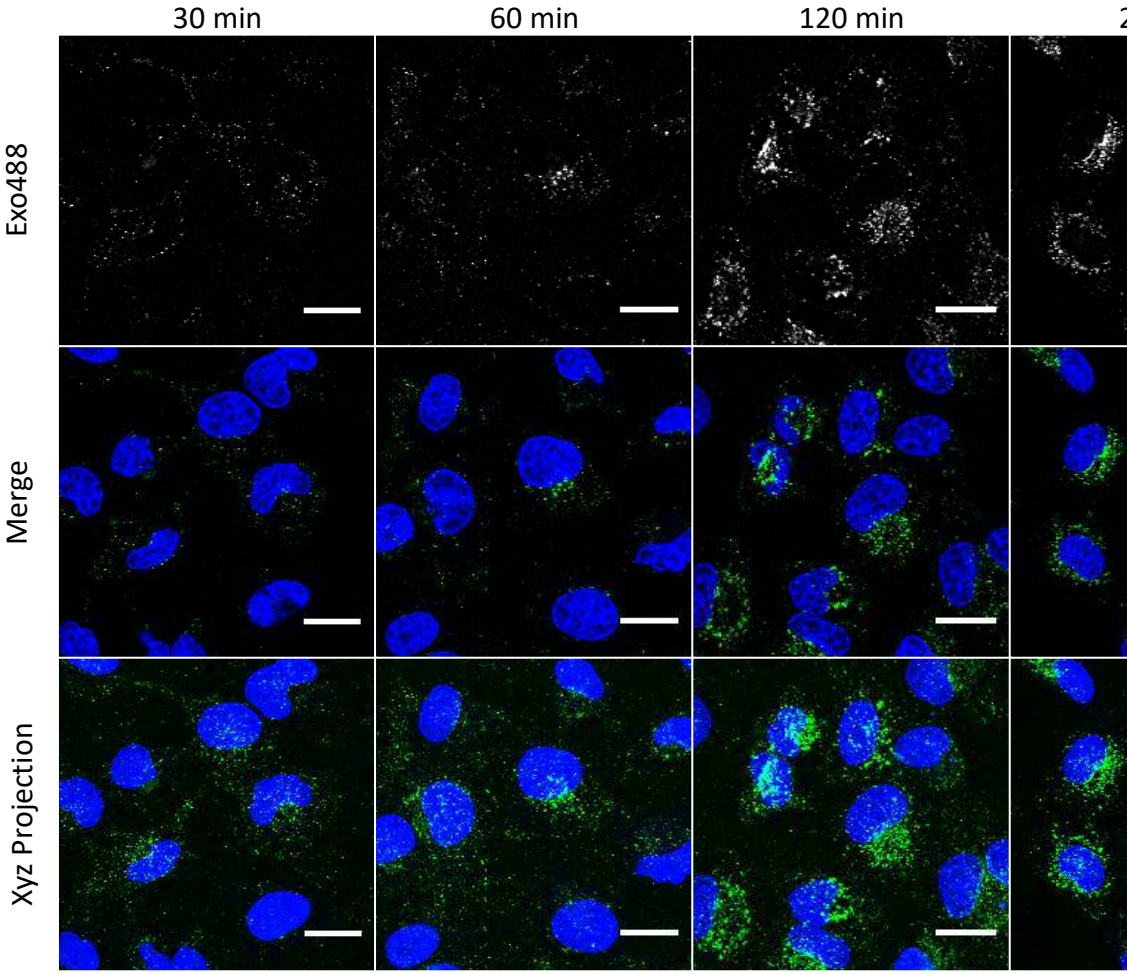

Fig. 5.5. ***Zoomed images of Exo488 internalisation in HeLa cells.*** Cells were pulsed with 60 µg/ml Exo488 for 30, 60, 12
imaging. Cells were incubated with Hoechst33342 for 5 min before imaging. Scale bar: 20 µm.

As these exosomes were internalising into endosomal like structures it was then important to learn more about their traffic and whether the final destination for these structures was the lysosome. We have previously used fluorescent dextran as a marker of fluid-phase endocytosis that is trafficked to lysosomes (Al-Taei et al., 2006; Moody et al., 2015). It can be pulsed into cells for approximately 2 hours and then following washing the cells can be further incubated in the absence of the probe to 'chase' the previously internalised fraction to lysosomes overnight (described in Section 2.10). Here, only lysosomes are labelled but via a simple 2 hour pulse, dextran can be used to label the entire endolysosomal pathway of fluid-phase endocytosis including early endosomes and lysosomes. For these reasons colocalisation of Exo488 with Dex647 labelled lysosomes was investigated and performed using different pulse and pulse chase methods described in Section 2.10. Cells previously pulse chased with dextran were incubated with exosomes for 30-360 min and showed a gradual time dependant accumulation of exosome fluorescence in the perinuclear region that contained the labelled dextran in lysosomes (Figure 5.6a). Colocalisation between Exo488 and 647-lysosomes was barely detected at 30 min and then increased over a period of six hours to the point that after 360 min approximately 60% of the identified exosomes were contained in labelled lysosomes (Figure 5.6b). Experiments by which dextran was similarly used to label lysosomes were then performed but following a two hour pulse of exosome endocytosis the cells were washed and the material already associated with the cells was chased for a further 4 hours. This revealed that over 60% of exosome associated labelling had reached and remained at the lysosomes by the end of this chase period (Figure 5.7).

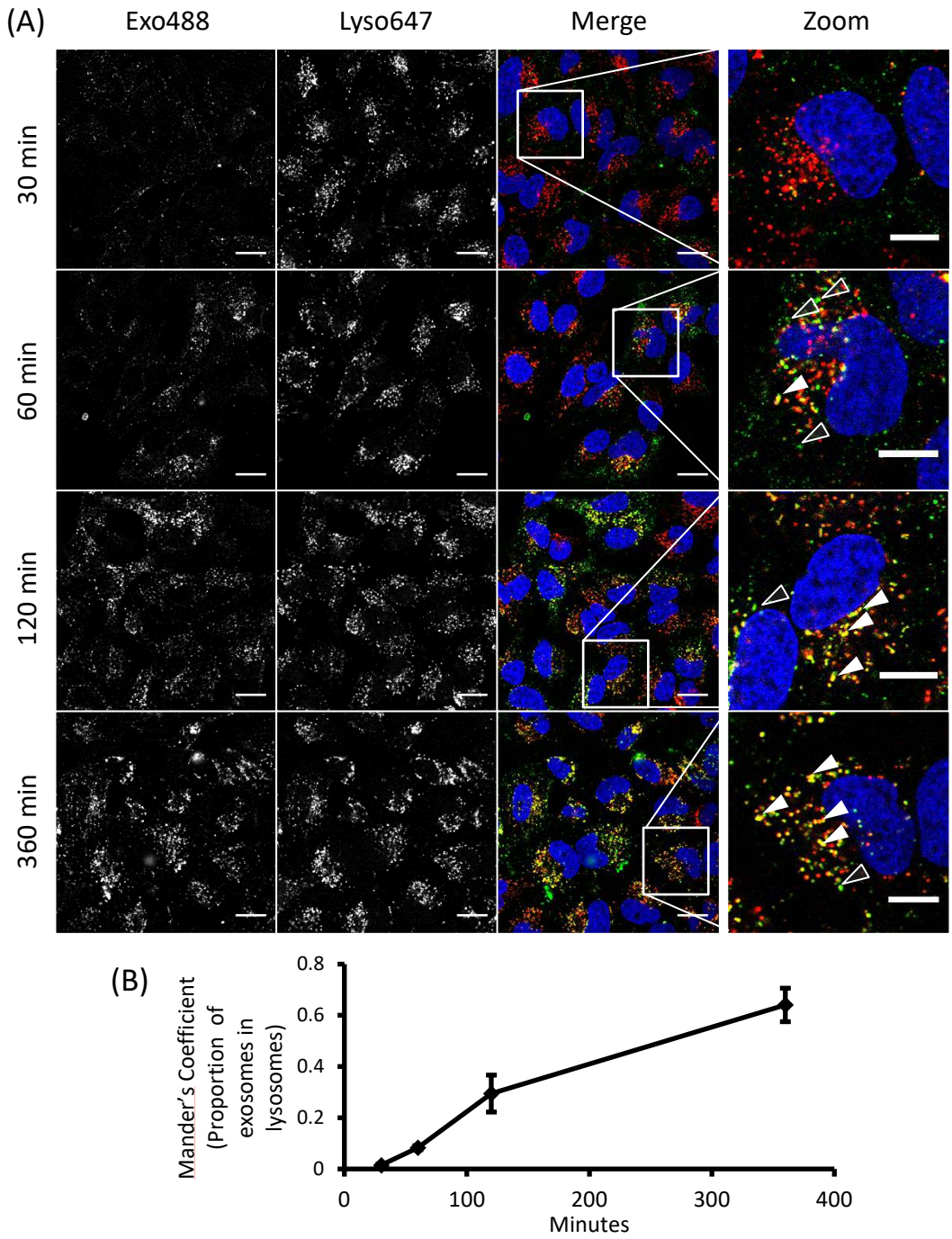

Fig. 5.6. Colocalisation of 488-labelled exosomes with dextran-loaded lysosomes in HeLa cells. (A) Cells were incubated with Dx647 (100 µg/ml) for 2 h, washed with PBS and incubated for a further 18 h in culture media. Cells were then incubated with Exo488 (60 µg/ml) for either 30, 60, 120 or 360 min before treatment with Hoechst33342 for 5 min and imaging. Solid arrowheads indicate colocalisation between exosomes and lysosomes and transparent arrowheads indicate exosomes not colocalised with lysosomes. Scale bars: 20 µm and 10 µm in zoomed images. Images representative of three separate experiments. (B) Mander's correlation coefficient analysis of the proportion of green fluorescence (exosomes) associated with far-red fluorescence (lysosomes) based on the experiments performed to generate images. Error bars: Standard error. n=3.

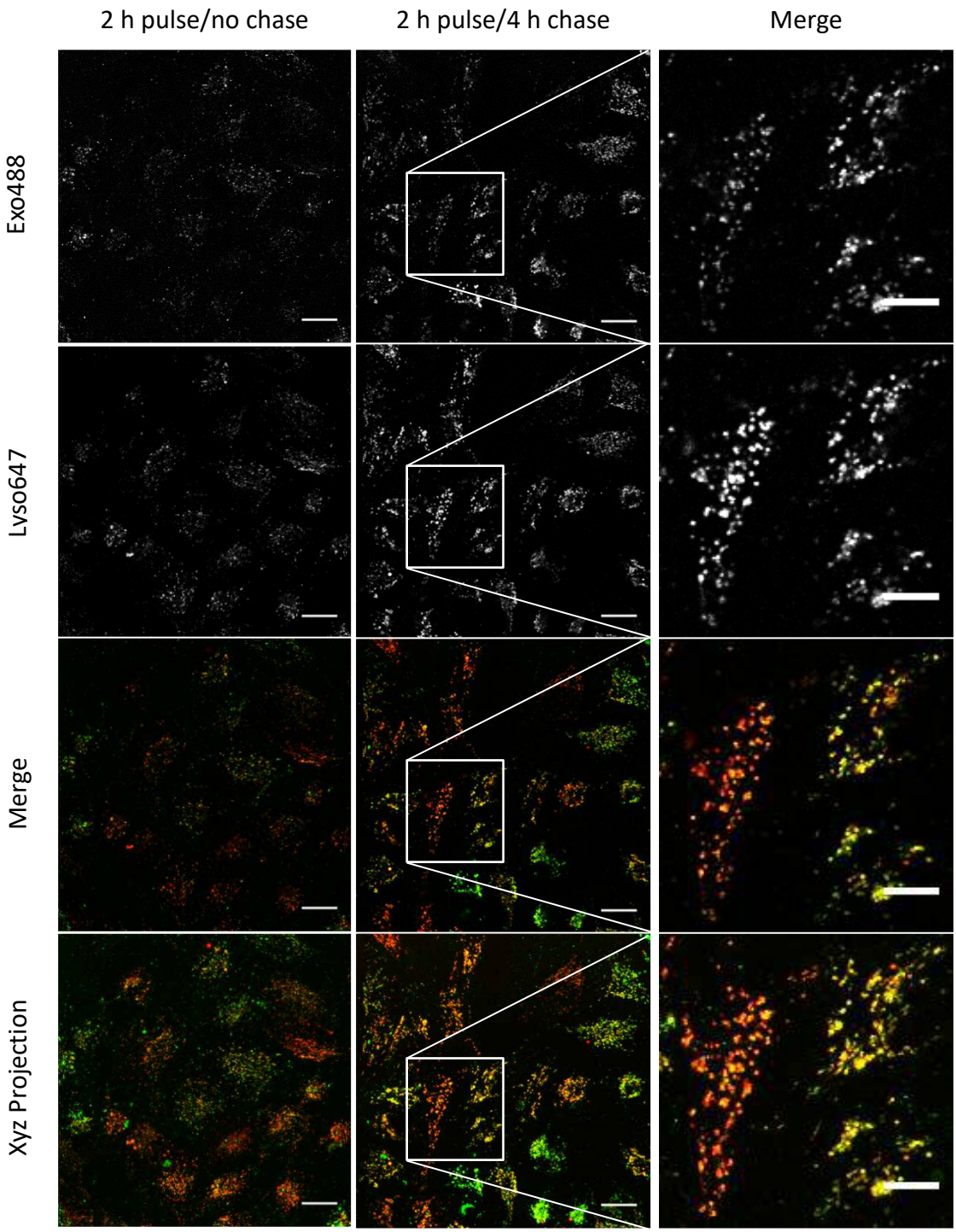

Fig. 5.7. Colocalisation of 488-labelled exosomes with dextran-loaded lysosomes in HeLa cells. Cells were incubated with Dx647 (100 µg/mL) for 2 h, washed with PBS and incubated for a further 18 h in culture media. Cells were then incubated with Exo488 (60 µg/mL) for 2 h with no chase or for 2 h followed by washing and a 4 h chase. Scale bars: 20 µm and 10 µm on zoomed images. Images representative of three separate experiments.

5.3.3 Endocytic Uptake of Exosomes in Clathrin-Mediated Endocytosis (CME) Compromised Cells

CME has been extensively characterised in *in vitro* models including HeLa cells (McMahon and Boucrot, 2011; Robinson, 2015), and this process can be attenuated using a range of methods as described in Chapter 3 of this thesis and previous members of the Jones lab (Al Soraj et al., 2012; Vercauteren et al., 2011). These include siRNA depletion of a key member of the of the CME adaptor complex AP2, known as AP2µ2 or AP50. AP2 is essential for the anchorage of cargo at the plasma membrane and subsequent recruitment of clathrin and further regulatory proteins to allow the process of internalisation to proceed (Jackson et al., 2010). Members of the Jones lab and others have shown that siRNA depletion of AP2µ2 prevents the uptake of transferrin via the transferrin receptor (Moody et al., 2015; Motley et al., 2003). In this thesis these methods were employed to initially target CME and then other proteins known to regulate other endocytic pathways. As previously demonstrated in Chapter 3 of this thesis, endocytosis of the CME probe transferrin was significantly reduced in cells depleted of AP2µ2 (Figure 3.1). Cells were transfected with control siRNA (si-control) or siRNA targeting AP2µ2 depleted cells and then incubated with Exo488 for 60 min prior to analysing cell fluorescence. Figure 5.8a shows no noticeable difference in either the cell fluorescence or the distribution of vesicular labelling between these two conditions. This was further confirmed by quantification of the MFI from three separate analyses including cells that were not transfected (Figure 5.8b).

Exosome uptake was also evaluated in cells treated with a widely used dynamin II inhibitor, Dynasore, previously used in numerous studies to evaluate the uptake of different entities via dynamin-dependant endocytic processes, such as CME and caveolae (Macia et al., 2006). Cells were pre-incubated with Dynasore for 30 min prior to addition of Tf488 for 15 min both the confocal microscopy images and MFI data highlight the strong and significant inhibition ($p<0.001$) of Tf488 uptake by this drug (Figure 5.9).

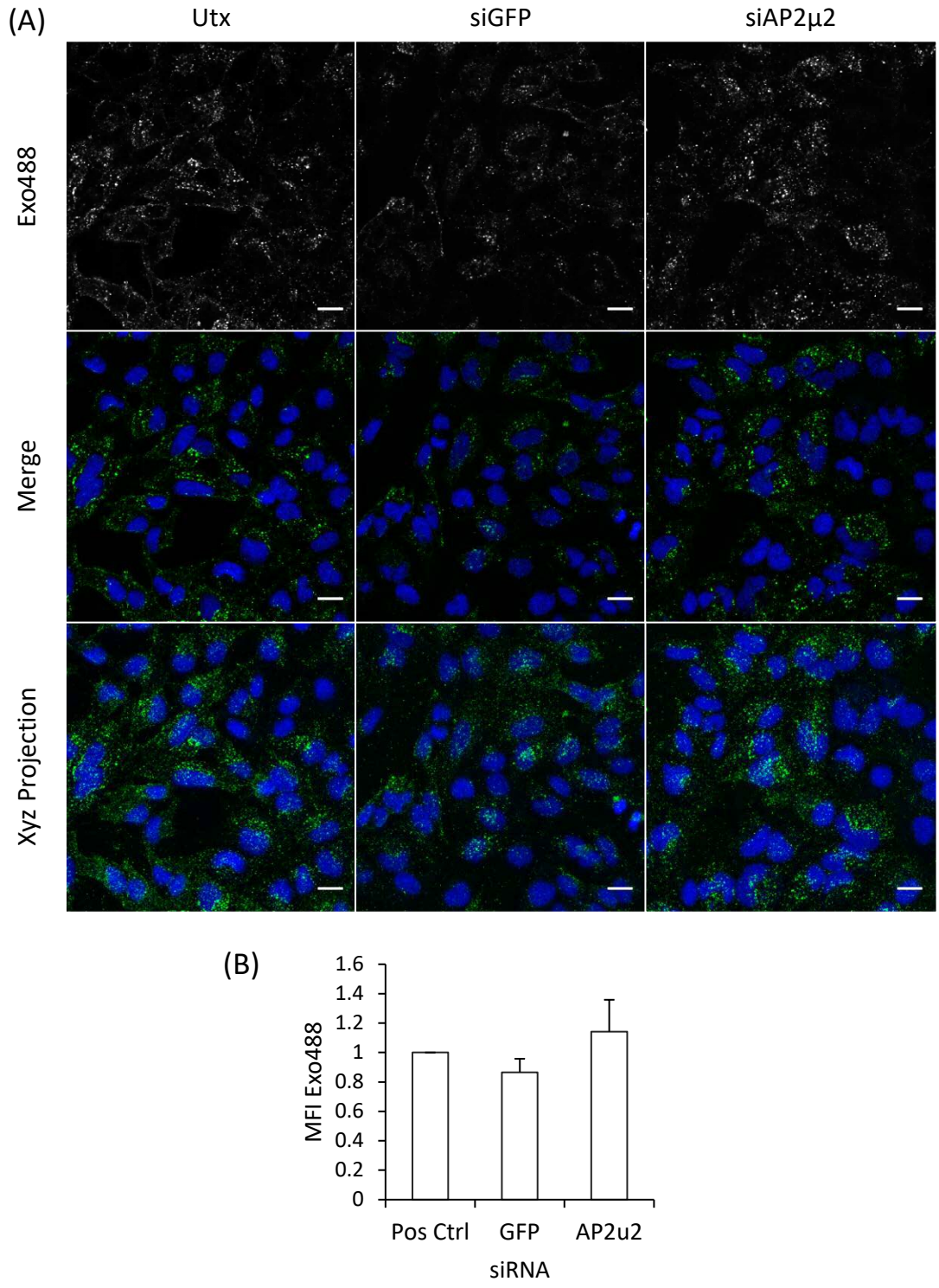

Fig. 5.8. ***Uptake of Alexa488 labelled exosomes in HeLa cells depleted of the CME adaptor protein AP2µ2*** (A) Following 48 h siRNA transfection cells were pulsed with 60 µg/ml Exo488 for 60 min (37°C, 5% CO_2). Cells were incubated with Hoechst33342 for 5 min before imaging live (R/T). Scale bar: 20 µm. (B) MFI quantification of each cell population. Error bars: Standard error. Images and graph summarise three separate experiments.

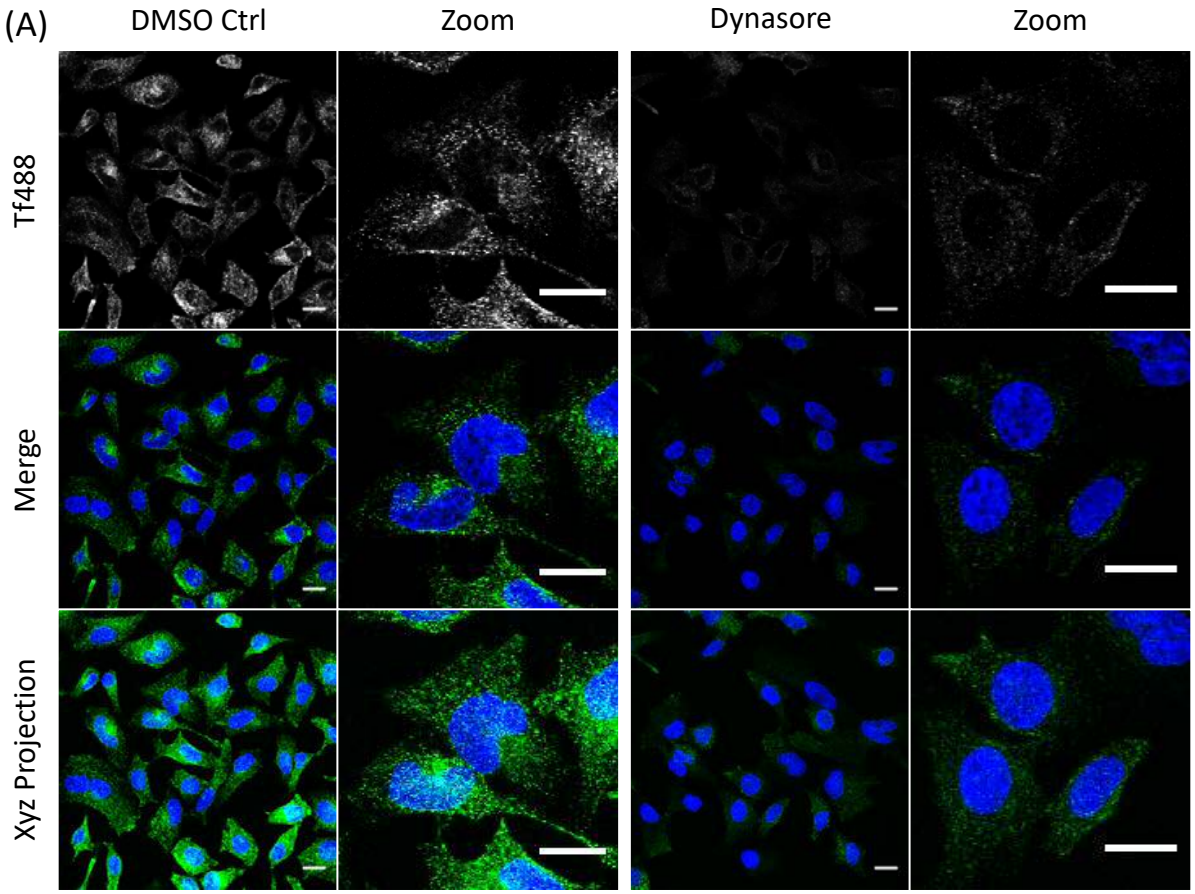

Fig. 5.9. ***Uptake of Tf488 in HeLa cells treated with Dynasore is significantly reduced in comparison to uptake in control trea***

(80 µm) pre-treatment, cells were pulsed with Tf488 (5 µg/mL) for 15 min whilst in the continued presence of the inhibitor (3

Hoechst33342 for 5 min before imaging live (R/T). Scale bar: 20 µm. (B) MFI quantification of Tf488 of the cell populations i

and graphs summarise three separate experiments. ***p<0.001

Unlike the AP2µ2 phenotype showing strong Tf488 labelling on the plasma membrane, Dynasore treated cells (Section 2.5.2) were almost devoid of any labelling; the reason for this is currently unknown but suggests that transferrin is unable to access its receptor in Dynasore treated cells. This was highly unexpected and as the zoomed images indicate, transferrin fluorescence was observed to be more disperse throughout the cytoplasm of Dynasore treated cells, rather than within the distinct punctate structures of control treated cells (Figure 5.9b). The ability of Dynasore treated cells to internalise dextran via fluid-phase endocytosis was investigated to access the effects of dynaminII inhibition on this process, as the protein has reported involvement in this pathway (Cao et al., 2007). This is also important when investigating the effect of Dynasore treatment on other endocytic pathways in this cell model. Following 60 min uptake, Dx488 could be observed as characteristic punctate structures within control treated cells and Dynasore treated cells (Figure 5.10a). There was no decrease in fluorescence intensity of Dx488 between the two populations, further indicating that the inhibitor had no effect on the fluid-phase uptake of dextran (Figure 5.10b). With regards to the effects of this inhibitor on exosome internalisation, there was a much smaller yet significant decrease in exosome uptake in Dynasore treated cells (Figure 5.11). This observation shows that a proportion of exosomes are entering via a dynamin II-dependant mechanism that based on data in Figure 5.8 is not CME. Interestingly cells transfected with a dominant negative dynamin II mutant were also shown to have reduced exosome uptake in RAW 264.7 macrophages (Feng et al., 2010). This observation of exosome uptake, by a Dynasore but not an AP2µ2 dependent process, could be due to the fact dynamin II has been implicated in the regulation of other endocytic pathways such as fluid-phase uptake and caveolae (Cao

et al., 2007; Henley et al., 1998). Furthermore, it has recently been demonstrated that Dynasore elicits additional dynamin independent effects on the cholesterol organisation of plasma membrane lipid rafts (Preta et al., 2015). Alteration of the plasma membrane in this way could affect the wider endocytic network, thereby affecting the designated uptake route of these structures. These studies led to further investigations targeting other endocytic proteins and pathways.

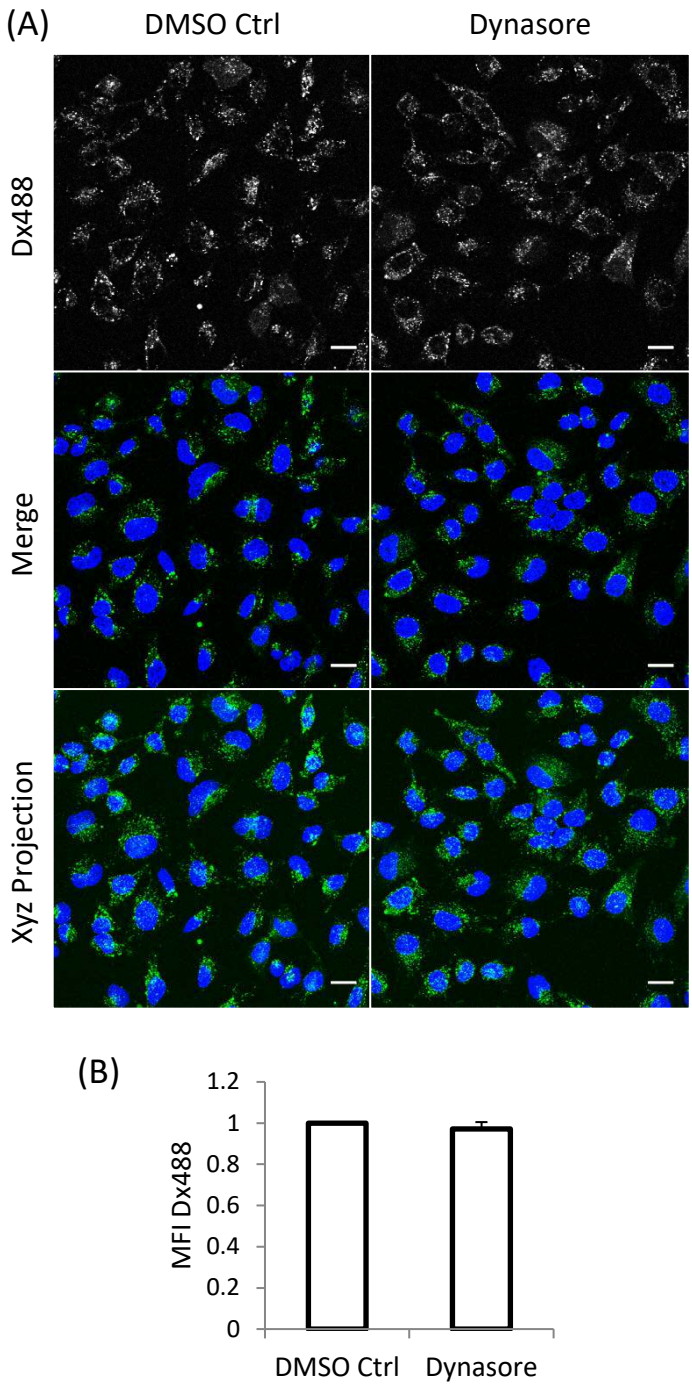

Fig. 5.10. Endocytic Uptake of *Dx488 in HeLa cells treated with Dynasore is not affected.* (A) Following 30 min Dynasore (80 µM) pre-treatment, cells were pulsed with Dx488 (100 µg/mL) for 60 min whilst in the continued presence of the inhibitor (37°C, 5% CO_2). Cells were incubated with Hoechst33342 for 5 min before imaging live (R/T). Scale bar: 20 µm. (B) MFI quantification of Dx488 of the cell populations presented in (A). Error bars: Standard error. Images and graph summarise three separate experiments.

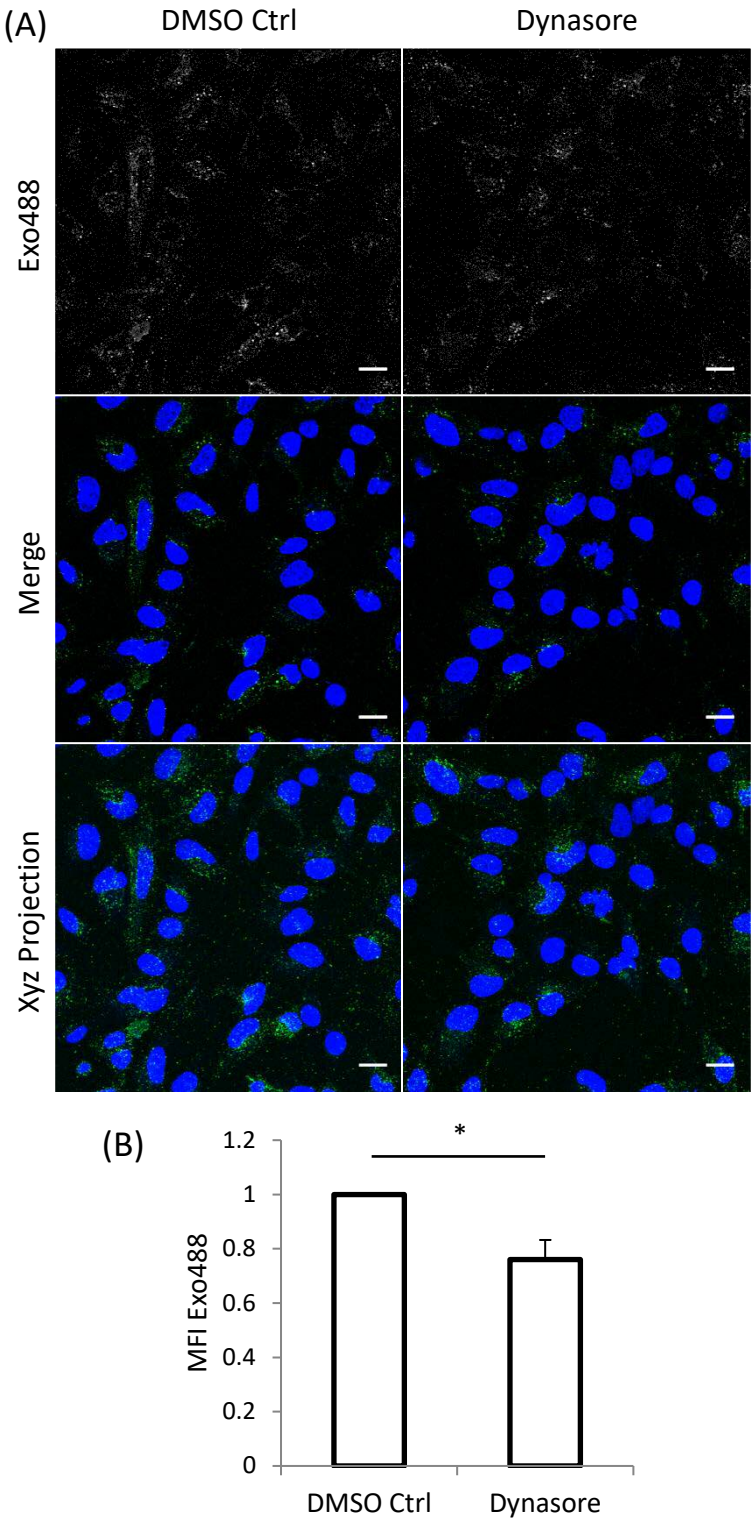

Fig. 5.11. Uptake of *Exo488 in HeLa cells treated with Dynasore is significantly reduced.* (A) Following 30 min Dynasore (80 µM) pre-treatment, cells were pulsed with Exo488 (60 µg/mL) for 60 min whilst in the continued presence of the inhibitor (37°C, 5% CO_2). Cells were incubated with Hoechst33342 for 5 min before imaging live (R/T). Scale bar: 20 µm. (B) MFI quantification of each cell population presented in (A) Error bars: Standard error. Images and graph summarise three separate experiments. *p<0.05

5.3.4 Exosome Uptake in Caveolin-1 and Flotillin-1 depleted cells

Using the same siRNA-based approach both Cav1 and Flot1 proteins were successfully depleted as indicated by Western blot analysis (Figure 5.12) but this did not significantly affect cellular uptake of the labelled exosomes (Figure 5.13). We and others have shown that endocytosis of LacCer and an anti-CD59 antibody have previously been shown to be reduced, respectively, in Cav1 and Flot1 depleted cells (Al Soraj et al., 2012; Vercauteren et al., 2011). These were not performed here due to: 1. the fact that the anti-CD59 antibodies that have been previously used by the Jones lab (Al Soraj et al., 2012) and the commercial variant used by Bitsikas et al (Bitsikas et al., 2014) to demonstrate the existence of this pathway are no longer available, and 2. that analysing LacCer uptake is technically very difficult in that it involves multiple rounds of washes in fatty acid free BSA (Al Soraj et al., 2012).

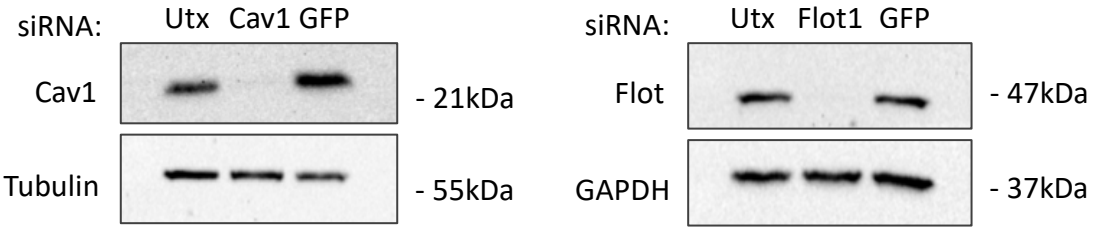

Fig. 5.12. ***Western blot analysis indicates successful depletion of Cav1 and Flot1 expression following siRNA transfection in HeLa cells.*** Following a 48 h period of siRNA transfection (100 nM) with siRNA targeting either Cav1, Flot1 or GFP, cells were lysed and Western blotting performed on the lysates. Western blots indicate Cav1 and Flot1 protein levels in comparison to the loading controls Tubulin and GAPDH.

For these reasons the discovery of novel and more specific probes for the analysis of Cav1 and Flot1 mediated endocytosis is crucial for the continued analysis of this pathway. In this thesis both proteins were successfully depleted giving us confidence that we could then perform endocytic uptake assays in these cells. It should also be noted that depletion of either of these proteins could have significant cellular effects beyond that of reducing endocytic processes as both have been implicated as important modulators of cell signalling and organisation of lipid rafts (Lajoie and Nabi, 2010). Of interest was that the distribution of exosome labelling was more peripheral in siCav1 and siFlot1 cells compared with controls suggesting alterations in downstream endocytic traffic. Overall these observations strongly suggest that endocytic processes involving Cav1 and Flot1 are not the primary mode of exosome entry, but these proteins may be involved in their subsequent traffic.

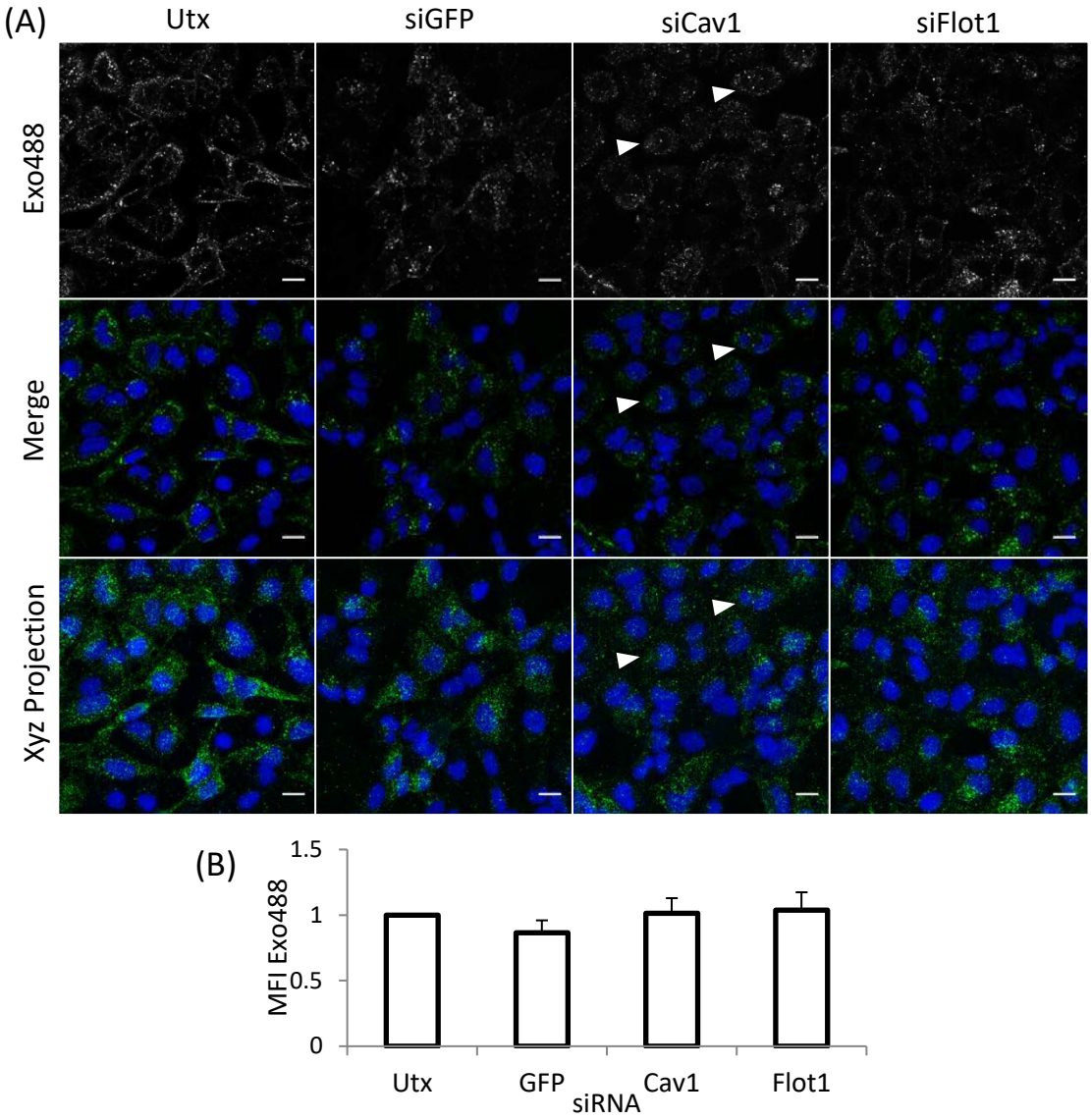

Fig. 5.13. ***Uptake of Exo488 in HeLa cells depleted of Cav1 or Flot1*** (A) Following 48 h siRNA transfection (100nM), cells were pulsed with Exo488 (60µg/ml) for 60 min (37°C, 5%CO_2). Cells were incubated with Hoechst33342 for 5 min before imaging live (R/T). Arrows indicate surface localised exosomes. Scale bar: 20µm. (B) MFI quantification of Exo488 of the cell populations in (A). Error bars: Standard error. Images and graphs summarise three separate experiments.

5.3.5 Exosome uptake in cells depleted of proteins regulating actin dynamics, fluid-phase endocytosis and macropinocytosis

Macropinocytosis has been described as a mechanism that is activated upon growth factor stimulation and could be conceived as an activated form of fluid-phase endocytosis (Jones, 2007; Kerr and Teasdale, 2009; Lim and Gleeson, 2011; Swanson and Watts, 1995). It is still unknown whether macropinocytosis can be viewed as a constitutive process in cells. Both fluid-phase endocytosis and macropinocytosis lack a specific master regulatory protein that could be targeted for siRNA depletion without affecting other processes. Macropinocytosis is highly reliant upon the organisation of actin, indicating that actin regulating proteins are candidate siRNA targets for inhibition of this process. Actin may also have involvement in constitutive fluid phase uptake (Shurety et al., 1998). PAK1 has been identified as an important regulatory factor in the events associated with actin dynamics and macropinocytosis (Dharmawardhane et al., 2000; Liberali et al., 2008). Cdc42 is also a regulator of actin dynamics, having also demonstrated an involvement in fluid-phase endocytosis/macropinocytosis (Yoshida et al., 2009). These proteins were therefore targeted with siRNA to investigate whether their depletion caused any effects on dextran endocytosis and the uptake of exosomes.

Cells were transfected with siRNA sequences targeting PAK1 and Cdc42 as performed in Chapter 4 of this thesis. Previous studies have indicated that PAK1 was involved in the cellular uptake of cationic cell penetrating peptides (CPPs) that may be inducing a form of macropinocytosis for cell entry (Al Soraj et al., 2012; Nakase et al., 2004).

Despite some visual evidence of a reduction of dextran uptake in PAK1 depleted cells, quantitative analysis showed that this was not significant and no effects were also noted for Cdc42 depletion (Chapter 3, Figure 3.17). Following a 60 min endocytic pulse in the cells depleted of either PAK1 or Cdc42, a small decrease (Figure 5.14) in exosome uptake was observed. Localisation of punctate exosome structures in Cdc42 depleted cells was noticeably different from control cells. Exosome density was greater at the cell periphery (Figure 5.14), suggesting an inability of these structures to be trafficked beyond the plasma membrane region. As noted for Flot1 and Cav1 the effects of depleting these proteins extend beyond just endocytic processes but the data suggest that traffic of exosomes beyond the plasma membrane is regulated by Cdc42 and most probably actin. As discussed in Chapter 4, actin targeting agents such as Cytochalasin D, latrunculin B and jasplakinolide are routinely used to monitor the involvement of actin on endocytosis but they also cause gross morphological effects on cells (He et al. Manuscript in preparation) making data interpretation very difficult. These drugs were not used in this thesis.

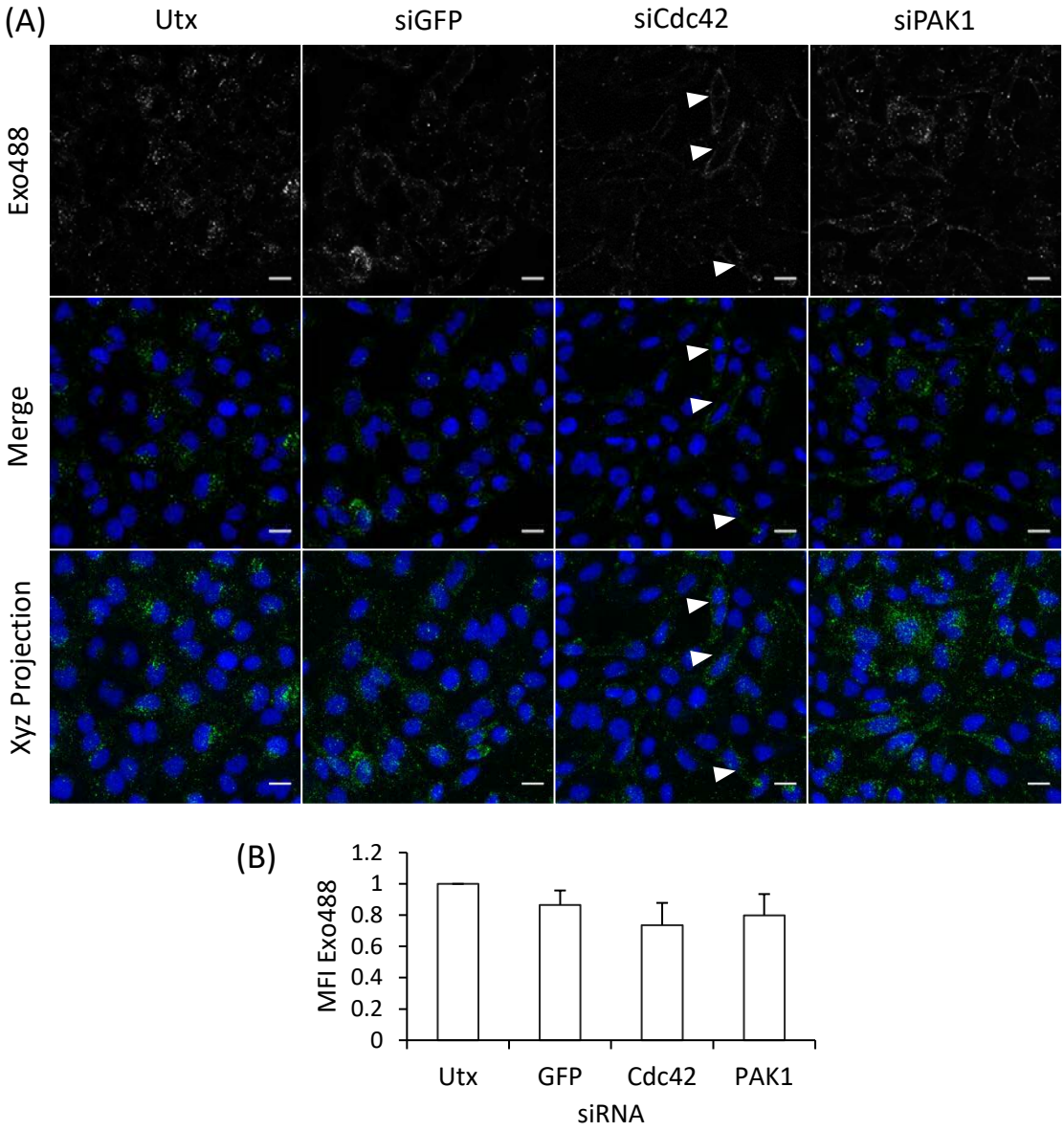

Fig. 5.14. ***Uptake of Exo488 in HeLa cells depleted of Cdc42 or PAK1*** (A) Following 48 h siRNA transfection (100 nM), cells were pulsed with Exo488 (60 µg/ml) for 60 min (37°C, 5% CO_2). Cells were incubated with Hoechst33342 for 5 min before imaging live (R/T). Arrows indicate surface localised exosomes. Scale bar: 20 µm. (B) MFI quantification of Exo488 of each cell population in (A). Error bars: Standard error. Images and graphs summarise three separate experiments.

5.3.6 Exosome uptake in cells treated with fluid-phase endocytosis/macropinocytosis inhibitors

Endocytosis inhibitors can be used in conjunction with siRNA transfection studies to provide a more comprehensive analysis of the endocytic uptake of different probes (Vercauteren et al., 2011). Following PAK1 and Cdc42 siRNA studies the inhibitors characterised in Chapter 5 targeting fluid-phase endocytosis and macropinocytosis were utilised to further explore the involvement of these pathways in exosome uptake.

EIPA is a commonly utilised Na^+/H^+ exchange inhibitor, and most probably prevents macropinocytosis by lowering the submembranous pH of the macropinocytic cup (Koivusalo et al., 2010), as discussed in Chapters 1 and 4. Although EIPA did not affect fluid-phase uptake of dextran in this cell line, it caused a small observable decrease in exosome uptake (Figure 5.15). Although endocytosis measures as fluorescence intensity was unaffected, exosome localisation in EIPA treated cells was more confined to the periphery of the cell (Figure 5.15a), further indicating the role of actin-dependant processes on the downstream traffic of these exosomes. Previous studies in PC12 cells incubated with PC12 exosomes have shown by flow cytometry that EIPA significantly reduces uptake of DiD labelled PC12 exosomes (Tian et al., 2014).

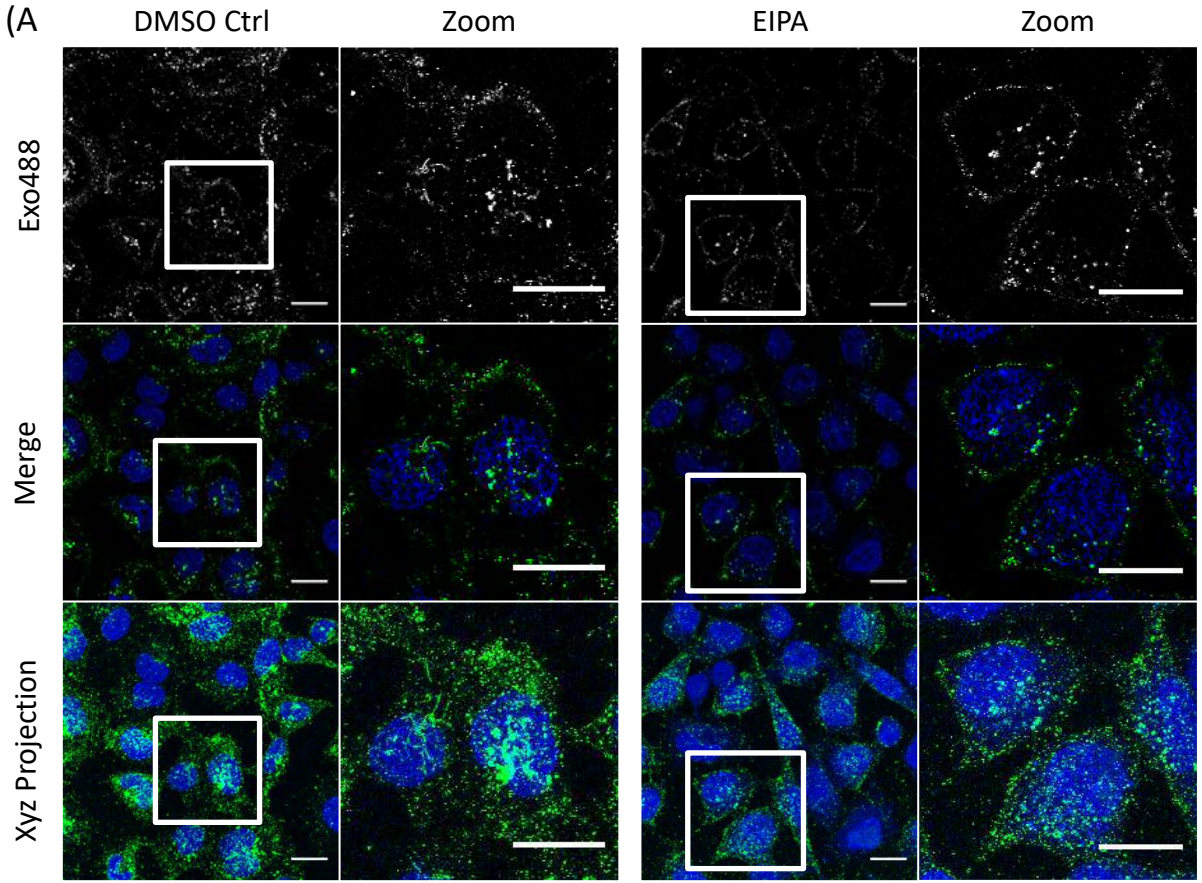

Fig. 5.15. ***Reduced uptake and membrane localisation of Exo488 in HeLa cells treated with EIPA*** (A) Following 30 min EIPA (
with Exo488 (60 µg/mL) for 60 min whilst in the continued presence of the inhibitor (37°C, 5% CO_2). Cells were incubate
imaging live (R/T). Scale bar: 20 µm. (B) MFI quantification of Exo488 of the cell populations in (A). Error bars: Standard err
separate experiments.

Rottlerin is an inhibitor primarily utilised to target fluid-phase endocytosis rather than macropinocytosis (Hufnagel et al., 2009). Exosome uptake was significantly decreased in Rottlerin treated cells (Figure 5.16), further suggesting that some of these entities are simply entering with the fluid.

The PAK1 inhibitor IPA-3 (Deacon et al., 2008), has previously been used to suggest macropinocytosis as a mechanism for viral cell entry (Krzyzaniak et al., 2013; Wen et al., 2013). This drug induced a significant decrease in dextran uptake indicating a disruption of fluid-phase endocytosis in these cells (Chapter 4, Figure 4.13). Exosome uptake was also significantly reduced in cells treated with IPA-3 (Figure 5.17) further suggesting that a fraction of these exosomes are gaining intracellular access via the fluid-phase. Collectively observations with these inhibitors suggest that a major fraction of exosomes enter these cells by fluid phase endocytosis rather than macropinocytosis.

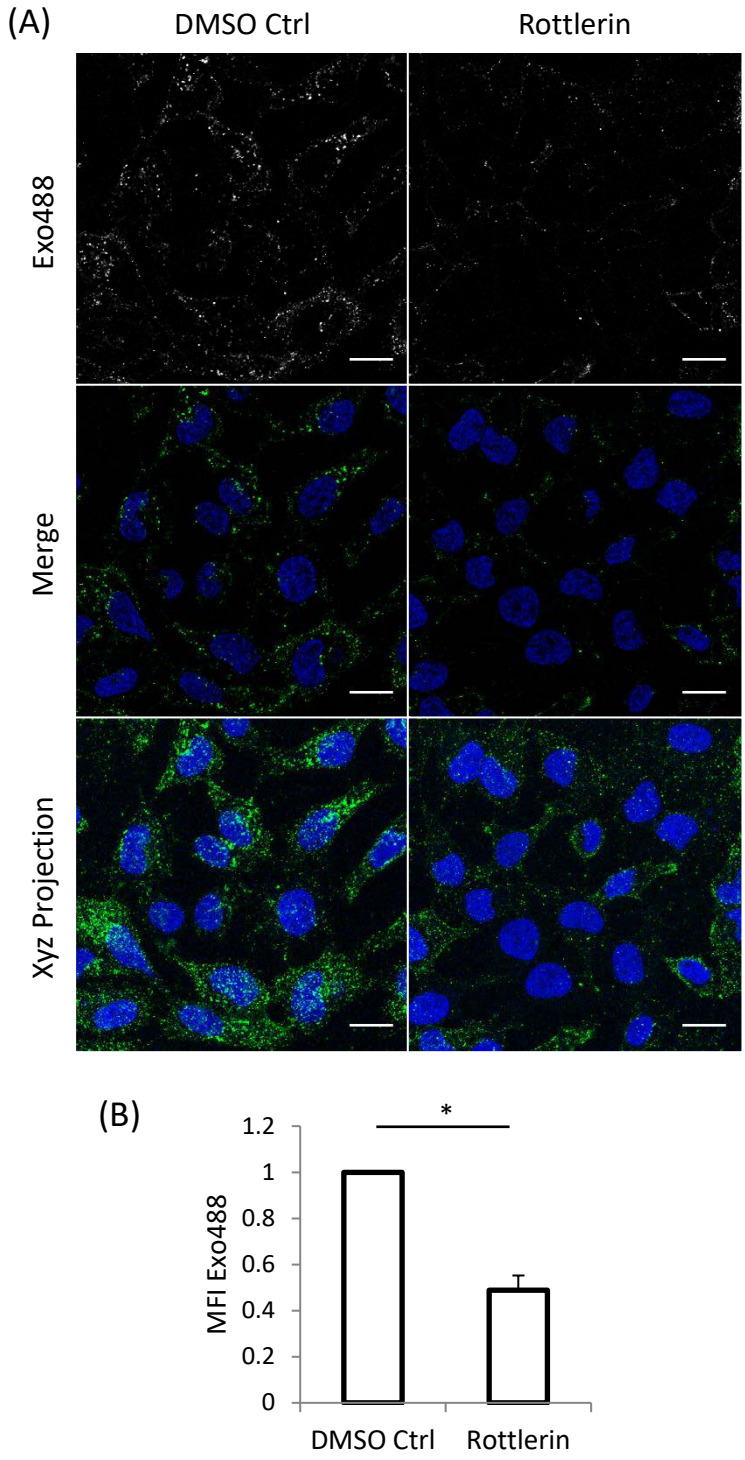

Fig. 5.16. Significant inhibition of *Exo488 in Rottlerin treated HeLa cells.* (A) Following 30 min Rottlerin (10 µm) pre-treatment, cells were pulsed with Exo488 (60 µg/mL) for 60 min whilst in the continued presence of the inhibitor (37°C, 5% CO_2). Cells were incubated with Hoechst33342 for 5 min before imaging live (R/T). Scale bar: 20 µm. (B) MFI quantification of Exo488 of the cell populations in (A). Error bars: Standard error. Images and graphs summarise three separate experiments. *p<0.05

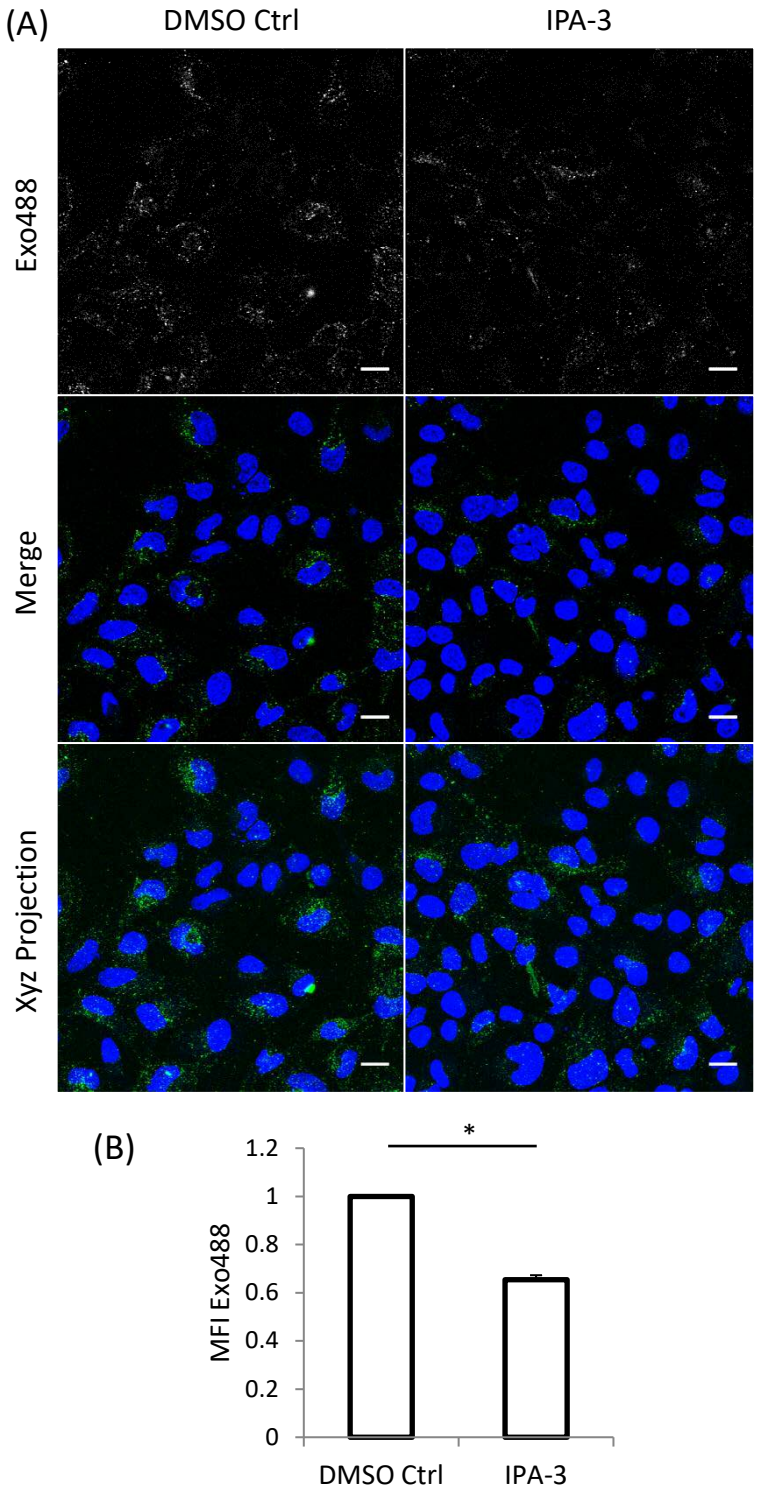

Fig. 5.17. ***Significant inhibition of Exo488 uptake in IPA-3 treated HeLa cells.*** (A) Following 30 min IPA-3 (10 µm) pre-treatment, cells were pulsed with Exo488 (60 µg/mL) for 60 min whilst in the continued presence of the inhibitor (37°C, 5% CO_2). Cells were incubated with Hoechst33342 for 5 min before imaging live (R/T). Scale bar: 20 µm. (B) MFI quantification of Exo488 of the cell populations in (A). Error bars: Standard error. Images and graphs summarise three separate experiments. *p<0.05

5.3.7 Establishment of an in vitro cell model to analyse the siRNA delivery potential of exosomes

Several different formulations have been investigated, based a library of different delivery vectors, to transport nucleotides to the inside of cells. Vectors include lipids as lipoplexes, polymers as polyplexes, combinations of these and other systems based on CPPs. As preliminary studies and to establish an *in vitro* model for siRNA delivery this thesis also investigated the capacity of the prostate derived exosomes to deliver siRNA. This was via provision the non-small lung cancer cell line (H1299) that stably expresses eGFP (kind gift from Professor Camila Foged at the University of Copenhagen).

Initial experiments were performed to ensure eGFP could be depleted in these cells using Oligofectamine, the transfection reagent that is routinely used in the Jones laboratory to deliver siRNA. Using our established protocols (Section 2.3), Oligofectamine was complexed with siRNA targeting eGFP that was either unlabelled, or labelled with the fluorophore Cy5, before the complexes were incubated with cells for 48 hours in this cell line (H1299eGFP). Cells transfected with both Cy5 and unlabelled siRNA demonstrated reduced expression of eGFP that was uniform across all cells of the population indicating that this protocol was sufficient for delivering siRNA into the cytosol of these cells (Figure 5.18). Cy5-labelled siRNA was observed within cells as punctate vesicular structures with and without Oligofectamine complexation, suggesting that the siRNA alone can gain intracellular access but not as an active entity in the cytosol. Wildtype H1299 cells (H1299WT) were utilised to provide an observable baseline fluorescence to compare eGFP depletion against. These

control studies provided a useful tool to further investigate the drug delivery potential of Du145 exosomes.

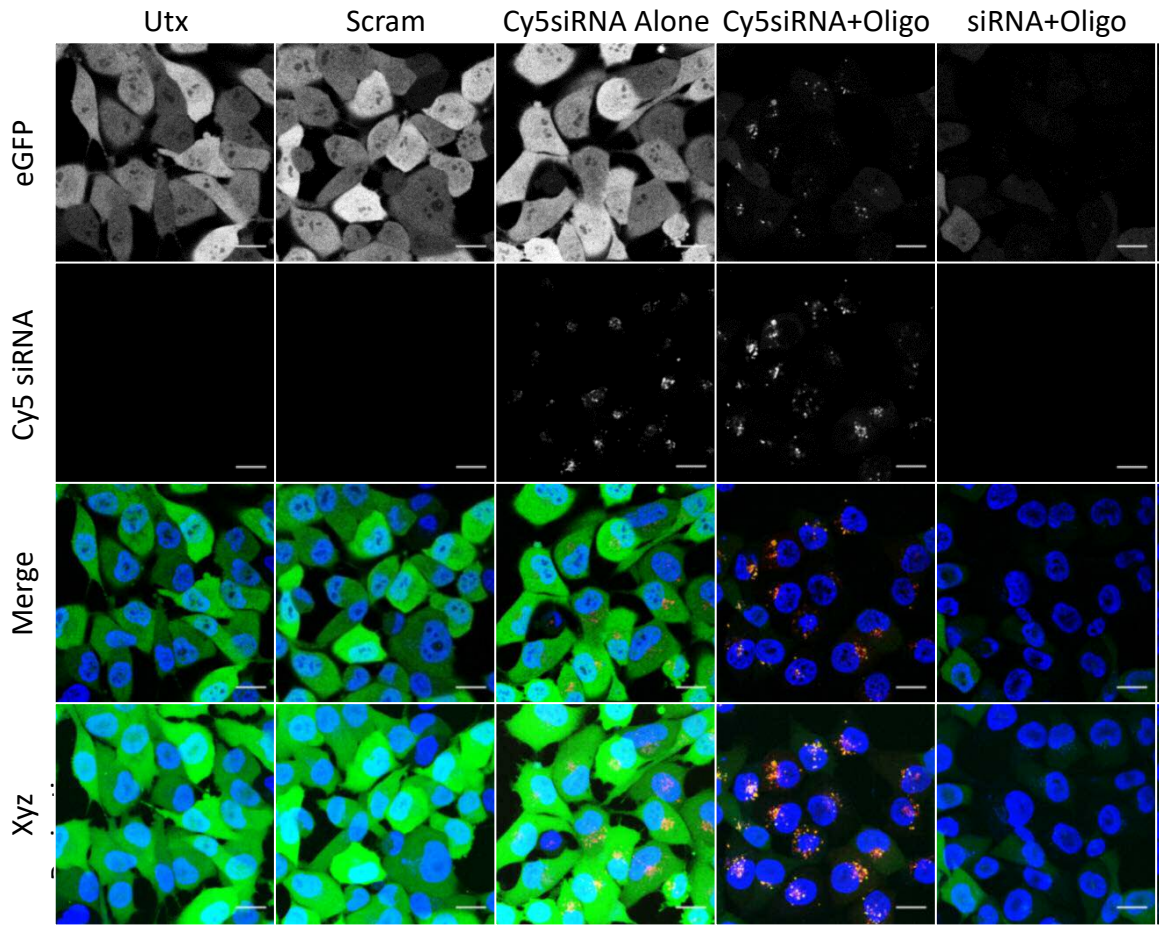

Fig. 5.18. Reduction of eGFP expression in H1299eGFP cells transfected with Oligofectamine and siRNA (Cy5-labelled and

transfected with 100 nM of either scrambled siRNA (+Oligo), Cy5siRNA (no Oligo), Cy5siRNA (+Oligo) or unlabelled siRNA (

incubated with Hoechst33342 for 5 min before imaging live (R/T). Scale bar: 20 µm. Images representative of three separate e

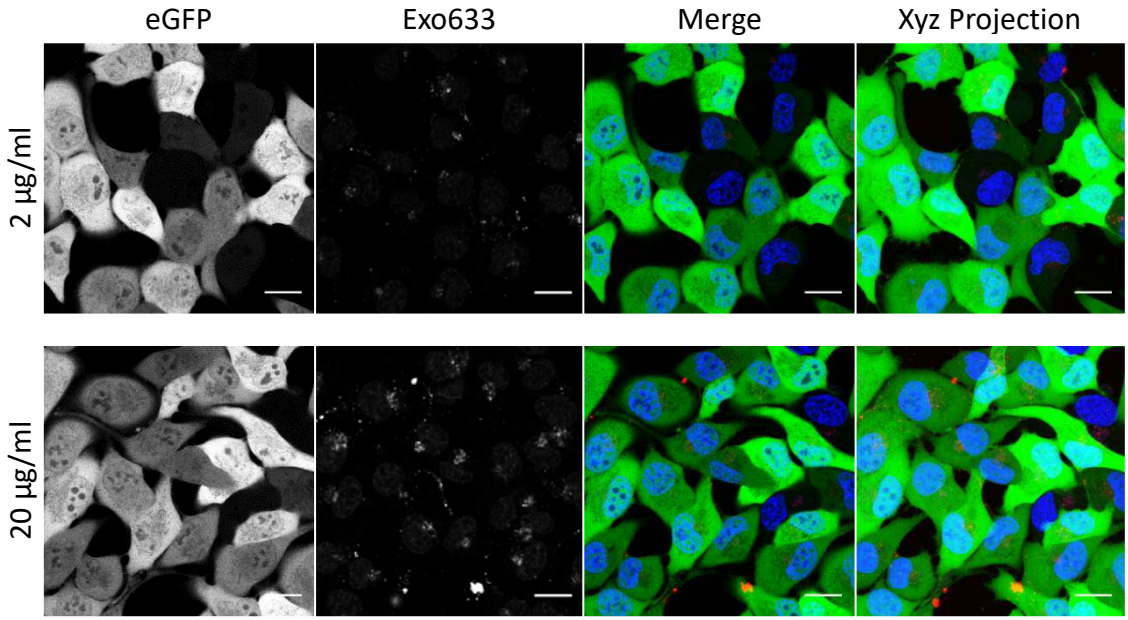

Fig. 5.19. ***Uptake of Exo633 in H1299eGFP cells.*** Cells were pulsed with either 2 µg/ml or 20 µg/ml Exo633 for 4 h (37°C, 5% CO_2). Cells were incubated with Hoechst33342 for 5 min before imaging live (R/T). Scale bar: 20 µm.

Exosomes were incubated with both labelled and unlabelled siRNA for a period of 30 min at R/T in a manner similar to Oligofectamine/siRNA complexation. Following a 48 hour transfection, depletion in eGFP expression was not observed in cells treated with exosome 'complexed' siRNA unlike cells treated with Oligofectamine complexed siRNA, which displayed a reduced expression of eGFP (Figure 5.19).

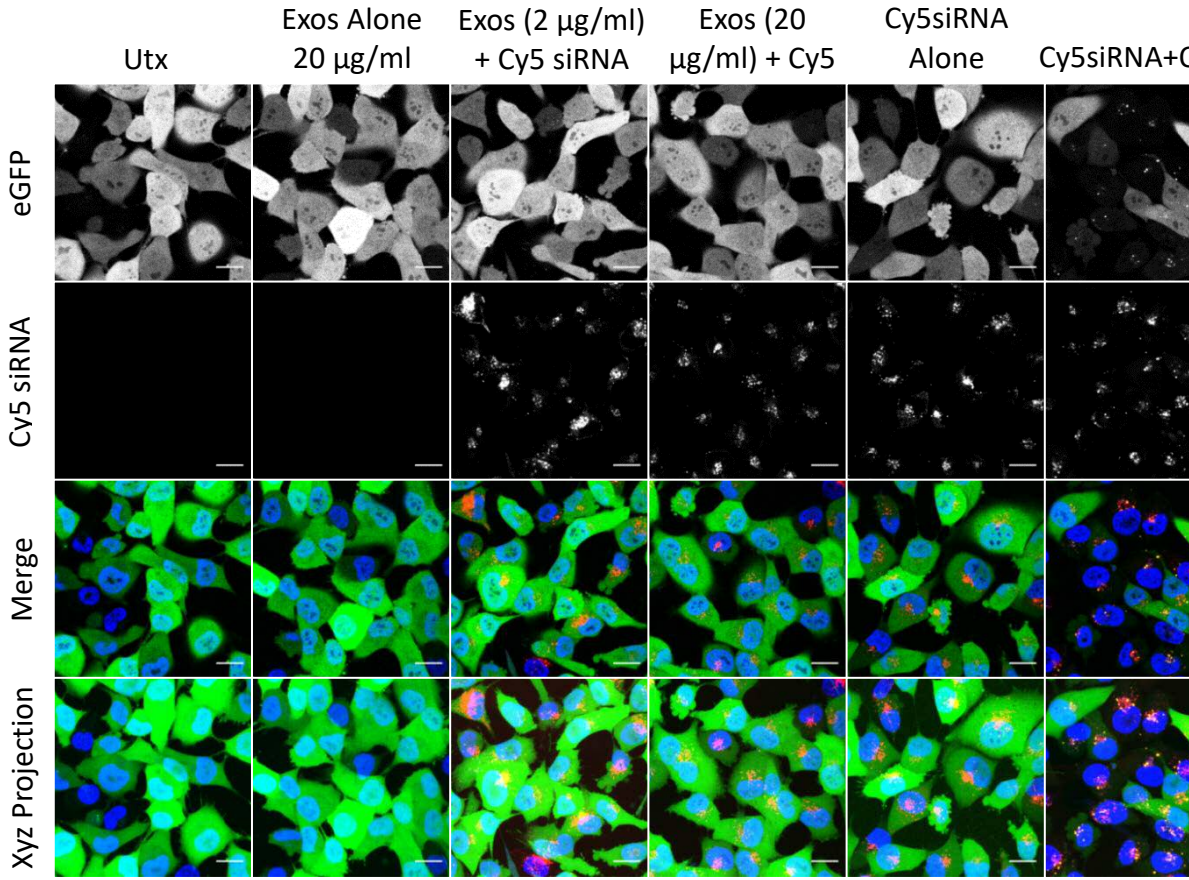

Fig. 5.20. eGFP expression in H1299eGFP cells transfected with Oligofectamine, exosomes and siRNA (Cy5-labelled and transfected with either 20 µg/ml exosomes alone, exosomes (2 µg/ml or 20 µg/ml) and Cy5siRNA (100 nM), Cy5siRNA (100 and Oligofectamine, for a period of 48 h. Cells were incubated with Hoechst33342 for 5 min before imaging live (R/T). Scale three separate experiments.

Cy5siRNA could be observed as punctate structures within the perinuclear region of: exosome complexed siRNA, Oligofectamine complexed siRNA and siRNA only treated cells (Figure 5.20), indicating that exosomes do not interfere with the ability of siRNA to reach the cell interior. No visible differences in the localisation of siRNA could be observed between siRNA alone and exosome 'complexed' siRNA further indicating that exosomes have no effects on the uptake and trafficking of siRNA within the cell, although they do not aid transfection. Indeed, it is likely that the exosomes did not complex with siRNA, causing inefficient transfection. Due to time limitations and the need for methods to load exosomes with siRNA these studies were not continued.

5.4 Discussion

In this chapter an efficient and novel method to fluorescently label exosomes for subsequent high content microscopy analysis of their interactions with cells and in endocytic traffic has been explored. Unlike other current labelling methods, this technique provides flexibility with regards to choice of fluorophore used and also provides the ability to easily label exosomes from different cell types. In the case of prostate cancer Du145 derived exosomes the labelling procedure did not affect their capacity to induce complex cellular responses such as fibroblast to myofibroblast differentiation and induction of HGF secretion. It however remains to be determined whether this labelling method influences the other numerous functional effects documented for exosomes.

These studies strongly suggest that these exosomes enter cells as components of the extracellular fluid in both primary lung fibroblasts and HeLa cells, and like dextran are mostly trafficked to lysosomes in HeLa. The localisation and dynamic activity of exosome positive vesicles suggest cellular entry via endocytosis rather than plasma membrane-exosome membrane fusion, as has been previously demonstrated in ovarian cancer cells (Escrevente et al., 2011) and discussed in a review from the Society of Extracellular Vesicles (Mulcahy et al., 2014). Approximately 60% of exosomes were fated for the lysosome, and if a longer chase were performed it may be that a greater percentage of exosomes would be found within these regions. The interference of endocytic pathways with inhibitors and siRNA depletion of endocytosis mediators together provided greater knowledge of the ways in which exosomes are

gaining access to the cell interior. Depletion of the CME moderator AP2µ2 indicated that this pathway is not primarily involved in exosome uptake. The Dynasore studies however suggest that a dynamin II dependent mechanism may be involved. Indeed, Dynasore treatment may have a global effect on the cell, as a variety of cellular processes require the function of this scission protein, meaning that the effects on exosome uptake could be due to secondary effects of the inhibitor treatment. The effects of dynasore of transferrin uptake was highly unexpected as it was expected that a dynamin II inhibitor would not prevent binding of the ligand to its receptor but only its uptake into the cells. This support previous warnings regarding the selectivity of this inhibitor to dynamin II effects (Preta et al., 2015). It also highlights how microscopy can give additional information to FACS studies that here would have given the 'expected' decrease in transferrin fluorescence.

Caveolin-1 and Flotillin-1 depletion did not affect exosome uptake with regards to internalisation intensity however localisation of exosome positive vesicles was altered. Accumulation at the plasma membrane indicates that these proteins may be required for downstream trafficking of these entities. It should also be noted that a reduced expression of Cav1 and Flot1 does not necessarily mean that their associate pathways are no longer active within the cell. Previous members have indeed indicated a reduction in the probes LacCer and anti-CD59 (Cav1-dependent and Flot1-dependent, respectively) through FACS analysis (Al Soraj et al., 2012). It could be proposed that a reduced expression of these proteins is sufficient to affect trafficking, so should follow and also affect endocytosis, in which instance it can be stated that Cav1 and Flot1 dependant pathways are not primarily involved in the uptake of these exosomes.

Indeed, the involvement of lipid-raft dependant endocytosis in exosome uptake has been previously demonstrated through siRNA depletion of Cav1. Here, uptake of exosomes increased following depletion of Cav1 suggesting that the protein can negatively regulate uptake (Svensson et al., 2013).

From the observations presented here, the most likely route utilised by these exosomes to gain intracellular access is via a fluid-phase endocytic or macropinocytosis-like mechanism. Depletion of Cdc42 and PAK1, proteins highly involved in actin dynamics (as discussed in Chapter 1), caused a small but insignificant decrease in exosome uptake. The most likely reason for this lack of significance is the large variability in uptake intensity between cells in the same population. Successful transfection does not often occur in every cell of a treated population, meaning that some cells will therefore retain the capacity to perform the pathways targeted. Cdc42 depletion has been shown in Chapter 3 to cause a decrease in transferrin uptake, indicating that pathways generally involving actin rearrangement such as CME are also affected. PAK1 depletion however did not demonstrate these effects on the uptake of other endocytic probes indicating that the reduction in exosome uptake is likely due to a reduction in a fluid-phase or macropinocytosis-like mechanism. Exosome uptake in cells treated with the chemical inhibitors of fluid-phase endocytosis and PAK1, Rottlerin and IPA-3, however was significantly reduced. Unlike siRNA transfection, chemical inhibition affects all cells in the population resulting in a smaller variability in uptake between cells. The small but not significant decrease in EIPA treated cells also alludes to the fact that exosomes are gaining access primarily through a fluid-phase endocytic/macropinocytosis like mechanism. Previous exosome studies have indicated

this also through the use of EIPA and other chemical inhibitors of fluid-phase endocytosis/macropinocytosis including Nystatin and MβCD (Tian et al., 2014). For the reasons discussed in Chapter 1, the latter inhibitors were not utilised in this thesis, but the use of EIPA demonstrated a similar decrease in uptake as observed in this thesis. Macropinocytosis has previously been designated as an exosome uptake route in microglial cells, where they are also found to localise to late endosomes/lysosomes (Fitzner et al., 2011). Pharmacological inhibitors of these processes were also used here, with amiloride and dynasore again indicating a reduction in exosome uptake. At this point it is interesting to suppose that exosomes are acting on the plasma membrane in a manner similar to a growth factor, thereby activating the actin ruffles associated with macropinocytosis. For instance, activation of the EGFR has previously been shown to increase the uptake of exosomes and this activation is accompanied by the hallmarks of macropinocytosis: actin reorganisation and ruffling (Nakase et al., 2015). As previously discussed in Chapter 1, in this instance however the EGF used originates from exosomes that have already been internalised and it is proposed that the growth factor is trafficked back to the cell surface in order to induce these effects. It is unlikely that such an engineered system would occur naturally.

The ability to successfully package or load exosomes with macromolecular or indeed small molecule therapeutics is essential to their potential use as drug delivery vectors, but methods to do this are lacking. Most current techniques utilise electroporation, which involves passing an electric current through the preparation to create pores in the membrane bilayer of the exosome (Alvarez-Erviti et al., 2011; Kooijmans et al., 2013), but other methods include sonification, transfection reagents and liposomal

techniques (Lee et al., 2016; Lu et al., 2017). Furthermore, such techniques have induced more efficient loading of porphyrins into exosomes when compared to lysosomes, another potential drug delivery vector (Fuhrmann et al., 2015). Optimising these loading techniques to improve the intracellular delivery of a range of therapeutics would indeed unlock the drug delivery potential of exosomes and other extracellular vesicles. Their use would greatly benefit the treatment of a multitude of diseases, particularly those in which biological barriers impair efficient treatment due to the natural passage of exosomes across them. For instance, exosomes are able to cross the BBB to carry therapeutics to tissues in which access to most entities is prevented by this structure (Rufino-Ramos et al., 2017).

From the results presented here it is likely that Du145 exosomes are primarily gaining access to the cell interior through a fluid-phase endocytosis/macropinocytosis-like mechanism that is dependent on dynamin II and actin dynamics, whereby the majority are trafficked to the lysosome. The techniques established and used here are now being utilised for the endocytic analysis of these exosomes in the primary lung fibroblasts in which they induce a phenotypic effect. A PhD student in the Clayton lab, Alex Cocks, is now optimising these techniques for use in this cell line, studies that will aid the overall aim of finding how Du145 exosomes interact with the cell to transfer functional cargo. The implications of these endocytic characteristics for the use of exosomes as drug delivery vectors remain to be determined but their trafficking profiles may be beneficially exploited if they can be packaged with small molecule drugs for lysosomal release into the cytosol.

5.5 References

Al-Taei, S., N.A. Penning, J.C. Simpson, S. Futaki, T. Takeuchi, I. Nakase, and A.T. Jones. 2006. Intracellular traffic and fate of protein transduction domains HIV-1 TAT peptide and octaarginine. Implications for their utilization as drug delivery vectors. *Bioconjugate chemistry*. 17:90-100.

Al Soraj, M., L. He, K. Peynshaert, J. Cousaert, D. Vercauteren, K. Braeckmans, S.C. De Smedt, and A.T. Jones. 2012. siRNA and pharmacological inhibition of endocytic pathways to characterize the differential role of macropinocytosis and the actin cytoskeleton on cellular uptake of dextran and cationic cell penetrating peptides octaarginine (R8) and HIV-Tat. *Journal of controlled release : official journal of the Controlled Release Society*. 161:132-141.

Alvarez-Erviti, L., Y. Seow, H. Yin, C. Betts, S. Lakhal, and M.J. Wood. 2011. Delivery of siRNA to the mouse brain by systemic injection of targeted exosomes. *Nature biotechnology*. 29:341-345.

Batrakova, E.V., and M.S. Kim. 2015. Using exosomes, naturally-equipped nanocarriers, for drug delivery. *Journal of controlled release : official journal of the Controlled Release Society*. 219:396-405.

Bitsikas, V., I.R. Corrêa, and B.J. Nichols. 2014. Clathrin-independent pathways do not contribute significantly to endocytic flux.

Cao, H., J. Chen, M. Awoniyi, J.R. Henley, and M.A. McNiven. 2007. Dynamin 2 mediates fluid-phase micropinocytosis in epithelial cells. *Journal of cell science*. 120:4167-4177.

Deacon, S.W., A. Beeser, J.A. Fukui, U.E.E. Rennefahrt, C. Myers, J. Chernoff, and J.R. Peterson. 2008. An Isoform-Selective, Small-Molecule Inhibitor Targets the Autoregulatory Mechanism of p21-Activated Kinase. *Chemistry & biology*. 15:322-331.

Dharmawardhane, S., A. Schurmann, M.A. Sells, J. Chernoff, S.L. Schmid, and G.M. Bokoch. 2000. Regulation of macropinocytosis by p21-activated kinase-1. *Molecular biology of the cell*. 11:3341-3352.

Enjeti, A.K., L. Lincz, and M. Seldon. 2008. Bio-maleimide as a generic stain for detection and quantitation of microparticles. *International journal of laboratory hematology*. 30:196-199.

Escrevente, C., S. Keller, P. Altevogt, and J. Costa. 2011. Interaction and uptake of exosomes by ovarian cancer cells. *BMC cancer*. 11:108.

Feng, D., W.L. Zhao, Y.Y. Ye, X.C. Bai, R.Q. Liu, L.F. Chang, Q. Zhou, and S.F. Sui. 2010. Cellular internalization of exosomes occurs through phagocytosis. *Traffic (Copenhagen, Denmark)*. 11:675-687.

Fitzner, D., M. Schnaars, D. van Rossum, G. Krishnamoorthy, P. Dibaj, M. Bakhti, T. Regen, U.K. Hanisch, and M. Simons. 2011. Selective transfer of exosomes from

oligodendrocytes to microglia by macropinocytosis. *Journal of cell science*. 124:447-458.

Fuhrmann, G., A. Serio, M. Mazo, R. Nair, and M.M. Stevens. 2015. Active loading into extracellular vesicles significantly improves the cellular uptake and photodynamic effect of porphyrins. *Journal of controlled release : official journal of the Controlled Release Society*. 205:35-44.

Grafe, I., S. Alexander, J.R. Peterson, T.N. Snider, B. Levi, B. Lee, and Y. Mishina. 2017. TGF-beta Family Signaling in Mesenchymal Differentiation. *Cold Spring Harbor perspectives in biology*.

Headland, S.E., H.R. Jones, A.S.V. D'Sa, M. Perretti, and L.V. Norling. 2014. Cutting-Edge Analysis of Extracellular Microparticles using ImageStreamX Imaging Flow Cytometry. *Scientific reports*. 4:5237.

Henley, J.R., E.W. Krueger, B.J. Oswald, and M.A. McNiven. 1998. Dynamin-mediated internalization of caveolae. *The Journal of cell biology*. 141:85-99.

Hufnagel, H., P. Hakim, A. Lima, and F. Hollfelder. 2009. Fluid phase endocytosis contributes to transfection of DNA by PEI-25. *Molecular therapy : the journal of the American Society of Gene Therapy*. 17:1411-1417.

Jackson, L.P., B.T. Kelly, A.J. McCoy, T. Gaffry, L.C. James, B.M. Collins, S. Honing, P.R. Evans, and D.J. Owen. 2010. A large-scale conformational change couples

membrane recruitment to cargo binding in the AP2 clathrin adaptor complex. *Cell*. 141:1220-1229.

Jones, A.T. 2007. Macropinocytosis: searching for an endocytic identity and role in the uptake of cell penetrating peptides. *Journal of cellular and molecular medicine*. 11:670-684.

Kerr, M.C., and R.D. Teasdale. 2009. Defining macropinocytosis. *Traffic (Copenhagen, Denmark)*. 10:364-371.

Koivusalo, M., C. Welch, H. Hayashi, C.C. Scott, M. Kim, T. Alexander, N. Touret, K.M. Hahn, and S. Grinstein. 2010. Amiloride inhibits macropinocytosis by lowering submembranous pH and preventing Rac1 and Cdc42 signaling. *The Journal of cell biology*. 188:547-563.

Kooijmans, S.A., S. Stremersch, K. Braeckmans, S.C. de Smedt, A. Hendrix, M.J. Wood, R.M. Schiffelers, K. Raemdonck, and P. Vader. 2013. Electroporation-induced siRNA precipitation obscures the efficiency of siRNA loading into extracellular vesicles. *Journal of controlled release : official journal of the Controlled Release Society*. 172:229-238.

Krzyzaniak, M.A., M.T. Zumstein, J.A. Gerez, P. Picotti, and A. Helenius. 2013. Host cell entry of respiratory syncytial virus involves macropinocytosis followed by proteolytic activation of the F protein. *PLoS Pathog*. 9:e1003309.

Lajoie, P., and I.R. Nabi. 2010. Lipid rafts, caveolae, and their endocytosis. *International review of cell and molecular biology*. 282:135-163.

Lee, J., H. Lee, U. Goh, J. Kim, M. Jeong, J. Lee, and J.H. Park. 2016. Cellular Engineering with Membrane Fusogenic Liposomes to Produce Functionalized Extracellular Vesicles. *ACS applied materials & interfaces*. 8:6790-6795.

Liberali, P., E. Kakkonen, G. Turacchio, C. Valente, A. Spaar, G. Perinetti, R.A. Bockmann, D. Corda, A. Colanzi, V. Marjomaki, and A. Luini. 2008. The closure of Pak1-dependent macropinosomes requires the phosphorylation of CtBP1/BARS. *The EMBO journal*. 27:970-981.

Lim, J.P., and P.A. Gleeson. 2011. Macropinocytosis: an endocytic pathway for internalising large gulps. *Immunology and cell biology*. 89:836-843.

Lotvall, J., A.F. Hill, F. Hochberg, E.I. Buzas, D. Di Vizio, C. Gardiner, Y.S. Gho, I.V. Kurochkin, S. Mathivanan, P. Quesenberry, S. Sahoo, H. Tahara, M.H. Wauben, K.W. Witwer, and C. Thery. 2014. Minimal experimental requirements for definition of extracellular vesicles and their functions: a position statement from the International Society for Extracellular Vesicles. *Journal of extracellular vesicles*. 3:26913.

Lu, M., H. Xing, Z. Yang, Y. Sun, T. Yang, X. Zhao, C. Cai, D. Wang, and P. Ding. 2017. Recent advances on extracellular vesicles in therapeutic delivery: challenges, solutions, and opportunities. *European journal of pharmaceutics and*

biopharmaceutics : official journal of Arbeitsgemeinschaft fur Pharmazeutische Verfahrenstechnik e.V.

Macia, E., M. Ehrlich, R. Massol, E. Boucrot, C. Brunner, and T. Kirchhausen. 2006. Dynasore, a cell-permeable inhibitor of dynamin. *Developmental cell*. 10:839-850.

Martínez, Z.A., and M. Yáñez-Mó. 2014. Tetraspanins in Extracellular Vesicle formation and function. *Frontiers in immunology*. 5.

McMahon, H.T., and E. Boucrot. 2011. Molecular mechanism and physiological functions of clathrin-mediated endocytosis. *Nature reviews. Molecular cell biology*. 12:517-533.

Montecalvo, A., A.T. Larregina, W.J. Shufesky, D.B. Stolz, M.L. Sullivan, J.M. Karlsson, C.J. Baty, G.A. Gibson, G. Erdos, Z. Wang, J. Milosevic, O.A. Tkacheva, S.J. Divito, R. Jordan, J. Lyons-Weiler, S.C. Watkins, and A.E. Morelli. 2012. Mechanism of transfer of functional microRNAs between mouse dendritic cells via exosomes. *Blood*. 119:756-766.

Moody, P.R., E.J. Sayers, J.P. Magnusson, C. Alexander, P. Borri, P. Watson, and A.T. Jones. 2015. Receptor Crosslinking: A General Method to Trigger Internalization and Lysosomal Targeting of Therapeutic Receptor:Ligand Complexes. *Molecular therapy : the journal of the American Society of Gene Therapy*. 23:1888-1898.

Motley, A., N.A. Bright, M.N. Seaman, and M.S. Robinson. 2003. Clathrin-mediated endocytosis in AP-2-depleted cells. *The Journal of cell biology*. 162:909-918.

Mulcahy, L.A., R.C. Pink, and D.R. Carter. 2014. Routes and mechanisms of extracellular vesicle uptake. *Journal of extracellular vesicles*. 3.

Nakase, I., and S. Futaki. 2015. Combined treatment with a pH-sensitive fusogenic peptide and cationic lipids achieves enhanced cytosolic delivery of exosomes. *Scientific reports*. 5:10112.

Nakase, I., N.B. Kobayashi, T. Takatani-Nakase, and T. Yoshida. 2015. Active macropinocytosis induction by stimulation of epidermal growth factor receptor and oncogenic Ras expression potentiates cellular uptake efficacy of exosomes. *Scientific reports*. 5:10300.

Nakase, I., M. Niwa, T. Takeuchi, K. Sonomura, N. Kawabata, Y. Koike, M. Takehashi, S. Tanaka, K. Ueda, J.C. Simpson, A.T. Jones, Y. Sugiura, and S. Futaki. 2004. Cellular uptake of arginine-rich peptides: roles for macropinocytosis and actin rearrangement. *Molecular therapy : the journal of the American Society of Gene Therapy*. 10:1011-1022.

Preta, G., J.G. Cronin, and I.M. Sheldon. 2015. Dynasore - not just a dynamin inhibitor. *Cell communication and signaling : CCS*. 13:24.

Robinson, M.S. 2015. Forty Years of Clathrin-coated Vesicles. *Traffic (Copenhagen, Denmark)*. 16:1210-1238.

Rufino-Ramos, D., P.R. Albuquerque, V. Carmona, R. Perfeito, R.J. Nobre, and L. Pereira de Almeida. 2017. Extracellular vesicles: Novel promising delivery systems for therapy of brain diseases. *Journal of controlled release : official journal of the Controlled Release Society*. 262:247-258.

Sagar, G., R.P. Sah, N. Javeed, S.K. Dutta, T.C. Smyrk, J.S. Lau, N. Giorgadze, T. Tchkonia, J.L. Kirkland, S.T. Chari, and D. Mukhopadhyay. 2016. Pathogenesis of pancreatic cancer exosome-induced lipolysis in adipose tissue. *Gut*. 65:1165-1174.

Shurety, W., N.L. Stewart, and J.L. Stow. 1998. Fluid-Phase Markers in the Basolateral Endocytic Pathway Accumulate in Response to the Actin Assembly-promoting Drug Jasplakinolide. *Molecular biology of the cell*. 9:957-975.

Svensson, K.J., H.C. Christianson, A. Wittrup, E. Bourseau-Guilmain, E. Lindqvist, L.M. Svensson, M. Morgelin, and M. Belting. 2013. Exosome uptake depends on ERK1/2-heat shock protein 27 signaling and lipid Raft-mediated endocytosis negatively regulated by caveolin-1. *The Journal of biological chemistry*. 288:17713-17724.

Swanson, J.A., and C. Watts. 1995. Macropinocytosis. *Trends in cell biology*. 5:424-428.

Temchura, V.V., M. Tenbusch, G. Nchinda, G. Nabi, B. Tippler, M. Zelenyuk, O. Wildner, K. Uberla, and S. Kuate. 2008. Enhancement of immunostimulatory properties of exosomal vaccines by incorporation of fusion-competent G protein of vesicular stomatitis virus. *Vaccine*. 26:3662-3672.

Tian, T., Y.L. Zhu, Y.Y. Zhou, G.F. Liang, Y.Y. Wang, F.H. Hu, and Z.D. Xiao. 2014. Exosome uptake through clathrin-mediated endocytosis and macropinocytosis and mediating miR-21 delivery. *The Journal of biological chemistry*. 289:22258-22267.

Vader, P., E.A. Mol, G. Pasterkamp, and R.M. Schiffelers. 2016. Extracellular vesicles for drug delivery. *Advanced drug delivery reviews*. 106:148-156.

van Dommelen, S.M., P. Vader, S. Lakhal, S.A. Kooijmans, W.W. van Solinge, M.J. Wood, and R.M. Schiffelers. 2012. Microvesicles and exosomes: opportunities for cell-derived membrane vesicles in drug delivery. *Journal of controlled release : official journal of the Controlled Release Society*. 161:635-644.

Vercauteren, D., M. Piest, L.J. van der Aa, M. Al Soraj, A.T. Jones, J.F. Engbersen, S.C. De Smedt, and K. Braeckmans. 2011. Flotillin-dependent endocytosis and a phagocytosis-like mechanism for cellular internalization of disulfide-based poly(amido amine)/DNA polyplexes. *Biomaterials*. 32:3072-3084.

Webber, J., and A. Clayton. 2013. How pure are your vesicles? *Journal of extracellular vesicles*. 2.

Webber, J., R. Steadman, M.D. Mason, Z. Tabi, and A. Clayton. 2010. Cancer exosomes trigger fibroblast to myofibroblast differentiation. *Cancer research*. 70:9621-9630.

Webber, J.P., L.K. Spary, A.J. Sanders, R. Chowdhury, W.G. Jiang, R. Steadman, J. Wymant, A.T. Jones, H. Kynaston, M.D. Mason, Z. Tabi, and A. Clayton. 2015. Differentiation of tumour-promoting stromal myofibroblasts by cancer exosomes. *Oncogene*. 34:290-302.

Wen, Z., B. Zhao, K. Song, X. Hu, W. Chen, D. Kong, J. Ge, and Z. Bu. 2013. Recombinant lentogenic Newcastle disease virus expressing Ebola virus GP infects cells independently of exogenous trypsin and uses macropinocytosis as the major pathway for cell entry. *Virol J*. 10:331.

Wiklander, O.P., J.Z. Nordin, A. O'Loughlin, Y. Gustafsson, G. Corso, I. Mager, P. Vader, Y. Lee, H. Sork, Y. Seow, N. Heldring, L. Alvarez-Erviti, C.I. Smith, K. Le Blanc, P. Macchiarini, P. Jungebluth, M.J. Wood, and S.E. Andaloussi. 2015. Extracellular vesicle in vivo biodistribution is determined by cell source, route of administration and targeting. *Journal of extracellular vesicles*. 4:26316.

Yoshida, S., A.D. Hoppe, N. Araki, and J.A. Swanson. 2009. Sequential signaling in plasma-membrane domains during macropinosome formation in macrophages. *Journal of cell science*. 122:3250-3261.

6 General Discussion

A higher level of understanding of the ways in which drug delivery systems, incorporating macromolecular therapeutics, interact with cells could greatly improve their capacity to cross important biological barriers such as the BBB and the gut epithelium. Incorporating such therapeutics with a variety of vectors is absolutely required to improve their capacity for intracellular access and targeting across a range of cell types (Ke et al., 2009; Midoux et al., 2009; Regberg et al., 2016; Srimanee et al., 2016). Exosomes and other types of extracellular vesicles represent natural vectors that are now gaining increasing attention as potential delivery vectors (El Andaloussi et al., 2013; Jiang and Gao, 2017; Vlassov et al., 2012). Wanting are robust *in vitro* models that allow the true mechanisms of cell entry of drug delivery to be determined.

Establishment of platforms to analyse in detail (high-content) the endocytic uptake of various drug delivery systems would benefit from greater knowledge of the proteins involved in regulating the different pathways that have now been described. Also needed are inhibitors that are truly specific for inhibiting defined pathways. Most of the described endocytic pathways have, however, only been partially characterised. The work carried out in this project aimed to address this issue and was initially successful in providing a robust *in vitro* model for clathrin-mediated endocytosis (CME) in more than one cell line. CME has been extensively studied and benefits form the fact that to date is the only pathway that allows uptake of transferrin. The establishment of a model to study fluid-phase endocytosis and macropinocytosis was more difficult due to lack of specific probes and identification of proteins that only

regulate these processes over other pathways and other cellular processes. This overall problem was partially addressed through the use of chemical inhibitors of these pathways together with siRNA depletion of key proteins. The techniques established were eventually successfully utilised to provide important information on the uptake characteristics of exosomes that were the main focus of these studies.

High capacity endocytic screening of drug delivery systems provided by collaborators, across a range of cell lines, was the initial goal of the project. This in part was achieved through the work of Dr Edd Sayers in the lab. This project ran in parallel with the work of Dr Sayers to provide higher content analysis and focused primarily on improving our capacity to study individual pathways using endocytic probes and then moving on to test these systems using labelled exosomes and model drug delivery vectors. All the analysis here was performed using live cell confocal microscopy rather than fixed cell analysis. This eliminated one potential source of error in data interpretation and also allowed concomitant analysis of the subcellular distribution and quantification of probes and exosomes. This can also not be achieved using flow cytometry.

Initially, only qualitative analysis of the differences in uptake of various entities (whether endocytic probes or exosomes) between cell samples was provided via confocal microscopy, and largely the images failed to provide a reliable indication of levels representative of cell populations as a whole. For this reason, quantitative methods of evaluating uptake was explored and developed. The optimised technique involved the quantification of mean fluorescence intensity of individual cells using the method described in Section 2.13.1. This method allowed the calculation of statistically

significant differences between the intracellular fluorescence values of different cell populations. Performing this analysis is however time-consuming due to the requirement of having to manually identify the outline of hundreds of cells per sample. Automation of this process, such as that provided by platforms such as Cell Profiler, would be extremely beneficial for this process and is currently being explored in the lab. Systems that perform this automation have been described via the composition of macros working through software such as MetaMorph (Araki et al., 2014). This study involved the automatic quantification of wide-field microscopy images, but this process is distinct from setting up a system to automatically quantify confocal images. With regards to endocytosis, this idea has been applied further to quantify the extent of macropinocytosis occurring in a cell population in a cell population (Wang et al., 2014). Using this method it was found that following starvation, EGF stimulation was efficient in the activation of macropinocytosis in HEK239 cells, a process that was also reduced following EIPA treatment.

Techniques such as flow cytometry provide quantitative data on thousands of cells per sample and experimental time point, negating the need for such a rigorous process. Important qualitative data is, however, missed using such methods. Employing the technique used and developed in this project produces quantitative data relating directly to the qualitative data provided by the microscopy images. FACS analysis also requires several wash steps and detachment of the cells, potentially altering the cellular system being analysed.

The work surrounding CME benefitted greatly from the huge amount of information relating to its molecular organisation in numerous cell types (Godlee and Kaksonen, 2013; McMahon and Boucrot, 2011; Robinson, 2015; Xing et al., 2010). AP2µ2 depletion provided an efficient method of inhibiting CME without noticeably, to our knowledge, affecting other processes. Cells depleted of AP2µ2 in this project did not present with differences in cell morphology and the uptake of the CIE probes dextran and albumin was not affected, indicating that the extended endocytic network was not affected. Further analysis investigation metabolic viability/cell division of cells depleted of AP2µ2 may well reveal that depleting this protein may have other non-endocytic effects. This needs further investigation.

The use of Dynasore as a CME inhibitor is extensive in the literature but its effects on other cellular processes has now been reviewed (Preta et al., 2015). Furthermore, its target dynamin II is involved in endocytic processes other than CME (Cao et al., 2007; Henley et al., 1998; Kokotos and Low, 2015) and also in processes distinct from endocytosis (Menon and Schafer, 2013). This was exemplified by the uptake of transferrin in Dynasore treated cells, where transferrin was not observed, as expected, to label the plasma membrane only due to the fact that the GTPase activity of Dynamin is required to pinch the clathrin coated vesicle from the membrane to allow internalisation. Reasons for this could include the inefficient recycling of the transferrin receptor to the plasma membrane, leaving nothing for extracellular transferrin to bind to. Alternatively the drug may affect the capacity of the transferrin to bind to its receptor. Future studies may benefit from the use of other chemical inhibitors related to Dynasore, such as the Dyngo molecules (McCluskey et al., 2013). Studies in this

thesis clearly highlighted how this anomaly would have been missed had we relied entirely on flow cytometry analysis.

The distinction between fluid-phase endocytosis and macropinocytosis generally identifies macropinocytosis as a growth factor activated process (Kerr and Teasdale, 2009) rather than constitutive like fluid-phase endocytosis. Both are independent of the requirement for clathrin (Stromhaug et al., 1997; Synnes et al., 1999). This project highlighted many of the issues that influence our ability to study these pathways, including choice of probe, cell line being studied and in general, the cell-wide reorganisation of the cytoskeleton involved in this processes, particularly macropinocytosis. It could be expected that the constitutive nature of fluid-phase endocytosis means that fluid-phase probes, such as dextran, can be internalised by most cell lines. Macropinocytosis however requires the ability of the cell to respond to growth factor stimulation, a reaction that depends upon expression of the growth factor receptor by a particular cell line. For instance, the actin cytoskeleton of HeLa cells did not respond to EGF stimulation to the extent that A549 cells do, suggesting that the latter cell line expresses more EGFR or has a greater capacity to respond to EGFR activation. Although described in the literature, western blot analysis of EGFR levels would further confirm this. Notably, analysis of dextran uptake in EGF stimulated cells (classical depiction of macropinocytosis) was not performed in this project, mainly because of time constraints. Furthermore, studies analysing EGF mediated promotion of micropinocytosis involve, in some cases, long periods of serum starvation. To the best of our ability we avoided this kind of cell manipulation to allow better correlation regarding what happens in vitro to what may happen *in vivo*.

Following the establishment of these inhibitory methods, the project moved on to using them to characterise the uptake of interesting molecules that were known to influence cell physiology and were of interest in the COMPACT consortium as potential drug delivery vectors. These were exosomes and an existing collaboration was in place with Dr Clayton and colleagues at the Velindre Hospital who had published work on the differentiation capacity of prostate cancer derived Du145 exosomes. Working with members of the Jones lab that had identified a novel technique to fluorescently label these structures.

Exosomes have been shown to internalise into cells using a variety of mechanisms, including via CME and macropinocytosis (Tian et al., 2014), but this presented thesis indicated that CME was not primarily utilised by these Du145 exosomes in HeLa cells. It is likely that a macropinocytosis-like pathway with a dependence on dynamin is used; noting the earlier discussion on issues relating to the specificity of dynasore. Using colocalisation analysis it would appear that lysosomes are major depots for these exosomes raising interesting questions regarding their usefulness for delivering therapeutics to these hydrolytic organelles and how they are able to naturally release cargo such as miRNA into the cytosol before degradation.

The uptake mechanism used by any extracellular vesicle is likely to depend on a variety of factors including the recipient cell line. Another issue to consider is the identity/profile of the vesicles present in the isolate. The distinction between exosomes and other extracellular vesicles in the isolation of vesicle preparations is much debated. It is difficult to state that an isolate contains exclusively exosomes, with

a collection of different types of extracellular vesicle much more likely. The Clayton group performs rigorous tests to define an isolate as mainly exosomes (Webber and Clayton, 2013), (as described in Appendix B and C), so this work describes all extracellular vesicles used as exosomes, though it may be possible that other types of vesicles are present.

Delineating the uptake mechanism(s) of Du145 exosomes, fluorescently labelled using this novel technique was used in conjunction with an innovative way of quantifying fluorescence as a measure of exosome uptake. The ways in which this developed high content endocytic platform, can be used to explore endocytosis of a potential drug delivery vector was demonstrated. These platforms are now currently being used by members of the Clayton lab to study the uptake of Du145 exosomes in primary lung fibroblasts, and also by members of the Jones lab to aid their individual project aims. The work performed in this project to establish these models highlighted the need for a collection of different methods, comprising both siRNA depletion methods and chemical inhibitors to study different pathways, as these processes have both strengths and weaknesses that can almost be counterbalanced when used in conjunction with each other. There is however a need for better inhibitors and a higher level of understanding of endocytic pathways.

Preliminary experiments were also performed to assess whether simple mixing of siRNA with exosomes would result in protein depletion following addition to the cells. These experiments in H1299eGFP cells were not successful, which is not unexpected due to the fact that optimisation studies were lacking. It is clear that loading exosomes

with cargo represents a major challenge and considered also should be the possibility that these entities, like Du145 exosomes, may have other effects. These effects such as the differentiation mentioned here could be detrimental or could be exploited for therapeutic gain. The preliminary deliver studies presented here in H1299eGFP cells now provide a suitable platform to study the siRNA delivery potential within the Jones group and with collaborators sharing new drug delivery formulations.

It is also worthwhile considering how exosomes and other extracellular vesicles could be produced industrially if found to be utilised as a successful drug delivery vector. The processes required to collect and isolate exosomes in the small amounts used for this project are currently extremely rigorous; escalating these would be expensive, time-consuming, and require high levels of industrial cell culture. If efficient loading of exosomes were to be optimised and targeting to different tissues was successful, the use of exosomes as novel drug delivery vectors for packaging macromolecular therapeutics is an exciting prospect for the future of drug delivery.

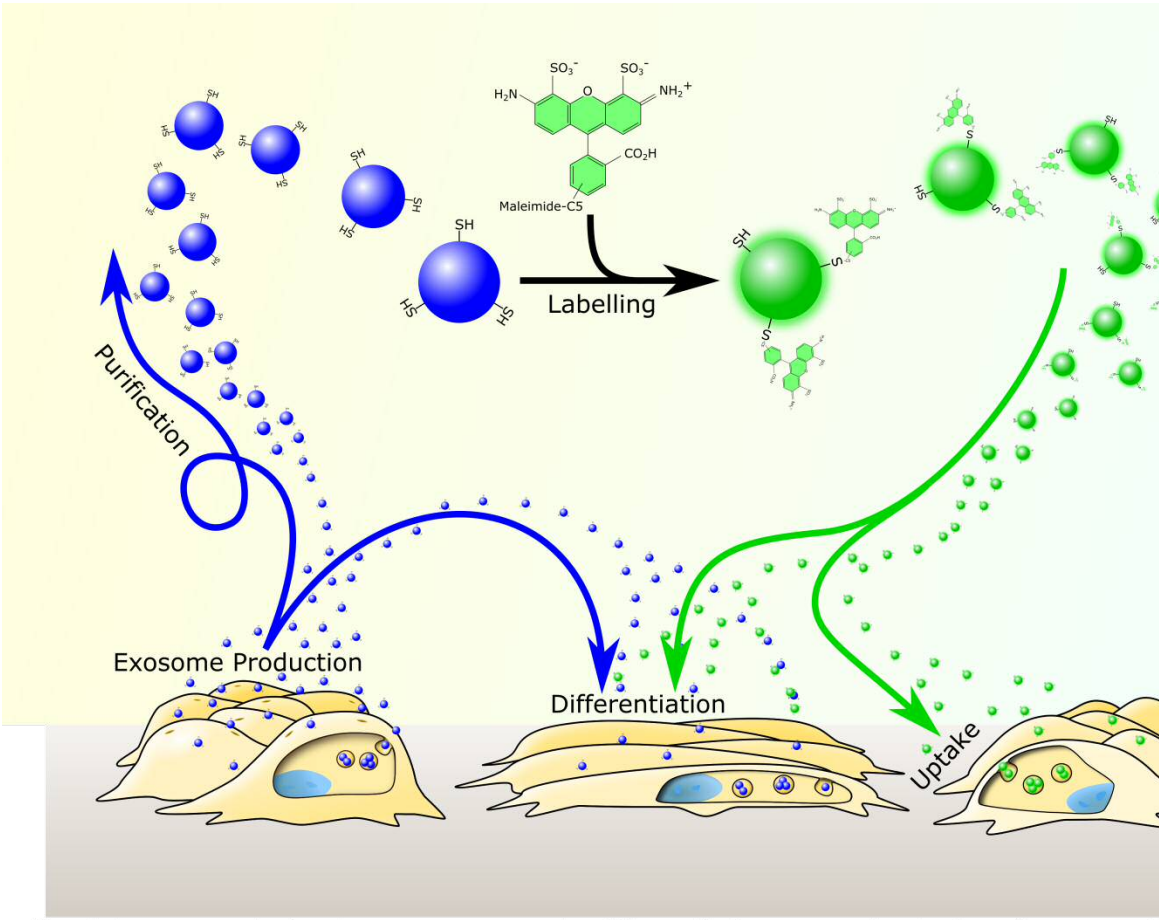

Fig. 6.1 Prostate cancer derived exosomes remain differentiation competent when fluorescent
thiol-based method, allowing exploration of their cellular uptake and trafficking mecha
content microscopy analysis.

Courtesy of Edd Sayers

6.1 References

Araki, N., Y. Ikeda, T. Kato, K. Kawai, Y. Egami, K. Miyake, N. Tsurumaki, and M. Yamaguchi. 2014. Development of an automated fluorescence microscopy system for photomanipulation of genetically encoded photoactivatable proteins (optogenetics) in live cells. *Microscopy (Oxford, England)*. 63:255-260.

Cao, H., J. Chen, M. Awoniyi, J.R. Henley, and M.A. McNiven. 2007. Dynamin 2 mediates fluid-phase micropinocytosis in epithelial cells. *Journal of cell science*. 120:4167-4177.

El Andaloussi, S., S. Lakhal, I. Mager, and M.J. Wood. 2013. Exosomes for targeted siRNA delivery across biological barriers. *Advanced drug delivery reviews*. 65:391-397.

Godlee, C., and M. Kaksonen. 2013. Review series: From uncertain beginnings: initiation mechanisms of clathrin-mediated endocytosis. *The Journal of cell biology*. 203:717-725.

Henley, J.R., E.W. Krueger, B.J. Oswald, and M.A. McNiven. 1998. Dynamin-mediated internalization of caveolae. *The Journal of cell biology*. 141:85-99.

Jiang, X.C., and J.Q. Gao. 2017. Exosomes as novel bio-carriers for gene and drug delivery. *International journal of pharmaceutics*. 521:167-175.

Ke, W., K. Shao, R. Huang, L. Han, Y. Liu, J. Li, Y. Kuang, L. Ye, J. Lou, and C. Jiang. 2009. Gene delivery targeted to the brain using an Angiopep-conjugated

polyethyleneglycol-modified polyamidoamine dendrimer. *Biomaterials*. 30:6976-6985.

Kerr, M.C., and R.D. Teasdale. 2009. Defining macropinocytosis. *Traffic (Copenhagen, Denmark)*. 10:364-371.

Kokotos, A.C., and D.W. Low. 2015. Myosin II and dynamin control actin rings to mediate fission during activity-dependent bulk endocytosis. *The Journal of neuroscience : the official journal of the Society for Neuroscience*. 35:8687-8688.

McCluskey, A., J.A. Daniel, G. Hadzic, N. Chau, E.L. Clayton, A. Mariana, A. Whiting, N.N. Gorgani, J. Lloyd, A. Quan, L. Moshkanbaryans, S. Krishnan, S. Perera, M. Chircop, L. von Kleist, A.B. McGeachie, M.T. Howes, R.G. Parton, M. Campbell, J.A. Sakoff, X. Wang, J.Y. Sun, M.J. Robertson, F.M. Deane, T.H. Nguyen, F.A. Meunier, M.A. Cousin, and P.J. Robinson. 2013. Building a better dynasore: the dyngo compounds potently inhibit dynamin and endocytosis. *Traffic (Copenhagen, Denmark)*. 14:1272-1289.

McMahon, H.T., and E. Boucrot. 2011. Molecular mechanism and physiological functions of clathrin-mediated endocytosis. *Nature reviews. Molecular cell biology*. 12:517-533.

Menon, M., and D.A. Schafer. 2013. Dynamin: expanding its scope to the cytoskeleton. *International review of cell and molecular biology*. 302:187-219.

Midoux, P., C. Pichon, J.J. Yaouanc, and P.A. Jaffres. 2009. Chemical vectors for gene delivery: a current review on polymers, peptides and lipids containing histidine or imidazole as nucleic acids carriers. *British journal of pharmacology*. 157:166-178.

Preta, G., J.G. Cronin, and I.M. Sheldon. 2015. Dynasore - not just a dynamin inhibitor. *Cell communication and signaling : CCS*. 13:24.

Regberg, J., L. Vasconcelos, F. Madani, Ü. Langel, and M. Hällbrink. 2016. pH-responsive PepFect cell-penetrating peptides. *International journal of pharmaceutics*. 501:32-38.

Robinson, M.S. 2015. Forty Years of Clathrin-coated Vesicles. *Traffic (Copenhagen, Denmark)*. 16:1210-1238.

Srimanee, A., J. Regberg, M. Hallbrink, O. Vajragupta, and U. Langel. 2016. Role of scavenger receptors in peptide-based delivery of plasmid DNA across a blood-brain barrier model. *International journal of pharmaceutics*. 500:128-135.

Stromhaug, P.E., T.O. Berg, T. Gjoen, and P.O. Seglen. 1997. Differences between fluid-phase endocytosis (pinocytosis) and receptor-mediated endocytosis in isolated rat hepatocytes. *European journal of cell biology*. 73:28-39.

Synnes, M., K. Prydz, T. Lovdal, A. Brech, and T. Berg. 1999. Fluid phase endocytosis and galactosyl receptor-mediated endocytosis employ different early endosomes. *Biochimica et biophysica acta*. 1421:317-328.

Tian, T., Y.L. Zhu, Y.Y. Zhou, G.F. Liang, Y.Y. Wang, F.H. Hu, and Z.D. Xiao. 2014. Exosome uptake through clathrin-mediated endocytosis and macropinocytosis and mediating miR-21 delivery. *The Journal of biological chemistry*. 289:22258-22267.

Vlassov, A.V., S. Magdaleno, R. Setterquist, and R. Conrad. 2012. Exosomes: current knowledge of their composition, biological functions, and diagnostic and therapeutic potentials. *Biochimica et biophysica acta*. 1820:940-948.

Wang, J.T.H., R.D. Teasdale, and D. Liebl. 2014. Macropinosome quantitation assay. *MethodsX*. 1:36-41.

Webber, J., and A. Clayton. 2013. How pure are your vesicles? *Journal of extracellular vesicles*. 2.

Xing, Y., T. Bocking, M. Wolf, N. Grigorieff, T. Kirchhausen, and S.C. Harrison. 2010. Structure of clathrin coat with bound Hsc70 and auxilin: mechanism of Hsc70-facilitated disassembly. *The EMBO journal*. 29:655-665.

Appendices

Appendix A – List of Products and Suppliers

Biorad (Hemel Hempstead, UK):
- Precision plus protein dual colour standards (#161-0374)
- Clarity, Western ECL substrate (#170-5060)
- 10% Mini-PROTEAN TGX Precast Gel (#456-1033)

DAKO (Ely, UK):
- Fluorescence mounting medium “Dako oil” / (#S3023)

Fisher Scientific (Loughborough, UK):
- Coverslips No. 1 circle 16mm diameter (#12313138)
- PVDF membrane (#10344661)
- SuperSignal West Femto Chemiluminescent Substrate (#34094)

Life Technologies (Paisley, UK):
- DMEM (#21885)
- DMEM (Phenol red free + 20mM HEPES) (#21063-029)
- RPMI 1640 (#21875)
- DMEM/F12 (#11330)
- Sensicell MEM (#A15156-01)
- Ham’s F-12K (#21127-022)
- FBS (#16000-044)
- Opti-MEM (#31985-047)
- NEAA (#11140050)
- Sodium Pyruvate (#11530396)
- 0.05% Trypsin EDTA (#25300062)
- Hoechst 33342 (#H3570)
- Cell Mask deep red (#C10046)
- Cell Mask orange (#C10045)
- Rhodamine Phalloidin (#R415)
- Transferrin Alexa 488 (#T13342)
- Transferrin Alexa 647 (#T23366)
- 10kDa Dextran Alexa 488 (#D22910)
- 10kDa Dextran Alexa 647 (#D22914)
- C_5-maleimide Alexa 488 (#A10254)
- C_5-maleimide Alexa 633 (#A20342)
- BODIPY – LacCer (#B34402)

- BSA Alexa 647 (#A34785)
- Oligofectamine transfection reagent (#12252-011)
- Exosome Elution Columns (MW3000) (#4484449)

Roche Diagnostics (Burgess Hill, UK):
- cOmplete Protease Inhibitor Cocktail Tablets (#11836153001)

Sigma Aldrich (Poole, UK):
- EGF (#E9644)
- EIPA (#A3085)
- Rottlerin (#R5648)
- IPA-3 (#I2285)
- ML-7 (#I2764)
- Triton X-100 (#X100)
- BSA (#A7906)
- Bicinchoninic Acid solution (#B9643)
- Copper (II) Sulphate solution (#C2284)
- TEMED (#T9281)
- Ponceau S solution (#P7170)
- Tween 20 (#P1379)
- Trypan Blue (#T8154)

Appendix B – Roberts-Dalton et al. *Nanoscale*. 2017. In press.

Nanoscale

PAPER

Fluorescence labelling of extracellular vesicles using a novel thiol-based strategy for quantitative analysis of cellular delivery and intracellular traffic†

Cite this: DOI: 10.1039/c7nr04128d

H. D. Roberts-Dalton,[a] A. Cocks,[b] J. M. Falcon-Perez,[c] E. J. Sayers,[a] J. Webber,[b] P. Watson,[d] A. Clayton*[b] and A. T. Jones *[a]

Extracellular vesicles, including exosomes, are naturally derived nanovesicles generated in and released by numerous cell types. As extracellular entities they have the capacity to interact with neighbouring cells and distant tissues and affect physiological processes as well as being implicated in numerous diseases including tumorigenesis and neurodegeneration. They are also under intense investigation as delivery vectors for biotherapeutics. The ways in which EVs interact with recipient cells to influence cell physiology and deliver a macromolecular payload are at the early stages of exploration. A significant challenge within these studies is the ability to label EVs directly or indirectly with fluorescent probes to allow visualization without compromising functionality. Here, we present a thiol-based fluorescence labelling method allowing comprehensive analysis of the cellular uptake of prostate cancer derived EVs in live cells using confocal microscopy. Labelling of the EVs in this way did not influence their size and had no effect on their ability to induce differentiation of lung fibroblasts to myofibroblasts. For endocytosis analyses, depletion of key endocytic proteins and the use of chemical inhibitors (Dynasore, EIPA, Rottlerin and IPA-3) indicated that fluid-phase endocytosis and/or macropinocytosis was involved in EV internalisation. Over a period of six hours EVs were observed to increasingly co-localise with lysosomes, indicating a possible termination point following internalisation. Overall this method provides new opportunities for analysing the cellular dynamics of EVs as biological entities affecting cell and whole body physiology as well as investigating their potential as drug delivery vectors.

Received 9th June 2017,
Accepted 22nd August 2017
DOI: 10.1039/c7nr04128d
rsc.li/nanoscale

1 Introduction

Exosomes, a subpopulation of extracellular vesicles (EVs), are secreted 30–150 nm sized vesicles manufactured within multivesicular endosomes and trafficked to the extracellular space through Rab-GTPase dependent mechanisms.[1,2] These structures comprise a phospholipid bilayer that is particularly enriched in membrane proteins such as tetraspanins, MHC Class-I proteins, integrins and many others.[3,4] The vesicle lumen also encompasses complex entities derived from the cell of origin, including cytosolic proteins and a subset of cellular RNAs.[5,6] Exosomes naturally serve as a means of shuttling this cargo intercellularly as a mode of communication, which can modulate important physiological and pathological processes such as cancer, cardiovascular diseases, and neurodegeneration, as well as in transfer of pathogenic virulence factors.[6]

This natural ability to functionally transfer a spectrum of macro-molecular cargo between cells raises opportunities for exploiting exosomes as vectors for drug delivery.[7,8] However, little is known about the ways in which exosomes initially interact with the cell, gain intracellular access and are trafficked through the cell to their final destination. Even less is known about how intravesicular cargo is released and directed towards the intended target within the cytosol or other intracellular compartments. The capacity of exosomes to mediate these effects, possibly through endocytosis, requires further characterisation in order to fully understand their natural roles in disease pathogenesis and also unlock their potential for drug delivery.

[a]Cardiff School of Pharmacy and Pharmaceutical Sciences, Cardiff University, Cardiff, CF10 3NB, UK. E-mail: jonesat@cardiff.ac.uk
[b]Division of Cancer & Genetics, Tenovus Institute, Heath park, Cardiff University, Cardiff CF14 4XN, UK. E-mail: claytona@cf.ac.uk
[c]CIC bioGUNE, CIBERehdParque Tecnológico, Bldg. 801-A, Derio, 48160 Bizkaia, Spain
[d]School of Biosciences, Cardiff University, Cardiff, CF10 3AX, UK
†Electronic supplementary information (ESI) available. See DOI: 10.1039/c7nr04128d

Endocytosis involves the envelopment of materials from the exterior region of the cell by the plasma membrane. Several endocytic pathways have now been described, each utilising proteins that regulate single and multiple uptake routes.[9,10] Clathrin-mediated endocytosis is by far the most well-defined mechanism, characterised by the formation of a clathrin coated pit that eventually buds into the cytoplasm to form a clathrin coated vesicle that is uncoated before fusing with an early or sorting endosome.[9–11] Endocytosis mediating from distinct platforms of the plasma membrane termed lipid rafts has also been described, with these processes demonstrating involvement of Caveolin-1[9,12] or Flotillin-1.[9,13] Other pathways include fluid-phase endocytosis and macropinocytosis, which are defined as cargo non-specific mechanisms, with the latter process demonstrating a reliance on extensive plasma membrane reorganisation by the actin cytoskeleton. This is often in response to growth factor stimulation.[14–16] Distinguishing between macropinocytosis and fluid phase uptake as constitutive processes is very difficult as they may share similar protein mediators. Proteins that have been implicated in the organisation of macropinocytosis include PAK-1 and Cdc42 that function as actin regulators.[17–19]

Exosome entry and cargo release has been proposed to occur *via* endocytosis[20] and/or through direct exosome-plasma membrane fusion;[21] reviewed in ref. 22. These studies labelled purified exosome preparations with fluorescent probes and then used either microscopy or flow cytometry to monitor cell interaction and uptake. Labelling strategies include the use of lipophilic dyes such as PKH26[23,24] and the carbocyanine dyes (DiI, DiO),[25,26] which embed non-covalently within the membrane bilayer of the exosome. Such dyes can however form dye aggregates or micelles in aqueous solutions, of similar proportions to exosomes, potentially giving misleading information in uptake experiments.[27] Exosome permeable compounds including carboxyfluorescein succinimidyl ester (CFSE) and 5(6) carboxyfluorescein succinimidyl diacetate (CFDA) have also been used for this purpose.[20,28] Any structural modifications on exosomes following labelling with these dyes will alter their physical characteristics but may also affect their functional properties. For cell uptake analysis this functional impact is rarely considered. Other labelling methods include the use of stable cell lines that fuse Green Fluorescent protein (GFP), or variants of, on to a protein enriched in exosomes, such as the tetraspanin CD63. This consequently produces a sub-population of exosomes, of uncertain proportion, that are GFP-tagged.[29,30] This approach also produces cells overexpressing tetraspanins; proteins that are known to be important in the biogenesis and function of these vesicles,[31] and this is therefore a major modification of the composition of the vesicles being produced. Furthermore, tetraspanins are also present on linear membrane fragments, various forms of cellular debris and larger plasma-membrane derived vesicles, and hence does not entirely alleviate the need for rigorous exosome-purifications.

In this report, we have developed a simple and rapid method for covalent fluorescent labelling of purified EVs. The method takes advantage of thiol (sulph-hydryl) groups on the EV surface and our labelling approach does not alter their documented capacity to induce fibroblast differentiation *in vitro*;[32,33] suggesting they retain at least a fraction of their biological effects. We thereafter investigated the potential pathways involved in EV uptake, using the well characterised endocytic HeLa cell model. This was performed with chemical inhibitors of endocytic pathways or siRNA-based depletion of specific endocytosis regulating proteins, and thus pathways.[34] Our findings show that EV uptake is clathrin-independent, with an endocytic profile indicative of macropinocytosis with eventual delivery to lysosomes.

2 Materials and methods

2.1 Reagents

Transferrin Alexa488 (Tf488), Alexa488/647 10 kDa dextran (Dx488/647), C_5-maleimide-Alexa488/633, Cell Mask Deep Red Plasma Membrane Stain, Dulbecco's Modified Eagle Medium (DMEM), Oligofectamine, Opti-MEM I reduced serum medium were purchased from Invitrogen (Paisley, UK). Bovine serum albumin (BSA), Dynasore, 5-(*N*-ethyl-*N*-isopropyl) amiloride (EIPA), 1,1′-disulfanediyldinaphthalen-2-ol (IPA-3) and Rottlerin were obtained from Sigma-Aldrich (Dorset, UK). Complete mini-protease inhibitor cocktail tablets were purchased from Roche Diagnostics (Sussex, UK). Single sequence (21–23 residues) siRNAs listed in Table 1 were purchased from Eurofins MWG Operon (Ebesburg, Germany). Sucrose and D_2O for EV isolations were from Sigma-Aldrich and Optiseal™ ultracentrifugation tubes from Beckman Coulter.

2.2 Cell culture

All culture materials were purchased from Invitrogen (Paisley, UK). DU145 prostate cancer cells (ATCC) were maintained in Integra Bioreactors (CellLine 1000AD) as described[35] with the outer chamber housing RPMI and 5% foetal calf serum (FCS), with the inner cell-containing chamber holding RPMI with 5% FCS that has previously been made devoid of bovine EVs by overnight ultracentrifugation and filtration. All were cultured in a humidified incubator at 5% CO_2, 37 °C. Primary lung fibroblasts (AG02262, Coriell Institute of Medical Research) were cultured as sub-confluent monolayers in DMEM F-12 (1 : 1 mix) supplemented with 10% EV-depleted FCS. HeLa cervical cancer cells (CCL-2; ATCC, Teddington, UK) were main-

Table 1 siRNA sequences used to deplete key endocytic proteins

siRNA target	Sequence	Ref.
AP2μ2	GUGGAUGCCUUUCGGGUCAdTdT	Custom designed
Cav-1	AGACGAGCUGAGCGAGAAGdTdT	34
Cdc42	GACUCCUUUCUUGCUUGUUdTdT	Custom designed
Flot-1	UGAGGCCAUGGUGGUCUCCdTdT	Custom designed
PAK1	AUAACGGCCUAGACAUUCAdTdT	34
GFP	GGCUACGUCCAGGAGCGCAdTdT	34

tained in sensi-cell MEM medium supplemented with 10% FCS, as a sub-confluent monolayer.

2.3 Antibodies

Listed antibodies were from the following manufacturers: AP50 (AP2μ2) and flotillin-1 BD Transduction Laboratories (Oxford, UK); Caveolin-1, GAPDH, PAK-1 Cell Signalling Technologies (Hertfordshire, UK); Anti-TSG101, Alix, Calnexin (Santa Cruz Biotechnology, Dallas, TX, USA); anti MHC Class-I (eBioscience, ThermoFisher Scientific, Paisley, UK). Anti-Cdc42 and horseradish peroxidase (HRP) -anti-δ-tubulin (Sigma-Aldrich, Dorset, UK); secondary HRP conjugated goat anti-mouse/anti-rabbit (Thermo-Scientific Pierce, Loughborough, UK).

2.4 Extracellular vesicle isolation, purification and characterisation

Using the methodology outlined in ESI,† the isolation and subsequent analyses satisfy the criterion set by the International Society for Extracellular Vesicles (ISEV), for defining this specimen as exosomes.[36] However, as discussion continues within the field on isolation and characterisation of exosomes as pure entities we refer here on in to our purified particles as EVs.

2.5 Labelling of extracellular vesicles with Alexa488/633

C_5-Maleimide-Alexa488 or C_5-maleimide-Alexa633 (200 μg ml^{-1}–2.5 μl) was added to a 30 μl EV aliquot containing 60 to 100 μg protein, and made up to 50 μl with PBS before incubation, with no agitation, for 60 min in the dark at room temperature (R/T). During incubation exosome spin columns (Invitrogen) were prepared according to manufacturer's instructions and powdered resin was hydrated for 15–30 min at R/T. Spin columns placed in the collection tubes were centrifuged for 2 min (750*g*), in a swing-out rotor. The collection tubes were discarded before the addition of the labelled EV aliquot to the resin. Columns were placed in 1.5 ml eppendorf tubes and centrifuged for 3 min (750*g*) to collect labelled EVs. Non-incorporated, excess dye was retained by the resin, and controls involving dye but no EVs were performed in parallel to confirm dye retention by the column. For microscopy analysis, labelled EVs (referred to as EV488 or EV633) were gently mixed to 1000 μl in phenol red free DMEM, before filtration through a 0.22 μm filter (Millex), aliquoted and stored at −80 °C until required.

2.6 Fibroblast differentiation assay

To test the impact of labelling on EV function, we used a well-established fibroblast differentiation assay as described.[33] Briefly, 80% confluent primary lung fibroblasts (Coriell Institute for Medical Research) were serum deprived for 72 h prior to stimulation with native or fluorescently labelled DU145 EVs (at 200 μg ml^{-1}). This dose provides vesicle-associated TGFβ equivalent to a dose of 1.5 ng ml^{-1} of soluble TGFβ.[32] As a positive control, soluble rhTGFβ (Promocell) was used at 1.5 ng ml^{-1}. After 72 h, ice cold acetone: methanol (1 : 1 ratio) was added as fixative for 5 min. Following solvent evaporation in air, cells were blocked in 1% BSA/PBS for 1 h. Monoclonal antibody against alpha-smooth muscle actin (αSMA) (Santa Cruz Biotechnology, Dallas, TX, USA) followed by secondary goat anti-mouse IgG Fab'-Alexa594 conjugate (ThermoFisher Scientific) was used to visualise onset of αSMA stress-fibres. This is a hallmark of the myofibroblastic phenotype visualised by fluorescence microscopy (Zeiss Observer, Cambridge, UK). Fibroblast secretion of Hepatocyte Growth Factor (HGF) was assessed by DuoSet ELISA (R&D Systems), performed on fibroblast conditioned medium 72 h post-treatment, following manufacturers protocol.

2.7 Cell internalisation of Alexa488 labelled extracellular vesicles in HeLa and primary lung fibroblasts

Cells were seeded in 35 mm MatTek imaging dishes (MatTek Corporation, MA, USA) and cultured for 24 h to reach 80–90% confluency. On the day of the experiment, EVs in imaging medium (phenol-red free DMEM, 20 mM HEPES) containing 0.05% w/v BSA were added to cells at 50–60 μg ml^{-1} for 30–360 min before live cell confocal microscopy was performed. Cells were incubated with the nuclear label Hoechst for 5 min before washing with imaging medium followed by imaging. For time-lapse imaging, cells were incubated with Hoechst and Cell Mask Deep Red Plasma Membrane Stain (1 : 5000) for 5 min before washing with imaging medium and time lapse confocal microscopy.

2.8 Labelling of lysosomes with dextran-Alexa647

Cells were seeded to be 50–60% confluent on the day of dextran incubation. Dextran647 (Dx647, 100 μg ml^{-1}) was incubated with cells for 2 h (5% CO_2, 37 °C), before washing with PBS and re-addition of complete cell culture media. Cells were then incubated for 18 h (5% CO_2, 37 °C) before incubating with 50–60 μg ml^{-1} EV488 for colocalisation analysis.

2.9 Incubation of cells with endocytosis inhibitors

All inhibitors were diluted from DMSO stocks to working solutions in imaging medium containing 0.05% BSA. Cells were seeded in 35 mm MatTek dishes 24 h before the day of the experiment to be 80–90% confluent. They were then washed three times with imaging medium containing 0.05% BSA and subjected to 30 min inhibitor pre-incubation with either Dynasore (80 μM), EIPA (25 μM), IPA-3 (50 μM) or Rottlerin (10 μM). Cells were then incubated with the stated concentration of experimental probe (Dx488/647, Tf488, EV488) for the specified time period in the continued presence of the inhibitor. They were then washed with imaging medium prior to performing live cell confocal microscopy.

2.10 siRNA depletion of proteins regulating endocytosis

Performed as described in ESI.†

2.11 Internalisation of Tf488, Dx488/647 into cells

Cells were seeded in 35 mm MatTek dishes and cultured for 24 h to be 80–90% confluent on the day of the experiment. For transferrin uptake analysis, cells were washed three times and

incubated with imaging medium supplemented with 0.05% BSA for 30 min before the addition of Tf488 (5 μg ml^{-1}) for 15 min. For dextran uptake, 100 μg ml^{-1} of Dx488/647 in imaging medium supplemented with 0.05% BSA was added to cells for 60 min without 30 min pre-incubation. Cells were incubated with Hoechst in imaging medium for 5 min before washing with fresh imaging medium followed by performing live cell confocal microscopy.

2.12 SDS PAGE and Western blotting for siRNA depletion

Performed as detailed in ESI.†

2.13 Fluorescence microscopy

2.13.1 Live-cell imaging confocal microscopy. Fluorescent images were taken using a Leica SP5 Confocal Microscope system and captured using LAS AF software. Cells were imaged at R/T with either a 40× 1.25 NA or a 63× 1.4 NA oil objective. Alexa488 was excited by a 488 Argon laser (20% intensity), and Alexa633/647 excited by a 633 helium–neon laser (20% intensity). Bi-directional, sequential scanning was applied to ensure spectral separation of fluorophores. The presented movie was acquired using the same microscopy settings but with cells maintained at 37 °C.

2.13.2 Calculation of colocalisation coefficients. To determine the proportion of EVs (green fluorescence) associated with lysosomes (red fluorescence) the M1 Mander's coefficient was calculated using the JaCop ImageJ plug-in and thresholded using the automated default algorithm. Six fields of view (approximately 60 cells) per time point were analysed and the mean calculated to provide an average colocalisation value for each repeat. The mean of the average colocalisation value for three separate experiments was plotted.

2.13.3 Mean fluorescence intensity (MFI) quantification. Individual cells from LAS AF files were manually selected as regions of interest (ROIs) using ImageJ software. Mean fluorescence intensity (MFI) of each was calculated, resulting in the quantification of approximately 150–160 cells per experimental sample. The geometric mean of each sample group was calculated to provide an average MFI for repeat experiments; the mean of the geometric mean from three independent experiments was calculated and used for statistical calculations.

2.14 Statistical analysis

To compare control treated samples against experimental samples, a Student's unpaired *t*-test was utilised using the geometric mean of each separate experiment. Significance was specified as $*p < 0.05$, $**p < 0.01$, or $***p < 0.001$.

3 Results and discussion

3.1 Characterisation and labelling of purified extracellular vesicles

Cells produce a variety of debris and different types of vesicle, we therefore utilised our established approach for the specific isolation of EVs.[37] Following the clearance of gross debris from cell-conditioned medium, by centrifugation (2000*g*), the medium were filtered (0.22 μm) to remove the majority of larger microvesicles. The medium was thereafter ultracentrifuged, capturing vesicles floating in an isotonic cushion of sucrose, preventing vesicles of classical densities 1.1–1.2 g ml^{-1} from pelleting.

Cryo-electron microscopy was performed on EVs purified by this method, revealing the presence of genuine vesicle structures, with a lipid-bilayer boundary (Fig. 1A). There was some heterogeneity in sizes, and the structures are typical for EVs analysed by Cryo-EM as reported.[38] Nanoparticle tracking analysis (NTA) using the NanoSight™ platform, revealed particulates with a modal hydrodynamic diameter of ~100 nm, and a low proportion of larger particulates (Fig. 1B), comparable to sizes seen by Cryo-EM. We also examined the preparation for the presence of proteins typically enriched in EVs. EV-preparations immobilised on microtitre plates were stained with antibodies specific for CD9, CD81, CD63 and respective isotype-matched controls.

This highlighted strong, specific signals for these tetraspanins (Fig. 1C), which is a particular trait of exosomes.[39] In addition, by comparing the parent DU145 cancer cells with EV preparations by western blotting, we also reveal an enrichment of some classical EV-associated proteins such as TGS101, Alix and MHC Class-I (Fig. 1C, inset). In contrast, the endoplasmic reticulum marker, Calnexin, was not detectable in these preparations, yet abundant in cell lysates, demonstrating the paucity of cellular contamination of these EV preparations. Furthermore, using a combination of BCA-protein assay and NanoSight™-concentration measurements, the particle to protein ratio for purified EVs was calculated. This gives an indication of specimen purity as we describe[40] and for all preparations used in the study a particle : protein ratio of $>2 \times 10^{10}$ particles per μg protein was achieved.

The EV is an environment that is cysteine rich, through, for example, the presence of tetraspanin webs.[39] We therefore postulated that the thiol (–S–H groups) present on these structures would react with a maleimide functional group, to form a stable, non-reversible, thio-ether linkage. Fluorophore conjugated maleimides are often used to fluorescently label biomolecules and here we used C_5-maleimide conjugated to Alexafluor488. Other groups have exploited this labelling protocol in order to study micro-particle populations whereby whole blood samples were labelled with BODIPY-maleimide for analysis *via* flow cytometry.[41,42] However, BODIPY itself is used to label membranes, and is therefore likely to integrate onto the EV bilayer.

We examined the capacity for maleimide-Alexa488 to react with EV thiols. Part of this procedure however, involves the removal of non-bound dye from the EV-preparations. Initial experiments used ultracentrifugation washes to achieve this, but the method was refined thereafter by using a spin-column (Invitrogen), that retains molecules of <3000 Da. Initial experiments explored incubating a constant quantity of purified EVs

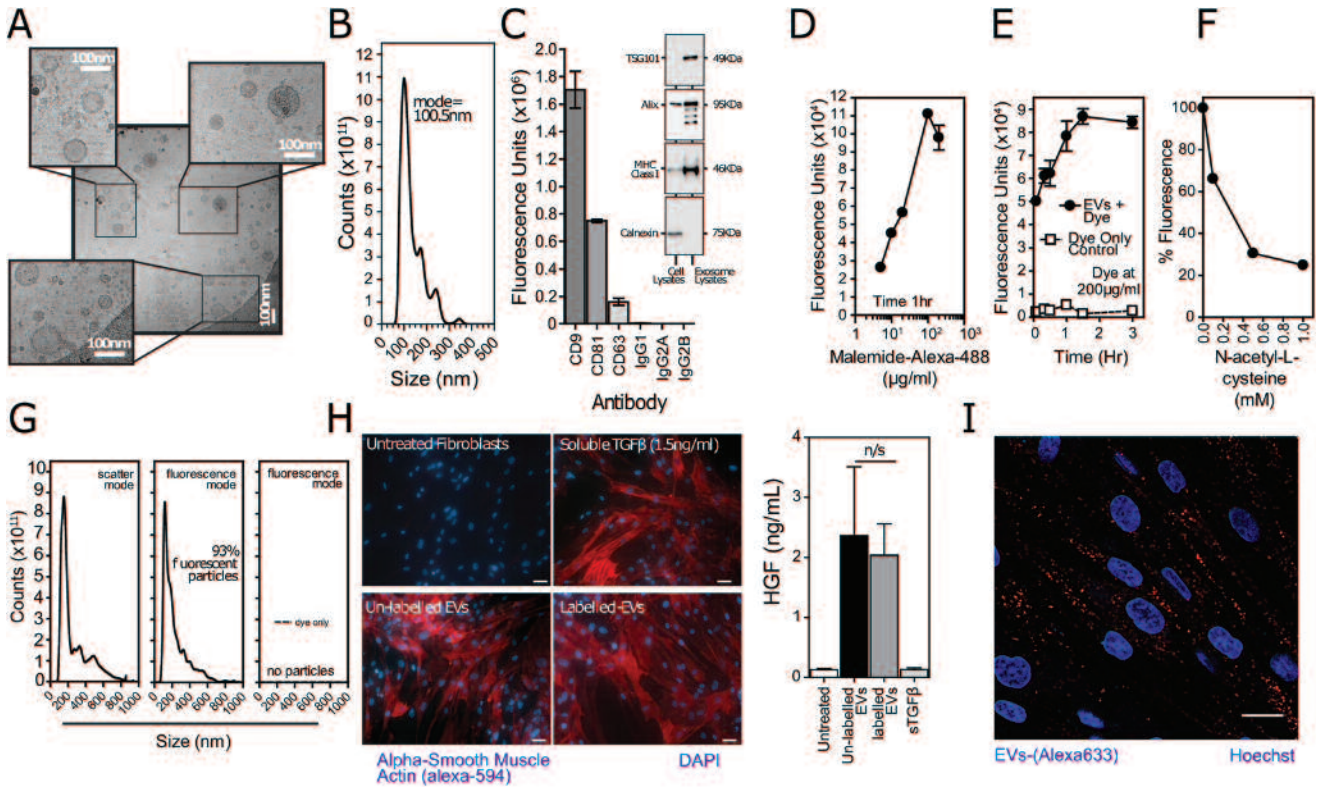

Fig. 1 Labelling of EVs with malemide-Alexa488. (a) Cryo-electron microscopy of a typical preparation of DU145 EVs, with examples of small vesicular structures. Higher magnification micrographs highlight some heterogeneity in sizes. (b) Nanoparticle tracking analysis of DU145 EV size distribution. (c) Plate-immobilised EVs with surface staining for tetraspanin proteins, as indicated. (c, inset) Western blot panel with cell lysates compared to EV lysates (each with 20 μg protein per lane), stained for exosomal or cellular markers as indicated. (d) Malemide-Alexa488 (5–200 μg ml^{-1}) was incubated with EVs for 1 h prior to separation of free dye and analysis by fluorometry. (e) EVs were labelled with malemide-Alexa488 at 200 μg ml^{-1} up to 3 h (circles) and retention of free dye by the column (squares). (f) EVs were pre-incubated with *N*-acetyl-cysteine up to 1 mM for 30 min prior to labelling with malemide-488 (200 μg ml^{-1} for 1 h). (g) Malemide-Alexa488 labelled EVs analysed by NTA, (left) shows a similar size distribution profile measured in light scatter mode or measured with fluorescence filter revealing high proportion of fluorescent vesicles (middle); absence of fluorescent dye-particles in the absence of EVs (right). (h) Growth arrested fibroblasts were stimulated with treatments as indicated, and 72 h later fixed and stained for detection of α-smooth muscle actin (red, scale bar: 50 μm). (h, bars) Medium harvested from stimulated fibroblasts after 72 h, were assessed for levels of HGF by ELISA, showing mean ± standard deviation of triplicates. N/S: not significantly different, n = 3. (i) Primary lung fibroblasts were incubated with maleimide-633 labelled EVs (60 μg ml^{-1}) for 1 h before live cell confocal microscopy was performed. Cells were incubated with Hoechst for 5 min before imaging to label the nucleus. Scale bar: 20 μm.

with varying fluorophore concentrations (Fig. 1D), showing saturating levels of labelling at ≥100 μg ml^{-1} after an incubation of 1 h. At the saturating fluorophore concentration 200 μg ml^{-1}, we also examined various incubation times revealing most of the fluorophore-EV labelling occurs very rapidly within the first 5 min, and saturation was reached at 1 to 2 h (Fig. 1E, circles). A control for fluorophore-only (no EVs) to assess its possible retention by the spin column is also shown, revealing negligible signal (Fig. 1E). We chose labelling conditions of 200 μg ml^{-1} for 1 h for the remainder of the study. To ascertain whether or not the fluorophore was actually forming a covalent bond through the thiol groups, or merely binding passively to the vesicle surface, we added a competitor that works by capping the available reactive thiol groups. Pre-incubating EVs with doses of *N*-acetyl-L-cysteine showed a potent (~80%) inhibition of labelling under these same conditions (Fig. 1F).

Nanoparticle tracking analysis revealed a similar size distribution profile following incubations with maleimide-Alexa488, suggesting a paucity of gross complexation due to maleimide-vesicle cross-linking (Fig. 1G, left). Importantly, NTA-analysis in the presence of a low-pass 500 nm filter showed the majority (>90%) of vesicles were fluorescent (Fig. 1G, middle). The capacity to monitor fluorescent nanovesicles by this method is a challenge, and successful tracking here points to strong fluorescence output from each vesicle. We also analysed the stock maleimide-Alexa488 reagent, by NTA. Unlike for some other fluorescent labels, particularly PKH26, there were negligible particles detected in scatter mode, and there were no particles seen with a fluorescent filter in place (Fig. 1G, right graph). An example of nanoparticulate PKH26 fluorescent aggregates in the absence of EVs are shown (Fig. S1†). Particulate material spanning the size range of exosomes was present in the stock solution, and a high proportion (52%) of

these are fluorescent. We conclude this method is a simple, rapid and highly effective modality for EV labelling, and is free of artefacts related to insoluble dye nanoparticulate.

We next investigated the functional impact of coating EVs with our fluorescent label; an aspect that is rarely considered in previous studies. To do this, we relied on a well-established functional assay whereby prostate cancer exosomes trigger the differentiation of fibroblasts to myofibroblasts.[32] This process requires delivery of exosome-associated TGFβ to fibroblasts, but also is likely to involve additional exosome-cargo as the myofibroblasts generated are distinct from those formed by soluble TGFβ-stimulation in that secretion of hepatocyte growth factor (HGF) is triggered.[33] Stimulation of fibroblasts either with native or with maleimide-Alexa488 labelled EVs successfully triggered the onset of stress fibres visualized *via* αSMA labelling; soluble TGFβ also did this as expected (Fig. 1H). When evaluating the secretion of HGF however, there was clear difference in levels of HGF whether stimulations were by EVs or soluble TGFβ (Fig. 1H, bars), as we have previously observed.[33] The labelled or unlabelled EVs were equally proficient at stimulating HGF secretion.

In this assay, which represents a major and complex cell differentiation process, our maleimide-Alexa488 labelling approach shows no signs of attenuating EV function.

3.2 Endocytic analysis of Alexa488 extracellular vesicles in cells

We investigated the possibility of visualising the labelled EVs following incubation with the fibroblasts. These cells had high background cellular autofluorescence at 488 nm excitation (data not shown) and the purified EVs were therefore labelled with Alexa633 using the same procedure. Fig. 1I demonstrates these EVs were internalised to label punctate structures indicative of endosomes. These cells are however poorly characterised with respects to characterisation of endocytosis. We and others have performed detailed studies of the involvement of individual endocytic pathways in HeLa cells as model for uptake of drug delivery vectors.[34] Previous studies on exosome and EV uptake have also been published using HeLa cells.[30,43,44] We therefore decided to focus our subsequent experiments on the well characterised HeLa cell line.

HeLa cells incubated with Alexa488 labelled EVs (EV488) for 30 and 60 min demonstrated a scattered punctate distribution throughout the cell cytoplasm (Fig. 2A). Time lapse imaging of EV488 incubated with HeLa cells over a period of 3 min (after a 120 min pre-incubation) shows these structures to be highly motile with little evidence of extensive accumulation at the plasma membrane (Video S1†). There was a noticeable time dependant increase in fluorescence intensity from 30 min to 240 min (Fig. 2B) and at this later time point fluorescence was more polarised to the perinuclear regions. This confirmed that these labelled EVs also have endocytic capacity in this cell line, allowing further analysis of cell entry mechanisms.

3.3 Traffic of Alexa488 extracellular vesicles to lysosomes

Cells incubated with EVs for >60 min showed the accumulations of fluorescence in the perinuclear region suggesting a fraction were being trafficked to lysosomes that are also prominent in this region in HeLa cells (Fig. 2).[45] EV traffic from the plasma membrane was then studied at different time points in cells containing labelled lysosomes *via* a pulse-chase incubation. Colocalisation between 488-EVs and 647-lysosomes was

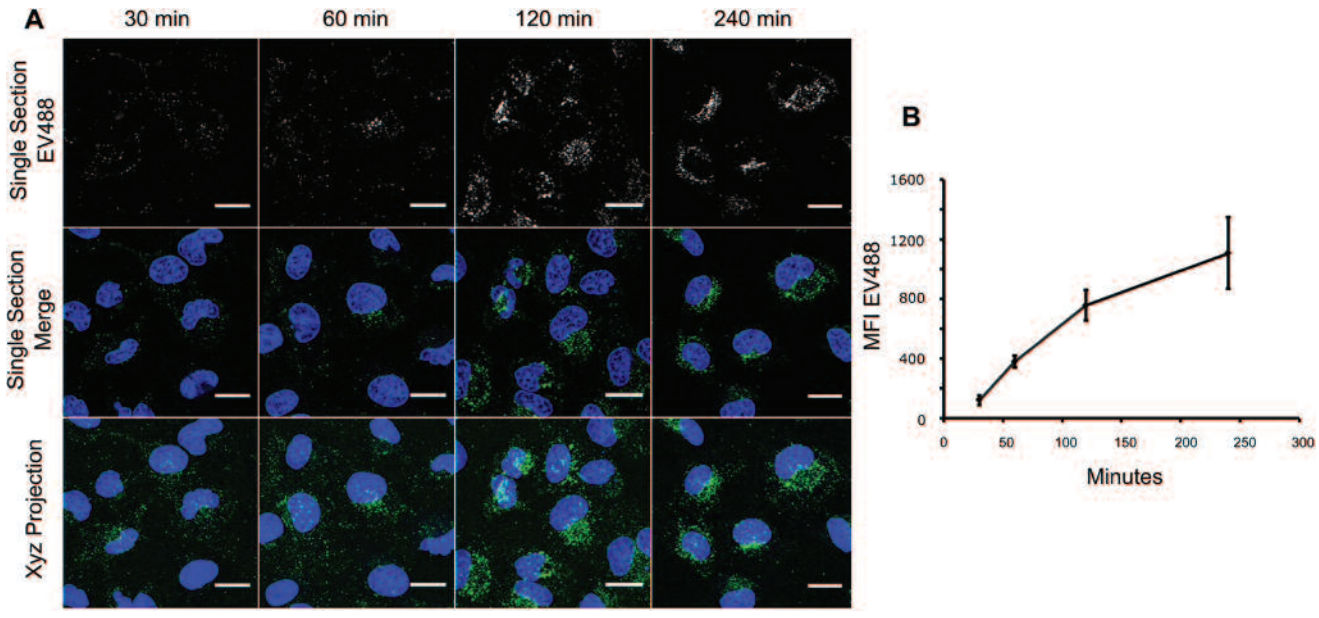

Fig. 2 Time dependent EV endocytosis in HeLa cells. (a) Cells were incubated with EV488 (60 μg ml^{-1}) for 30, 60, 120 or 240 min and incubated with Hoechst for 5 min before live cell confocal imaging. Scale bars: 20 μm. Images representative of three separate experiments. (b) MFI quantification of the experiments presented. Error bars: standard error. Representative of three separate experiments.

barely detected at 30 min and then increased over a period of six hours to the point that after 360 min ~60% of detected EVs were contained in labelled lysosomes (Fig. 3). This method measures the location of EVs in early and late endocytic compartments including lysosomes. We then performed experiments by which dextran was similarly used to label lysosomes but following a two hour pulse of EV endocytosis the cells were washed and the material already associated with the cells was chased for a further 4 hours revealing that over 60% of EV associated labelling had reached and remained at the lysosomes by the end of this chase period (Fig. S2†).

3.4 Endocytic uptake of extracellular vesicles in clathrin-mediated endocytosis (CME) compromised cells

CME has been extensively characterised in *in vitro* models including HeLa cells,[10,11] and this process can be attenuated using a range of methods.[34] These include siRNA depletion of a key member of the of the CME adaptor complex AP2, known as AP2μ2 or AP50. This subunit is essential for the anchorage of cargo at the plasma membrane and subsequent recruitment of clathrin and further regulatory proteins to allow the process of internalisation to proceed.[46] We and others have shown that siRNA depletion of AP2μ2 prevents the uptake of transferrin *via* the transferrin receptor.[45,47] Following a 48 hours transfection with siRNA the AP2μ2 protein (50 kDa) was effectively depleted *versus* a control siRNA (Fig. 4A). A second siAP2μ2 insensitive lower molecular weight band was identified with this antibody that was insensitive to siRNA AP2μ2, this has previously been shown but not explained.[48] In these siAP2μ2 treated cells incubated with Tf488 for 15 min, the probe was mainly sequestered at the plasma membrane compared to internalised punctate structures in control cells (Fig. 4B). si-Control and AP2μ2 depleted cells were also incubated with EV488 for 60 min prior to analysing cell fluorescence. Fig. 4C shows no noticeable difference in either the cell fluorescence or the distribution of vesicular labelling between these two conditions. This was further confirmed by quantification of the mean fluorescence intensity (MFI) from three separate analyses including cells that were not transfected (Fig. 4D).

Extracellular vesicle uptake was also evaluated in cells treated with a widely used dynamin II inhibitor, Dynasore, previously used in numerous studies to evaluate the uptake of different entities *via* dynamin-dependant endocytic processes, such as CME and caveolae.[49] Cells were pre-incubated with

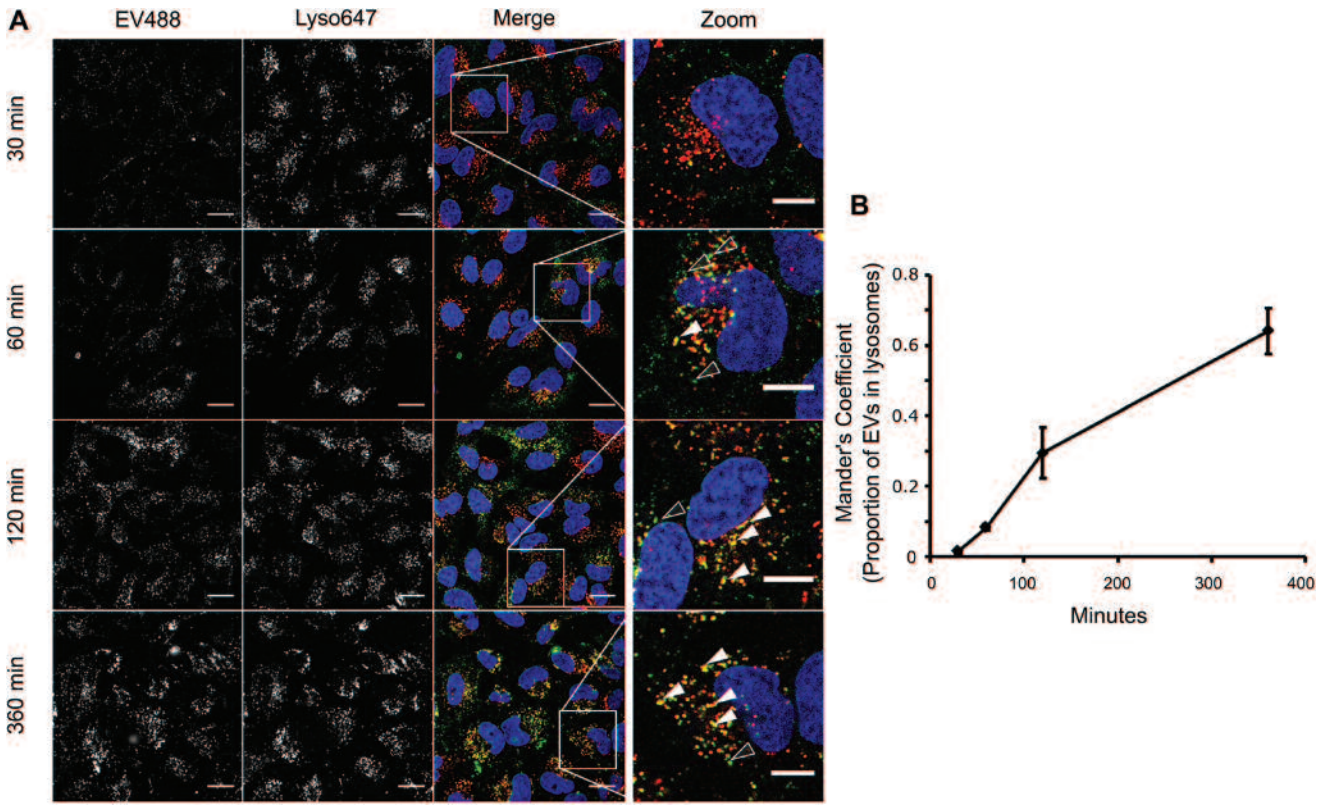

Fig. 3 Co-localisation of 488-labelled EVs with dextran-loaded lysosomes in HeLa cells. (a) Cells were incubated with Dx647 (100 μg ml^{-1}) for 2 h, washed with PBS and incubated for a further 18 h in culture media. Cells were then incubated with EV488 (60 μg ml^{-1}) for either 30, 60, 120 or 360 min before treatment with Hoechst for 5 min and live cell confocal imaging. Solid arrowheads indicate colocalisation between EVs and lysosomes and transparent arrowheads indicate EVs not colocalised with lysosomes. Scale bars: 20 μm and 10 μm in zoomed images. Images representative of three separate experiments. (b) Mander's correlation coefficient analysis of the proportion of green fluorescence (EVs) associated with far-red fluorescence (lysosomes) based on the experiments performed to generate Fig. 3(A). Error bars: standard error. Representative of three separate experiments.

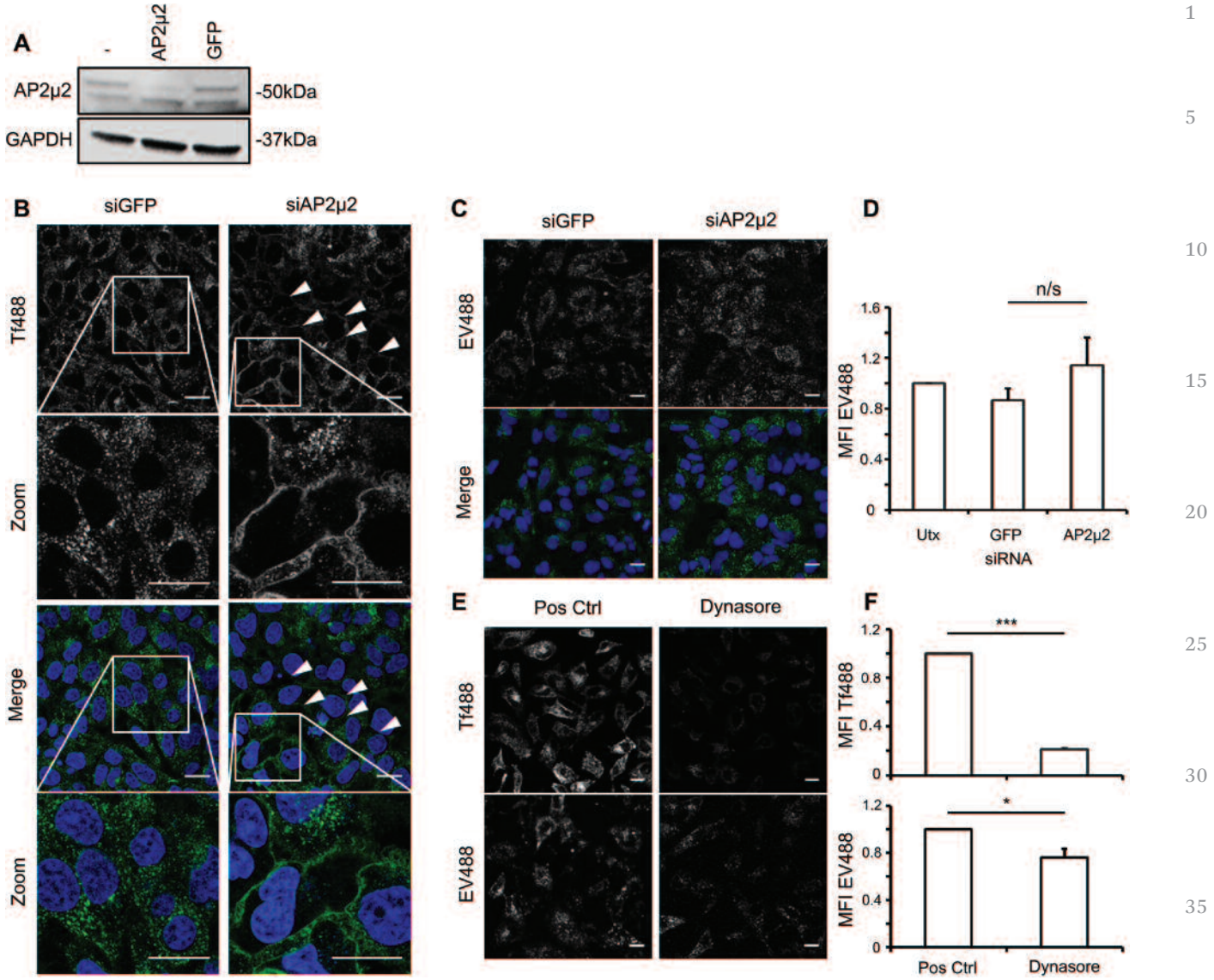

Fig. 4 Internalisation of EVs in CME compromised HeLa cells. (a) Western blot analysis of AP2μ2 protein levels 48 h following siRNA transfection in comparison with loading GAPDH loading control. (b) Cells were depleted of either AP2μ2 *via* siRNA transfection for 48 h before incubation with either (b) Tf488 (5 μg ml^{-1}) for 15 min or (c) EV488 (50 μg ml^{-1}) for 60 min. White arrowheads indicate surface bound Tf488. (e) Cells were pre-incubated with Dynasore (80 μM) for 30 min before incubation with either Tf488 (5 μg ml^{-1}) for 15 min or EV488 (50 μg ml^{-1}) for 60 min. All were incubated with Hoechst for 5 min before live cell imaging. Scale bars: 20 μm. Images representative of three separate experiments. (d), (f) MFI quantification of the experiments presented in (c), (e), respectively. Utx: untransfected. Error bars represent standard error. *$p < 0.05$, ***$p < 0.001$, n/s: no significance. Representative of three separate experiments.

Dynasore for 30 min prior to addition of Tf488 for 15 min or EV488 for 60 min. Both the confocal microscopy images and MFI data highlight the strong inhibition of Tf488 uptake by this drug (Fig. 4E and F). Unlike the AP2μ2 phenotype showing strong Tf488 labelling on the plasma membrane, Dynasore treated cells were almost devoid of any labelling; the reason for this is currently unknown but suggests that Tf is unable to access its receptor in Dynasore treated cells. There was a much smaller but significant decrease in EV uptake in Dynasore treated cells (Fig. 4E and F). This observation shows that a significant proportion of EVs are entering *via* a dynamin II-dependant mechanism that based on data in Fig. 4C is not CME. Interestingly cells transfected with a dominant negative dynamin II mutant were also shown to have reduced exosome uptake in RAW 264.7 macrophages.[23] Our observation of EV uptake, by a Dynasore but not an AP2μ2 dependent process, could be due to the fact dynamin II has been implicated in the regulation of other endocytic pathways such as fluid-phase uptake and caveolae.[50,51] Furthermore, it has recently been demonstrated that Dynasore elicits additional dynamin independent effects on the cholesterol organisation of plasma membrane lipid rafts.[52] Alteration of the plasma membrane in

this way could affect the wider endocytic network, thereby affecting the designated uptake route of these structures. These studies led to further investigations targeting other endocytic proteins and pathways.

3.5 Extracellular vesicle uptake in Caveolin-1 and Flotillin-1 depleted cells

Using the same siRNA-based approach, both Caveolin-1 and Flotillin-1 proteins were successfully depleted but the loss of these proteins, and the endocytosis that they organise, did not significantly affect cellular uptake of the labelled EVs (Fig. 5). Although not performed for the studies presented here, we and others have however shown that endocytosis of lactosylceramide and an anti-CD59 antibody have previously been shown to be reduced, respectively, in Caveolin-1 and Flotillin-1 depleted cells.[34,53] It should be noted that depletion of either of these proteins could have significant cellular effects beyond that of reducing endocytic processes as both have been implicated as important modulators of cell signalling and organisation of lipid rafts.[54] Of interest is that the distribution of EV labelling was more peripheral in siRNA Flotillin-1 cells compared with controls suggesting alterations in downstream endocytic traffic. Overall these observations strongly suggest that endocytic processes involving Caveolin-1 and Flotillin-1 are not the primary mode of EV entry.

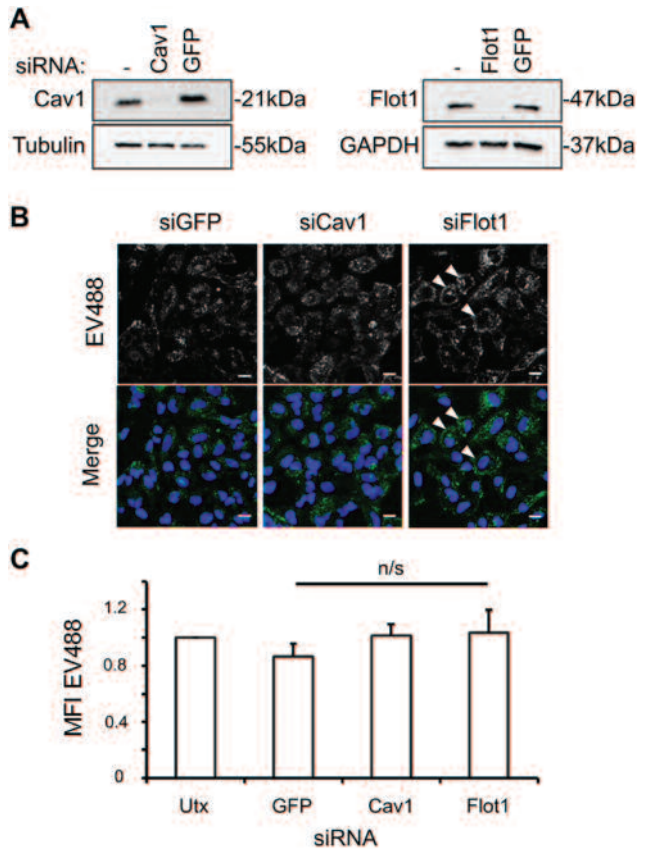

Fig. 5 Internalisation of EVs in HeLa cells depleted of Cav-1 and Flot-1. (a) Western blot analysis of Cav-1 and Flot-1 protein levels in HeLa cells 48 h following siRNA transfection in comparison with loading proteins Tubulin or GAPDH. (b) Cells were depleted of either Cav-1 or Flot-1 *via* siRNA transfection for 48 h before 60 min incubation with EV488 (50 μg ml^{-1}). Cells were incubated with Hoechst for 5 min before live cell imaging. Scale bar: 20 μm. Images representative of three separate experiments. Arrowheads in B represent peripheral EVs (c) MFI quantification of the experiments presented in (b). Utx: untransfected. Error bars represent standard error. n/s: no significance. Representative of three separate experiments.

3.6 Extracellular vesicle uptake in cells depleted of proteins regulating actin dynamics, fluid-phase endocytosis and macropinocytosis

Fluid-phase endocytosis could be viewed as a process of constitutive plasma membrane turnover performed important for functions such as nutrient gathering and sampling of the extracellular environment. Macropinocytosis has been described as a mechanism that is activated upon growth factor stimulation and could be conceived as an activated form of fluid-phase endocytosis.[14,15,55,56] Both lack a specific master regulatory protein that could be targeted for siRNA depletion without affecting other processes. Macropinocytosis is highly reliant upon the organisation of actin, thus actin regulating proteins are candidate siRNA targets for inhibition of this process. Actin may also have involvement in constitutive fluid phase uptake.[57] The p21-activated kinases (PAKs) regulate numerous modifications of the cytoskeleton, particularly through their interactions with the Rho GTPases, Cdc42 and Rac1.[58,59] PAK-1 has been identified as an important regulatory factor in the events associated with macropinocytosis.[18,19] Cells were successfully transfected with siRNA sequences targeting PAK-1 and Cdc42 (Fig. 6A) to investigate the roles of these proteins on initially the uptake of dextran that represents in the absence of growth factor activation, a constitutive fluid phase probe.[60,61] Our previous studies indicated that PAK-1 was involved in the cellular uptake of cationic cell penetrating peptides that may be inducing a form of macropinocytosis for cell entry.[34,62] Despite some visual evidence of a reduction of dextran uptake in PAK-1 depleted cells (Fig. 6B), quantitative analysis showed that this was not significant and no effects were also noted for Cdc42 depletion (Fig. 6C). Following a 60 min endocytic pulse in the cells depleted of either PAK-1 or Cdc42 (Fig. 6D), a small but insignificant decrease (Fig. 6E) in EV uptake was observed. Localisation of punctate EV structures in Cdc42 depleted cells was noticeably different from control cells, being much more apparent at the cell periphery suggesting an inability of these structures to be trafficked beyond the plasma membrane region (Fig. 6D). These observations are further represented in the additional fields of view presented in Fig. S3.† As noted for Flotillin-1 and Caveolin-1 the effects of depleting these proteins scope wider than endocytosis but the data suggest that traffic of EVs beyond the plasma membrane is regulated by Cdc42 and most probably actin. Actin regulating agents such as Cytochalasin D are routinely used to monitor the involvement of actin on endocytosis but they also cause gross morphological effects on cells (data not shown) making data interpretation very difficult.

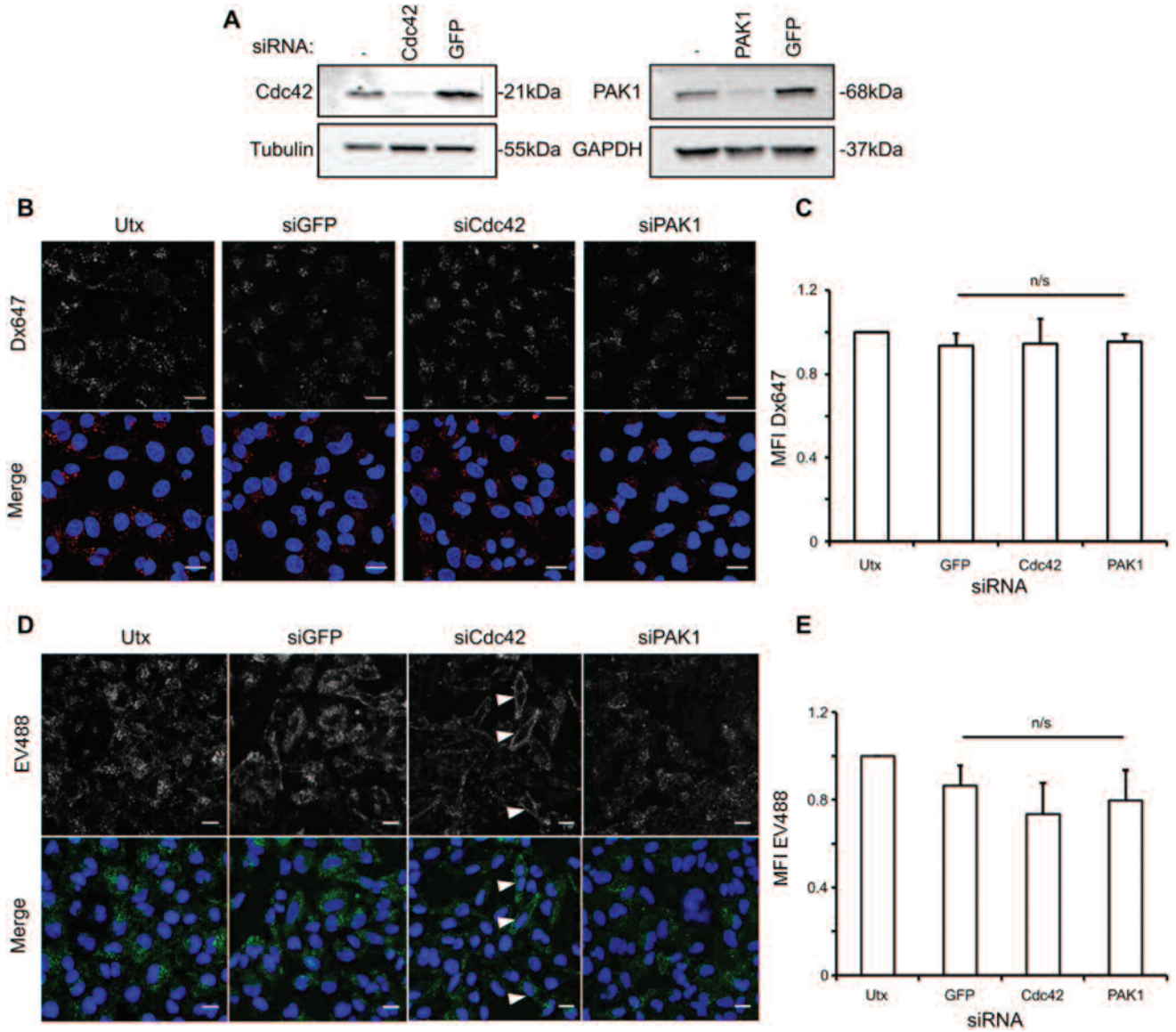

Fig. 6 Internalisation of EVs in HeLa cells depleted of fluid-phase/macropinocytosis related proteins. (a) Western blot analysis of Cdc42 and PAK-1 protein levels in cells 48 h following siRNA transfection in comparison with loading proteins Tubulin or GAPDH. (b) Cells were depleted of either Cdc42 or PAK-1 *via* siRNA transfection for 48 h before 60 min incubation with either (b) Dx488 (100 μg ml^{-1}) or (d) EV488 (50 μg ml^{-1}). Cells were incubated with Hoechst for 5 min before live cell imaging. Arrowheads in D represent peripheral EVs. Utx: untransfected. Scale bar: 20 μm. Images representative of three separate experiments, respectively. (c), (e) MFI quantification of the experiments presented in (b), (d), respectively. Error bars represent standard error. n/s: no significance. Representative of three separate experiments, respectively.

3.7 Extracellular vesicle uptake in cells treated with fluid-phase/macropinocytosis inhibitors

Endocytosis inhibitors can be used in conjunction with siRNA transfection studies to provide a more comprehensive analysis of the endocytic uptake of different probes.[53] Following our observations in siPAK-1 and siCdc42 cells, inhibitors targeting fluid-phase endocytosis and macropinocytosis were utilised to further explore the involvement of these pathways in EV uptake.

5-(*N*-Ethyl-*N*-isopropyl) amiloride (EIPA) is a commonly utilised Na^+/H^+ exchange inhibitor, and most probably prevents macropinocytosis by lowering the submembranous pH of the macropinocytic cup.[63] A small but insignificant (p = 0.61) decrease in dextran uptake was observed in EIPA treated cells (Fig. 7A and B), suggesting that it has little effect on fluid-phase endocytosis. Transferrin internalisation in these cells in comparison with control treated cells was significantly reduced, indicating that EIPA affects CME to a certain degree (Fig. S4†). Notably, differences in the localisation of transferrin loaded vesicles was apparent, agreeing with our previous studies showing effects on the subcellular localisation of early and late endosomes/lysosomes in cells treated with this drug.[64] Previous studies in PC12 cells incubated with self-

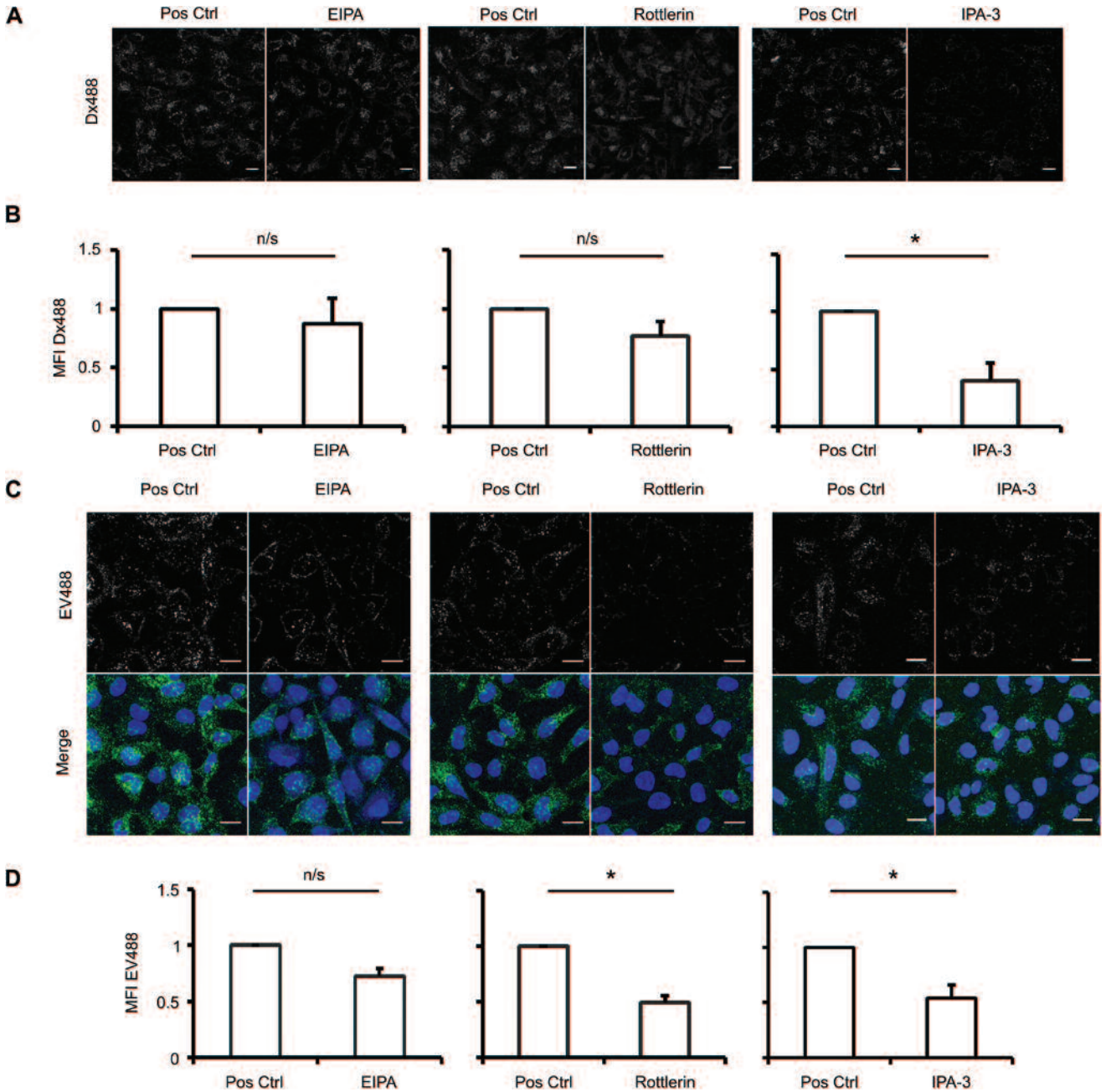

Fig. 7 Internalisation of EVs in HeLa cells treated with fluid-phase/macropinocytosis inhibitors. (a, c) Cells were pre-incubated with EIPA (25 μM), Rottlerin (10 μM), IPA-3 (50 μM), or 0.05% DMSO as 'Pos Ctrl' for 30 min before 60 min incubation with either (a) Dx488 (100 μg ml^{-1}) or (c) EV488 (50 μg ml^{-1}). Cells were incubated with Hoechst for 5 min before live cell imaging. Scale bar: 20 μm. Images representative of three separate experiments. (b), (d) MFI quantification of the experiments presented in (a), (c), respectively. Error bars represent standard error. *$p < 0.05$. n/s: no significance. Representative of three separate experiments.

derived exosomes have shown by flow cytometry that EIPA significantly reduces uptake of DiD labelled PC12 exosomes.[26] In our study EIPA cells caused a small but insignificant decrease in EV uptake (Fig. 7C and D). Rottlerin is an inhibitor primarily utilised to target fluid-phase endocytosis rather than macropinocytosis.[61] Its effects have previously been connected with inhibition of PKCδ activity,[65] though other Rottlerin targets have been identified.[66,67] Rottlerin did not affect the uptake of dextran but was a significant inhibitor of Tf and EV uptake in these cells (44% and 51% respectively) (Fig. 7 and S4†). The PAK-1 inhibitor IPA-3,[68] has previously been used to propose macropinocytosis as a mechanism for viral cell entry.[69,70] This drug induced a significant decrease in dextran uptake (60%) and EVs (50%, Fig. 7) with Tf488 showing a slight, non-significant decrease. However, Tf488 localisation was more scattered in treated cells (Fig. S4†) with a concomitant loss of juxta-

nuclear polarisation that is indicative of the localisation of Tf recycling compartments in this cell line. Collectively observations with these inhibitors suggest that a major fraction of EVs enter cells by fluid phase endocytosis rather than macropinocytosis.

4 Conclusions

Here we describe an efficient and novel method to fluorescently label EVs characterised as exosomes for subsequent high content microscopy analysis of their interactions with cells and endocytic traffic. Unlike other current labelling methods, this technique provides flexibility with regards to choice of fluorophore used and also provides the ability to easily label EVs from different cell types. In the case of prostate cancer DU145 derived EVs the labelling procedure did not affect their capacity to induce complex cellular responses such as fibroblast to myofibroblast differentiation and induction of HGF secretion. It however remains to be determined whether this labelling method influences the other numerous functional effects documented for EVs. It will also be interesting to compare our data with exosomes labelled using the same procedure but with different fluorophores, noting that they have unique characteristics that could affect cell uptake[71] and differentiation. Interference of endocytic pathways with inhibitors and siRNA depletion of endocytosis mediators together with endocytic trafficking studies strongly suggest our EVs enter cells as components of the extracellular fluid and like dextran are mostly trafficked to lysosomes. Approximately 40% of endocytosed EVs however are not fated for lysosomes, at least within the time-frame that we have explored. The implications of these endocytosis characteristics for the use of EVs as drug delivery vectors remain to be determined but their trafficking profiles may be beneficially exploited if they can be packaged with small molecule drugs for lysosomal release into the cytosol.

Conflicts of interest

Q3 ■■■■

Acknowledgements

The research leading to these results has received support from the Innovative Medicines Initiative Joint Undertaking under grant agreement no. [115363], resources of which are composed of financial contribution from the European Union's Seventh Framework Programme (FP7/2007–2013) and EFPIA companies' in kind contribution (HDRD, EJS, PW, ATJ). This work was also supported by Tenovus (ACo, ACl, PW, ATJ) and Prostate Cancer UK (PCUK – award no. CDF13-001, JW).

References

1 G. Raposo, H. W. Nijman, W. Stoorvogel, R. Liejendekker, C. V. Harding, C. J. Melief and H. J. Geuze, *J. Exp. Med.*, 1996, **183**, 1161–1172.
2 M. Ostrowski, N. B. Carmo, S. Krumeich, I. Fanget, G. Raposo, A. Savina, C. F. Moita, K. Schauer, A. N. Hume, R. P. Freitas, B. Goud, P. Benaroch, N. Hacohen, M. Fukuda, C. Desnos, M. C. Seabra, F. Darchen, S. Amigorena, L. F. Moita and C. Thery, *Nat. Cell Biol.*, 2010, **12**, 19–30.
Q4
3 H. Kalra, R. J. Simpson, H. Ji, E. Aikawa, P. Altevogt, P. Askenase, V. C. Bond, F. E. Borras, X. Breakefield, V. Budnik, E. Buzas, G. Camussi, A. Clayton, E. Cocucci, J. M. Falcon-Perez, S. Gabrielsson, Y. S. Gho, D. Gupta, H. C. Harsha, A. Hendrix, A. F. Hill, J. M. Inal, G. Jenster, E. M. Kramer-Albers, S. K. Lim, A. Llorente, J. Lotvall, A. Marcilla, L. Mincheva-Nilsson, I. Nazarenko, R. Nieuwland, E. N. Nolte-'t Hoen, A. Pandey, T. Patel, M. G. Piper, S. Pluchino, T. S. Prasad, L. Rajendran, G. Raposo, M. Record, G. E. Reid, F. Sanchez-Madrid, R. M. Schiffelers, P. Siljander, A. Stensballe, W. Stoorvogel, D. Taylor, C. Thery, H. Valadi, B. W. van Balkom, J. Vazquez, M. Vidal, M. H. Wauben, M. Yanez-Mo, M. Zoeller and S. Mathivanan, *PLoS Biol.*, 2012, **10**, e1001450.
4 Z. Andreu and M. Yanez-Mo, *Front. Immunol.*, 2014, **5**, 442.
5 M. P. Zaborowski, L. Balaj, X. O. Breakefield and C. P. Lai, *Bioscience*, 2015, **65**, 783–797.
6 M. Yanez-Mo, P. R. Siljander, Z. Andreu, A. B. Zavec, F. E. Borras, E. I. Buzas, K. Buzas, E. Casal, F. Cappello, J. Carvalho, E. Colas, A. Cordeiro-da Silva, S. Fais, J. M. Falcon-Perez, I. M. Ghobrial, B. Giebel, M. Gimona, M. Graner, I. Gursel, M. Gursel, N. H. Heegaard, A. Hendrix, P. Kierulf, K. Kokubun, M. Kosanovic, V. Kralj-Iglic, E. M. Kramer-Albers, S. Laitinen, C. Lasser, T. Lener, E. Ligeti, A. Line, G. Lipps, A. Llorente, J. Lotvall, M. Mancek-Keber, A. Marcilla, M. Mittelbrunn, I. Nazarenko, E. N. Nolte-'t Hoen, T. A. Nyman, L. O'Driscoll, M. Olivan, C. Oliveira, E. Pallinger, H. A. Del Portillo, J. Reventos, M. Rigau, E. Rohde, M. Sammar, F. Sanchez-Madrid, N. Santarem, K. Schallmoser, M. S. Ostenfeld, W. Stoorvogel, R. Stukelj, S. G. Van der Grein, M. H. Vasconcelos, M. H. Wauben and O. De Wever, *J. Extracell. Vesicles*, 2015, **4**, 27066.
7 E. V. Batrakova and M. S. Kim, *J. Controlled Release*, 2015, **219**, 396–405.
8 P. Vader, E. A. Mol, G. Pasterkamp and R. M. Schiffelers, *Adv. Drug Delivery Rev.*, 2016, **106**, 148–156.
9 G. J. Doherty and H. T. McMahon, *Annu. Rev. Biochem.*, 2009, **78**, 857–902.
10 H. T. McMahon and E. Boucrot, *Nat. Rev. Mol. Cell Biol.*, 2011, **12**, 517–533.
11 M. S. Robinson, *Traffic*, 2015, **16**, 1210–1238.
12 B. Nichols, *J. Cell Sci.*, 2003, **116**, 4707–4714.
13 T. Ait-Slimane, R. Galmes, G. Trugnan and M. Maurice, *Mol. Biol. Cell*, 2009, **20**, 3792–3800.

14 A. T. Jones, *J. Cell. Mol. Med.*, 2007, **11**, 670–684.
15 M. C. Kerr and R. D. Teasdale, *Traffic*, 2009, **10**, 364–371.
16 J. A. Swanson, *Nat. Rev. Mol. Cell Biol.*, 2008, **9**, 639–649.
17 J. Mercer, S. Knebel, F. I. Schmidt, J. Crouse, C. Burkard and A. Helenius, *Proc. Natl. Acad. Sci. U. S. A.*, 2010, **107**, 9346–9351.
18 S. Dharmawardhane, A. Schurmann, M. A. Sells, J. Chernoff, S. L. Schmid and G. M. Bokoch, *Mol. Biol. Cell*, 2000, **11**, 3341–3352.
19 P. Liberali, E. Kakkonen, G. Turacchio, C. Valente, A. Spaar, G. Perinetti, R. A. Bockmann, D. Corda, A. Colanzi, V. Marjomaki and A. Luini, *EMBO J.*, 2008, **27**, 970–981.
20 C. Escrevente, S. Keller, P. Altevogt and J. Costa, *BMC Cancer*, 2011, **11**, 108.
21 A. Montecalvo, A. T. Larregina, W. J. Shufesky, D. B. Stolz, M. L. Sullivan, J. M. Karlsson, C. J. Baty, G. A. Gibson, G. Erdos, Z. Wang, J. Milosevic, O. A. Tkacheva, S. J. Divito, R. Jordan, J. Lyons-Weiler, S. C. Watkins and A. E. Morelli, *Blood*, 2012, **119**, 756–766.
22 L. A. Mulcahy, R. C. Pink and D. R. Carter, *J. Extracell. Vesicles*, 2014, **3**.
23 D. Feng, W. L. Zhao, Y. Y. Ye, X. C. Bai, R. Q. Liu, L. F. Chang, Q. Zhou and S. F. Sui, *Traffic*, 2010, **11**, 675–687.
24 G. Sagar, R. P. Sah, N. Javeed, S. K. Dutta, T. C. Smyrk, J. S. Lau, N. Giorgadze, T. Tchkonia, J. L. Kirkland, S. T. Chari and D. Mukhopadhyay, *Gut*, 2016, **65**, 1165–1174.
25 O. P. Wiklander, J. Z. Nordin, A. O'Loughlin, Y. Gustafsson, G. Corso, I. Mager, P. Vader, Y. Lee, H. Sork, Y. Seow, N. Heldring, L. Alvarez-Erviti, C. I. Smith, K. Le Blanc, P. Macchiarini, P. Jungebluth, M. J. Wood and S. E. Andaloussi, *J. Extracell. Vesicles*, 2015, **4**, 26316.
26 T. Tian, Y. L. Zhu, Y. Y. Zhou, G. F. Liang, Y. Y. Wang, F. H. Hu and Z. D. Xiao, *J. Biol. Chem.*, 2014, **289**, 22258–22267.
27 J. D. Tario, Jr., K. Humphrey, A. D. Bantly, K. A. Muirhead, J. S. Moore and P. K. Wallace, *J. Visualized Exp.*, 2012, e4287, DOI: 10.3791/4287.
28 V. V. Temchura, M. Tenbusch, G. Nchinda, G. Nabi, B. Tippler, M. Zelenyuk, O. Wildner, K. Uberla and S. Kuate, *Vaccine*, 2008, **26**, 3662–3672.
29 A. Suetsugu, K. Honma, S. Saji, H. Moriwaki, T. Ochiya and R. M. Hoffman, *Adv. Drug Delivery Rev.*, 2013, **65**, 383–390.
30 I. Nakase, N. B. Kobayashi, T. Takatani-Nakase and T. Yoshida, *Sci. Rep.*, 2015, **5**, 10300.
31 D. Perez-Hernandez, C. Gutierrez-Vazquez, I. Jorge, S. Lopez-Martin, A. Ursa, F. Sanchez-Madrid, J. Vazquez and M. Yanez-Mo, *J. Biol. Chem.*, 2013, **288**, 11649–11661.
32 J. Webber, R. Steadman, M. D. Mason, Z. Tabi and A. Clayton, *Cancer Res.*, 2010, **70**, 9621–9630.
33 J. P. Webber, L. K. Spary, A. J. Sanders, R. Chowdhury, W. G. Jiang, R. Steadman, J. Wymant, A. T. Jones, H. Kynaston, M. D. Mason, Z. Tabi and A. Clayton, *Oncogene*, 2015, **34**, 290–302.
34 M. Al Soraj, L. He, K. Peynshaert, J. Cousaert, D. Vercauteren, K. Braeckmans, S. C. De Smedt and A. T. Jones, *J. Controlled Release*, 2012, **161**, 132–141.
35 J. P. Mitchell, J. Court, M. D. Mason, Z. Tabi and A. Clayton, *J. Immunol. Methods*, 2008, **335**, 98–105.
36 J. Lotvall, A. F. Hill, F. Hochberg, E. I. Buzas, D. Di Vizio, C. Gardiner, Y. S. Gho, I. V. Kurochkin, S. Mathivanan, P. Quesenberry, S. Sahoo, H. Tahara, M. H. Wauben, K. W. Witwer and C. Thery, *J. Extracell. Vesicles*, 2014, **3**, 26913.
37 C. Thery, S. Amigorena, G. Raposo and A. Clayton, in *Current protocols in cell biology*, ed. J. S. Bonifacino, *et al.*, 2006, ch. 3, Unit 3.22.
38 R. Linares, S. Tan, C. Gounou and A. R. Brisson, *Methods Mol. Biol.*, 2017, **1545**, 43–54.
39 Z. A. Martínez and M. Yáñez-Mó, *Front. Immunol.*, 2014, **5**.
40 J. Webber and A. Clayton, *J. Extracell. Vesicles*, 2013, **2**.
41 A. K. Enjeti, L. Lincz and M. Seldon, *Int. J. Lab. Hematol.*, 2008, **30**, 196–199.
42 S. E. Headland, H. R. Jones, A. S. V. D'Sa, M. Perretti and L. V. Norling, *Sci. Rep.*, 2014, **4**, 5237.
43 I. Nakase and S. Futaki, *Sci. Rep.*, 2015, **5**, 10112.
44 K. J. Svensson, H. C. Christianson, A. Wittrup, E. Bourseau-Guilmain, E. Lindqvist, L. M. Svensson, M. Morgelin and M. Belting, *J. Biol. Chem.*, 2013, **288**, 17713–17724.
45 P. R. Moody, E. J. Sayers, J. P. Magnusson, C. Alexander, P. Borri, P. Watson and A. T. Jones, *Mol. Ther.*, 2015, **23**, 1888–1898.
46 L. P. Jackson, B. T. Kelly, A. J. McCoy, T. Gaffry, L. C. James, B. M. Collins, S. Honing, P. R. Evans and D. J. Owen, *Cell*, 2010, **141**, 1220–1229.
47 A. Motley, N. A. Bright, M. N. Seaman and M. S. Robinson, *J. Cell Biol.*, 2003, **162**, 909–918.
48 J. E. Alford, J. Gumbs and E. C. Anderson, *PLoS One*, 2014, **9**, e91429.
49 E. Macia, M. Ehrlich, R. Massol, E. Boucrot, C. Brunner and T. Kirchhausen, *Dev. Cell*, 2006, **10**, 839–850.
50 H. Cao, J. Chen, M. Awoniyi, J. R. Henley and M. A. McNiven, *J. Cell Sci.*, 2007, **120**, 4167–4177.
51 J. R. Henley, E. W. Krueger, B. J. Oswald and M. A. McNiven, *J. Cell Biol.*, 1998, **141**, 85–99.
52 G. Preta, J. G. Cronin and I. M. Sheldon, *Cell Commun. Signaling*, 2015, **13**, 24.
53 D. Vercauteren, M. Piest, L. J. van der Aa, M. Al Soraj, A. T. Jones, J. F. Engbersen, S. C. De Smedt and K. Braeckmans, *Biomaterials*, 2011, **32**, 3072–3084.
54 P. Lajoie and I. R. Nabi, *Int. Rev. Cell Mol. Biol.*, 2010, **282**, 135–163.
55 J. A. Swanson and C. Watts, *Trends Cell Biol.*, 1995, **5**, 424–428.
56 J. P. Lim and P. A. Gleeson, *Immunol. Cell Biol.*, 2011, **89**, 836–843.
57 W. Shurety, N. L. Stewart and J. L. Stow, *Mol. Biol. Cell*, 1998, **9**, 957–975.
58 D. C. Edwards, L. C. Sanders, G. M. Bokoch and G. N. Gill, *Nat. Cell Biol.*, 1999, **1**, 253–259.
59 C. Vidal, B. Geny, J. Melle, M. Jandrot-Perrus and M. Fontenay-Roupie, *Blood*, 2002, **100**, 4462–4469.

60 J. P. Lim, P. Gosavi, J. D. Mintern, E. M. Ross and P. A. Gleeson, *J. Cell Sci.*, 2015, DOI: 10.1242/jcs.174359.

61 H. Hufnagel, P. Hakim, A. Lima and F. Hollfelder, *Mol. Ther.*, 2009, **17**, 1411–1417.

62 I. Nakase, M. Niwa, T. Takeuchi, K. Sonomura, N. Kawabata, Y. Koike, M. Takehashi, S. Tanaka, K. Ueda, J. C. Simpson, A. T. Jones, Y. Sugiura and S. Futaki, *Mol. Ther.*, 2004, **10**, 1011–1022.

63 M. Koivusalo, C. Welch, H. Hayashi, C. C. Scott, M. Kim, T. Alexander, N. Touret, K. M. Hahn and S. Grinstein, *J. Cell Biol.*, 2010, **188**, 547–563.

64 M. Fretz, J. Jin, R. Conibere, N. A. Penning, S. Al-Taei, G. Storm, S. Futaki, T. Takeuchi, I. Nakase and A. T. Jones, *J. Controlled Release*, 2006, **116**, 247–254.

65 M. Gschwendt, H. J. Muller, K. Kielbassa, R. Zang, W. Kittstein, G. Rincke and F. Marks, *Biochem. Biophys. Res. Commun.*, 1994, **199**, 93–98.

66 S. P. Soltoff, *Trends Pharmacol. Sci.*, 2007, **28**, 453–458.

67 S. P. Soltoff, *J. Biol. Chem.*, 2001, **276**, 37986–37992.

68 S. W. Deacon, A. Beeser, J. A. Fukui, U. E. E. Rennefahrt, C. Myers, J. Chernoff and J. R. Peterson, *Chem. Biol.*, 2008, **15**, 322–331.

69 Z. Wen, B. Zhao, K. Song, X. Hu, W. Chen, D. Kong, J. Ge and Z. Bu, *Virol. J.*, 2013, **10**, 331.

70 M. A. Krzyzaniak, M. T. Zumstein, J. A. Gerez, P. Picotti and A. Helenius, *PLoS Pathog.*, 2013, **9**, e1003309.

71 A. T. Jones and E. J. Sayers, *J. Controlled Release*, 2012, **161**, 582–591.

Appendix C – Supplementary Information for Roberts-Dalton et al. *Nanoscale.* 2017. In press.

Supplementary Materials

Supplementary Materials and Methods

1. Exosome isolation, purification and characterisation

Exosomes were purified from 7-day cell conditioned media, pre-cleared of cell debris and microvesicles by differential centrifugation followed by filtration through a 0.22 µm filter (Millipore). Exosome vesicles were purified based on their density by ultracentrifugation at 100,000 x *g* on a 30% sucrose/D_2O cushion as described [1]. Purified exosomes were resuspended in around 100 µl PBS, aliquoted, before storage at -80°C. Total protein was quantified by microBCA protein assay (ThermoFisher Scientific, Paisley, UK). The number, and size distribution of nano-particles was assessed by nanoparticle tracking analysis (Nanosight; Malvern Instruments, Worcestershire, UK). As a measure of exosome purity, protein and nanoparticle concentrations were used to calculate a ratio of particle to protein. All preparations had a particle to protein ratio of >$2x10^{10}$ particles per µg of protein, as described [2]. The presence of tetraspanins at the outer exosome surface was determined using a plate-immobilisation of purified exosomes, and indirect staining with antibodies against CD9 (R&D Systems, Abingdon, UK), CD81 or CD63 (BioRad, Hertfordshire, UK), a secondary anti-Mouse IgG-biotin conjugate (PerkinElmer) and streptavidin-Europium detection. Primary antibodies against relevant isotypes, IgG1 and IgG2b (eBioscience, ThermoFisher Scientific), were used as a control. Time resolved fluorometry was performed on a Pherastar FS instrument (BMGlabtech, Germany) as described [3]. Whole cell lysates, prepared using RIPA-buffer (Santa Cruz Biotechnology) were compared to exosome lysates, prepared by boiling in SDS-sample buffer containing 20 mM DTT, by western blotting running 10 µg protein per lane. After transfer to PVDF membranes (GE Healthcare), and blocking with 5% non-fat powdered milk with 0.1% Tween-20 in PBS for 1 hr, primary monoclonal antibody at a concentration of 1-4 µg/ml was added at 4°C overnight. Antibodies for expected exosome proteins TSG101, Alix, LAMP1 (Santa Cruz Biotechnology), MHC Class I

(eBioscience, ThermoFisher Scientific) were used, and to assess cellular contaminants, blots were also probed for calnexin expression (Santa Cruz). After washes in 0.1% Tween-20/PBS bands were detected using an anti-mouse IgG-horseradish peroxidase conjugated antibody (Santa Cruz) and chemiluminescence substrate (PicoWest, ThermoFisher Scientific). Images of membranes were collected using the C-DiGit Chemiluminescence Blot Scanner (LI-COR Biotechnology, Cambridge, UK).

2. Exosome analysis by Nano particle Tracking Analysis (NanoSight™)

Freshly prepared exosomes, or those following fluorescent labelling were diluted in particle free water (Fresenius Kabi, Runcorn, UK) to concentrations up to $2x10^9$ particles/ml, which is within the linear range of the NanoSight instrument. Analysis was performed on a NanoSight™ NS300 system configured with a temperature controlled LM14 laser module with a 488 nm laser and a high sensitivity sCMOS camera system and a syringe-pump system (Malvern Instruments, Malvern, UK). Three videos of 30-60 s were taken under controlled fluid flow with a pump speed set to 80, and temperature set to 25°C. Videos were taken in light scatter mode. On some occasions, videos were also taken following application of a long-pass fluorescence filter, so that only particles emitting light at >500 nm were visible. This required corrections for focusing, and an adjustment to the camera settings to maximise chances of visualising, and tracking fluorescent nano-particles. Videos were analysed using the batch analysis tool of NTA 2.3 software (version 2.3 build 2.3.5.0033.7-Beta7), where minimum particle size, track length and blur were set at "automatic". The area under the histogram for each triplicate measurement was averaged and used as a particle concentration measurement.

3. Cryo-electron microscopy of purified exosomes

Exosome preparations were adsorbed onto glow-discharging holey carbon 200-mesh copper grids (Quantifoil Micro Tools GmbH). Grids were vitrified with the aid of a

Vitrobot (Maastricht Instruments BV). Vitrified samples were imaged at liquid nitrogen temperature using a JEM-2200FS/CR transmission cryo-electron microscope (JEOL) equipped with a field emission gun and operated at an acceleration voltage of 200 kV.

4. siRNA transfection

In a 6 well plate (or 35 mm imaging dish) 100 pmols siRNA was diluted in 185 µl Opti-MEM while in a separate container 2 µl Oligofectamine was diluted with 13 µl OptiMEM. The two solutions were gently mixed and incubated at room temperature for 30 min. The cells were washed with Opti-MEM and 800 µl of Opti-MEM was added before dropwise addition of the siRNA complex mixture. Cells were returned to the incubator for 4 h before addition of 500 µl Opti-MEM containing 30% FCS and incubated for 44 h.

5. SDS PAGE and Western blotting

5.1. Following siRNA depletion

Following 48 h transfection, cells were washed with PBS followed by incubation on ice for 5 min in 100 µl ice-cold lysis buffer - 150 mM NaCl, 50 mM Tris-base pH 8.0, 1% Triton X-100 containing protease inhibitor cocktail. Cells were scraped from the plastic surface, placed in eppendorf tubes and then centrifuged for 10 min (13000 x *g*) at 4°C. The protein concentration of each sample was calculated via BCA assay and 18 µg protein per sample was mixed with 3x SDS PAGE sample buffer, heated to 95°C and loaded on to 8%, 10% or 12% SDS-PAGE gels. Following gel electrophoresis, proteins were transferred to PVDF membranes before blocking (5% w/v dried milk in PBS 0.0025% v/v Tween 20 (PBSTM)) and incubation with primary antibodies recognising AP2µ2, Caveolin-1 (Cav-1), Cdc42, Flotillin-1 (Flot-1), p21-activated kinase-1 (PAK-1), or GAPDH in 2% PBSTM. Secondary antibody incubation with goat anti-rabbit HRP conjugate, goat anti-mouse HRP conjugate or HRP conjugated anti-δ-

tubulin was then performed and chemiluminescence was detected on a ChemiDoc imager using ImageLab software (Bio-Rad).

6. Optimisation and characterization of exosome labelling

C_5-maleimide-Alexa488 (5-200 µg/ml) was added to a 30 µl exosome aliquot containing 60 to 100 µg protein, and made up to a final volume of 50 µl with PBS. Incubations, with no agitation, for 60 min in the dark at room temperature (R/T), were followed by removal of unbound dye using exosome spin columns (Invitrogen) according to manufacturer's instructions. Collected labelled exosomes were added to black-walled 96-well plates and the average fluorescence of triplicate wells measured on a PHERAstar FS plate reader (BMG Labtech, Ortenberg, Germany). Similarly, at a fixed dose of 200 µg dye, incubations for up to 3 h were performed before assessing intensity of labelling. In parallel, dye in the absence of exosomes were included in these experiments, to assess the efficacy of free-dye capture by the exosome spin columns. For some experiments, the free sulph-hydryl bonds at the exosome surface were capped by pre incubations with N-acytyl-L-cysteine (up to 1 mM) for 30 min prior to dye labelling (200 µg/ml, 1 h) and fluorescence assessment; revealing approximately 80% inhibition of labelling at maximal N-acetyl-L-cysteine dose.

Supplementary Figures

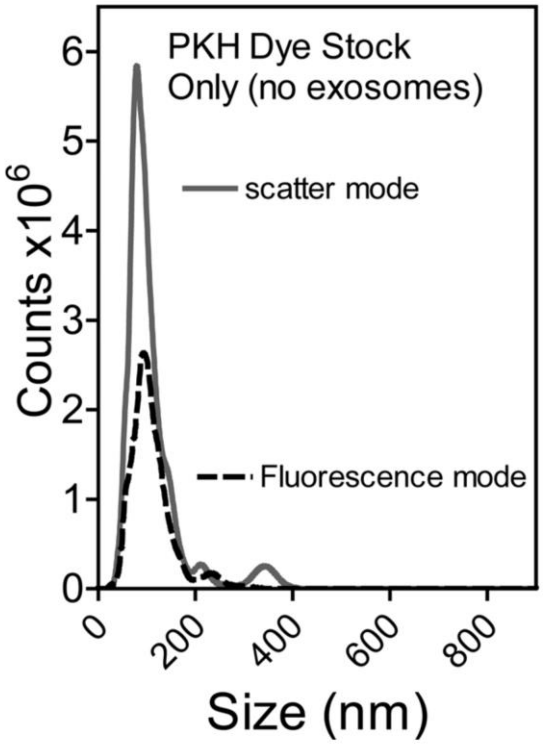

Supplementary Figure. 1. PKH26 dye was diluted 1 in 1000 in the provided dilution buffer, and analysed by NTA. The analysis was performed in light scatter mode (grey), and then following application of fluorescence filter where only fluorescing particles are visible (black, dashed line). We conclude that small particulate material spanning the size range of exosomes is present in the stock solution, and a proportion (52%) of these are fluorescent.

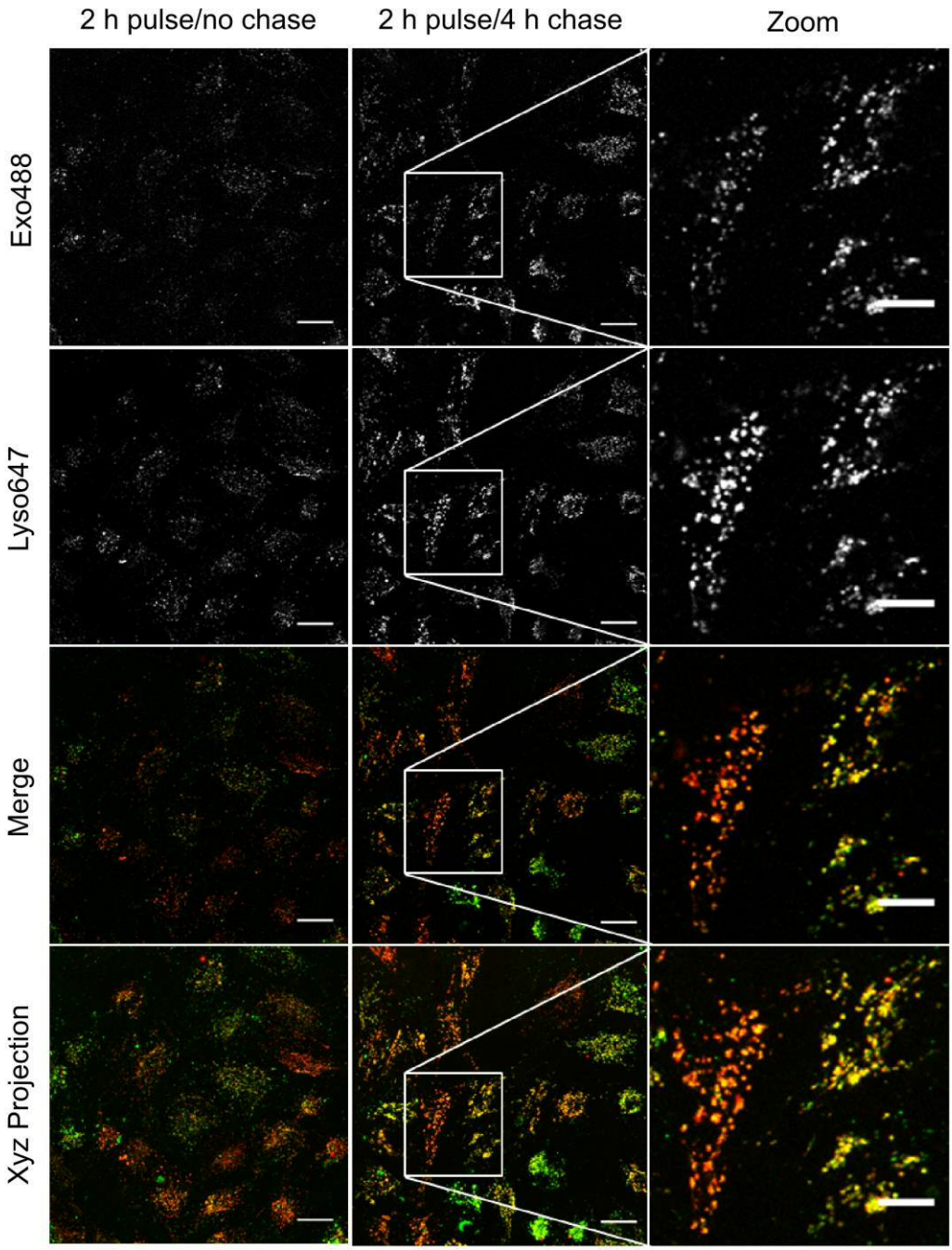

Supplementary Figure. 2. Colocalisation of 488-labelled exosomes with dextran-loaded lysosomes in HeLa cells. Cells were incubated with Dx647 (100 µg/ml) for 2 h, washed with PBS and incubated for a further 18 h in culture media. Cells were then incubated with Exo488 (60 µg/ml) for 2h with no chase or for 2 h followed by washing and a 4 hr chase. Scale bars: 20 µm and 10 µm on zoomed images. Images representative of three separate experiments.

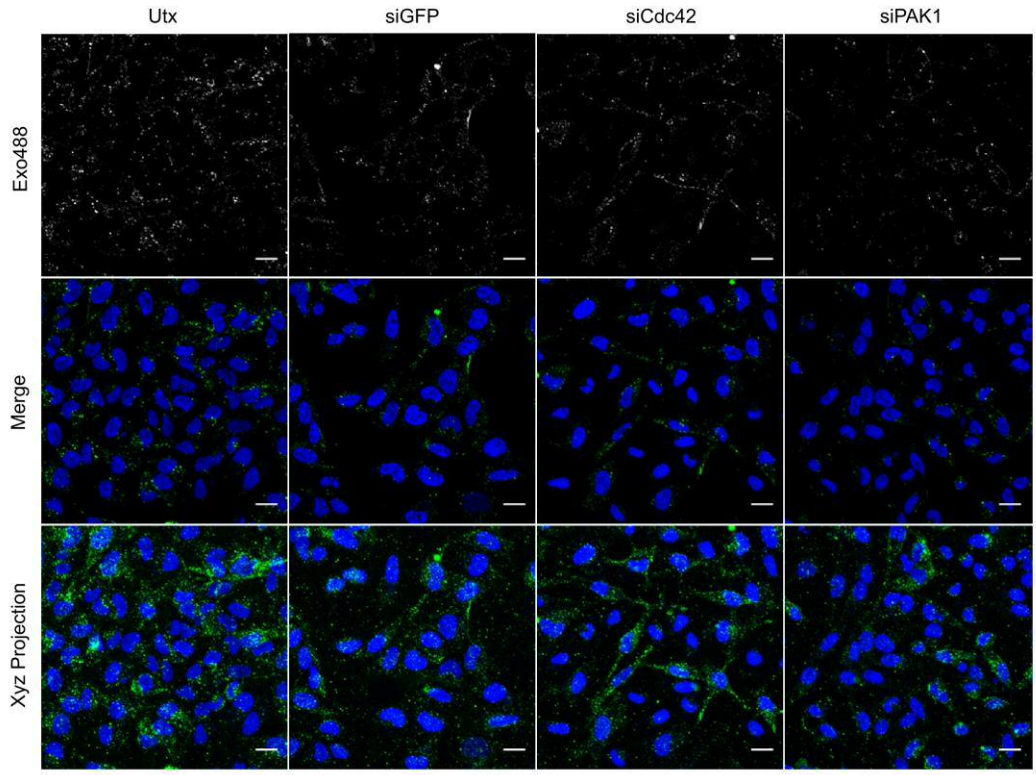

Supplementary Figure. 3. Additional fields of view showing internalisation of exosomes in HeLa cells depleted of fluid-phase/macropinocytosis related proteins. Cells were depleted of either Cdc42 or PAK-1 via siRNA transfection for 48 h before 60 min incubation with Exo488 (50 µg/ml). Cells were incubated with Hoechst for 5 min before live cell imaging. Utx: Untransfected. Scale bar: 20 µm. Images representative of three separate experiments.

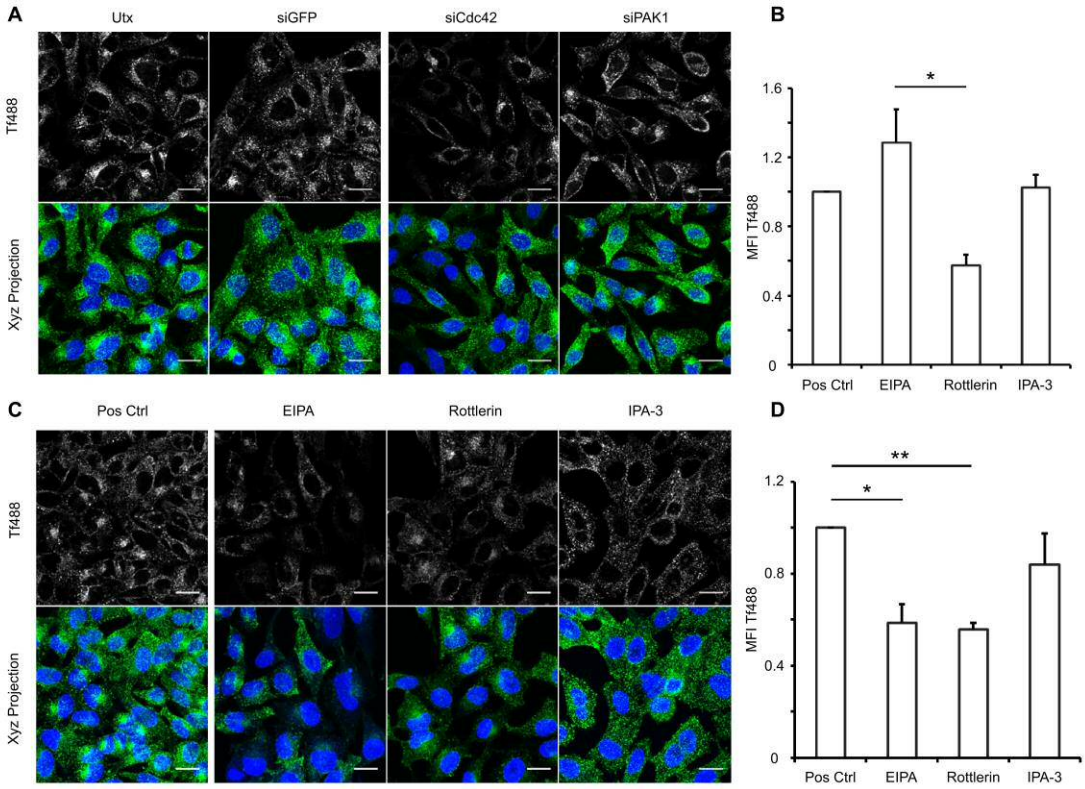

Supplementary Figure. 4. Transferrin internalisation in HeLa cell models of fluid-phase/macropinocytosis inhibition. (a) Cells were depleted of either Cdc42 or PAK1 via siRNA transfection for 48 h, or (c) pre-incubated with either EIPA (25 µM), Rottlerin (10 µM), IPA-3 (50 µM), or 0.05% DMSO as 'Pos Ctrl' for 30 min before 15 min incubation with Tf488 (5 µg/ml). Cells were incubated with Hoechst for 5 min before live cell imaging. Scale bar: 20 µm. Images representative of three separate experiments. (b) and (d) MFI quantification of the experiments presented in (a) and (c), respectively. Error bars represent Standard error. *p<0.05, **p<0.01. Representative of three separate experiments.

Supplementary Video.1. Time lapse images of Exo488 uptake in HeLa cells. Exo488 (60 µg/ml) were added for a period of either 120 min before confocal time lapse imaging. Hoechst and cell mask deep red were added for the final 5 min before imaging. Imaging was continuously performed for a period of 2 min.

Supplementary References

1. C. Thery, S. Amigorena, G. Raposo and A. Clayton, *Current protocols in cell biology / editorial board, Juan S. Bonifacino ... [et al.]*, 2006, **Chapter 3**, Unit 3.22.
2. J. Webber and A. Clayton, *Journal of extracellular vesicles*, 2013, **2**.
3. J. Webber, T. C. Stone, E. Katilius, B. C. Smith, B. Gordon, M. D. Mason, Z. Tabi, I. A. Brewis and A. Clayton, *Molecular & cellular proteomics : MCP*, 2014, **13**, 1050-1064.